Mechanisms of Soft-Tissue Mineralization Induced by the Inhibition of the MEK/ERK Pathway or the Inhibition of Fibroblast Growth Factor Receptors

João Alberto Zenhas Graça

PhD Thesis 2016

Summary

Currently in development as anti-cancer drugs, MEK/ERK and FGFR inhibitors have induced soft-tissue mineralization and increased plasma Pi and 1,25-dihydroxyvitamin D_3 ($1,25D_3$) levels in pre-clinical studies. AstraZeneca in-house data reported soft-tissue mineralization in stomach, kidney and heart of rats administered for >7d with MEK (MEKi) or FGFR (FGFRi) inhibitors. In this study, I aimed to unravel the mechanisms of soft-tissue mineralization associated with MEK/ERK or FGFR inhibition by assessing key processes for mineral homeostasis in rats treated with these inhibitors. The main findings of this study are:

1) Supporting previous studies, MEKi and FGFRi treatment (8d) resulted in soft-tissue mineralization and increases in plasma Pi and FGF23. Importantly, similar effects were observed for the first time in animals treated with an ERK inhibitor (ERKi).

2) Renal CaSR expression remained unchanged following MEKi or FGFRi treatment (8d), suggesting that the CaSR is not key for the mineralization induced by these inhibitors. Additionally, CaSR expression was detected throughout the nephron which supports previously hypothesised roles for this receptor in different processes including $1,25D_3$ production and Pi reabsorption.

3) Acute dosing (6h) with ERKi or FGFRi resulted in reduced plasma FGF23 and altered renal expression of proteins involved in $1,25D_3$ production (Cyp27b1, Cyp24a1) and Pi reabsorption (NaPiIIa), effects indicative of an impared FGF23 signalling. These results are consistent with MEK/ERK and FGFR inhibition promoting soft-tissue mineralization by analogous mechanisms: a blockage of FGF23 signalling that results in increased $1,25D_3$ production and in the consequent toxicity.

4) Repeated dosing (8d) with MEKi and FGFRi resulted in increased renal expression of Ca^{2+}-transport (TRPV5, calbindin-D28k, PMCA) and of calcification-inducing (alkaline phosphatase) proteins. These increases may contribute to mineralization by locally raising Ca^{2+}xPi product and inducing a pro-calcifying environment. Since the identified proteins contain VDREs, these effects are likely to be induced by increased plasma $1,25D_3$ levels.

Acknowledgements

Contents

List of abbreviations

$1,25D_3$	1,25-dihydroxyvitamin D_3
ADAM	A disintegrin and metalloproteinase domain
Al^{3+}	Aluminium
ALP	Alkaline phosphatase
ANK	Progressive ankyloses protein
AQP2	Aquaporin-2
ASARM	Acidic serine aspartate-rich MEPE-associated motif
ATP	Adenosine-5'-triphosphate
BCA	Bicinchoninic acid
Bcl-x	B-cell lymphoma-x
BID	Bi-daily administration
BMP2	Bone morphogenetic protein 2
BSP	Bone sialoprotein
C_{12h}	Drug concentration at 12h post-dose
Ca^{2+}	Free ionized calcium
cAMP	Cyclic adenosine monophosphate
CaSR	Calcium sensing receptor
CaSR-HEK	HEK293 cells stably transfected with the human CaSR
CD	Collecting duct
CLC-Kb	Chloride channel *Kb*;
C_{max}	Maximum drug concentration
CNT	Connecting tubule
CTX	Carboxy-terminal collagen crosslinks
CREB	cAMP response element-binding protein
DCT	Distal convoluted tubule
DKK1	Dickkopf-1
DMEM	Dulbecco's modified Eagle medium
DMEM/F12	Dulbecco's modified Eagle medium / nutrient mixture F-12
DMP1	Dentin matrix protein 1
DNA	Deoxyribonucleic acid
DSPP	Dentin sialophosphoprotein

DT	Distal tubule
EDTA	Ethylenediaminetetraacetic acid
EGFR	Epidermal growth factor receptor
ELISA	Enzyme-linked immunosorbent
ERKi	ERK 1/2 inhibitor used in this study
FGF	Fibroblast growth factor
FGF23	Fibroblast growth factor 23
FGFR	Fibroblast growth factor receptor
FGFRi	FGFR 1-3 inhibitor used in this study
FFPE	Formalin fixed paraffin embedded
FRS2	Fibroblast growth factor receptor substrate 2
Gd^{3+}	Gadolinium
GPCRs	G protein-coupled receptors
H&E	Hematoxylin and eosin
HCD	Human collecting duct
HEK	Human embryonic kidney
HK-2	Human kidney 2
HPMC	Hydroxypropyl methylcellulose
hRPTEC	Human renal proximal tubular epithelial cell
HTA	Human Tissue Act
HRP	Horseradish peroxidase
IHC	Immunohistochemistry
ISH	*In situ* hybridization
JAK	Janus kinase
JGA	Juxtaglomerular apparatus
JNK	c-Jun N-terminal kinase
Kir4.1	Inwardly rectifying potassium channel 4.1
MAPKAPK-2	Mitogen-activated protein kinase-activated protein kinase 2
MDCT	Mouse distal convoluted tubule
MEPE	Matrix extracellular phosphoglycoprotein
Mg^{2+}	Free ionised magnesium
MGP	Matrix Gla Protein
MEKi	MEK 1/2 inhibitor used in this study
mpkDCT4	Murine distal convoluted tubule 4

mRNA	Messenger ribonucleic acid
NaPi-IIa	Type IIa sodium-phosphate co-transporter
NaPi-IIb	Type IIb sodium-phosphate co-transporter
NaPi-IIc	Type IIc sodium-phosphate co-transporter
NBC	Sodium bicarbonate co-transporter;
NCC	Thiazide-sensitive Na+/Cl−cotransporter
NCX1	Na^+/Ca^{2+} exchanger
NFkB	Nuclear factor kappa-light-chain-enhancer of activated B cells
NHE3	Sodium hydrogen exchanger 3;
NKCC2	Sodium potassium 2-chloride co-transporter
NPP1	Nucleotide pyrophosphatase phosphodiesterase 1
OK	Opossum kidney
OPG	Osteoprotegerin
PARP	Poly ADP ribose polymerase
PBS	Phosphate-buffered saline
PEG	Polyethylene glycol 400
PLA	Proximity ligation assay
PLC	Phospholipase C
Pi	Inorganic phosphate
Pit-1	Sodium-dependent phosphate transporter 1
Pit-2	Sodium-dependent phosphate transporter 2
PKA	Protein kinase A
PKC	Protein kinase C
PMCA	Plasma membrane Ca^{2+} ATPase
PT	Proximal tubule
PTH	Parathyroid hormone
PTH1R	Parathyroid hormone receptor type 1
PTH2R	Parathyroid hormone receptor type 2
PTHrP	Parathyroid hormone related protein
qPCR	Real time polymerase chain reaction
RANK	Receptor activator of NF-kB
RANKL	Receptor activator of NF-kB ligand
RIPA	Radioimmunoprecipitation assay
RNA	Ribonucleic acid

ROMK	Renal outer medullary potassium channel
RPPA	Reverse phase protein array
RSK	p90 ribosomal S6 kinase
RT-PCR	Reverse transcription polymerase chain reaction
SEM	Standard error of the mean
SGLT	Sodium-dependent glucose cotransporter
SIBLING	Small integrin-binding ligand N-linked glycoprotein
SMA	Smooth muscle actin
STAT	Signal transducer and activator of transcription
$t_{1/2}$	Drug half-life
TAL	Thick ascending limb of Henle's loop
TBST	Tris-buffered saline containing 0.1%Tween
TNF	Tumour necrosis factor
TRPV5	Transient receptor potential cation channel subfamily V member 5
TRPV6	Transient receptor potential cation channel subfamily V member 6
VDR	Vitamin D receptor
VDREs	Vitamin D response elements
VEGFR	Vascular endothelial growth factor receptor
VSMC	Vascular smooth muscle cell

List of figures

List of tables

1 Introduction

1.1 Biomineralization

Biomineralization is the process of mineral production by a biological system (Weiner 2003). In mammals, biomineralization consists mainly of the deposition of calcium phosphate crystals in the form of hydroxyapatite. Under physiological conditions biomineralization only occurs in hard tissues such as bone, calcified cartilage and teeth (Bonucci 2013), however under pathological conditions this process can also occur in soft-tissues (ectopic mineralization), most frequently in kidney, skin, articular cartilage and cardiovascular tissue (Kirsch 2006). The consequences of ectopic mineralization depend on the affected tissue. For instance, mineralization of articular cartilage, associated with osteoarthritis, results in cartilage destruction and joint stiffness (Ea et al. 2011) whilst mineralization of blood vessels, associated with pathologies such as atherosclerosis and chronic kidney disease, results in the stiffening of these vessels and increased risk for myocardial infarction (Wexler et al. 1996). The mechanism of biomineralization is very complex and appears to be regulated by several factors, including levels of free ionized calcium (Ca^{2+}) and inorganic phosphate (Pi) (Bethke et al. 1932); formation of matrix vesicles / apoptotic bodies (Golub 2009) and presence of proteins and other molecules that regulate mineralization (Orimo 2010, Moochhala 2012). These factors are depicted in Figure 1.1 and will be further described in sections 1.2-1.4.
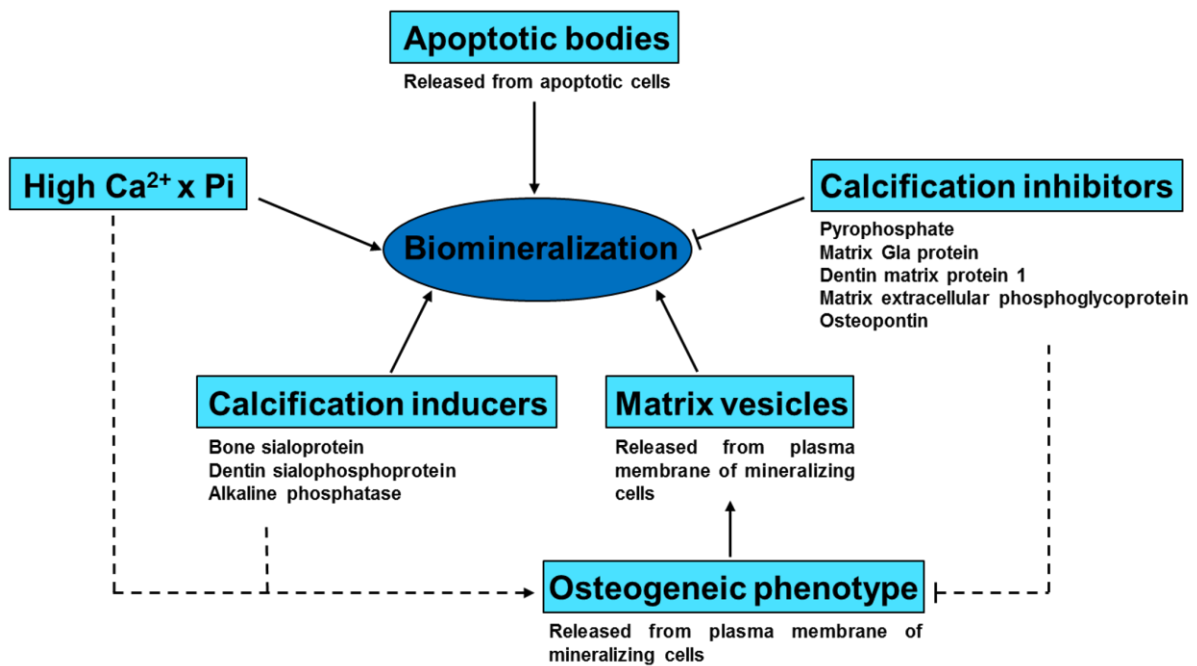
Figure 1.1: Schematic representation of the mechanisms that contribute to the occurrence of biomineralization. The scheme integrates data from different studies showing the complexity of biomineralization mechanisms and modulation by diverse processes including $Ca^{2+}xPi$ product, matrix vesicles, apoptotic bodies, induction of osteogenic phenotype, proteins/ molecules with pro-calcifying and anti-calcifying effects. Figure adapted from (Speer and Giachelli 2004).

1.2 Calcium and phosphate

High levels of Ca^{2+} and/or Pi in blood or body tissues contribute to the occurrence of soft-tissue mineralization (Haut et al. 1980, Giachelli et al. 2001). Initially, soft-tissue mineralization was thought to be a passive deposition of Ca^{2+} and Pi, since the production of hydroxyapatite is thermodynamically favourable (Johnsson and Nancollas 1992, Nancollas 1992). In the last few decades, however, Ca^{2+} and Pi were described to have an active role in this process (Speer and Giachelli 2004). High levels of Ca^{2+} and Pi were reported to promote soft-tissue mineralization by inducing changes in cellular phenotype. These effects were first observed in vascular smooth muscle cells (VSMCs) cultured in media containing high levels of Ca^{2+} and Pi, which showed the presence of soft-tissue mineralization associated with the suppression of smooth muscle cell specific genes such as *SM22α* and the induction of osteogenic genes, such as *Runx2* and alkaline phosphatase (Jono et al. 2000, Steitz et al. 2001, Yang et al. 2004). Mutations in genes encoding key regulators of Ca^{2+} and Pi homeostasis, such as the calcium sensing receptor (CaSR) and fibroblast growth factor 23 (FGF23), have been associated with the occurrence of soft-tissue mineralization (Hough et al. 2004, Masi et al. 2009). Moreover, soft-tissue mineralization is frequently observed in pathologies that comprise perturbations in Ca^{2+} and/or Pi homeostasis, such as chronic kidney disease (Evenepoel and Wolf 2013) and diabetes mellitus (Chen and Moe 2003).

1.3 Matrix vesicles / apoptotic bodies

Matrix vesicles are extracellular particles that originate from the plasma membrane of mineralizing cells. These vesicles contribute to mineralization by acting as mineral nucleation sites (Anderson 1969, Anderson 2003) and by decreasing the pyrophosphate/Pi ratio (Bobryshev et al. 2014). The mineralization functions of matrix vesicles involve the expression of pro-calcifying proteins, including alkaline phosphatase (Montessuit et al. 1995), annexins (Chen et al. 2008) and phospho-1 (Roberts et al. 2007). Similarly to matrix vesicles, apoptotic bodies, small particles released from cells undergoing apoptosis, contribute to mineralization by acting as mineral nucleation sites (Proudfoot et al. 2000, Proudfoot et al. 2001). Nevertheless, the mechanisms by which matrix vesicles and apoptotic bodies induce mineralization may differ as the latter lack the expression of pro-calcifying proteins such as alkaline phosphate and annexins (Kirsch et al. 2003).

1.4 Regulators of mineralization

1.4.1 Pyrophosphate

Pyrophosphate is a molecule that inhibits mineralization by binding to and preventing the growth of hydroxyapatite crystals (Fleisch 1981). Pyrophosphate is formed by different processes including the cleavage of adenosine-5'-triphosphate (ATP) or other nucleotides by the nucleotide pyrophosphatase phosphodiesterase 1 (NPP1) (Terkeltaub 2006). Consistent with the inhibitory role of pyrophosphate in the mineralization process, inactivating mutations of the gene that encodes NPP1 have been associated with the occurrence of soft-tissue mineralization (Mackenzie et al. 2012). Pyrophosphate is mainly produced intracellularly in the mitochondria (Johnson et al. 2000), however it can also be produced extracellularly by the transmembranous and secreted forms of NPP1 (Johnson et al. 1999). Pyrophosphate is extruded from the cells to the extracellular space by the progressive ankylosis protein (ANK) (Ho et al. 2000). Similarly to NPP1, inactivating mutations of the gene that encodes ANK have been associated with the occurrence of soft-tissue mineralization (Morava et al. 2011).

1.4.2 Matrix Gla protein

Matrix Gla protein (MGP) is a vitamin K-dependent protein expressed in different tissues including bone, kidney and heart (Fraser and Price 1988). MGP inhibits mineralization by binding to and preventing the growth of hydroxyapatite crystals (Price et al. 2002). Besides, MGP may prevent mineralization through other processes such as the inhibition of the pro-calcifying protein bone morphogenic protein 2 (BMP2) (Sweatt et al. 2003). MGP deficiency has been associated with soft-tissue mineralization in MGP knockout mice (Luo et al. 1997, El-Maadawy et al. 2003) and in patients with Keutel syndrome (Munroe et al. 1999). Also, MGP polymorphisms have been associated with vascular calcification (Herrmann et al. 2000, Crosier et al. 2009).

1.4.3 SIBLING

The small integrin-binding ligand N-linked glycoprotein (SIBLING) family consists in five different proteins, bone sialoprotein (BSP), dentin sialophosphoprotein, (DSPP),

dentin matrix protein 1 (DMP1), matrix extracellular phosphoglycoprotein (MEPE) and osteopontin, which are expressed in different organs including bone (Huang et al. 2008), kidney (Ogbureke and Fisher 2005) and salivary glands (Ogbureke and Fisher 2004). The SIBLINGs have both inhibitory and promoter roles in the mineralization process, which are conditioned by post-translational modifications such as phosphorylation and cleavage (Staines et al. 2012). Nevertheless, BSP (Wang et al. 2006) and DSPP (Prasad et al. 2010) are generally associated with the promotion and DMP1 (Tartaix et al. 2004), MEPE (Gowen et al. 2003) and osteopontin (Steitz et al. 2002) with the prevention of mineralization. At least partially, the inhibitory effects of the SIBLINGs in the mineralization process are associated with the release of a peptide containing an acidic serine aspartate-rich MEPE-associated motif (ASARM). This peptide is able to bind and prevent the development of hydroxyapatite crystals (Addison et al. 2008).

1.4.4 Alkaline phosphatase

The alkaline phosphatase protein family is composed by four distinct pro-calcifying isozymes. The intestinal, germ cell and placental isozymes show a tissue specific expression whilst the tissue nonspecific isozyme is expressed in different tissues including kidney, bone and liver (Sharma et al. 2014). The pro-calcifying effects of the alkaline phosphatases are mainly associated with the hydrolysis of pyrophosphate through a process that generates Pi (Hessle et al. 2002). Also, alkaline phosphatases can produce Pi through the breakdown of other molecules such as phosphoethanolamine and pyridoxal-5′-phosphate (Sharma et al. 2014). Mice lacking tissue nonspecific alkaline phosphatase show skeletal hypomineralization and defective growth of hydroxyapatite crystals in the vicinity of matrix vesicles (Anderson et al. 2004). These effects are ablated with the knockout of NPP1, the enzyme that catalyses the production of pyrophosphate from nucleotides, which suggests that the pro-calcifying effects of alkaline phosphatase are associated with the inhibition of pyrophosphate, rather than the production of phosphate (Hessle et al. 2002).

1.4.5 RANK, RANKL and osteoprotegerin

Receptor activator of NF-kB ligand (RANKL) is a protein from the tumour necrosis factor (TNF) superfamily that has key roles in processes that include bone turnover and vascular calcification. RANKL is expressed in different tissues including bone and

kidney (Kartsogiannis et al. 1999). This protein exerts its biological function by activating the receptor activator of NF-kB (RANK), which modulates different signalling pathways such as NF-Kb, Src, and MEK/ERK (Wada et al. 2006). In bone, RANK activation by RANKL promotes bone resorption by inducing differentiation, maturation and activation of osteoclasts (Wada et al. 2006). In the vasculature, RANK activation by RANKL induces vascular calcification by a process that is not completely understood but appears to include an increased expression of pro-inflammatory factors such as interleukin 6 and TNFα and osteogenic markers such as alkaline phosphatase and Runx2 (Deuell et al. 2012). RANKL signalling through RANK is inhibited by osteoprotegerin, which acts as a decoy receptor for RANKL and prevents its binding to RANK. Through the inhibition of RANKL-RANK signalling, osteoprotegerin has key roles in the regulation of bone turnover and vascular calcification. These roles are evident in the osteoprotegerin knockout mouse, which develops osteoporosis and extensive vascular calcification (Bucay et al. 1998).

1.4.6 Modulators of Wnt signalling

The Wnt family consists of 19 known glycoproteins that signal through 3 distinct pathways, a canonical pathway, which regulates the activation of the transcription co-activator beta-catenin and two non-canonical pathways. Wnt signalling is modulated by various proteins including the inducers leptin and parathyroid hormone (PTH) and the inhibitors Dickkopf-1 (DKK1) and sclerostin. Different studies have reported that VSMCs cultured in high Pi conditions show activation of the canonical Wnt pathway associated with the presence of mineral deposits and increased expression/activity of osteogenic markers such as BMP2 and alkaline phosphatase (Martinez-Moreno et al. 2012, Guerrero et al. 2014). Moreover, these effects were reduced or enhanced respectively by adding a Wnt inhibitor (DKK1) or Wnt activators (lithium chloride, CHIR98014 or leptin) to the culture media (Zeadin et al. 2012, Guerrero et al. 2014). Besides, the addition of magnesium to the culture medium reduced phosphate-induced calcification and beta-catenin activation in VSMC, suggesting that the process by which magnesium prevents the calcification process may involve the modulation of Wnt signalling (Montes de Oca et al. 2014). *In vivo* studies have reported that vascular calcification is associated with increased levels of plasma sclerostin (Kuipers et al. 2015), DKK1 (Kim et al. 2011) and leptin (Reilly et al. 2004). While high levels of plasma leptin likely contribute to the occurrence of calcification, the increase in

sclerostin and DKK1 levels may be due to an increased expression of these proteins in calcified tissue, with the objective of preventing further calcification. To support this observation, a different *in vivo* study has reported that calcified heart valves express sclerostin, which is not expressed in non-calcified valves (Brandenburg et al. 2013).

1.5 Extracellular free ionised calcium (Ca^{2+}o) and phosphate (Pi) homeostasis

Besides constituting mineral tissue and regulating the mineralization process, Ca^{2+} and Pi are key molecules for different biological processes. Extracellular free ionised Ca^{2+} levels are important to physiological processes such as hormonal secretion (Leclercq-Meyer et al. 1981), apoptosis (Lin et al. 1998) and proliferation (Kanatani et al. 1991). Additionally, intracellular Ca^{2+} levels are important for the cellular function since Ca^{2+} is a co-factor for different enzymes and a second messenger in a number of signalling pathways (Clapham 2007). Extracellular Pi levels also regulates different physiological processes including apoptosis (Mansfield et al. 1999) and cellular differentiation (Mozar et al. 2008). The signalling effects of Pi involve the modulation of different pathways including RANK (Mozar et al. 2008) and MEK/ERK (Yamazaki et al. 2010). In addition to its roles as an extracellular signalling molecule, Pi is a component of different nucleotides including ATP, an important energy source for different physiological processes (McClare 1975). The levels of extracellular Ca^{2+} and Pi need to be maintained respectively at 1.1-1.4 mmol/L and 0.8-1.4 mmol/L in order to preserve mineral homeostasis (Chang et al. 2014). The maintenance of extracellular Ca^{2+} and Pi levels involves the activation of different hormones including 1,25-dihydroxyvitamin D$_3$ (1,25D$_3$), FGF23, and PTH, which regulate the processes of intestinal absorption, bone resorption of these ions (Bergwitz and Juppner 2010). In addition to hormonal regulation, extracellular Ca^{2+} and Pi levels are also maintained locally, through the action of different proteins including the CaSR, the transient receptor potential cation channel subfamily V members 5 and 6 (TRPV5 and TRPV6) and sodium-dependent phosphate transporter 1 (Pit-1) (Zoidis et al. 2004, Civitelli and Ziambaras 2011).

1.5.1 Ca^{2+} and Pi reabsorption in kidney

The kidney is an important homeostatic organ that filters the blood and excretes the waste products by producing urine. The functions of the kidney include the excretion of toxins, regulation of circulating levels of different ions and control of blood pH (Preuss 1993). The kidney contributes to mineral ion homeostasis by tightly regulating the reabsorption of Ca^{2+} and Pi from urine into the plasma. Following glomerular filtration, around 70% of the filtered Pi is reabsorbed by transcellular transport in the

proximal tubule (PT) in a process mediated by the type IIa (NaPi-IIa) and IIc (NaPi-IIc) sodium-phosphate co-transporters (Prasad and Bhadauria 2013). Further Pi reabsorption may occur in the distal convoluted tubule (DCT), however the associated mechanisms are not completely understood (Lassiter and Colindres 1982). Conversely to Pi, the majority of the filtered Ca^{2+} is reabsorbed paracellularly, 60-70% in the PT and 20% in the thick ascending limb of Henle's loop (TAL) (Blaine et al. 2015). The paracellular reabsorption of Ca^{2+} is dependent on the electrochemical gradients of sodium and chloride and subject to regulation by tight junction proteins such as claudins (Blanchard et al. 2001). A further 10-15% of the filtered Ca^{2+} is actively reabsorbed by transcellular transport in the DCT and connecting tubule (CNT) segments in response to the physiological needs for this ion (Boros et al. 2009). Distal Ca^{2+} reabsorption is mediated by the proteins TRPV5, calbindin D_{28k}, Na^+/Ca^{2+} exchanger (NCX1) and plasma membrane Ca^{2+} ATPase (PMCA). TRPV5 promotes Ca^{2+} entry into the cell through the apical membrane; calbindin D_{28k} transports Ca^{2+} through the cytosol to the basolateral membrane and acts as Ca^{2+} buffer; and NCX1 and PMCA mediate Ca^{2+} extrusion through the basolateral membrane (Boros, Bindels et al. 2009). The processes associated with renal reabsorption of Ca^{2+} and Pi are represented in Figure 1.2.
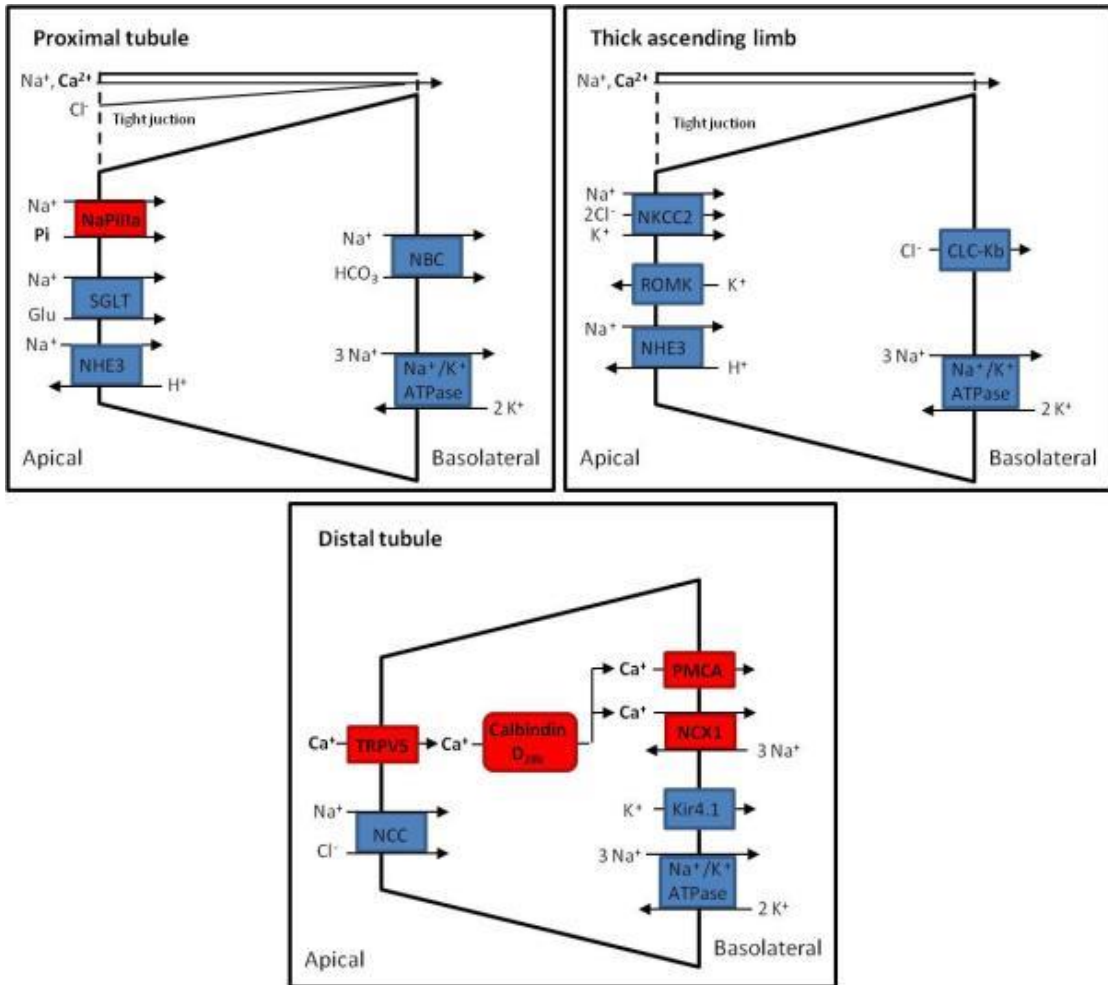
Figure 1.2: Schematic representation of Ca²⁺ and Pi reabsorption along the nephron. Proteins directly involved in Ca²⁺ and Pi transport are represented in red and proteins indirectly involved in Ca²⁺ and Pi transport are represented in blue. Abbreviations: NaPi-IIa, type II sodium-phosphate co-transporter; SGLT, sodium-dependent glucose cotransporter ; NHE3, sodium hydrogen exchanger 3; NBC, sodium bicarbonate co-transporter; NKCC2, sodium potassium 2-chloride co-transporter; ROMK, renal outer medullary potassium channel; CLC-Kb, chloride channel *Kb*; TRPV5, transient receptor potential cation channel subfamily V member 5; PMCA, plasma membrane Ca²⁺ ATPase; NCX1, Na+/Ca2+ exchanger; NCC, thiazide-sensitive Na+/Cl−cotransporter; NCX1, Na⁺/Ca²⁺ exchanger, Kir4.1, Inwardly rectifying potassium channel 4.1. Figure adapted from (Riccardi and Kemp 2012).

1.6 Parathyroid-Bone-Kidney axis

The kidney, bone and parathyroid axis and their respectively associated hormones, $1,25D_3$, FGF23 and PTH, ensure Ca^{2+} and Pi homeostasis (Bergwitz and Juppner 2010, Kuro-o 2010, Haussler et al. 2012). The levels and activity of these hormones are altered as a direct response to physiological changes in Ca^{2+} and / or Pi, and also as a consequence of complex feedback mechanisms. The metabolism and roles of $1,25D_3$, FGF23 and PTH in Ca^{2+} and Pi homeostasis are depicted in Figure 1.3 and described below.
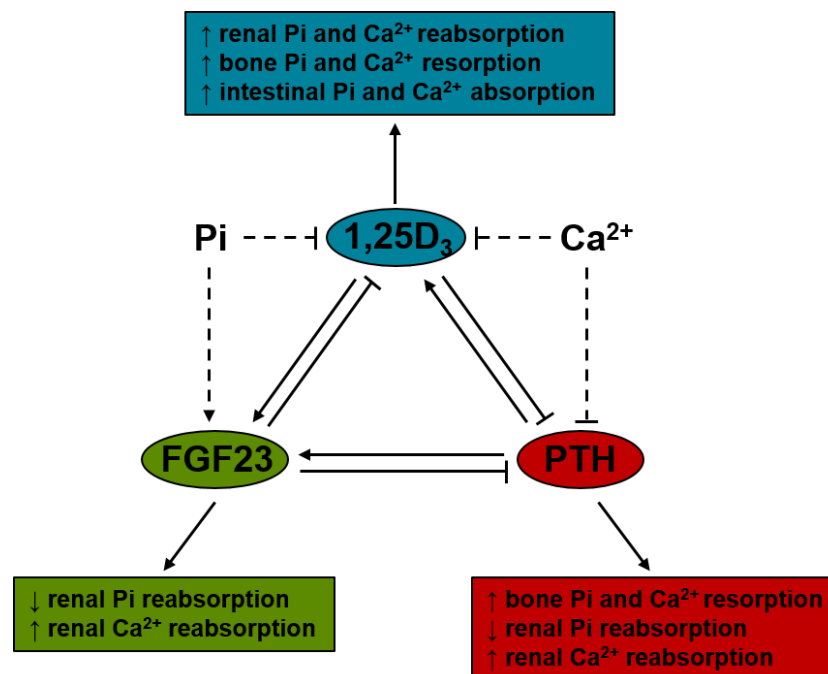
Figure 1.3: Schematic representation of the parathyroid-bone-kidney axis. The scheme depicts the effects of Ca^{2+} and Pi and inter-regulatory mechanisms in the production/secretion of PTH, FGF23 and $1,25D_3$ hormones. Figure adapted from (Silver and Naveh-Many 2009).

1.7 Vitamin D

1.7.1 Vitamin D metabolism

The concept of a vitamin involved in Ca^{2+} regulation was first suggested in 1922, following the discovery that cod liver oil oxidised to destroy vitamin A was able to promote Ca^{2+} deposition in bones of rats suffering from rickets (McCollum et al. 1922). In the 1930s, vitamins D_2 and D_3, the two major forms of vitamin D were identified respectively as products of the ultra-violet irradiation of ergosterol (Askew et al. 1930) and 7-dehydrocholesterol (Windaus and Bock 1937). Studies carried out in the subsequent decades have elucidated the metabolism and physiological roles of vitamin D. Vitamin D_3, the most important form of vitamin D for mammalian physiology, is obtained by exposure to sunlight and dietary intake (Bikle 2014). Then, this vitamin is activated in two sequential steps. First, CYP2R1 catalyses the production of 25-hydroxyvitamin D_3 from vitamin D_3 in the liver. Subsequently, in the rate limiting step of this process, CYP27B1 catalyses the production of 1,25-dihydroxyvitamin D_3 $(1,25D_3)$ from 25-hydroxyvitamin D_3 mostly in the kidney (Takeyama et al. 1997). To a lesser extent than the kidney, $1,25D_3$ is also produced in other tissues including breast, parathyroid gland and placenta, by the action of extra-renal CYP27B1 (Zehnder et al. 2001, Adams and Hewison 2012).

The production of $1,25D_3$ is regulated by different factors including the inducer PTH (Armbrecht et al. 2003) and the inhibitors Ca^{2+}, Pi (Fukumoto 2014) and FGF23 (Perwad et al. 2007). Renal $1,25D_3$ targets the kidney through autocrine/paracrine actions and it is secreted to the circulation and targets other organs by functioning as an endocrine factor. Conversely, extra-renal $1,25D_3$ has mainly local actions by functioning as an autocrine/paracrine factor (Zehnder et al. 2002, Morris and Anderson 2010). Whilst renal $1,25D_3$ is a key molecule for mineral homeostasis, extra-renal $1,25D_3$ seems to have more important roles in other processes including immunological response, proliferation and apoptosis (Adams and Hewison 2012, Hobaus et al. 2013).

The effects of $1,25D_3$ are mainly triggered by its genomic actions, which are mediated by the nuclear vitamin D receptor (VDR). Upon the activation by $1,25D_3$, the nuclear VDR functions as a transcription factor and regulates the expression of different genes containing vitamin D response elements (VDREs) (Haussler et al. 1997). In addition

to the genomic effects, $1,25D_3$ is able to signal through a membrane VDR that modulates different signalling pathways including protein kinase A (PKA) and protein kinase C (PKC) (Revelli et al. 1998). The inactivation of vitamin D_3 occurs through the 24-hydroxylation of $1,25D_3$, a process catalysed by CYP24A1 in different tissues including kidney, intestine, bone and skin (Armbrecht et al. 1992). The inactivation of vitamin D_3 is regulated by different factors including the inducers Ca^{2+} and Pi, $1,25D_3$ and FGF23 and the inhibitor PTH (Shinki et al. 1992, Shimada et al. 2004).

1.7.2 *Vitamin D and mineral ion homeostasis*

The production of $1,25D_3$ is promoted under conditions of hypocalcemia and/or hypophosphatemia. In order to restore mineral homeostasis, $1,25D_3$ increases serum levels of Ca^{2+} and Pi by stimulating the intestinal absorption and renal reabsorption of these ions and by enhancing bone resorption (Eisman and Bouillon 2014, Wranicz and Szostak-Wegierek 2014). The direct effects of $1,25D_3$ in intestinal absorption and renal reabsorption are associated with the induction of the expression of proteins involved in the transport of Ca^{2+} and Pi including TRPV5/6, calbindin D_{9K}/D_{28K}, PMCA, NaPi-IIa/b (Bindels et al. 1991, Hoenderop et al. 2001, van de Graaf et al. 2004, Kido et al. 2013). Although the mechanisms have not been fully elucidated so far, the direct effects of $1,25D_3$ in bone resorption appear to be associated with the regulation of the expression of RANKL (Kitazawa et al. 2003, Suda et al. 2003). In addition to the direct effects in the expression of proteins involved in bone resorption and Ca^{2+} and Pi reabsorption, $1,25D_3$ also encompasses indirect effects in mineral homeostasis including the induction of FGF23 (Barthel et al. 2007) and inhibition of PTH (Naveh-Many and Silver 1990) hormones. Most of the effects of $1,25D_3$ in mineral homeostasis are associated with the activation of nuclear VDR and regulation of genes that contain VDREs (Kumar et al. 2012).

1.8 FGF23 and Klotho

1.8.1 FGF23 structure and metabolism

Fibroblast growth factor 23 (FGF23), a 251 amino acid protein with key roles in Ca^{2+} and Pi regulation, was identified in mouse brain and thymus in 2000 (Yamashita et al. 2000). Shortly after the identification, the observation that a missense mutation in the FGF23 gene resulted in autosomal dominant hypophosphatemic rickets shed light on the importance of FGF23 to mineral homeostasis (White et al. 2000). FGF23 is produced mainly by osteocytes in bone (Bonewald and Wacker 2013) and unlike most fibroblast growth factors (FGFs), it is secreted to the circulation and functions as an endocrine factor (Kuro-o 2008). The production and secretion of FGF23 is regulated by different factors, including the inducers Pi (Vervloet et al. 2011), $1,25D_3$ (Kolek et al. 2005) and PTH (Lavi-Moshayoff et al. 2010). The effects of FGF23 encompass signalling through the fibroblast growth factor receptors (FGFRs) (Yu et al. 2005). There are four FGFRs, namely FGFR1-3, which possess two isoforms (b/c) originated by alternative splicing; and FGFR4 which only possesses one isoform (c) (Gong 2014). The interaction between FGF23 and the FGFRs has a low affinity, which is greatly enhanced by the protein alpha-Klotho (Klotho) (Urakawa et al. 2006). Although most of the biological effects of FGF23 require the presence of Klotho, some Klotho-independent effects were reported including the processes of PTH secretion (Olauson et al. 2013) and cardiovascular disease (Faul et al. 2011). FGF23 signalling occurs mainly via the fibroblast growth factor receptor substrate 2 (FRS2) and phospholipase C (PLC) gamma and involves the activation of different signalling pathways including the MEK/ERK pathway (Yamazaki et al. 2010, Brooks et al. 2012).

1.8.2 Klotho structure and metabolism

Klotho, the 1014 amino acid transmembrane co-receptor for FGF23, was identified in 1997 in a study that associated inactivating mutations in its encoding gene with the occurrence of a syndrome resembling premature ageing (Kuro-o et al. 1997). Nevertheless, the role of Klotho in FGFR signalling was only unravelled in 2006 (Kurosu et al. 2006), as the result of a study driven by the similarities between *Klotho* and *Fgf23* knockout mice (Shimada et al. 2004). Klotho was reported to function as a co-receptor for FGF23 by increasing the affinity of the c isoforms of the FGFRs 1, 3 and 4 for FGF23 (Kurosu et al. 2006). The expression of Klotho is regulated by

different factors including the inducer 1,25D$_3$ (Forster et al. 2011), and the inhibitors FGF23 (Marsell et al. 2008) and TNF alpha (Moreno et al. 2011). In addition to its function as a transmembrane co-receptor for FGF23, a secreted form of Klotho regulates different biological processes by acting as an endocrine factor (Huang 2010). The secretion of Klotho can be induced either by alternative splicing of the *Klotho* gene or by the cleavage of its extracellular domain by the proteases a disintegrin and metalloproteinase domain (ADAM) 10 and 17 (Chen et al. 2007).

1.8.3 FGF23, Klotho and mineral homeostasis

The production and secretion of FGF23 is promoted in conditions of hyperphosphatemia (Gupta et al. 2004). In order to restore mineral ion homeostasis, FGF23 inhibits the expression of NaPi-IIa and NaPi-IIc in the kidney, resulting in decreased renal Pi reabsorption (Shimada et al. 2004). Additionally, FGF23 induces the expression of TRPV5 in the kidney, resulting in increased renal Ca^{2+} reabsorption (Andrukhova et al. 2014). In addition to the direct effects of FGF23 on the expression of NaPi-IIa, NaPi-IIc and TRPV5, this hormone indirectly regulates Ca^{2+} and Pi metabolism by inhibiting the expression of PTH in the parathyroid (Ben-Dov et al. 2007) and the production of 1,25D$_3$ in the kidney (Gattineni et al. 2011). Although the associated mechanisms are not completely understood, the secreted form of Klotho appears to contribute to mineral ion homeostasis independently of FGF23 by inhibiting NaPi-IIa (Hu et al. 2010) and activating TRPV5 (Chang et al. 2005). The importance of FGF23 and Klotho in mineral ion homeostasis is evident from the phenotypes of mice carrying mutations in these genes, which encompass increased mineralization of soft-tissues associated with high serum levels of Pi and 1,25D$_3$ (Tsujikawa et al. 2003, Shimada et al. 2004).

1.9 Parathyroid hormone

1.9.1 Parathyroid hormone structure and metabolism

Parathyroid hormone (PTH), an 84 amino acid protein with key roles in Ca^{2+} and Pi homeostasis, was identified in 1925 as the hormone that mediates the actions of the parathyroid glands in regulation of blood Ca^{2+} levels (Collip 1925). PTH is produced and stored in the parathyroid glands. The production of active PTH (84 amino acid) involves the synthesis of a 115 amino acid precursor (pre-pro-PTH), followed by the sequential cleavages of a signal peptide (25 amino acid) and a prosequence (6 amino acid) (Habener et al. 1979). Active PTH is then stored in secretory vesicles that are released to the circulation under hypocalcemic (Felsenfeld et al. 2007) or hyperphosphatemic (Almaden et al. 1996) conditions. Other molecules regulate the production and secretion of PTH in addition to Ca^{2+} and Pi including the inhibitors CaSR (Chen and Goodman 2004), $1,25D_3$ (Cantley et al. 1985) and FGF23 (Ben-Dov et al. 2007). The biological effects of PTH involve signalling through the PTH receptors type 1 (PTH1R) and 2 (PTH2R), which are G protein-coupled receptors (GPCRs) (Mahon 2012). The activation of PTH1R and PTH2R by PTH results in the activation of different G proteins and modulation of various signalling pathways including PKC (Yang et al. 2006) and MEK/ERK (Lederer et al. 2000). PTH1R can also be activated by parathyroid hormone related protein (PTHrP), a hormone that shares some structural homology with PTH but exerts different biological roles (Wysolmerski 2012).

1.9.2 Parathyroid hormone and mineral homeostasis

The production and secretion of PTH is promoted under conditions of hypocalcemia (Felsenfeld et al. 2007) and hyperphosphatemia (Almaden et al. 1996). In order to restore mineral ion homeostasis, PTH directly targets the kidney, inhibiting NaPi-IIa in order to decrease in Pi reabsorption (Riccardi et al. 2000); and upregulating TRPV5, calbindin D_{28K} and NCX1 in order to increase renal Ca^{2+} reabsorption (van Abel et al. 2005, de Groot et al. 2009). Besides, PTH also targets the bone, where it induces different biological effects according to the length of the exposure. A prolonged exposure to PTH promotes bone resorption whilst an intermittent exposure promotes bone formation (Kroll 2000). In addition to the direct effects on processes of bone resorption and renal Ca^{2+} and Pi reabsorption, PTH also regulates the metabolism of

Ca^{2+} and Pi indirectly by inducing the expression of FGF23 in the bone (Lavi-Moshayoff et al. 2010) and the production of 1,25D$_3$ in the kidney (Bajwa et al. 2008).

1.10 Calcium sensing receptor

1.10.1 Structure and metabolism

The extracellular calcium sensing receptor (CaSR), a 1085 amino acid GPCR with a key role in mineral ion homeostasis, was first molecular identified from bovine parathyroid glands in 1993 (Brown et al. 1993). In the years that followed its identification, the expression and functional roles for the CaSR were reported in different tissues, including kidney (Riccardi et al. 1995), bone (Kameda et al. 1998) and intestine (Chattopadhyay et al. 1998). The main function of the CaSR is to monitor free ionised Ca^{2+} and magnesium (Mg^{2+}) in order to preserve divalent mineral ion homeostasis. In response to any changes in the serum levels of these ions, the CaSR regulates local processes such renal Ca^{2+} reabsorption (Loupy et al. 2012) and systemic processes such as PTH secretion (Chen and Goodman 2004) and $1,25D_3$ production (Bland et al. 2002). The affinity of the CaSR for Ca^{2+} can be modified by allosteric ligands such as glutathione and amino acids (Cavanaugh et al. 2012). Also, the CaSR can be activated by orthosteric ligands other than Ca^{2+} and Mg^{2+} including trivalent cations, such as gadolinium (Gd^{3+}) and aluminium (Al^{3+}); polyamines such as spermine; and aminoglycoside antibiotics such as neomycin (McLarnon et al. 2002, Cheng et al. 2004, Geibel 2010). The CaSR is involved in other processes besides mineral ion homeostasis, including taste perception (Ohsu et al. 2010), nutrient sensing (Conigrave and Brown 2006) and synaptic transmission (Phillips et al. 2008). The biological effects of the CaSR involve the induction of different G proteins and the modulation of several downstream signalling pathways, including PKC (Godwin and Soltoff 2002), cyclic adenosine monophosphate (cAMP) (Conigrave and Avlani 2012) and MEK/ERK (Kifor et al. 2001). The biological effects of the CaSR are dependent on the ligand activating the receptor since each ligand is able to stabilize a subset of receptor conformations that selectively activate downstream signalling pathways (ligand-biased signalling) (Leach et al. 2014). Besides, the downstream signalling of the CaSR may be influenced by the interaction with binding partners such as filamin-A, 14-3-3 proteins and caveolin (Awata et al. 2001, Riccardi and Brown 2010).

1.10.2 CaSR and mineral homeostasis

In physiological or hypercalcemic conditions, the CaSR inhibits the production and secretion of PTH in the parathyroid gland (Chen and Goodman 2004) and the production of $1,25D_3$ in the kidney (Bland et al. 2002), thus preventing Ca^{2+} levels from increasing. Besides, in hypercalcemic conditions, the CaSR promotes a decrease in serum Ca^{2+} levels by eliciting the secretion of calcitonin from the thyroid (Fox et al. 1999). Opposite to PTH and $1,25D_3$, calcitonin inhibits the processes of bone resorption and renal Ca^{2+} reabsorption (Masi and Brandi 2007). In addition to the systemic effects associated with the modulation of PTH, $1,25D_3$ and calcitonin, the CaSR also counteracts hypercalcemia by directly preventing bone resorption (Theman and Collins 2009) and by inhibiting renal Ca^{2+} reabsorption. The direct effects of the CaSR in renal Ca^{2+} reabsorption involve the modulation of the transepithelial potential in the TAL (Loupy et al. 2012) and the regulation of TRPV5 (Topala et al. 2009) and PMCA (Blankenship et al. 2001) in the DCT. Also, the CaSR regulates Pi reabsorption in the kidney by preventing the PTH-induced inhibition of NaPi-IIa (Ba et al. 2003). In hypocalcemic conditions, the inhibitory effects of the CaSR in the production and secretion of PTH and $1,25D_3$ are removed, thus leading to an increase in the serum levels of these hormones and a consequent raise in serum Ca^{2+} (Bland et al. 2002, Chen and Goodman 2004).

1.11 Scope and aims

Mineralization of soft-tissues is frequently observed during preclinical drug safety testing. MEK/ERK and FGFR inhibitors are two classes of compounds currently being developed to treat cancer (Knights and Cook 2010, McCubrey et al. 2010). In toxicology studies with rodents, the administration of these compounds resulted in the mineralization of soft-tissues associated with increased serum levels of Pi and $1,25D_3$ (Brown et al. 2005, Brown and Gad 2010, Diaz et al. 2012, Yanochko et al. 2013). Nevertheless, the molecular mechanisms associated with this toxicity have not been fully elucidated. Preliminary studies carried out at AstraZeneca have shown that the administration of a MEK 1/2 inhibitor (MEKi) or an FGFR 1-3 (FGFRi) inhibitor for >7d to rats results in soft-tissue mineralization in different organs including stomach, kidney and heart.

In this thesis I set out to unravel the mechanisms of soft-tissue mineralization induced by the inhibition of the MEK/ERK pathway or FGFRs. The work carried out for this thesis is focused on the kidney since the kidney is the organ where $1,25D_3$ is mainly produced and one of the organs displaying mineralization in animals treated with these inhibitors.

I hypothesised that FGFR and MEK/ERK inhibitors prevent FGF23 signalling in the kidney and consequently increase the production of $1,25D_3$. Then, the elevated levels of $1,25D_3$ promote the occurrence of soft-tissue mineralization through different effects including the increase in renal Ca^{2+} and Pi reabsorption and the increase in the expression of mineralization inducers such as alkaline phosphatase. Besides, I hypothesised that the renal CaSR is involved in this process, since the CaSR was previously described to regulate $1,25D_3$ production (Bland et al. 2002) and Ca^{2+} (Loupy et al. 2012) and Pi (Ba et al. 2003) reabsorption.

These hypothesis were tested by administering an ERK inhibitor (ERKi), MEKi or FGFRi to rats and assessing the effects of these inhibitors in key processes for mineral ion homeostasis.

The key aims of this work, which are addressed in Chapters 2-4, are described below.

- Clarification of the intra-renal distribution of the CaSR and assessment of the role of this receptor in the soft-tissue mineralization induced by MEKi or FGFRi.
- Identification of the cell signalling pathways that mediate the effects of ERKi, MEKi and FGFRi in mineral ion homeostasis and soft-tissue mineralization in the kidney.
- Evaluation of the role of the hormones $1,25D_3$, FGF23 and PTH in the process of soft-tissue mineralization induced by ERKi, MEKi and FGFRi.
- Assessment of the effects of ERKi, MEKi and FGFRi in the processes of renal reabsorption of Ca^{2+} and Pi.
- Assessment of the effects of ERKi, MEKi and FGFRi in the expression of circulating and renal calcification modulator proteins.
- Establishment and use of an *ex vivo* kidney slice model to further explore the findings of the *in vivo* experiments.

2 Intra-renal distribution and role of the CaSR in the mineralization induced by inhibition of MEK/ERK pathway and FGF receptors

2.1 Introduction

Mineralization of soft-tissues including kidney, bone and heart has been reported in toxicology studies with MEK and FGFR inhibitors (Brown et al. 2005, Brown and Gad 2010, Diaz et al. 2012, Yanochko et al. 2013). Both classes of compounds are currently being developed as drugs to target cancer, since mutations in the FGFRs or components of the MEK/ERK signalling pathway are on the origin of several tumours including breast, gastric tract, colorectal and thyroid tumours (Knights and Cook 2010, McCubrey et al. 2010). In addition to soft-tissue mineralization, the toxicological effects of MEK inhibitors (Brown and Gad 2010, Diaz et al. 2012, Yanochko et al. 2013) or FGFR inhibitors (Wohrle et al. 2011, Wohrle et al. 2013, Yanochko et al. 2013) in rodents include increased production of $1,25D_3$ and high plasma levels of Pi, observable as early as 12-24h after treatment. Similar to the studies mentioned above, soft-tissue mineralization in different organs and increased levels of plasma Pi were observed following the administration of a MEK 1/2 inhibitor (MEKi) or an FGFR 1-3 inhibitor (FGFRi) to rats in pre-clinical studies carried out at AstraZeneca. The CaSR is a receptor with key roles in mineral ion homeostasis including the regulation of blood free ionised Ca^{2+} and Pi. Activating mutations in the CaSR result in soft-tissue mineralization associated with hyperphosphatemia and hypocalcemia in the Nuf mouse model (Hough et al. 2004) and in patients with autosomal dominant hypocalcemia (Raue et al. 2011). Since the expression of the CaSR is induced by $1,25D_3$ (Canaff and Hendy 2002), it is plausible that this receptor is involved in the mineral homeostasis perturbations and soft-tissue mineralization observed in rodents treated with MEK/ERK or FGF inhibitors.

Previous studies have reported the involvement of the CaSR in different processes associated with mineral homeostasis including the secretion of "calciotropic" hormones such as PTH (Conigrave et al. 2004) and $1,25D_3$ (Bland et al. 2002); bone resorption (Kameda et al. 1998); and renal reabsorption of Ca^{2+} (Topala et al. 2009,

Toka et al. 2012) and Pi (Ba et al. 2003). Despite this, the renal localisation, and therefore the full physiological role of this receptor in the kidney, remain a matter of debate. Different studies have reported discrepant CaSR expression patterns in the kidney (Riccardi et al. 1996, Sands et al. 1997, Yang et al. 1997, Riccardi et al. 1998, Loupy et al. 2012), which creates uncertainty regarding some of the renal functions described for this receptor.

Molecular identification of the kidney CaSR was carried out in 1995 (Riccardi et al. 1995), shortly after the receptor was cloned from bovine parathyroid glands (Brown et al. 1993). Initial CaSR messenger ribonucleic acid (mRNA) expression studies in rat kidney, carried out by northern blot and *in situ* hybridization (ISH), detected CaSR transcripts predominantly in the outer medulla and medullary rays of the renal cortex. This distribution is consistent with the CaSR being primarily expressed in the thick ascending limb (TAL) of Henle's loop (Riccardi et al. 1995). A more detailed analysis of transcript distribution in rat kidney using ISH and reverse transcription polymerase chain reaction (RT-PCR) in dissected nephron segments showed additional CaSR expression in other nephron segments including glomeruli, proximal tubules (PT), medullary and cortical TAL, distal tubules (DT) and collecting ducts (CD) (Riccardi et al. 1996). Consistent with mRNA expression studies, CaSR protein distribution in rat kidney, examined by immunofluorescence showed receptor expression in PT, medullary and cortical TAL, macula densa cells, DT and type A intercalated cells in cortical CDs (Riccardi et al. 1998). Along with the observation of such a broad distribution, different functional roles were postulated for the CaSR in the different segments and a number of functional studies followed the initial characterization papers. In mouse, rat and human TAL, CaSR expression was detected basolaterally (Riccardi et al. 1998, Loupy et al. 2012) and described to regulate divalent cation reabsorption through the PTH-dependent transcellular (Motoyama and Friedman 2002) and paracellular (Wang et al. 1996, Loupy et al. 2012) pathways. Moreover, the effects of the CaSR in the paracellular divalent cation reabsorption were associated with the modulation of transepithelial potential difference (Wang et al. 1996) and paracellular permeability (Loupy et al. 2012, Gong and Hou 2014). In rat and human DT, CaSR expression was found to be present intracellularly/basolaterally (Riccardi et al. 1998, Topala et al. 2009) and it was described to regulate urinary Ca^{2+} reabsorption (Topala et al. 2009). In rat CD, the CaSR was detected in the cytoplasm and apical

and basolateral membranes of type A intercalated cells (Riccardi et al. 1998), where its activation was reported to reduce water permeability and to promote urine acidification (Renkema et al. 2009). In mouse and rat PT, CaSR expression was found at the apical membrane (Riccardi et al. 1998, Ba et al. 2003). Moreover, CaSR activation has been associated with $1,25D_3$ production in a human PT cell line (Bland et al. 2002), Pi reabsorption in mouse PT (Ba et al. 2003) and proton secretion and fluid reabsorption in mouse and rat PT (Capasso et al. 2013). In the mouse and human glomerulus, CaSR expression was detected in podocytes, where the activation of this receptor has been linked to pro-survival effects and to a reduction in toxin-induced glomerulosclerosis (Oh et al. 2011). In the rat juxtaglomerular apparatus (JGA) CaSR was found to be expressed basolaterally and it has been associated with the regulation of renin release (Atchison et al. 2010).

Although the expression and function of the CaSR has been reported in different nephron segments, controversies remain regarding the intra-renal CaSR expression and cellular polarity, as well as species differences between mouse, rat and human. The findings of CaSR mRNA and protein expression in TAL, DT and CD are supported by several studies (Riccardi et al. 1996, Sands et al. 1997, Yang et al. 1997, Riccardi et al. 1998, Topala et al. 2009, Quinn et al. 2013, Yasuoka et al. 2014). However, discrepant expression patterns have been reported within the CD (Riccardi et al. 1998, Yasuoka et al. 2014). CaSR expression in glomeruli (Riccardi et al. 1996, Caride et al. 1998, Oh et al. 2011) and JGA (Ortiz-Capisano et al. 2007, Maillard et al. 2009, Ortiz-Capisano et al. 2013), has only been reported in a small number of studies and expression of the CaSR in PT is still unclear since there are several studies that report conflicting data (Yang et al. 1997, Riccardi et al. 1998, Ba et al. 2003, Loupy et al. 2012, Wu et al. 2013, Yasuoka et al. 2014). A recent study analysed the mRNA and protein expression and functionality of the CaSR along the mouse, rat and human nephron and concluded that the CaSR is only present in TAL (Loupy et al. 2012).

The discrepancies in the various reports create some uncertainty in the CaSR expression pattern along the nephron, thus proscribing the understanding of CaSR renal functions. These discrepancies may be associated with differences between the approaches used in the different studies such as the biological material analysed (mRNA or protein), processing of the samples (eg. tissue fixation), analysis methodologies (eg. immunohistochemistry, Western blotting) and use of different

species. The use of such different approaches may result in a lack of sensitivity in some cases or non-specific detection of the CaSR in other cases.

In this chapter, I aimed to assess if the renal CaSR is involved in the process of soft-tissue mineralization induced by the inhibition of the MEK/ERK pathway or inhibition of the FGFRs. Due to the uncertainty about the localization of the CaSR in the kidney, I first took a comprehensive approach to assess the intra-renal distribution of this receptor. This approach consisted of a sensitive chromogenic branched deoxyribonucleic acid (DNA) ISH method, immunohistochemistry using a selection of antibodies raised against different epitopes of the CaSR and a highly sensitive and specific chromogenic *in situ* proximity ligation assay. After establishing the intra-renal distribution of the CaSR, I analysed the effects of the administration of MEKi for 28d or FGFRi for 25d in the renal expression of this receptor using IHC.

2.2 Methods

2.2.1 Origin of mouse, rat and human tissue

Animal kidney tissue was obtained from adult male CD-1 mice and Han Wistar rats, supplied by Harlan (Hillcrest, UK) or Charles River (Harlow, UK). Adult normal human kidney cortex tissue used for immunohistochemistry was obtained from the AstraZeneca Global Tissue Bank. The use of this tissue was compliant with the Human Tissue Act as well as Global AstraZeneca Policy. Adult human kidney tissue used for Western blotting was obtained from ethically-consented human kidneys surgically resected at The University Hospital Wales due to renal cell carcinoma (Research Ethics Committee approval reference number: 07/WSE04/53) in collaboration with the Wales Cancer Bank. Macroscopically normal kidney cortex tissue was taken from a region distant from the carcinoma.

2.2.2 In situ hybridization

Mouse, rat and human kidneys were fixed in 10% neutral-buffered formalin for 24 to 48h and embedded in paraffin. Five µm-thick sections were cut and *in situ* hybridization was performed using QuantiGene ViewRNA ISH tissue assay (Affymetrix, Santa Clara, USA) according to manufacturer's instructions, with the following modifications: incubation times were 5 min for pretreatment, 20 min for protease digestion, 40 min for PreAmp Hybridization, and 30 min for Amp Hybridization and Label Probe incubation. Rat CaSR probes (for mouse and rat sections) and human CaSR probes were obtained from Affymetrix (Affymetrix, Santa Clara, USA) and used at a concentration of 1:40 in the probe diluents provided by the kit. Sections were mounted using Immu-mount (Thermo Scientific, Waltham, USA). Negative controls were performed by omission of probes.

2.2.3 Immunofluorescence

Method performed by Dr. Martin Schepelmann (Cardiff University)

The different antibodies used in this study were screened by immunofluorescence patterns in human embryonic kidney (HEK) 293 cells stably transfected with the human CaSR (CaSR-HEK). Cultures of CaSR-HEK cells were performed as previously described (Maldonado-Perez et al. 2003). Cells were fixed in 4%

paraformaldehyde in phosphate-buffered saline (PBS), washed and incubated in PBS containing 50 mM of NH_4Cl. A blocking buffer composed of 1% bovine serum albumin/0.05% Triton-X 100 in PBS was used to prevent non-specific antibody binding. Primary antibodies (Table 2.1 except N-term6) were incubated overnight at 4ºC at a dilution of 1:100 in blocking buffer. Alexa Fluor 488 or Alexa Fluor 594 fluorescence-dye coupled secondary anti IgG antibodies (Life Technologies, Carlsbad, USA) were incubated at a dilution of 1:500 in blocking buffer to visualize primary antibody binding. Hoechst 34580 (Life Technologies, Carlsbad, USA) was used to stain the nuclei.

Table 2.1: Antibodies used to detect the expression of the CaSR

| Antibody | Manufacturer | Code | Epitope | | Host | Clone | Concentration IHC |
			Species	Region			
N-term1	Abcam / Thermo*	Ab19347 / MA1-934*	Human	N-term (ADD)	Mouse	Monoclonal	1:500
N-term2	Anaspec	53286	Rat	N-term	Rabbit	Polyclonal	1:500
N-term3	(W. Chang)	1C12	Human	N-term (ADD)	Mouse	Monoclonal	-
N-term4	(W. Chang)	3A8	Human	N-term (ADD)	Mouse	Monoclonal	-
N-term5	(D. Shoback)	-	Human	N-term (ADD)	Rabbit	Polyclonal	-
N-term6	Alomone	ACR-004	Human	N-term (ADD)	Rabbit	Polyclonal	1:500
C-term1	(W. Chang)	1C7E4B1	Mouse	C-term (C1)	Mouse	Monoclonal	1:150
C-term2	LS Bio	LS-C117834	Human	C-term	Rabbit	Polyclonal	-
Full length	Novus Bio	H00000846-B01P	Human	Full length	Mouse	Polyclonal	1:75

2.2.4 Western blotting

Mouse, rat and human kidney samples were homogenized separately in modified radioimmunoprecipitation assay (RIPA) buffer (25 mM Tris HCl pH 7.6, 150 mM NaCl, 1% NP40, 0.1% sodium dodecyl sulfate, 1% sodium deoxycholate, 1 mM n-ethylmaleimide, 1 mM phenylmethanesulfonylfluoride) containing Halt protease and phosphatase inhibitors (Pierce, Rockford, USA). Cell lysis was carried out using a Polytron (Kinematica, Bohemia, NY, USA) homogenizer. Following lysis, homogenates were centrifuged at 10,000 x g for 5 min to remove insoluble debris. CaSR-HEK cell extracts prepared by an analogous method were kindly provided by

Dr. Sarah Brennan (Cardiff University, UK). Protein extracts were quantified using a bicinchoninic acid (BCA) protein assay (Pierce, Rockford, USA). Twenty micrograms of each extract were electrophoresed on NuPage® 10% BisTris polyacrylamide gels (Invitrogen, Paisley, UK). Gels were transferred to nitrocellulose membranes and stained with Ponceau S to confirm even protein loading of wells. Non-specific protein binding was blocked using 5% low-fat dried milk in Tris-buffered saline containing 0.1% Tween (TBST) for 1h at room temperature. Primary antibodies were added at a concentration of 1:2000 in 5% milk/TBST overnight at 4ºC. An horseradish peroxidase (HRP) conjugated anti-mouse or anti-rabbit secondary antibody (Promega, Madison, USA) was added appropriately at a concentration of 1:20,000 or 1:6,000 in 5% milk/TBST before detection of immunoreactivity with ECL prime and developing on a ChemiDoc MP (Biorad, Hercules, USA).

2.2.5 Immunohistochemistry

Kidneys were fixed for 24 to 48h in 10% neutral-buffered formalin, embedded in paraffin, and 4 µm sections were cut. Sections were de-waxed using xylene and rehydrated using 100% and 95% ethanol. Immunostainings were performed using a Labvision autostainer (Labvision, Fremont, USA). Heat-mediated antigen retrieval was performed using a Milestone RHS-2 microwave (Milestone, Sorisole, Italy) at 110°C for 2 min in 1 mM ethylenediaminetetraacetic acid (EDTA) buffer, pH 8. Endogenous peroxidase activity was blocked with 3% (aq) hydrogen peroxide for 10 min. Nonspecific binding of the antibody was prevented by incubating slides with background blocker with casein (Menarini, Florence, Italy) for 20 min. Slides were incubated with primary antibodies (Table 2.1) for 1h at room temperature. X-Cell Plus HRP, Goat HRP (Menarini, Florence, Italy) Ultravision Quanto Mouse on Mouse (Thermo Scientific, Waltham, USA) or Envision anti-mouse labelled polymer (DAKO, Glostrup, Denmark) was applied to the slides, and peroxidase was then visualized with diamino benzidine (DAKO, Glostrup, Denmark). Identification of the nephron segments was carried out by double labelling the sections with antibodies against aquaporin 2 (1:4000, Sigma, St Louis, USA), Tamm-Horsfall (1:100, Santa Cruz Biotechnology, Santa Cruz, USA) or the thiazide-sensitive NaCl cotransporter, NCC (1:500, Millipore, Billerica, USA) for 1h at room temperature. Aquaporin 2, Tamm-Horsfall and NCC were detected by 30 min incubation with goat anti-rabbit antibody conjugated with alkaline phosphatase (Invitrogen, Paisley, UK), and visualized using

Quanto Fast Red Permanent (Thermo Scientific, Waltham, USA). Sections were counterstained using hematoxylin (Carazzi's) for 1 min before dehydrating in 95% and 100% ethanol, clearing in xylene, and mounting using Hystomount (TAAB Labs, Aldermaston, UK). Negative controls were performed using isotype controls or omission of the primary antibodies.

Whole slide images were scanned using a Scanscope® scanner (Aperio Technologies Incorporated, Vista, USA). Positive Pixel Count Algorithm of the ImageScope software (Aperio Technologies Incorporated, Vista, USA) was used to quantify the positive signal in whole kidney. Detection thresholds were manually set in order to obtain the best signal/noise ratio for the CaSR. The percentage of positive staining (relative stained area) was calculated as the sum of all stained pixels divided by the sum of all stained and unstained pixels.

2.2.6 Proximity ligation assay

Proximity ligation assays (PLA) were performed using the Duolink® assay with brightfield detection (Sigma, St Louis, USA) according to the manufacturer's instructions. Briefly, five µm-thick sections were antigen-retrieved and peroxidase quenching were carried out as described for immunohistochemistry (IHC). Sections were incubated with primary antibody pairs (N-term1/N-term2, N-term1/N-term6, N-term2/C-term1, N-term6/C-term1) for 1h at room temperature. Primary antibody pairs were detected by secondary antibodies conjugated with oligonucleotide probes (anti-Rabbit PLA probe Plus and anti-Mouse PLA probe Minus), incubated for 1h at 37º C. Ligation of the probes was performed by adding oligonucleotides capable of hybridizing to the two probes together with ligase enzyme for 30 min at 37º C. Amplification was carried out by adding nucleotides and polymerase enzyme together and incubating for 2h at 37 C. Detection was performed by incubation with HRP-conjugated oligonucleotide probes for 1h at room temperature. Peroxidase was then visualized with diamino benzidine (Menarini, Florence, Italy). Sections were counterstained with hematoxylin before dehydration in ethanol, clearing in xylene, and mounting using Hystomount (TAAB Labs, Aldermaston, UK). Negative controls were performed by omission of the primary antibodies, incubation with the corresponding immunoglobulin fractions (isotype control), or incubation of C-term1 with Ki-67 (1:200,

Novus, Littleton, USA) or N-term6 with smooth muscle actin (1:3000, Sigma. St Louis, USA).

2.2.7 Immunoprecipitation

Rat kidney samples were homogenized in RIPA buffer (Millipore, Billerica, USA) containing Halt protease inhibitors (Pierce, Rockford, USA). Cell lysis was carried out using a Polytron homogenizer (Kinematica, Bohemia, USA). Following lysis, homogenates were centrifuged at 10,000 x g for 5 min to remove insoluble debris. Immunoprecipitation was performed using µMACS Protein G MicroBeads and µ Columns (Miltenyi Biotec, Cologne, Germany). Protein extract was pre-cleared by incubation with MicroBeads during 45 min at 4º C and passage through the µ Column at RT. One mL of the pre-cleared extract was incubated with 3 µg of N-term1 CaSR antibody (Thermo Scientific, Waltham, USA), smooth muscle actin (Sigma, St Louis, USA) or IgG2a (Abcam, Cambridge, UK) for 45 min at 4º C. Fifty µL of MicroBeads were added and the incubated for further 45 min at 4º C. Lysates were loaded into the µ Columns at RT and washed with a buffer containing 150 mM NaCl, 50 mM Tris (pH 7.5) and 1% NP-40. Samples were eluted using 2x NuPage LDS sample buffer and reducing agent (Life Technologies, Carlsbad, USA). Twenty microliters of each immunoprecipitated sample, the bead flowthrough (negative control) and rat kidney extract (positive control) were electrophoresed on NuPage® 4-12% BisTris polyacrylamide gels (Invitrogen, Paisley, UK). Western blotting was performed as described above for smooth muscle actin (1:2000, Sigma, St Louis, USA) using a HRP-conjugated anti-mouse secondary antibody (Promega, Madison, USA). Controls for the Western blotting were performed by omission of primary antibody.

2.2.8 Animal Studies

The animal studies assessed in this thesis were designed and run by the Safety Assessment division at AstraZeneca UK, in compliance with regulations for repeated dose toxicity studies issued by European Medicines Agency, Ministry of Health Labour and Welfare and Food and Drug Administration. The studies were designed and carried out with the aim of assessing the toxicity of the oral administration of a MEK 1/2 inhibitor (MEKi) and an FGFR 1-3 inhibitor (FGFRi) to Han Wistar rats. These studies were planned for 28d dosing periods, to meet specific criteria for regulatory purposes. MEKi and FGFRi doses were respectively 300 mg/kg/day with bi-daily

administration (BID); 1.4 mg/kg/day; and 20 mg/kg/day, BID. These doses corresponded to the maximum tolerated doses, the highest drug concentrations administered in prior 7d (MEKi and FGFRi) tolerability studies that did not result in unacceptable toxicity. On the last day of each study animals were killed, plasma was collected and the major organs were embedded in paraffin. The FGFRi group in the 28d study had to be terminated earlier, at d25 due to animal welfare reasons. The study design, including the earlier terminations is described in Table 2.2.

Table 2.2: Design for the 28d rat *in vivo* studies using MEKi and FGFRi

Groups	Planed length	Effective length	Dose (mg/kg/d)	N	Vehicle
Vehicle	28d	28d	0	10	water containing 0.5% HPMC 0.1% Tween 80
MEKi			1.4	10	water containing 0.5% HPMC 0.1% Tween 80
Vehicle		25d	0 (BID)	10	30% PEG in water
FGFRi			20 (BID)	10	30% PEG in water

*PEG - Polyethylene glycol 400, HPMC - hydroxypropyl methylcellulose

2.2.9 Statistics

All data shown represents mean ± standard error of the mean. Statistical analysis was carried out with Microsoft Office Excel (Microsoft, Redmond, USA) using the Real Statistics Resource Pack. A two-tailed, Mann Whitney U test was employed and p values lower that 0.05 were considered to be significant.

2.3 Results

2.3.1 CaSR mRNA expression

The CaSR mRNA distribution was analysed using a sensitive chromogenic branched DNA ISH in mouse, rat and human kidney. The highest CaSR mRNA expression was observed in cortical medullary rays (Figure 2.1 A-C) and outer medulla (Figure 2.1 D-F) of all species, supporting a predominant expression of the CaSR in the TAL. Additionally, lower expression of CaSR mRNA was detected in kidney cortex, with a distribution and morphology consistent with DCT and CD (Figure 2.1 A-C). A high magnification picture of a CD showing CaSR signal is shown in Figure 2.10 A. In the PT and papilla (of mouse and rat only since the human kidney sections did not contain this region), CaSR mRNA expression was not distinguishable from the signal observed in negative controls performed by incubation with scrambled DNA probes. In these controls, the background signal was very low and generally localized in deposits with a relatively small size (Figure 2.1 G-I).

By ISH, CaSR mRNA was detected in the TAL, DCT and CD in mouse, rat and human kidney.
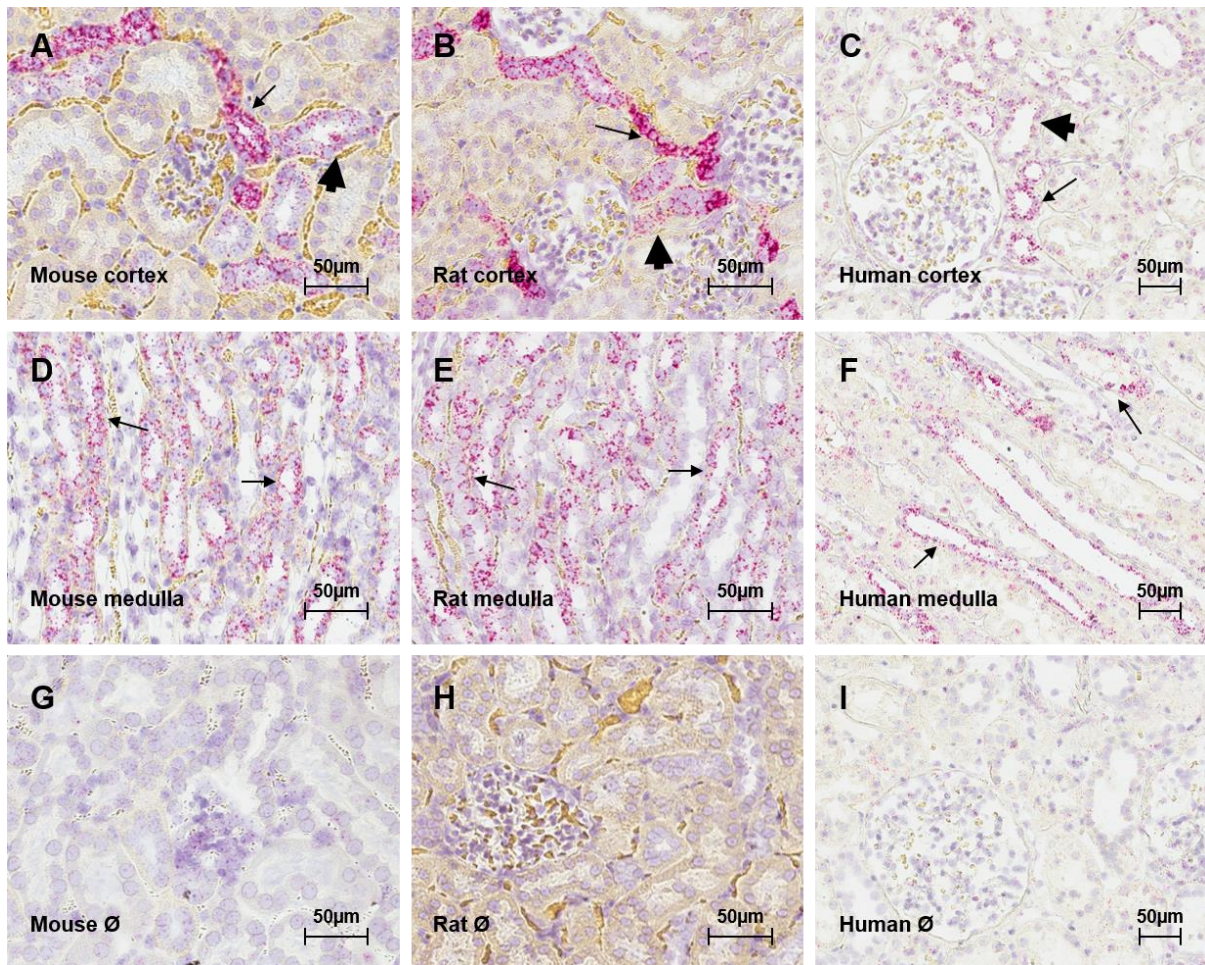
Figure 2.1: Expression of CaSR mRNA in mouse, rat and human kidney.
Photomicrographs of ISH against CaSR in mouse (A,D), rat (B,E) and human (C,F)
kidney. CaSR expression was present in kidney cortex (A-C) and medulla (D-F).
Negative controls were performed in mouse (G), rat (H) and human (I) kidney by
omission of probe (mouse, human) or use of scrambled probes (rat). CaSR signal
(red) corresponds to fast red staining. Scale bar = 50 µm. Arrow points to stronger
signal, consistent with TAL, and arrowhead points to weaker signal, consistent with
DT and CD. Pictures are representative of at least two experiments.

2.3.2 Antibody screening by immunofluorescence

The discrepancies in CaSR protein distribution reported in the literature could be ascribed to the use of different CaSR antibodies, which may differ in specificity or detect different forms of the receptor (eg. monomer vs dimer). An initial systematic study was undertaken using a panel of eight CaSR antibodies (Table 2.1, except N-term6) to identify and exclude antibodies that do not specifically detect the CaSR. This study was performed by analysing the immunofluorescence pattern of these antibodies in HEK293 cells stably transfected with the human CaSR (CaSR-HEK) (Figure 2.2), which were previously shown to express the CaSR (Maldonado-Perez et al. 2003). All the antibodies with the exception of C-term2 showed immunoreactivity mostly in the cytoplasm and plasma membrane, as it would be expected for the CaSR (Hjälm et al. 2001). Conversely, C-term2 showed nuclear immunoreactivity and for that reason was excluded from further experiments. No signal was observed in the negative controls, performed by omission of the primary antibody (not shown).

Seven out of eight tested CaSR antibodies showed a CaSR-like immunoreactivity by immunofluorescence. The remaining antibody showed a discrepant immunoreactivity pattern and therefore was excluded from further experiments.
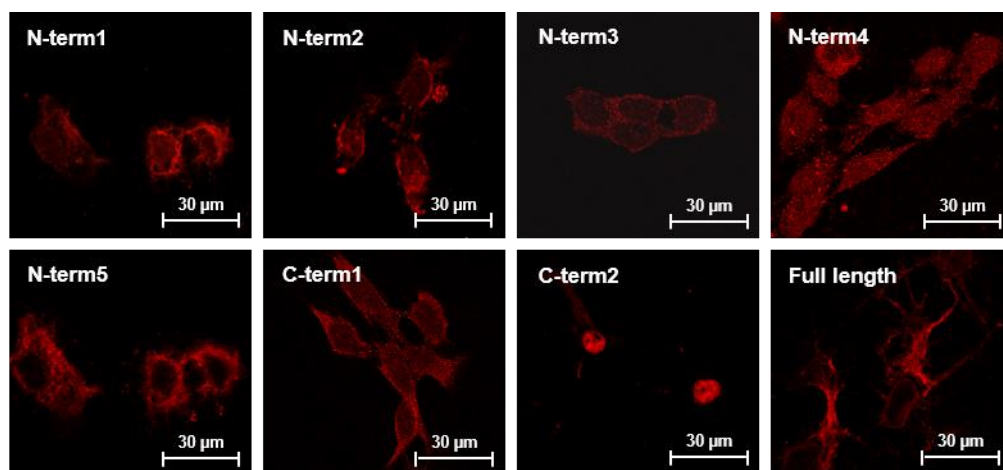
Figure 2.2: CaSR immunolocalization in CaSR-HEK cells. Immunofluorescence pattern of eight different anti-CaSR antibodies, N-term1 (Abcam), N-term2 (Anaspec), N-term3 (W. Chang), N-term4 (W. Chang), N-term5 (D. Shoback), C-term1 (W. Chang), C-term2 (Lifespan), Full length (Novus). Antibody signal corresponds to red staining. Scale bar = 30 µm.

2.3.3 Antibody validation by Western blotting

Since seven antibodies passed the initial immunofluorescence screening, four were selected to be used in further studies by considering the recognition of different CaSR epitopes. The antibodies N-term1, N-term3, N-term4 and N-term5 were raised against the same epitope, a human N-terminal ADD sequence that is conserved in mouse and rat. Out of these four antibodies, N-term1 was selected instead of the other ADD antibodies because it is commercially available and has been used in a vast number of studies (Weston et al. 2005, Heyeraas et al. 2008, Caudrillier et al. 2010, Loupy et al. 2012), whilst the remaining ADD antibodies are custom made by two collaborators and therefore not as easily accessible to all researchers. In addition to N-term1, the antibodies N-term2, Full length and C-term1 were also selected to be used in further studies. N-term2 was raised against a different N-terminal epitope from rat CaSR (according to the manufacturer), Full length was raised against the full length human CaSR protein and C-term1 was raised against a C-terminal epitope of mouse CaSR.

The specificity of the selected antibodies was confirmed by their ability to detect the correct molecular weight species by Western blotting in samples from mouse, rat and human kidneys and CaSR-HEK cell extracts (the latter included as a positive control) (Figure 2.3). Western blotting was performed using protein reducing conditions, which are consistent with the detection of CaSR-specific immunoreactivity at 130 kDa for the CaSR unglycosylated monomer, 140-170 kDa for the glycosylated CaSR monomer and 260-300 kDa for the CaSR dimer (Ray et al. 1998, Ward et al. 1998). Figure 7 shows that all antibodies tested showed CaSR-like immunoreactivity, with bands detected at the expected sizes for the glycosylated CaSR monomer and dimer. Possibly due to the resolution of the method, it was not possible to detect immunoreactivity for the CaSR unglycosylated monomer. Whilst N-term1 and N-term2 recognized all species, Full length only recognized the human CaSR (in tissue lysates and CaSR-HEK extracts) and C-term1 only detected mouse and rat CaSR. These observations are consistent with Full length and C-term1 being raised against human and mouse antigens, respectively. Besides the differences in species recognition, these antibodies showed some differences in the CaSR molecular species detected. N-term1 detected stronger immunoreactivity corresponding to the CaSR monomer than for the dimeric form of the receptor in mouse and rat samples, while it detected comparable immunoreactivity for both forms in human and CaSR-HEK samples. N-

term2 preferentially detected the dimeric rather than the monomeric form of the receptor in all species. Full length detected very weak CaSR immunoreactivity in human kidney, but a stronger signal in the CaSR-HEK samples. This antibody detected the CaSR monomer and dimer equally well. C-term1, similarly to N-term1, predominantly detected the CaSR monomer in mouse and rat samples.

By Western blotting, N-term1, N-term2, Full length and C-term1 specifically detected CaSR immunoreactivity. N-term2 preferentially detected the CaSR dimer, whilst the remaining antibodies detected comparable levels of both monomer and dimer (human) or preferentially the monomeric over the dimeric form of the CaSR protein (mouse and rat).
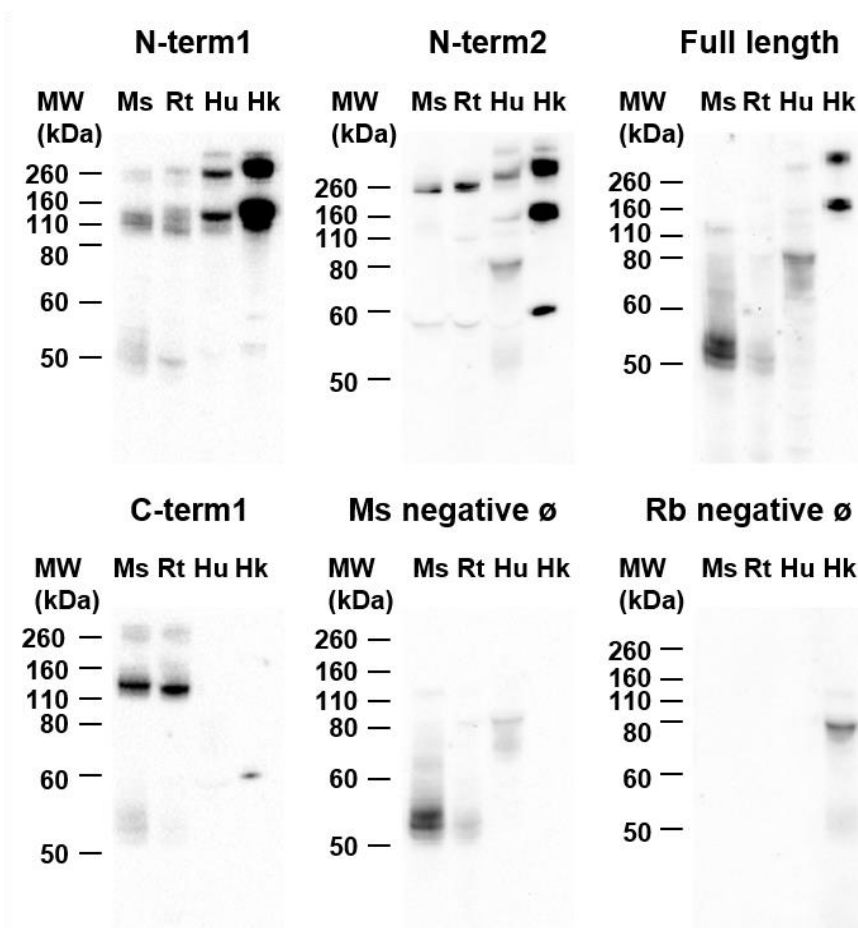
Figure 2.3: Western blotting immunoreactivities of the CaSR antibodies used in this study. Western blotting was performed using N-term1 (Thermo, ADD), N-term2 (Anaspec, N-term), Full length (Novus, fusion protein) and C-term1 (W. Chang, C-terminal) in mouse (Ms), rat (Rt) and human (Hu) kidney and CaSR-HEK (Hk) extracts. Predicted Immunoreactivity corresponding to the glycosylated CaSR monomer and dimer are 140-160 kDa and 260-300 kDa, respectively. Negative controls were performed by omission of the primary antibodies. MW=Molecular weight. Pictures are representative of at least two experiments.

2.3.4 CaSR protein expression by immunohistochemistry

Once the specificity of the four selected antibodies used was ascertained, the CaSR intra-renal distribution was investigated. Immunohistochemistry was performed on mouse (Figure 2.4) and rat (Figure 2.5) kidney sections using N-term1, N-term2 and C-term1 and in human kidney sections (Figure 2.6) using N-term1, N-term2 and Full length due to the lack of species cross-reactivity of Full length and C-term1. Similarly to the mRNA distribution, in all species, higher immunoreactivity was observed with all the antibodies in cortical medullary rays and outer medulla and lower immunoreactivity was observed in the kidney cortex. The presence of CaSR immunoreactivity in the different nephron segments was assessed by analysing cellular morphology and co-staining using the CaSR antibodies in combination with established segment-specific markers in mouse (Figure 2.7), rat (Figure 2.8), and human (Figure 2.9) sections. In the glomeruli and JGA, CaSR immunoreactivity was absent or undistinguishable from background. In the PT, identified through the presence of brush border, CaSR immunoreactivity was weak and variable between experiments in sections stained with N-term1, Full length and C-term1. Conversely, a relatively stronger and consistent immunoreactivity was observed in sections stained with N-term2. PT immunoreactivity generally increased from S1 to S3, although the staining pattern varied with the different antibodies. All antibodies demonstrated cytoplasmic CaSR expression, additionally N-term1 and N-term2 showed basolateral staining and N-term2 apical membrane staining of certain tubules, which were located mainly in the inner cortex, in the vicinity of cortical medullary rays. In TAL, identified by colocalization with Tamm-Horsfall protein, CaSR immunoreactivity was detected in the basolateral membrane and cytoplasm with all the antibodies. In agreement with the ISH results, the TAL was the nephron segment that showed higher CaSR immunoreactivity. In the DCT, identified by colocalization with NCC, CaSR immunoreactivity was detected in the cytoplasm and in the basolateral and apical membranes. In the CNT, identified by the analysis of cellular morphology and colocalization with aquaporin 2 (AQP2), CaSR was detected at the basolateral membrane and in the cytoplasm. In the CD, identified by the analysis of cellular morphology and colocalization with AQP2, CaSR immunoreactivity was heterogeneous and some expression differences were obtained between species and when different antibodies were used. In mouse and rat cortical CDs, all antibodies showed immunoreactivity in the cytoplasm and apical membrane

in a population of cells and basolateral immunoreactivity in a different population of cells. Conversely, in mouse and rat medullary CDs, only N-term2 showed immunoreactivity, which was present in the apical and basolateral membrane. In human tissue, all antibodies showed immunoreactivity in the cytoplasm and apical and basolateral membranes of most cortical and medullary CD cells, with N-term1 and N-term2 showing higher immunoreactivity in a population of cells. For all the species, all the antibodies showed CaSR CD immunoreactivity both in cells that expressed AQP2 (CaSR+/AQP2+) and in cells that did not express AQP2 (CaSR+/AQP2-). In cortical CDs, N-term2 showed immunoreactivity in all CD cells. Conversely, in medullary CDs stained with N-term2 and in cortical and medullary CDs stained with the remaining antibodies, some CD cells lacked CaSR immunoreactivity, whilst expressing (CaSR-/AQP2+) or not (CaSR-/AQP2-) AQP2. High magnification pictures of CaSR immunoreactivity in the CD are shown on Figure 2.10 B,D.

IHC with the CaSR antibodies N-term1, N-term2, Full length and C-term1 in mouse, rat and human kidney sections showed immunoreactivity in TAL, DCT, CNT and CD. Additionally, in the PT, relatively strong immunoreactivity was observed with N-term2 and weak and variable immunoreactivity was observed with the remaining antibodies
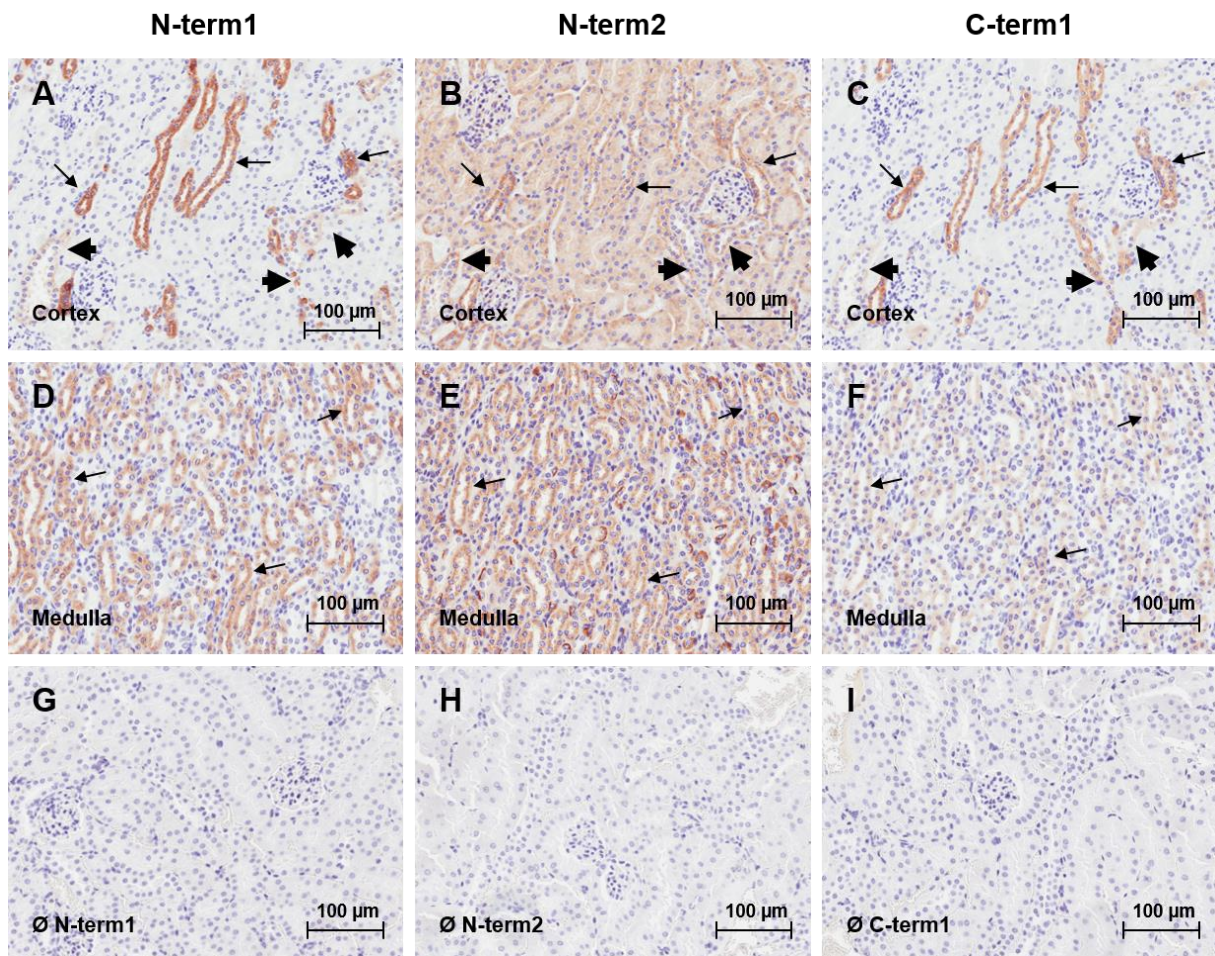
Figure 2.4: CaSR immunolocalization in mouse kidney sections. Photomicrographs of CaSR immunohistochemistry performed with N-term1 (Thermo, ADD, A,D), N-term2 (Anaspec, N-Term, B,E) and C-term1 (W. Chang, C-term, C,F) in kidney cortex (A-C) and medulla (D-F). Negative controls performed by omission of primary antibody (G-I). Positive signal corresponds to immunoperoxidase staining (brown). Arrow indicates stronger immunoreactivity consistent with TAL and arrowhead indicates weaker immunoreactivity consistent with DCT and CD. Scale bar = 100 µm. Pictures are representative of at least three experiments.
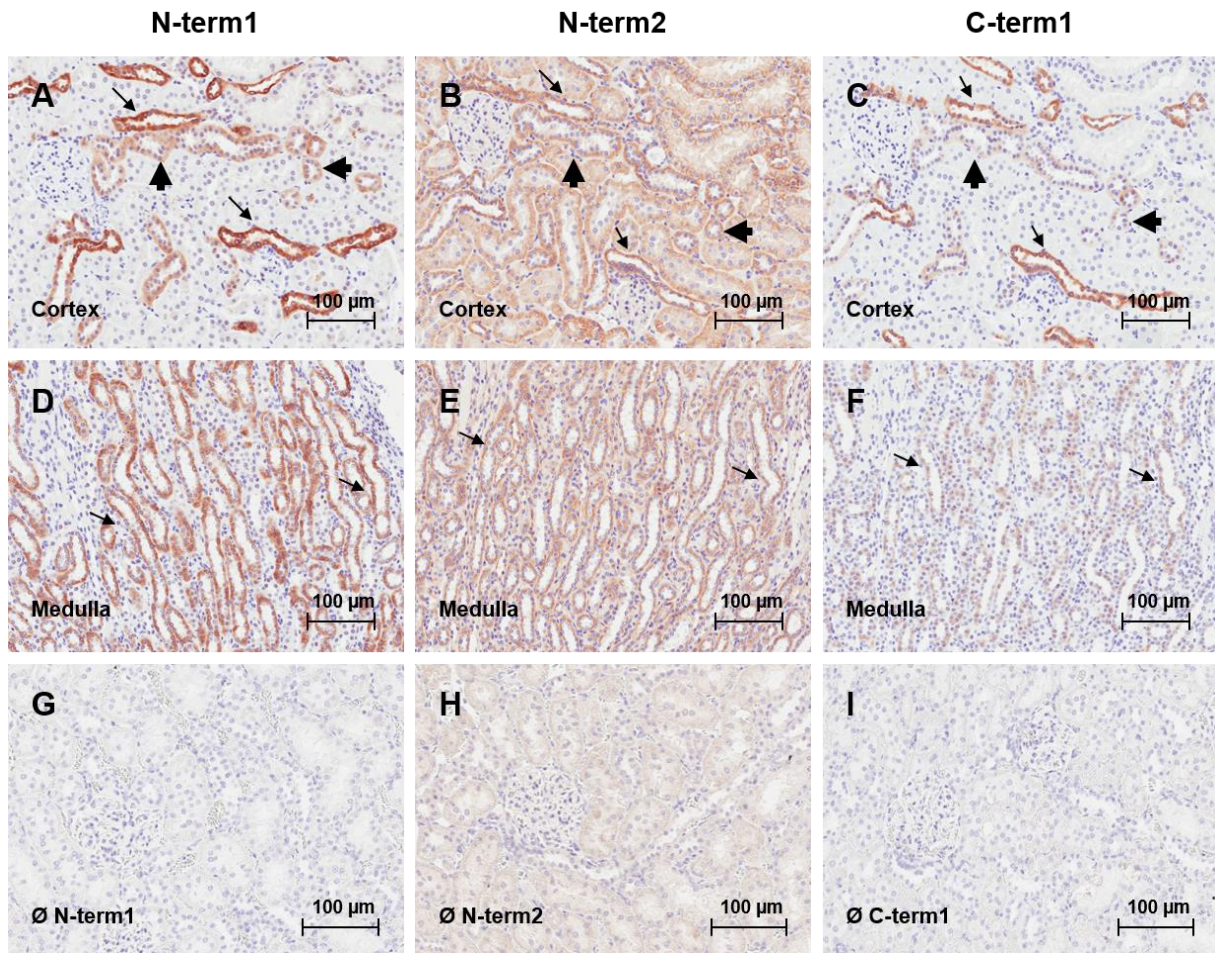
Figure 2.5: CaSR immunolocalization in rat kidney sections. Photomicrographs of CaSR immunohistochemistry performed with N-term1 (Thermo, ADD, A,D), N-term2 (Anaspec, N-Term, B,E) and C-term1 (W. Chang, C-term, C,F) in kidney cortex (A-C) and medulla (D-F). Negative controls performed by incubation with the Ig fraction correspondent to N-term1 (G), N-term2 (H) and C-term1 (I). Positive signal corresponds to immunoperoxidase staining (brown). Arrow indicates stronger immunoreactivity consistent with TAL and arrowhead indicates weaker immunoreactivity consistent with DCT and CD. Scale bar = 100 µm. Pictures are representative of at least three experiments.
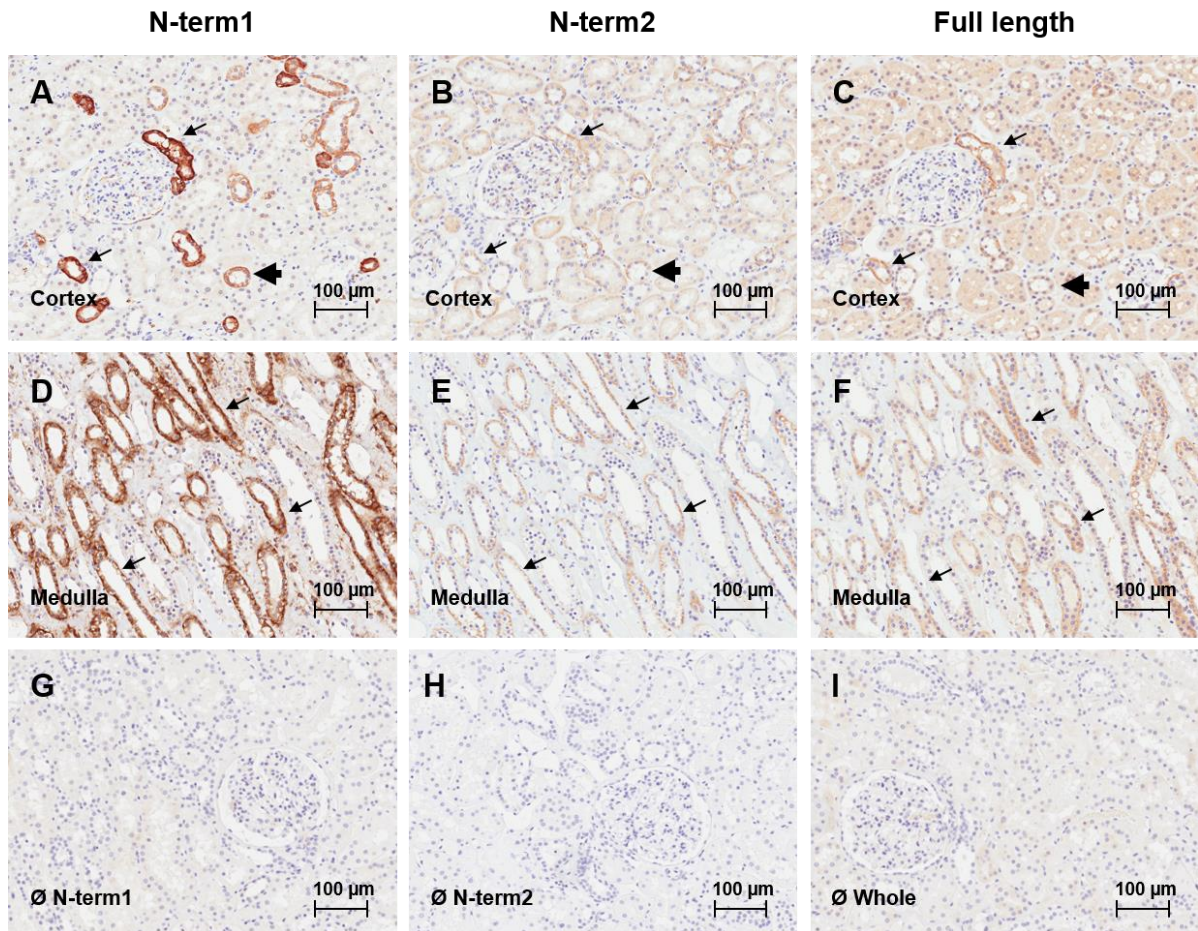
Figure 2.6: CaSR immunolocalization in human kidney sections. Photomicrographs of CaSR immunohistochemistry performed with N-term1 (Thermo, ADD, A,D), N-term2 (Anaspec, N-Term, B,E) and Full length (Novus, Whole protein C,F) in kidney cortex (A-C) and medulla (D-F). Negative controls performed by omission of primary antibody (G-I). Positive signal corresponds to immunoperoxidase staining (brown). Arrow indicates stronger immunoreactivity consistent with TAL and arrowhead indicates weaker immunoreactivity consistent with DCT and CD. Scale bar = 100 µm. Pictures are representative of at least three experiments.
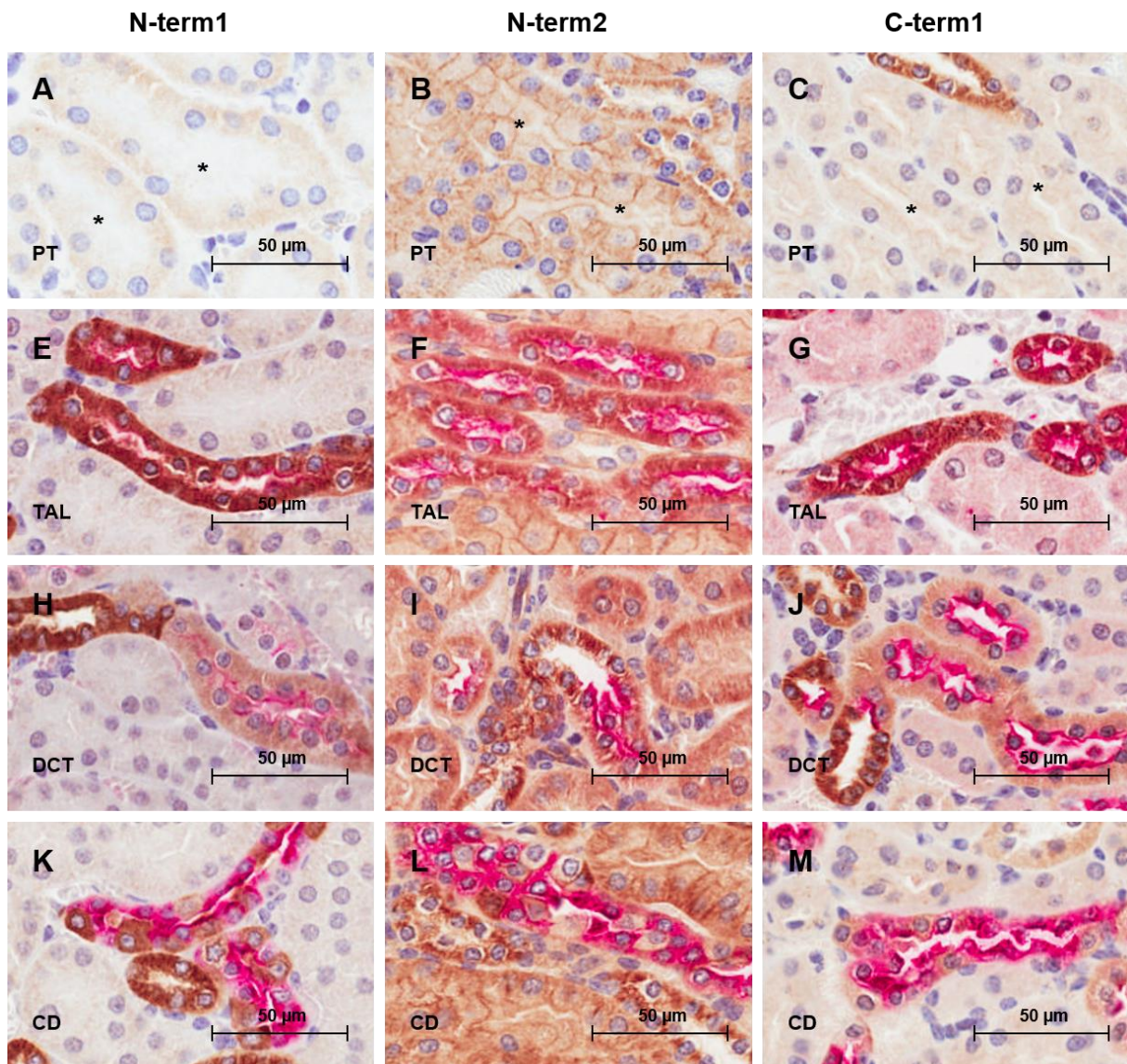
Figure 2.7: CaSR distribution along the nephron in mouse kidney sections. Photomicrographs of CaSR immunohistochemistry performed with N-term1 (Thermo, ADD, A,D,G,F), N-term2 (Anaspec, N-Term, B,E,G,H) and C-term1 (W. Chang, C-term, C,F,I,L) in kidney cortex. CaSR expression was detected in the PT, identified by the presence of brush border (A-C); TAL identified by dual staining with Tamm-Horsfall protein (D-F); DCT, identified through dual staining with thiazide-sensitive Na-Cl cotransporter (NCC, G-I); and CD identified through dual staining with aquaporin-2 (AQP2, J-L). Nephron segment marker signal corresponds to (red) fast red staining. Asterisk indicates PT. Scale bar = 50 μm. Pictures are representative of at least three experiments.

Figure 2.8: CaSR distribution along the nephron in rat kidney sections.
Photomicrographs of CaSR immunohistochemistry performed with N-term1 (Thermo, ADD, A,D,G,F), N-term2 (Anaspec, N-Term, B,E,G,H) and C-term1 (W. Chang, C-term, C,F,I,L) in kidney cortex. CaSR expression was detected in the PT, identified by the presence of brush border (A-C); TAL identified by dual staining with Tamm-Horsfall protein (D-F); DCT, identified through dual staining with thiazide-sensitive Na-Cl cotransporter (NCC, G-I); and CD identified through dual staining with aquaporin-2 (AQP2, J-L). Nephron segment marker signal corresponds to (red) fast red staining. Asterisk indicates PT. Scale bar = 50 µm. Pictures are representative of at least three experiments.

Figure 2.9: CaSR distribution along the nephron in human kidney sections. Photomicrographs of CaSR immunohistochemistry performed with N-term1 (Thermo, ADD, A,D,G,F), N-term2 (Anaspec, N-Term, B,E,G,H) and Full length (Novus, Whole protein, C,F,I,L) in kidney cortex. CaSR expression was detected in the PT, identified by the presence of brush border (A-C); TAL identified by dual staining with Tamm-Horsfall protein (D-F); DCT, identified through dual staining with thiazide-sensitive Na-Cl cotransporter (NCC, G-I); and CD identified through dual staining with aquaporin-2 (AQP2, J-L). Nephron segment marker signal corresponds to (red) fast red staining. Asterisk indicates PT. Scale bar = 50 μm. Pictures are representative of at least three experiments.
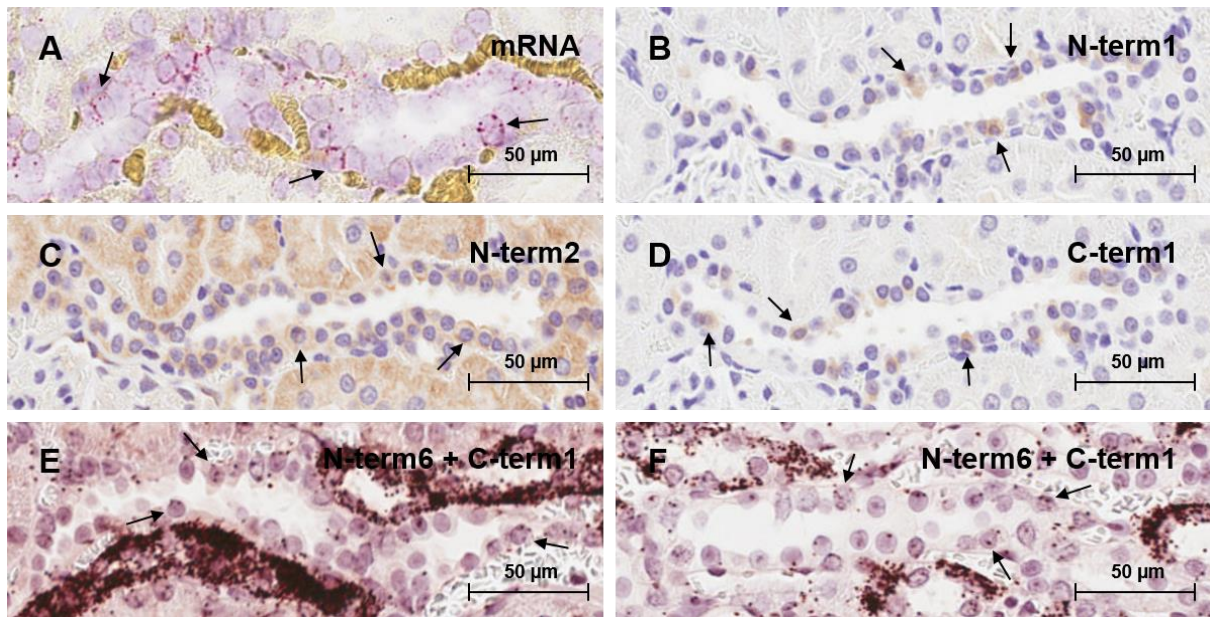
Figure 2.10: Expression of the CaSR in rat kidney CD. Photomicrographs of CaSR mRNA expression in CCD detected by ISH (A). CaSR signal (in red) corresponds to fast red staining. Photomicrographs of CaSR protein expression in CCD detected by IHC with N-term1 (Thermo, ADD, B), N-term2 (Anaspec, N-term, C), C-term1 (W. Chang, C-term, D) or PLA with C-term1 (W. Chang, C-term) and N-term6 (Alomone, ADD) (E). Photomicrographs of CaSR protein expression in OMCD, detected by PLA with C-term1 (W. Chang, C-term) and N-term6 (Alomone, ADD) (F). Arrows indicate CaSR expression. Scale bar = 50µm. Pictures are representative of at least two experiments.

2.3.5 Proximity ligation assay

CaSR protein expression was further analysed in rat kidney by chromogenic *in situ* PLA using the C-term1/N-term6 antibody pair in rat kidney sections (Figure 2.11). Stronger PLA signal was observed in the outer medulla and cortical medullary rays and weaker signal was observed in the cortex. This expression pattern is in agreement with the results obtained by ISH and IHC and suggests that the CaSR is strongly expressed in TAL and more weakly expressed in DT and cortical CD. In addition to these segments, PLA signal was also observed in the glomerulus, where CaSR expression was not detected by ISH and IHC and in the PT and medullary CDs (Figure 2.10 F), where the results ISH and IHC were discrepant. In the glomerulus, PLA signal was highly variable, with some glomeruli showing a signal clearly above the background levels and other glomeruli, even adjacent glomeruli, completely lacking PLA signal. Similar results were obtained when using N-term1/N-term2, N-term1/N-term6 or N-term2/C-term1 antibody pairs in rat kidney sections (Figure 2.12), C-term1/N-term6 in mouse kidney sections or Full length/N-term6 in human kidney sections (Figure 2.13). The negative controls, performed by incubation with the corresponding immunoglobulin fractions (Figure 2.11 B,D) showed a relatively low signal, localized to small deposits. Similarly, low signal was observed in sections incubated with C-term1 and an antibody against Ki-67, an unrelated protein expressed in the nuclei of proliferating cells. A further control was carried out by incubating N-term6 with smooth muscle actin (SMA), a protein predicted to interact with the CaSR, since both proteins interact with filamin (Lebart et al. 1994, Awata et al. 2001) (Figure 2.14). With the N-term6/SMA antibody pair, the PLA signal was only observed in the blood vessels and not along the nephron, consistent with SMA being expressed in the blood vessels but not in epithelial cells. The interaction between the CaSR and SMA was confirmed by immunoprecipitating rat kidney extracts with N-term1 and analysing SMA expression by Western blotting (Figure 2.14 D).

PLA with different CaSR antibody combinations showed CaSR immunoreactivity in different nephron segments including glomerulus, PT, TAL, DCT, CNT and CD.
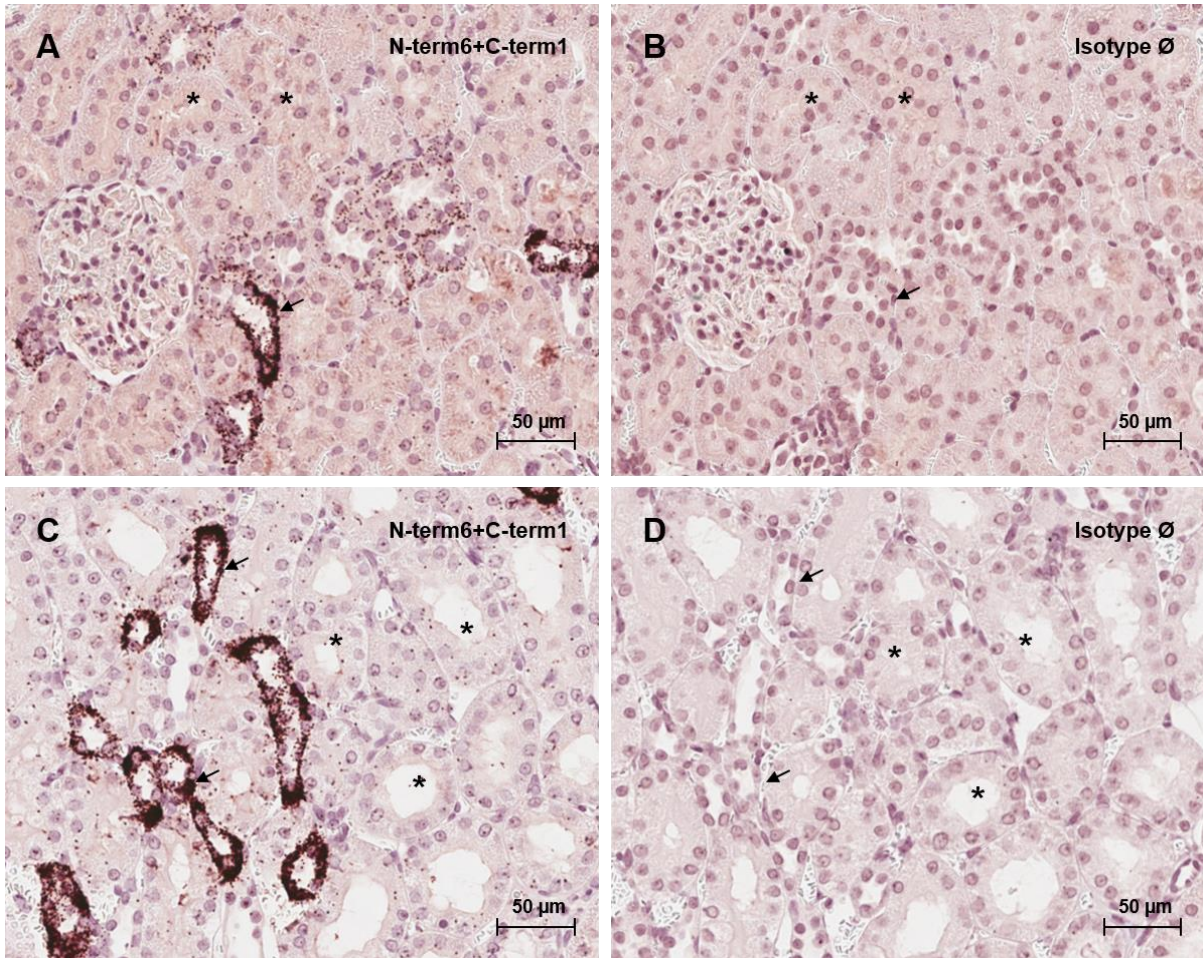
Figure 2.11: Proximity ligation assay to detect the CaSR in rat kidney. Photomicrographs from the proximity ligation assay performed using C-term1 (W.Chang, C-term) and N-term6 (Alomone, ADD): outer cortex (A) and inner cortex (C). Negative control performed by incubation with the Igs corresponding to the primary antibodies: outer cortex (B) and inner cortex (D). Positive staining corresponds to immunoperoxidase staining (brown dots). Arrow points to TAL and asterisk indicates PT. Scale bar = 50 µm. Pictures are representative of at least two experiments.
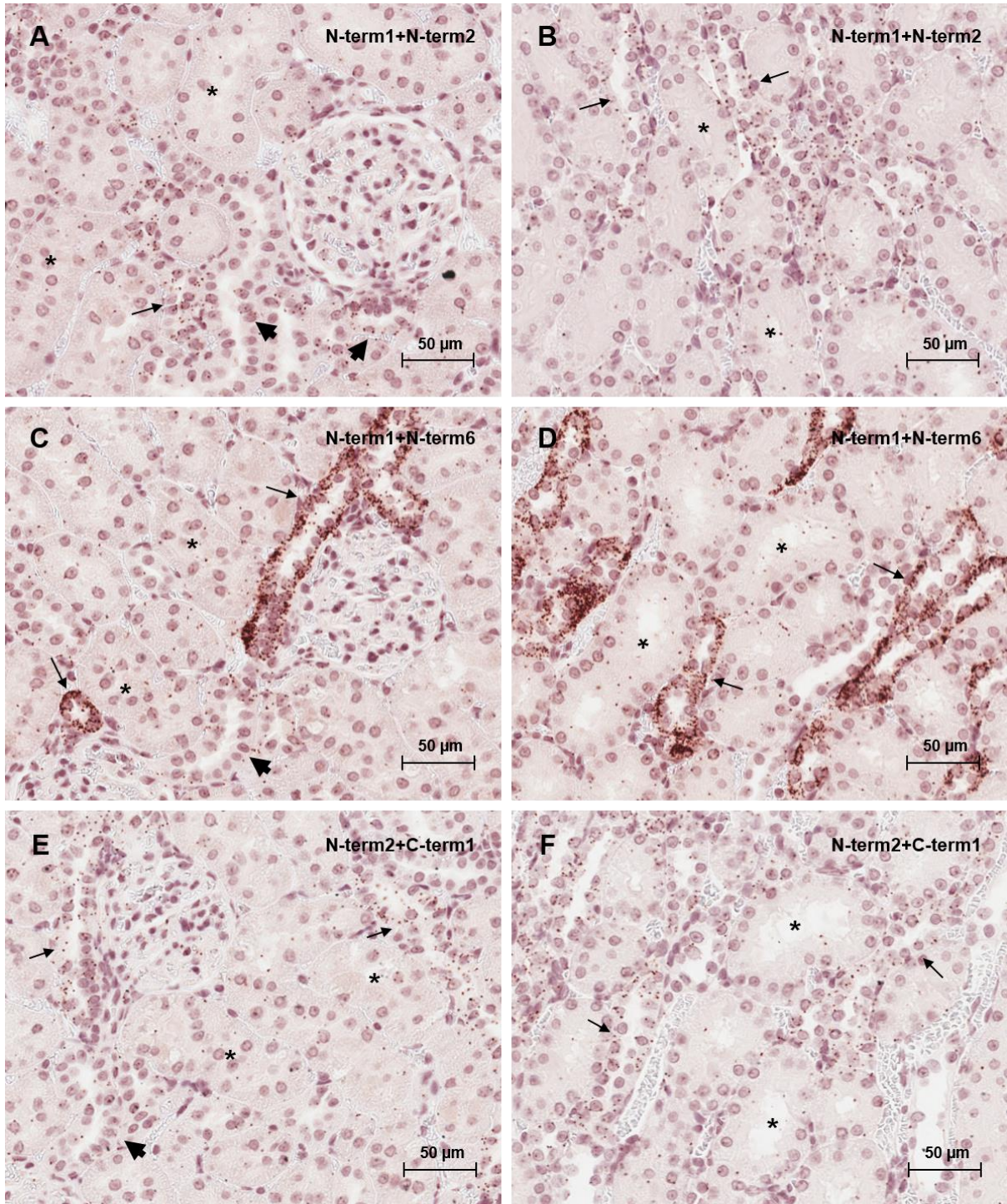
Figure 2.12: Proximity ligation assay to detect the CaSR in rat kidney. Photomicrographs from the proximity ligation assay performed using different antibody combinations: N-term1 (Thermo, ADD) and N-term2 (Anaspec, N-term) - outer cortex (A) and inner cortex (B); N-term1 (Thermo, ADD) and N-term6 (Alomone, ADD) - outer cortex (C) and inner cortex (D); N-term2 (Anaspec, N-term) and C-term1 (W. Chang, C-term) - outer cortex (E) and inner cortex (F). Positive staining corresponds to immunoperoxidase staining (brown dots). Arrow indicates TAL, arrowhead indicates DCT and CD and asterisk indicates PT. Scale bar = 50µm. Pictures are representative of at least two experiments.
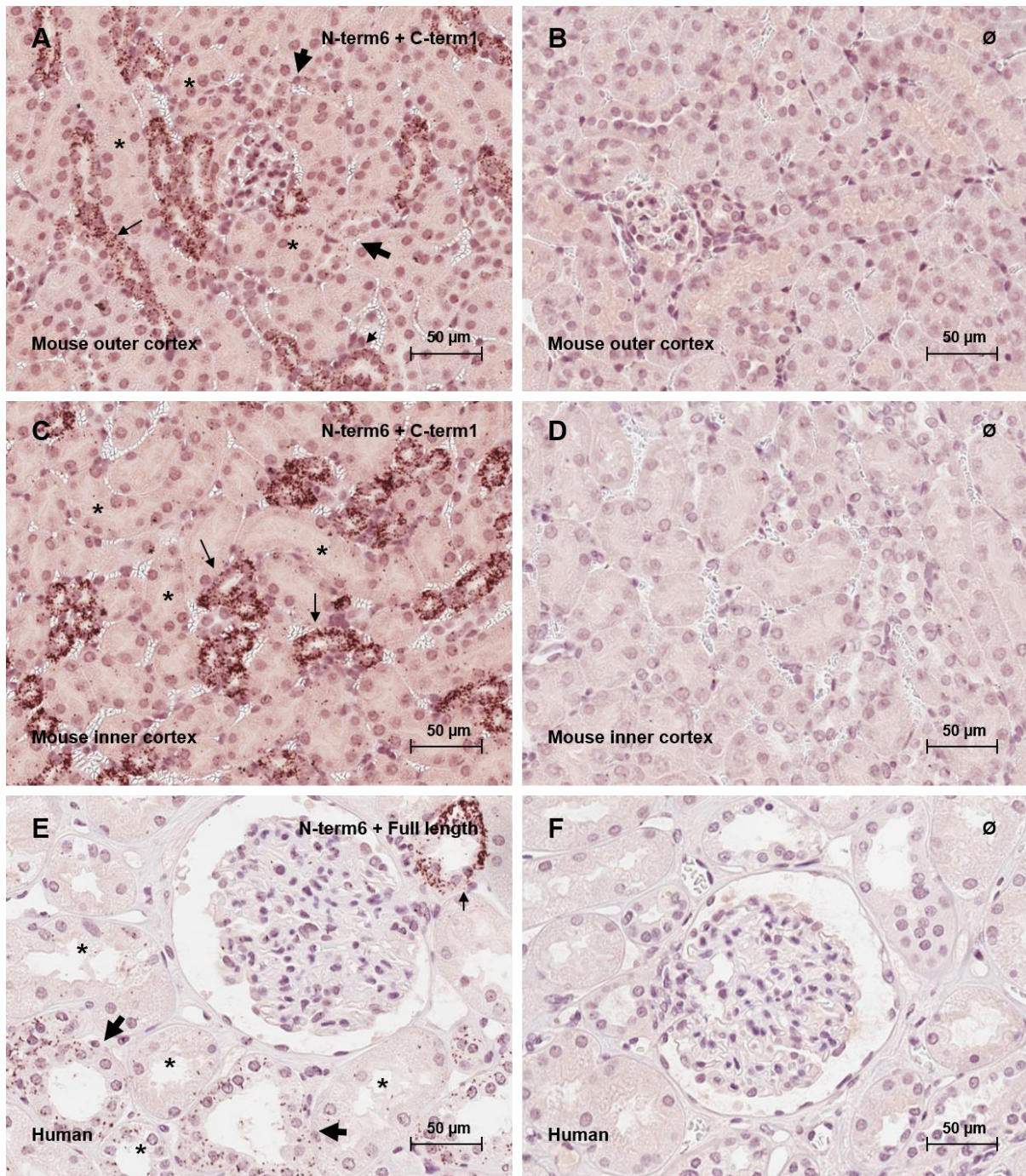
Figure 2.13: Proximity ligation assay to detect the CaSR in mouse and human kidney. Photomicrographs from the proximity ligation assay performed in mouse kidney sections using C-term1 (W. Chang, C-term) and N-term6 (Alomone, ADD) - outer cortex (A) and inner cortex (C); and in human kidney sections using C-term1 (Novus, fusion protein) and N-term6 (Alomone, ADD) - outer cortex (E). Negative controls for mouse outer cortex (B), inner cortex (D) and human outer cortex (F) were performed by omitting the incubation with primary antibodies. Positive staining corresponds to immunoperoxidase staining (brown dots). Arrow indicates TAL, arrowhead indicates DCT and CD and asterisk indicates PT. Scale bar = 50 µm.
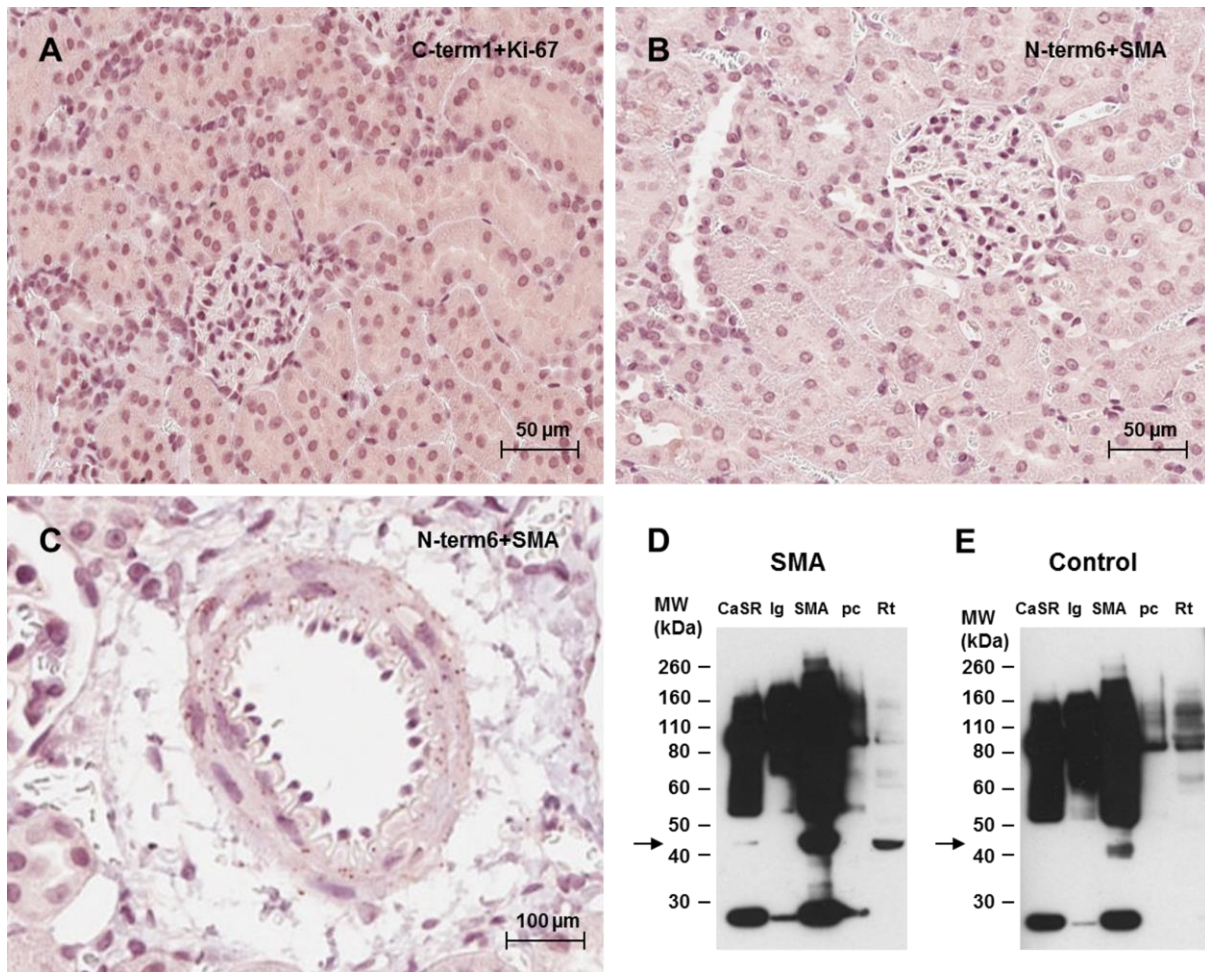
Figure 2.14: Controls for CaSR detection by proximity ligation assay in rat kidney. Controls for the proximity ligation assay were performed using C-term1 (W.Chang, C-term) and anti-Ki-67 antibodies - picture from the outer cortex (A); or N-term6 (Alomone, ADD) and anti-SMA antibodies - picture from the outer cortex (B) and a magnified blood vessel (C). Positive staining corresponds to immunoperoxidase staining (brown dots). Arrow indicates the blood vessel. Scale bar = 50 μm for the outer cortex pictures and 100 μm for the magnified blood vessel. The interaction between SMA and CaSR was confirmed by co-immunoprecipitation: Proteins from rat kidney extracts were pulled down with N-term1 (CaSR, Thermo, ADD), anti-SMA (SMA) or the corresponding isotype control (Ig, same for N-term1 and SMA). The pulled down proteins, together with the buffer used to pre-clear the pull-down assay columns (pc) and total protein extracts (Rt) were analysed by Western blotting with an anti-SMA antibody (D). Control for the Western blotting was performed by omitting the primary antibody (E). SMA MW = 42 kDa.

2.3.6 Summary of CaSR distribution

Table 2.3 shows a summary of the CaSR distribution detected by ISH, IHC and PLA in mouse rat and human kidney.

Table 2.3: Summary of the distribution of the expression of the CaSR observed by ISH, IHC and PLA.

		Glomerulus	PT	TAL	DCT	CNT	CCD	MCD
	ISH	-	-	++	+	+	+	+
IHC	**N-term1**	-	+/-	++	+	+	+	-
	N-term2	-	+	++	+	+	+	+
	Full length	-	+/-	++	+	+	+	-
	C-term1	-	+/-	++	+	+	+	-
PLA	**C-term1+ N-term6**	+	+	++	+	+	+	+

2.3.7 Effect of MEK and FGFR inhibition on the expression of the CaSR

In order to investigate the involvement of the renal CaSR in the soft-tissue mineralization induced by the inhibition of MEK/ERK pathway or FGFRs in rats, the expression of the CaSR was analysed in kidney sections from rats treated for 28d with MEKi or 25d with FGFRi. The tissue samples used to perform this assay were obtained from retrospective studies in which the administration of MEKi and FGFRi had resulted in soft-tissue mineralization in different organs including kidney, heart and stomach, and in increased levels of Pi and Ca^{2+} (only animals treated with MEKi) in plasma (Table 2.4).

In agreement with the intra-renal distribution described above, the study animals evidenced CaSR expression along the nephron, from the PT to the CD with the strongest signal detected in the TAL (Figure 2.15 A,D). Treatment with MEKi for 28d (Figure 2.15 B,C) or FGFRi for 25d (Figure 2.15 D,F) did not induce any evident changes in the expression or cellular distribution of the CaSR.

> Expression of the CaSR remained unchanged in animals treated with ERKi, MEKi or FGFRi.

Table 2.4: Data from retrospective studies showing plasma levels of Ca^{2+}, Pi and presence of soft-tissue mineralization in kidney, stomach and heart of animals treated with 1.4 mg/kg/day of MEKi for 28d or 20 mg/kg/day of FGFRi for 25d.

		Vehicle	MEKi	Vehicle	FGFRi
Ca^{2+}	d25	2.71 ± 0.01	2.67 ± 0.03	3.01 ± 0.04	3.28 ± 0.06*
Pi	d11/14	2.10 ± 0.06	2.89 ± 0.10*	1.93 ± 0.06	2.69 ± 0.08*
Pi	d25/d28	2.42 ± 0.12	2.70 ± 0.12	1.93 ± 0.10	2.62 ± 0.10*
Mineral deposition	Kidney	-	7/10	-	8/10
	Stomach	-	10/10	-	8/10
	Heart	-	4/10	-	4/10

Data representative of $N = 10$ rats + standard error of the mean (SEM). * $p<0.05$ vs vehicle control (Mann-Whitney). The data presented in this table was generated by the Pathology and Clinical Pathology department at AstraZeneca UK.
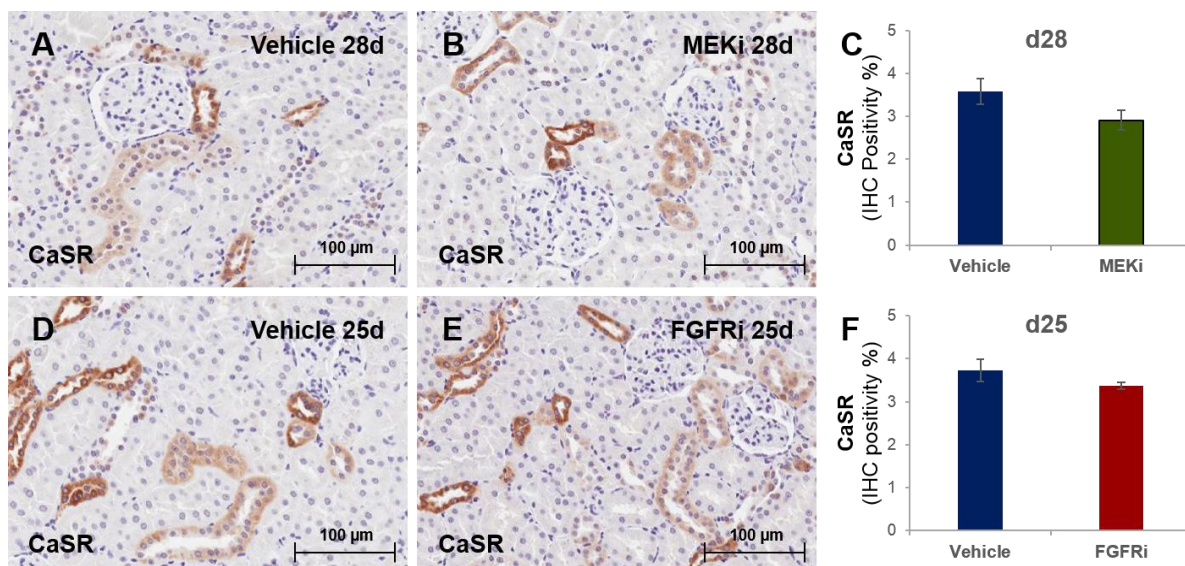
Figure 2.15: Expression of the CaSR in cortical kidney sections from rats treated with 1.4 mg/kg/day of MEKi or 20 mg/kg/day of FGFRi. Photomicrograph of CaSR immunostaining in sections of rats dosed for 28d with vehicle (A) or MEKi (B); or for 25d with vehicle (C) or FGFRi (D). Positive signal in immunohistochemistry corresponds to the brown staining. Histograms represent the quantification of CaSR expression (immunohistochemically stained area) in animals from the studies 1 (C) and 2 (F). Data representative of $N = 10$ rats + standard error of the mean (SEM). * $p<0.05$ vs vehicle control (Mann-Whitney). Scale bar = 100 µm.

2.4 Discussion

Different studies have reported various roles for the CaSR in the kidney, including regulation of the reabsorption of Ca^{2+} (Toka et al. 2012) and Pi (Ba et al. 2003), production of $1,25D_3$ (Bland et al. 2002) and urine acidification (Renkema et al. 2009). Since rats treated with MEK/ERK and FGFR inhibitors showed increased levels of plasma Ca^{2+}, Pi and $1,25D_3$ (Brown et al. 2005, Diaz et al. 2012, Yanochko et al. 2013), I decided to assess if the CaSR was involved in the soft-tissue mineralization induced by these inhibitors. In order to accomplish this, it was key to ascertain the intra-renal distribution and to develop sensitive methods to detect the CaSR, since the lack of consensus over the localization of this receptor in the kidney had generated some controversy regarding the its renal functions (Ba et al. 2003, Topala et al. 2009, Loupy et al. 2012, Toka et al. 2012). Also, it was important to clarify the intra-renal distribution of this receptor in order to allow the full understanding of its renal roles since positive CaSR modulators (calcimimetics) are currently in use in the clinic (Block et al. 2004) and negative modulators (calcilytics) are being developed for the treatment of autosomal dominant hypocalcemia (Nemeth and Shoback 2013).

In this study, I have established the CaSR expression pattern in mouse, rat and human kidney using the most sensitive and specific mRNA and protein detection methods currently available. The expression of CaSR mRNA was analysed by a branched DNA methodology in which the detection of the CaSR was performed using a probe set composed of 20 small oligonucleotide probe pairs. The detection of mRNA sequences with a probe set instead of a regular probe pair introduces higher specificity to this technique, allowing the distinction between sequences that share a great degree of homology (Player et al. 2001). This methodology also contained CaSR signal amplification through sequential steps of hybridization with synthetic DNA probes, conferring enough sensitivity to detect a single molecule of mRNA (Player et al. 2001). Moreover, the simple experimental design of this methodology allowed a faster and more reliable detection of mRNA molecules than the traditional radioactive ISH methods. The detection of CaSR protein was performed by IHC using automated immunostainers and by *in situ* PLA. The PLA technique was selected because it is extremely sensitive, since it comprises an amplification step, and also because it is highly specific, since it only produces signal when the epitopes detected by both antibodies are closely located (Gustafsdottir et al. 2005). Besides method sensitivity,

a factor that may account for discrepancies in protein and mRNA analysis is the use of different protocols to process the tissue, since increased exposure to fixatives (>48h) can lead to loss of mRNA integrity (Polidoro et al. 2013) and irreversible epitope masking which prevents antibody binding (Di Bartolo and Kavurma 2014). Also, mRNA fragmentation may be increased when the sections are not freshly cut or when the tissue blocks are stored at room temperature for a period longer than one year (von Ahlfen et al. 2007). In order to ensure the best RNA preservation, the samples used in this study were processed with a protocol that consisted of a strict 24-48h fixation in formalin followed by embedding in paraffin, tissue sectioning was carried out up to one year after embedding and ISH, IHC or PLA was performed up to 3 days (ISH) or 2 weeks (IHC and PLA) after sectioning. A significant problem associated with various methods of protein detection and analysis is the lack of specificity of some antibodies. Particularly, many antibodies that target GPCRs display a significant lack of specificity, possibly due to the high structural similarity between the various receptors (Absi and Ward 2013). In order to ensure an accurate determination of the CaSR expression, eight CaSR antibodies were initially screened by assessing the immunofluorescence pattern in CaSR-HEK cells. Out of these antibodies, seven specifically detected the CaSR, showing cytoplasmic and membrane immunoreactivity in CaSR-HEK cells; and one, C-term2, failed this initial screen by showing nuclear immunoreactivity. These data suggest that most CaSR antibodies are specifically detecting the CaSR and therefore the cross-detection of other proteins is not the most likely the explanation for the discrepancies between studies. Out of the seven antibodies that passed the initial screening, four were selected for further studies based on the recognition of different epitopes and the specificity of these four antibodies was confirmed by analysing the Western blot pattern in mouse, rat and human kidney or CaSR-HEK cell extracts. In line with previous reports, all the selected antibodies showed different forms of the receptor, consistent with the presence of homodimers/multimers and glycosylated forms (Bai et al. 1996, Bai et al. 1998, Ward et al. 1998). Moreover, the antibodies show slightly different Western blotting profiles, showing preferential detection of monomeric or dimeric forms of the receptor. N-term1, Full length and C-term1 seem to detect preferentially monomeric forms of the CaSR in mouse and rat or to detect equally the monomeric and dimeric forms in human. Conversely, N-term2 seems to preferentially detect the CaSR dimer in all species. By IHC, all antibodies show a generally consistent IHC pattern, with CaSR the strongest immunoreactivity observed

in TAL and a weaker immunoreactivity observed in CD and DT. In addition, N-term2 showed a relatively strong immunoreactivity the proximal tubule. Dimerization of the CaSR occurs in the endoplasmic reticulum in a process that is independent of agonist binding and precedes the trafficking of the receptor to the plasma membrane (Olauson et al. 2013), therefore it is plausible that N-term2 preferably detects more mature, dimeric forms of the CaSR, which are present in the proximal tubule. Alternatively, the signal observed with N-term2 in the PT may be associated with non-specific binding to formalin fixed paraffin embedded (FFPE) tissue.

Thick ascending limb

The highest CaSR mRNA and protein expression were observed in the TAL, the only segment unanimously recognized to express the CaSR. (Wang et al. 1996, Riccardi et al. 1998, Motoyama and Friedman 2002, Ba et al. 2003, Loupy et al. 2012, Meister et al. 2013). The physiological roles described for the CaSR in this nephron segment include the regulation of divalent cation reabsorption through PTH-dependent (Motoyama and Friedman 2002) and PTH-independent (Loupy et al. 2012) processes.

Distal convoluted tubule

CaSR mRNA and protein expression were also observed in the DCT, in agreement with a vast number of studies (Sands et al. 1997, McNeil et al. 1998, Riccardi et al. 1998, Riccardi et al. 2000, Topala et al. 2009, Quinn et al. 2013, Ronchetti et al. 2013, Yasuoka et al. 2014). In this nephron segment, the CaSR was described to regulate the expression of the Ca^{2+} channel TRPV5 (Topala et al. 2009) and the potassium channel Kir4.1 (Huang et al. 2007).

Collecting ducts

CaSR mRNA and protein expression were detected by all methods in a fraction of the cells (roughly 30%) of cortical CDs. Weaker CaSR immunoreactivity was observed in the remaining cells by IHC with N-term2 but not with the other methods. Conversely, only IHC with N-term2 and PLA showed expression of the CaSR in medullary CDs. Although it is possible that IHC with N-term2 shows a higher sensitivity than the other methods, it is more likely that this antibody is the only method that detects a specific form of the receptor. This hypothesis is supported by the Western blotting results showing a preferential detection of the dimer, when compared to the other CaSR antibodies. Alternatively, N-term2 may be recognizing non-specific signal in FFPE

tissue. Intra-tubular expression of the CaSR in the CD has been a controversial issue. In this study, a heterogeneous CaSR distribution was observed within the cytoplasm, apical and basolateral membranes of CD in agreement with the initial description of CaSR distribution in this segment (Riccardi et al. 1998). The CaSR expression was first described in type A intercalated cells, (Riccardi et al. 1998), where the CaSR was found to trigger urinary acidification by increasing H+-ATPase activity in response to high urinary Ca^{2+} levels (Renkema et al. 2009). Conversely, a more recent study described the CaSR expression as being restricted to type B intercalated cells and dependent of the pH (Yasuoka et al. 2014). Other studies supported the expression of the CaSR in the apical membrane of principal cells, where the receptor reduced arginine vasopressin-elicited osmotic water permeability by inhibiting Aqp2 expression (Sands et al. 1997, Bustamante et al. 2008, Procino et al. 2012). In this study CaSR expression was observed in a proportion of principal and intercalated cells, since populations of CaSR+/Aqp2+, CaSR+/Aqp2-, CaSR-/Aqp2+ and CaSR-/Aqp2- cells were observed. Further work will be necessary to understand the heterogeneity and polarity of the CaSR in CD and functional roles of the receptor in principal and intercalated cells.

Proximal tubule

The PT is the nephron segment where the CaSR expression is more controversial (Riccardi et al. 1998, Riccardi et al. 2000, Ba et al. 2003, Loupy et al. 2012, Quinn et al. 2013, Ronchetti et al. 2013, Wu et al. 2013). In this study, no specific PT CaSR expression was observed by ISH. By IHC, whilst N-term2 showed consistent immunoreactivity in the PT, all the other antibodies showed a high variation between experiments and it was difficult to distinguish CaSR specific signal from the background staining obtained in the negative controls. When observed, PT immunoreactivity generally increased from the outer cortex to the inner cortex (S1 to S3). Using PLA, it was possible to specifically detect a low level of CaSR expression in the proximal tubule. Similarly to the distribution observed in some of the IHC experiments, CaSR PLA signal increases from S1 to S3. Previous studies reported a decrease in CaSR immunoreactivity from the outer cortex to the inner cortex (S1 to S3) (Riccardi et al. 1998, Riccardi et al. 2000), the opposite of our findings. These discrepancies are possibly associated with differences in the processing of the sample, since our studies were performed using FFPE sections and the previous

studies were carried out using cryosections of kidneys fixed by perfusion with paraformaldehyde. This assumption was confirmed by carrying out IHC with N-term1 in sections of rat kidneys fixed (data not shown). The observation of the CaSR in the PT is in agreement with studies that have observed the expression of the receptor in this segment in tissue (Riccardi et al. 1996, Riccardi et al. 1998, Ward et al. 2001, Ba et al. 2003) and PT immortalized cell lines (Di Mise et al. 2015) and support functional studies that show a role for the CaSR in $1,25D_3$ production (Bland et al. 2002), PT fluid reabsorption (Capasso et al. 2013) and regulation of PTH inhibition of Pi reabsorption (Ba et al. 2003).

Glomerulus

A few studies have described the expression of the CaSR in the glomerulus (Caride et al. 1998, Oh et al. 2011), while most studies fail to detect the CaSR in this segment (Riccardi et al. 1996, Yang et al. 1997, Riccardi et al. 1998, Loupy et al. 2012, Yasuoka et al. 2014). In this study, the CaSR expression was only convincingly observed with PLA as the other techniques did not show any expression distinguishable from the background levels. By PLA, CaSR expression was highly variable within the glomeruli and adjacent glomeruli would frequently show very different CaSR expression levels. The observation of the CaSR in the glomerulus supports the functional role reported for the receptor in the regulation of apoptosis and cytoskeleton stabilization in the podocytes (Oh et al. 2011). Further experiments will be needed to clarify the physiological significance of the receptor within the glomeruli.

Blood vessels

CaSR expression was also observed in the blood vessels by PLA, where this receptor was found to interact with SMA. The interaction was further confirmed by a co-immunoprecipitation assay in which the SMA expression was observed by Western blotting in rat kidney extracts pulled down with the N-term1. The CaSR was previously shown to interact with the actin binding protein filamin A, which possibly acts as a scaffolding protein, regulating the localization and signalling of the CaSR within the cells (Awata et al. 2001, Hjälm et al. 2001). It is plausible that the interaction between SMA and CaSR is involved in the localization and signalling of the receptor within blood vessels, however further studies will be needed to understand the physiological significance of this interaction.

The intra-renal distribution of the CaSR observed in this study is consistent with this receptor playing roles in different processes associated with the mineralization induced by MEK/ERK or FGFR inhibitors including production of 1,25D$_3$ (Bland et al. 2002) and reabsorption of Ca^{2+} (Topala et al. 2009) and Pi (Ba et al. 2003). No changes in the expression or cellular localization of the CaSR were observed following treatment with MEKi or FGFRi. Although these findings may suggest that the CaSR is not involved in the process of mineralization induced by MEK/ERK or FGFR inhibitors, it is important to acknowledge the possibility of these drugs affecting the activation and consequently downstream signalling of the CaSR whilst having no effects in its expression levels. Since the FGFRs and the MEK/ERK pathway have a direct role in the regulation of 1,25D$_3$ production (Perwad et al. 2007), it is more likely that the mineralization induced by MEK/ERK and FGFR inhibitors is the consequence of an increased production of 1,25D$_3$ elicited independently of the CaSR. The high levels of 1,25D$_3$ in the kidney may directly promote the renal reabsorption of Ca^{2+} and Pi by inducing the expression of NaPi-IIa and TRPV5, since these proteins contain vitamin D$_3$ responsive elements (Taketani et al. 1998, Weber et al. 2001, Turunen et al. 2007). Although these studies did not show any evidence of a role of the CaSR in soft-tissue mineralization induced by MEKi or FGFRi, it is possible that the CaSR contributes to this process in other organs including parathyroid, where it regulates the expression of PTH. Further studies are required to assess a possible role of PTH and parathyroid CaSR in the soft-tissue mineralization induced by ERKi, MEKi or FGFRi.

2.5 Conclusions

In summary, this study has shown that the CaSR is expressed throughout the nephron with a similar pattern observed in mouse, rat and human kidney. Highest CaSR expression is observed in the TAL, however the receptor is also present in other segments including glomerulus, PT, DCT, CNT and DT. The expression of the CaSR in glomerulus and PT is only convincingly detected by PLA, which displays higher sensitivity and specificity than the IHC. These findings clarify the expression pattern of the CaSR in mouse, rat and human kidney, thus allowing the full physiological role of the receptor to be determined in this organ. The role of the CaSR in the soft-tissue mineralization induced by MEK/ERK or FGFR inhibition was analysed by assessing the renal expression of the CaSR in animals treated with MEKi or FGFRi. Neither of the drugs affected the expression or cellular distribution of the CaSR, which may suggest that this receptor is not involved in the soft-tissue mineralization induced by inhibition of MEK/ERK pathway or inhibition of the FGFRs.

3 Effects of the inhibition of the MEK/ERK pathway or the FGF receptors in mineral homeostasis and soft-tissue mineralization

3.1 Introduction

Soft-tissue mineralization is a relatively frequent finding during preclinical drug safety testing. Yet, the study of the mechanisms associated with drug-induced mineralization has only emerged over the last decade, following significant advances in the understanding of the biomineralization process. Biomineralization is now regarded as an active process, regulated by multiple factors including Ca^{2+}, Pi (Haut et al. 1980), calcification inducers such as alkaline phosphatase (Orimo 2010) and RANKL (Deuell et al. 2012) and calcification inhibitors such as pyrophosphate (Moochhala 2012), osteopontin (Staines et al. 2012) and osteoprotegerin (Bucay et al. 1998).

The administration of MEK (Brown and Gad 2010, Diaz et al. 2012, Yanochko et al. 2013) or FGFR (Brown et al. 2005, Yanochko et al. 2013) inhibitors to rodents has resulted in soft-tissue mineralization associated with altered production or plasma levels of $1,25D_3$, FGF23 and PTH in previous studies. Most of these studies show that the renal production and plasma levels of $1,25D_3$ are increased by MEK or FGFR inhibition. $1,25D_3$ is a hormone mainly produced in the kidney that contributes for mineral homeostasis by promoting an increase in Ca^{2+} and Pi absorption from intestine, reabsorption from kidney and resorption from bone (Dusso et al. 2005). Also, $1,25D_3$ regulates the mineralization process by inducing the expression of pro-calcifying proteins such as alkaline phosphatase (Jono et al. 1998), Pit-1 (Tatsumi et al. 1998) and RANKL (Cardus et al. 2007, Katsumata et al. 2014). The effects of MEK and FGFR inhibition in FGF23 and PTH are more unclear as some studies report that both types of inhibitors increase plasma FGF23 (Diaz et al. 2012, Yanochko et al. 2013) and / or decrease plasma PTH (Brown and Gad 2010, Diaz et al. 2012), while other studies report that FGFR inhibitors induce the opposite effects (Wohrle et al. 2011, Wohrle et al. 2013). FGF23 and PTH are two key hormones in mineral ion homeostasis, produced respectively mainly in bone and parathyroid glands. Both hormones are able to induce the reabsorption of Ca^{2+} and inhibit the reabsorption of Pi in kidney. In addition, PTH also induces Ca^{2+} and Pi resorption from bone. The

effects of FGF23 are mediated mainly by the FGFRs and require Klotho as a co-receptor (Jüppner and Wolf 2012).

The toxicological effects of MEK and FGFR inhibitors resemble the toxicity induced by high levels of $1,25D_3$ (Brown et al. 2005) which include soft-tissue mineralization associated with high plasma levels of $1,25D_3$, FGF23, Ca^{2+} and Pi and low plasma levels of PTH. Mice deficient in FGF23 (Shimada et al. 2004) or Klotho (Kuro-o et al. 1997) also show the presence of soft-tissue mineralization associated with increased levels of $1,25D_3$ and analogous effects in mineral homeostasis, which can be ablated through the knockout of Cyp27b1 (Razzaque et al. 2006, Ohnishi et al. 2009) or VDR (Hesse et al. 2007, Anour et al. 2012). Conversely, mice treated with a FGFR1-activating antibody show increased production of FGF23 and effects opposite to the toxicity of MEK inhibitors and FGFR inhibitors, namely hypophosphatemia, normocalcemia, downregulation of Cyp27b1 and upregulation of Cyp24a1 (Wu et al. 2013). Taking together the results from the studies mentioned above, increased production / high levels of $1,25D_3$ appear to be associated and perhaps a triggering event for the occurrence of soft-tissue mineralization.

Despite the comparable pathophysiology, it is not clear if the molecular mechanisms leading to increased production of $1,25D_3$ and occurrence of soft-tissue mineralization are similar in animals treated with FGFR inhibitors and animals treated with MEK inhibitors. The unravelling of such mechanisms is notoriously difficult due to the high complexity of the processes associated with mineral homeostasis. For instance, the expression/production of $1,25D_3$, FGF23 and PTH are regulated not only by plasma levels of Ca^{2+} and Pi, but also by complex cross-regulatory interactions between these three hormones (Kuro-o 2010, Haussler et al. 2012), by other ions such as Mg^{2+} (Matsuzaki et al. 2013) and by other hormones such as sclerostin (Ryan et al. 2013). Moreover, the expression and effects of $1,25D_3$, FGF23 and PTH involve signalling through different cell signalling pathways such as MEK/ERK, WNT and calcineurin/NFAT. Previous studies have shown that FGF23 is able to induce the expression of FGF23 in bone (Xiao et al. 2014) and to inhibit the production/expression of $1,25D_3$ in kidney (Ranch et al. 2011, Chanakul et al. 2013) and PTH in the parathyroid (Ben-Dov et al. 2007) by signalling through the FGF receptors and the MEK/ERK pathway. Taking these observations into account, it is plausible that the

dysregulations in 1,25D$_3$, FGF23 and PTH following MEK or FGFR inhibition are the consequence of a blockage in the FGF23-induced regulation of these hormones.

Most likely the kidney has a key role in the mineralization induced by MEK inhibitors or FGFR inhibitors since it is the organ where 1,25D$_3$ is mainly produced and one of the organs displaying more severe mineralization in animals treated with these inhibitors (Brown et al. 2005, Diaz et al. 2012). Also, the renal signalling of FGF23, which occurs through the FGFRs and the MEK/ERK pathway, results in the induction of TRPV5 and inhibition of NaPi-IIa, two important proteins for renal Ca^{2+} and Pi reabsorption, respectively (Andrukhova et al. 2012, Andrukhova et al. 2014). It is plausible that MEK or FGFR inhibitors directly affect renal Ca^{2+} and Pi reabsorption by blocking the FGF23 regulation of TRPV5 and NaPi-IIa. Consistent with these observations, NaPi-IIa expression is decreased in mice treated with a FGFR1-activating antibody (Wu et al. 2013) and increased in rats treated with a FGF23 inhibitor peptide (Goetz et al. 2010) and in mice lacking FGF23 or Klotho (Memon et al. 2008). One aspect proscribing the role of the kidney in the mineralization induced by MEK or FGFR inhibitors is the uncertainty about the intra-renal distribution of FGFRs and components of the MEK/ERK pathway. Regarding the FGFRs, although different studies have reported the expression of mRNA and protein from FGFR 1-4 in the kidney (Floege et al. 1999, Fuhrmann et al. 1999, Cancilla et al. 2001, Rossini et al. 2005, Liu et al. 2008), these show high discrepancies regarding the distribution of the four receptors along the nephron. Regarding the MEK/ERK pathway, whilst immunohistochemical studies have described ERK expression to be restricted to distal tubules and collecting ducts (Omori et al. 2000, Fujita et al. 2004), functional studies carried out in cell cultures suggest that ERK is expressed and attains functional roles also in the proximal tubule (Sengul et al. 2003, Su et al. 2006).

As described above, previous studies have shown that the inhibition of signalling through the FGFRs or through the MEK/ERK pathway in rats results in disturbances in mineral homeostasis and soft-tissue mineralization. I hypothesise that these effects are induced by a mechanism common to both types of inhibitors, which is represented in Figure 3.1 and described below:

- FGFR and MEK/ERK inhibitors may block the FGF23-induced regulation of Cyp27b1 and Cyp24a1 expression, thus promoting an increase in the production of 1,25D$_3$. The elevation in 1,25D$_3$ in turn may promote the following effects:

- Elevation in plasma Ca^{2+} and Pi through the increase of the renal reabsorption of these ions.

- Increase in the expression of mineralization inducers including alkaline phosphatase.

- Compensatory actions for the inhibition of FGFR or the MEK/ERK pathway including the negative feedback for $1,25D_3$ production and the induction of FGF23 production

- FGFR and MEK/ERK inhibitors may also block the FGF23-induced inhibition of NaPi-IIa expression, leading to increased Pi reabsorption.

- Soft-tissue mineralization may occur as a consequence of the increased levels of circulating Ca^{2+} and Pi and the increased expression of mineralization inducers.

The hypothesis described above was tested using an *in vivo* approach. A 6h (single dose) and two 8d (repeated dosing) rat *in vivo* studies were carried out using inhibitors of ERK 1/2 (ERKi), MEK 1/2 (MEKi) or FGFR 1-3 (FGFRi) (Table 3.1: Studies 1-3). Additionally, assays were carried out using samples collected in a previous 28d study with MEKi and FGFRi (Table 3.1: Study 4). The samples from these four studies were analysed for different biological readouts, grouped in 5 topics:

- Study execution and toxicokinetic analysis of ERKi, MEKi and FGFRi - This topic concerns the performance of the *in vivo* studies and addresses the problems encountered during its development, the solutions adopted and the plasma levels of the administered drugs during the course of the studies.

- Effects of ERKi, MEKi and FGFRi in soft-tissue mineralization and mineral homeostasis – This topic concerns the effects of the inhibitors in the occurrence of soft-tissue mineralization, plasma levels of Pi, Ca^{2+} and Mg^{2+} and production and plasma levels of the hormones $1,25D_3$, FGF23 and PTH.

- Effects of ERKi, MEKi and FGFRi on the activation of cell signalling pathways in the kidney - This topic addresses: a) The susceptibility of the different nephron segments to be directly targeted by the inhibitors through the analysis of the distribution of ERK, MEK, Klotho and FGFR1-4; b) The efficacy of the inhibitors in preventing the activation of the ERK pathway; c) The identification of downstream

signalling pathways affected by the inhibitors, which may be involved in the soft-tissue calcification process.

- Effects of ERKi, MEKi and FGFRi in renal reabsorption of Pi and Ca^{2+} – This topic addresses the effects of the inhibitors in the expression of proteins involved in the renal transport of Pi (NaPi-IIa), renal transport of Ca^{2+} (TRPV5, calbindin-D28k and PMCA) and key proteins for the regulation of these processes (Klotho).

- Effects of ERKi, MEKi and FGFRi in the expression of calcification modulator proteins – This topic addresses the effect of the inhibitors in a) the expression of alkaline phosphatase and Pit-1, two pro-calcifying proteins susceptible induction by $1,25D_3$; b) the expression of calcification inhibitors osteopontin, osteoprotegerin, DKK1, sclerostin, which were previously found to be upregulated in calcifying tissue.

It is important to mention that, at the start of this project, in 2011, soft-tissue mineralization and perturbations of mineral homeostasis had been reported with MEK (Brown and Gad 2010) and FGFR (Brown et al. 2005) inhibitors, however very little information was available regarding the mechanisms responsible for these effects. The mechanistic studies presented in the introduction were carried out and published during the course of this work (Wohrle et al. 2011, Diaz et al. 2012, Wohrle et al. 2013, Yanochko et al. 2013). Moreover, for some mechanistic aspects such as the effect of the MEK and FGFR inhibition in the alteration of vitamin D_3 metabolism and NaPi-IIa activation, I had obtained analogous findings at the time of the publication of these studies (Wohrle et al. 2011, Diaz et al. 2012).
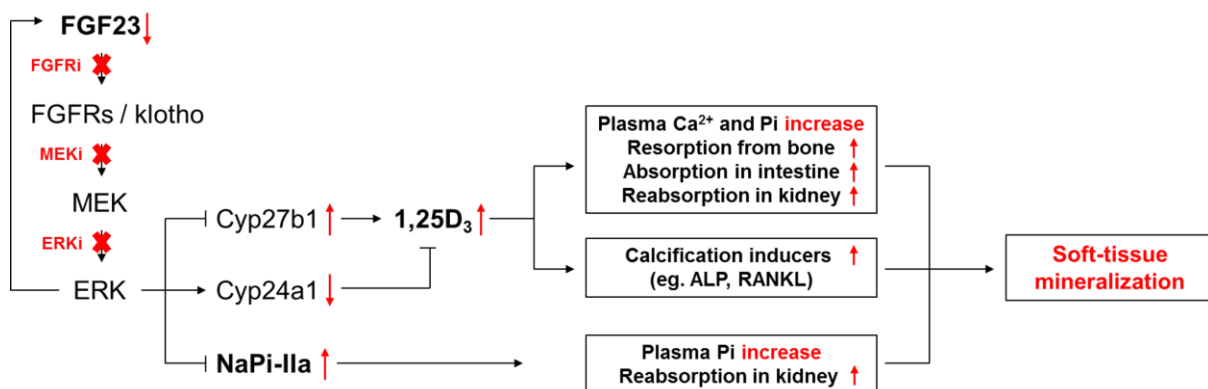
Figure 3.1: Hypothetical model for the mechanism of soft-tissue mineralization induced by inhibition of the FGFRs or MEK/ERK pathway. ALP, alkaline phosphatase.

3.2 Methods

3.2.1 Animal Studies

The animal studies assessed in this thesis were designed and run by the Safety Assessment division at AstraZeneca UK, in compliance with the regulations for repeated dose toxicity studies issued by European Medicines Agency, Ministry of Health Labour and Welfare and Food and Drug Administration. The studies were designed and carried out with the aim of assessing the toxicity of the oral administration of a MEK 1/2 inhibitor (MEKi) and a FGFR 1-3 inhibitor (FGFRi) to Han Wistar rats. These studies were planned for 8d (2 studies) and 28d dosing periods, to meet specific criteria for regulatory purposes. Additionally, a 6h, single dose study was designed to assess the effects of acute dosing with the inhibitors. Due to problems with the licensing of the MEKi, this compound had to be substituted with an ERK 1/2 inhibitor (ERKi) in two of the studies (6h and 8d). ERKi, MEKi and FGFRi dosages were respectively 300 mg/kg/day with bidaily administration (BID); 1.4 mg/kg/day; and 20 mg/kg/day, BID. These dosages corresponded to the maximum tolerated doses, the highest drug concentrations administered in prior 4d (ERKi) or 7d (MEKi and FGFRi) tolerability studies that did not result in unacceptable toxicity. In the last day of each study animals were killed, plasma was collected and the major organs were embedded in paraffin and/or flash frozen. In the 8d studies, the killing of the animals was carried out 2h after the last dosing, a time when the drugs were expected to reach the maximum concentrations in blood. The ERKi group in the 8d study and the FGFRi group in the 28d study had to be killed earlier due to animal welfare reasons, respectively at d3 and d25. The study design, including the earlier terminations is described in Table 3.1.

Table 3.1: Rat in vivo studies using ERKi, MEKi and FGFRi

	Groups	Planed length	Effective length	Dose (mg/kg/d)	N	Vehicle
Study 1	Vehicle	8d	8d	0	3	30% PEG in water
	MEKi			1.4	6 (4 for IHC)	water containing 0.5% HPMC 0.1% Tween 80
	FGFRi			20 (BID)	6 (5 for WB)	30% PEG in water
Study 2	Vehicle	8d	8d	0	6	10% PEG, 40.5% HP-b-CD
	ERKi		3d	300 (BID)	6 (4 for IHC)	10% PEG, 40.5% HP-b-CD
	FGFRi		8d	20 (BID)	6 (4 for IHC)	30% PEG in water
Study 3	Vehicle	6h	6h	0	6	10% PEG, 40.5% HP-b-CD
	ERKi			150	6	10% PEG, 40.5% HP-b-CD
	FGFRi			20	6	30% PEG in water
Study 4	Vehicle	28d	28d	0	10	water containing 0.5% HPMC 0.1% Tween 80
	MEKi			1.4	10	water containing 0.5% HPMC 0.1% Tween 80
	Vehicle		25d	0 (BID)	10	30% PEG in water
	FGFRi			20 (BID)	10	30% PEG in water

*PEG - Polyethylene glycol 400, HPMC - hydroxypropyl methylcellulose

3.2.2 Toxicokinetic analysis

Toxicokinetic analysis was carried out by the Drug Metabolism and Pharmacokinetics department at AstraZeneca UK.

ERKi, MEKi and FGFRi were analysed using liquid chromatography-tandem mass spectrometry in samples extracted from plasma with acetonitrile.

3.2.3 Ca^{2+}, Mg^{2+} and Pi determination

Plasma Ca^{2+}, Mg^{2+} and Pi were quantified by the Clinical Pathology department at AstraZeneca UK.

Plasma Ca^{2+}, Mg^{2+} and Pi were measured using a Roche Modular P analyser (Roche Diagnostics, West Surrey, UK). Pi and Mg^{2+} were quantified using assay kits supplied by Roche (Roche Diagnostics, West Surrey, UK). Ca^{2+} was quantified using a colorimetric end point method (Instrumentation Laboratory, Warrington, UK).

3.2.4 Mineralization assay

Kidneys were fixed for 24 to 48h in 10% neutral-buffered formalin, embedded in paraffin, and 4 µm sections were cut. Sections were de-waxed using xylene and rehydrated using 100% and 95% ethanol. Mineralization was assessed by staining the sections with Von Kossa's stain. Briefly, sections were incubated with a 2.5% silver nitrate solution for 20 min under an ultraviolet light. Sections were rinsed with water and the excess silver was removed by incubating with 5% sodium thiosulphate for 5 min. Sections were counterstained with nuclear fast red for 1 min before dehydrating in 95% and 100% ethanol, clearing in xylene, and mounting using Hystomount (TAAB Labs, Aldermaston, UK).

3.2.5 In situ hybridization

Rat kidneys were fixed in 10% neutral-buffered formalin for 24 to 48h and embedded in paraffin. Five µm-thick sections were cut and *in situ* hybridization was performed using QuantiGene ViewRNA ISH tissue assay (Affymetrix, Santa Clara, USA) according to manufacturer's instructions, with the following modifications: incubation times were 5 min for pretreatment, 20 min for protease digestion, 40 min for PreAmp Hybridization, and 30 min for Amp Hybridization and Label Probe incubation. Rat FGFR1-4 probes were obtained from Affymetrix (Affymetrix, Santa Clara, USA) and

used in concentration of 1:40 in the probe diluents provided by the kit. Sections were mounted using Immu-mount (Thermo Scientific, Waltham, USA). Negative controls were performed by omission of probes.

3.2.6 Immunohistochemistry

Kidneys were fixed for 24 to 48h in 10% neutral-buffered formalin, embedded in paraffin, and 4 µm sections were cut. Sections were de-waxed using xylene and rehydrated using 100% and 95% ethanol. Immunostainings were performed using a Labvision autostainer (Labvision, Fremont, USA) or a Ventana XT autostainer (Ventana, Tucson, USA). The sections stained with the Labvision autostainer had a previous heat-mediated antigen retrieval step performed in a Milestone RHS-2 microwave (Milestone, Sorisole, Italy) at 110°C for 2 min in 1 mM EDTA buffer, pH 8 or 10 mM Citrate buffer, pH 6. Endogenous peroxidase activity was blocked with 3% (aq) hydrogen peroxide for 10 min. Nonspecific binding of the antibody was prevented by incubating slides with background blocker with casein (Menarini, Florence, Italy) for 20 min. Slides were incubated with primary antibodies (Table 3.2) for 1h at room temperature. X-Cell Plus HRP, Goat HRP (Menarini, Florence, Italy), Ultravision Quanto Mouse on Mouse (Thermo Scientific, Waltham, USA) or Envision anti-mouse labelled polymer (DAKO, Glostrup, Denmark) was applied to the slides, and peroxidase was then visualized with diamino benzidine (DAKO, Glostrup, Denmark). Immunostainings with the Ventana XT autostainer were carried out using Ventana reagents (Ventana, Tucson, USA) and a pre-set immunostaining protocol that included antigen-retrieval and had antibody incubation times similar to the Labvision protocol. Sections were counterstained using hematoxylin (Carazzi's) for 1 min before dehydrating in 95% and 100% ethanol, clearing in xylene, and mounting using Hystomount (TAAB Labs, Aldermaston, UK). Negative controls were performed using isotype controls or omission of the primary antibodies.

Whole slide images were scanned in a Scanscope® scanner (Aperio Technologies Incorporated, Vista, USA). Positive Pixel Count Algorithm of the ImageScope software (Aperio Technologies Incorporated, Vista, USA)), was used to quantify the positive signal in whole kidney. Detection thresholds were manually set in order to obtain the best signal/noise ratio for each protein. The percentage of positive staining (relative

stained area) was calculated as the sum of all stained pixels divided by the sum of all stained and unstained pixels.

Table 3.2: Antibodies used for immunohistochemistry

Protein	Supplier/Code	Raised in	Dilution	Antigen retrieval
ALP [1]	Abcam / ab65834	Rabbit	1:200	CC1
Calbindin-D28k	Sigma / c9848	Mouse	1:3000	CC2 / Citrate
EGR1	CST[2] / CST4153	Rabbit	1:50	CC1
ERK	CST / CST4695	Rabbit	1:200	CC2 / Citrate
FGFR1	Abcam / ab31324*	Goat	1:500	Citrate
FGFR2	Abcam / ab10648*	Rabbit	1:2000	Proteinase K
FGFR3	Abcam / ab10651*	Rabbit	1:2000	Proteinase K
FGFR4	Abcam / ab41948	Rabbit	1:500	EDTA
Klotho	ADI[3] / KL11-A	Rabbit	1:200	CC1 / EDTA
MEK	CST / CST 9122	Rabbit	1:100	CC1 / EDTA
NaPi-IIa	ADI / NPT27-A	Rabbit	1:200	CC1 / EDTA
Osteopontin	IBL / 18628	Rabbit	1:100	CC1 / EDTA
Phopho-ERK	CST / CST4376	Rabbit	1:100	CC1 / EDTA
Phospho-MEK	CST / CST 9121	Rabbit	1:100	CC1 / EDTA
Phospho-RSK	Abcam / ab32413	Rabbit	1:75	CC1 / EDTA
Pit-1	Abcam / ab177147	Rabbit	1:800	CC2 / Citrate
PMCA	Santa Cruz / sc-20028	Mouse	1:300 / 1:100	CC2 / Citrate
RSK	BD / 610226	Mouse	1:150	CC2 / Citrate
TRPV5	Alomone / ACC-035	Rabbit	1:400 / 1:100	CC2 / Citrate
VDR	Santa Cruz / sc-13133	Mouse	1:100 / 1:500	CC1 / EDTA

1 - Alkaline phosphatase; 2 – Cell Signaling Technology; 3 – Alpha Diagnostics International

3.2.7 Quantitative reverse transcription polymerase chain reaction

Ribonucleic acid (RNA) was extracted from rat kidneys using an RNeasy Plus Mini Kit (QIAGEN, Venlo, Netherlands), according to the manufacturer's instructions. RNA was quantified using NanoDrop 2000 (Thermo Scientific, Waltham, USA) and RNA integrity was assessed using an Agilent 2100 Bioanalyzer with an Agilent RNA 6000 Nano Kit (Agilent, Stockport, UK). Reverse transcription was carried out using 800 ng of RNA into a final volume of 20 µl with SuperScript® III First-Strand Synthesis SuperMix for qRT-PCR (Life Technologies, Carlsbad, USA). Two µl from each sample were pooled and used to create a standard curve. The remaining 18 µl of each sample were diluted 10-fold with water. Real time polymerase chain reaction (qPCR) was performed in a MX3000P qPCR system (Agilent, Stockport, UK) using RT² SYBR® Green with ROX (QIAGEN, Venlo, Netherlands). The primers for Cyp24a1 (RT² qPCR Primer Assay for Rat Cyp24a1) were obtained from QIAGEN (QIAGEN, Venlo, Netherlands) and the primers for beta-actin, (Fw-GAGGCCCCTCTGAACCCTAA, Rv-ACCAGAGGCATACAGGGACAA), Cyp27b1 (Fw-TGGTGAAGAATGGCAGAG, Rv-GTCCAGAGTTCCAGCATA), and VDR (Fw-CAGTCTGAGGCCCAAGCTA, Rv-TCCCTGAAGTCAGCGTAGGT) were obtained from Sigma (Sigma, St Louis, USA). Relative mRNA expression of Cyp27b1, Cyp24a1 and VDR was calculated by interpolating the Ct values in the standard curves and normalizing the results to beta-actin expression. Negative controls were performed by omission of template and by omission of the reverse transcriptase during the complementary DNA synthesis step.

3.2.8 Plasma analysis

Analysis of plasma $1,25D_3$, Klotho, FGF23, PTH, DKK1, sclerostin and osteoprotegerin were carried out by the Clinical Pathology department at AstraZeneca UK.

Plasma $1,25D_3$ was analysed using 1,25-dihydroxyvitamin D_3 radioimmunoassay (Immunodiagnostics systems, Boldon, UK), according to the manufacturer's instructions.

Plasma Klotho was analysed using Rat Klotho ELISA Kit (Cusabio, Wuhan, China), according to the manufacturer's instructions.

Plasma FGF23 was analysed using a FGF23 ELISA Kit (Kainos laboratories, Tokyo, Japan), according to the manufacturer's instructions.

Plasma PTH, DKK1, sclerostin and osteoprotegerin were analysed using a multiplex assay, Rat Bone Magnetic Bead Panel 1 (Millipore, Billerica, USA), according to the manufacturer's instructions. Data collection was performed using a BioPlex 200 instrument (Biorad, Hercules, USA).

3.2.9 Western blotting

Rat kidney samples were homogenized in T-PER buffer (Pierce, Rockford, USA) containing Halt protease and phosphatase inhibitors (Pierce, Rockford, USA). Cell lysis was carried out using a Polytron (Kinematica, Bohemia, NY, USA) homogenizer. Following lysis, homogenates were centrifuged at 10,000 x g for 5 min to remove insoluble debris. Protein extracts were quantified using a BCA protein assay (Pierce, Rockford, USA). Twenty micrograms of each extract were electrophoresed on NuPage® 4-12% BisTris polyacrylamide gels (Invitrogen, Paisley, UK). Gels were transferred to nitrocellulose membranes and stained with Ponceau S to confirm even protein loading of wells. Non-specific protein binding was blocked using 5% low-fat dried milk in Tris-buffered saline containing 0.1%Tween (TBST) for 1h at room temperature. Primary antibodies were added at a concentration of 1:2000 in 5% milk/TBST overnight at 4ºC. An horseradish peroxidase conjugated anti-mouse or anti-rabbit secondary antibody (Promega, Madison, USA) was added appropriately at a concentration of 1:20,000 or 1:6,000 in 5% milk/TBST before detection of immunoreactivity with ECL prime and development and development on HyperfilmTM ECL (GE Healthcare, Little Chalfont, UK).

3.2.10 Reverse Phase Protein Array

Reverse phase protein array (RPPA) was carried out at the Edinburgh Cancer Research Centre using a ZeptoMARK platform (Bayer, Leverkussen, Germany). The samples used for the RPPA were snap frozen kidneys from study 3 (6h dosing with ERKi, FGFRi or vehicle).

3.2.11 Statistics

All data shown represent mean ± standard error of the mean. Statistical analysis was carried out with Microsoft Office Excel (Microsoft, Redmond, USA) using the Real Statistics Resource Pack. A two-tailed, Mann Whitney U test was employed and p values lower that 0.05 were considered to be significant.

3.3 Results - Study execution and toxicokinetic analysis of ERKi, MEKi and FGFRi

3.3.1 Study execution

All studies lasted for the designed duration, with the exception of the ERKi group in the 8d study, which had to be killed at d3 due to animal welfare reasons. Also, in the previous 28d study, the FGFRi group had been killed at d25 for the same reasons. The clinical signs that lead to the earlier termination of these studies include weight loss, staining around the uro/ano-genital region, piloerection, hunched posture and decreased motor activity.

3.3.2 Toxicokinetic analysis

Plasma drug concentrations were analysed during the 12h period following the administration of ERKi, MEKi or FGFRi at d1 (single dose) and d7 (repeated dose) of the 8d study. Due to the earlier termination of the study, the d7 plasma drug concentrations were not analysed for ERKi. A graphical representation of this analysis is shown in Figure 3.2 and the estimated toxicokinetic parameters of maximum drug concentration (C_{max}), drug concentration at 12h post-dose (C_{12h}) and drug half-life ($t_{1/2}$) are shown in Table 3.3.

ERKi – At d1, ERKi showed a C_{max} of 155±15 µmol/L, which was detected 2h after dosing. Also, ERKi evidenced a $t_{1/2}$ of 9.5h and the C_{12h} of 52±7 µmol/L, around 35% of the C_{max}. Considering that ERKi was administered twice daily, these results suggest that plasma concentrations of this compound remained high during the whole study.

MEKi – At d1, MEKi showed a C_{max} of 1.27±0.22 µmol/L, which was detected 2h after dosing. Also, MEKi evidenced a $t_{1/2}$ of 3.4h and the C_{12h} of 0.11±0.01 µmol/L, around 9% of the C_{max}. At d7, MEKi showed values of C_{max} (1.77±0.37 µmol/L), $t_{1/2}$ (3.7h) and C_{12h} (0.11±0.03) comparable to d1. The low $t_{1/2}$ and C_{12h} values, together with the fact that MEKi was only dosed once a day, suggest that the plasma concentrations of this drug decreased to very low levels between dosing intervals.

FGFRi – At d1, FGFRi showed a C_{max} of 2.94±0.27 µmol/L, which was detected 2h after dosing. Also, FGFRi evidenced a $t_{1/2}$ of 4.7h and the C_{12h} of 0.07±0.03 µmol/L,

around 2% of the C_{max}. Conversely, at d7, FGFRi showed a C_{max} of 2.00±0.38 µmol/L, a $t_{1/2}$ of 8.2h and the C_{12h} of 0.39±0.11 µmol/L, around 20% of the C_{max}. The increase in the values of $t_{1/2}$ and C_{12h} from d1 to d7 may be associated with the accumulation of FGFRi in the different tissues. The $t_{1/2}$ and C_{12h} values observed during the repeated dose phase, together with the fact that FGRi was dosed twice a day suggest that the plasma concentration of this compound remained high during most of the study.

ERKi, MEKi and FGFRi showed the highest plasma drug concentrations 2h after dosing.

t1/2 and C_{12h} suggest that the concentrations of ERKi and FGFRi remained high during most of the study, while the concentrations of MEKi decreased to extremely low levels between dosing intervals.

C_{max} and t1/2 suggest that the timing for the last dosing (2h before termination for 8d studies / 6h before termination for 6h study) was consistent the presence of high drug concentrations of ERKi, MEKi (only at 2h) and FGFRi in plasma.
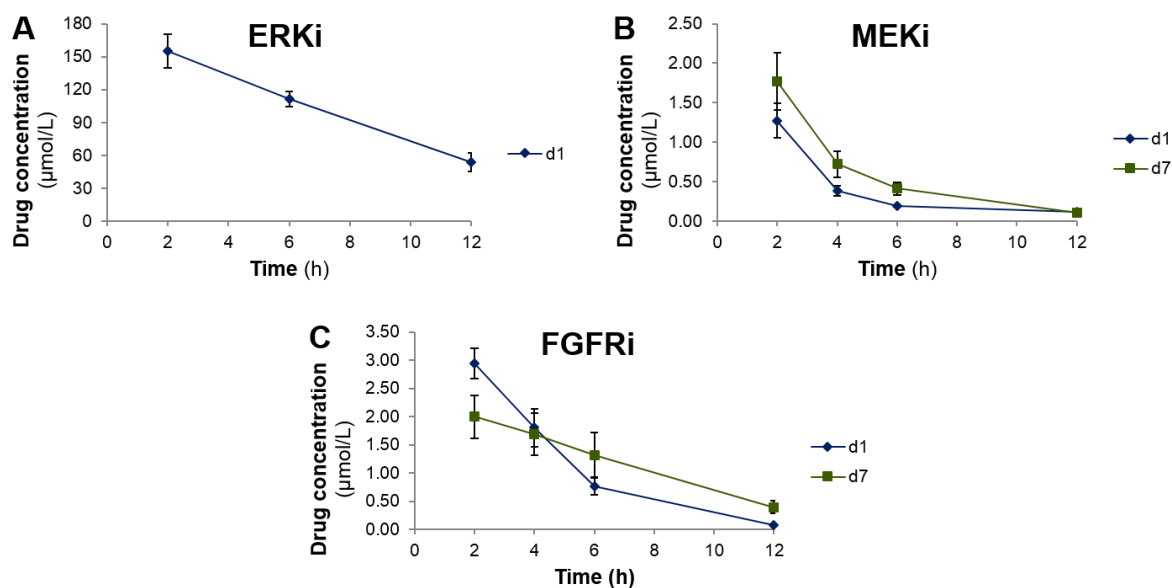
Figure 3.2: Plasma drug concentrations during a 12h period following the administration of 150 mg/kg of ERKi, 1.4 mg/kg of MEKi or 10 mg/kg of FGFRi to rats by oral gavage. Plasma drug concentrations of ERKi (A), MEKi (B) or FGFRi (C) were evaluated following a single dose (d1) and at d7 of a repeated dosing period (d7) with these inhibitors. Data representative of N = 3-6 rats + SEM. Plasma drug concentrations were analysed by the Drug Metabolism and Pharmacokinetics department at AstraZeneca UK.

Table 3.3: Maximum drug concentration (Cmax), drug concentration at 12h (C_{12h}) and drug half-life (t1/2) following the oral administration of ERKi, MEKi and FGFRi to rats, respectively at 150 mg/kg, 1.4 mg/kg or 10 mg/kg concentrations.

	Day	Cmax (µmol/L)	C12h (µmol/L)	t1/2 (h)
ERKi	d1	155±15	52±7	9.5
MEKi	d1	1.27±0.22	0.11±0.01	3.4
	d7	1.77±0.37	0.11±0.03	3.7
FGFRi	d1	2.94±0.27	0.07±0.03	4.7
	d7	2.00±0.38	0.39±0.11	8.2

Data representative of N = 3-6 rats + SEM. Toxicokinetic parameters were estimated by the Drug Metabolism and Pharmacokinetics department at AstraZeneca UK.

3.4 Results - Effects of ERKi, MEKi and FGFRi in soft-tissue mineralization and mineral homeostasis

3.4.1 Effect of ERK, MEK and FGFR inhibition on soft-tissue mineralization

Kidney, stomach and heart were analysed for the presence of mineralization using a von Kossa stain on sections of tissue obtained from animals treated with ERKi, MEKi and FGFRi. These analysis aimed not only to confirm that MEKi and FGFRi are able to induce the mineralization effects previously reported with other inhibitors of the same classes but also to assess if ERK inhibition also resulted in similar effects.

Mineralization of soft-tissues was observed in animals treated with ERKi for 3d or with MEKi or FGFRi for 8d or 25/28d (Table 3.4). For all the inhibitors, the stomach was the most affected organ, with mineralization detected in nearly all animals. In the heart, mineralization was observed in animals from all the MEKi and FGFRi treatment groups. In the kidney, mineralization was detected in the cortex the majority of the animals treated with MEKi for 28d or FGFRi for 8d or 25d. Kidney mineralization appeared to be mainly present in connective tissue adjacent to distal tubules. Conversely, mineralization was not detected in kidneys of animals treated with ERKi for 3d or MEKi for 7d. Figure 3.3 shows representative pictures of mineral deposition in kidney sections from rats treated with MEKi or FGRi, observed by von Kossa and hematoxylin and eosin (H&E) stainings.

Treatment with ERKi for 3d or MEKi or FGFRi for >8d resulted in soft-tissue mineralization in different organs including stomach, heart and kidney.

Table 3.4: Number of animals showing the presence of mineralization by von Kossa staining.

	Groups	Stomach	Kidney	Heart
Study 1 (8d)	MEKi	**6**/6	**0**/4	**1** /6
	FGFRi	**5**/6	**0**/6	**3** /6
Study 2 (3/8d)	ERKi	**3**/6	**0**/4	**0** /6
	FGFRi	**6**/6	**3**/4	**5** /6
Study 4 (25/28d)	MEKi	**10**/10	**7**/10	**4** /10
	FGFRi	**8**/10	**8**/10	**4** /10
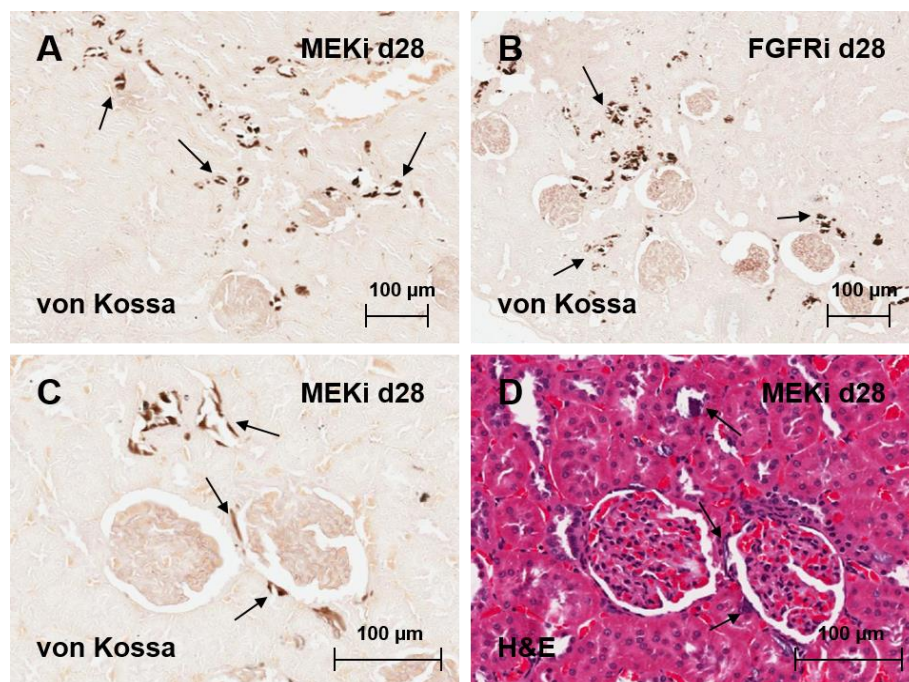
Figure 3.3: Mineralization in the kidney cortex of rats dosed with 1.4 mg/kg/day of MEKi for 28 days or 20 mg/kg/day of FGFRi for 25 days. Lower magnification photomicrographs of von Kossa staining in cortical kidney sections of rats dosed with MEKi (A) or FGFRi (B). Higher magnification photomicrographs of von Kossa (C) or H&E staining (D) in cortical kidney sections of rats treated with MEKi. Arrows illustrate focal deposits of angular crystals in the renal tubules. Scale bar = 100 µm.

3.4.2 Effect of ERK, MEK and FGFR inhibition on mineral homeostasis

Plasma levels of calcium (Ca^{2+}), phosphate (Pi) and magnesium (Mg^{2+}) were analysed at different time points in animals dosed for 6h or 3/8d with ERKi, MEKi and FGRi (Figure 3.4).

Treatment with ERKi, MEKi and FGFRi did not induce any increase in plasma Pi at 2h or 6h post-dose. In fact, a slight, but significant decrease in plasma Pi was even observed 2h after dosing with ERKi (-31%) or FGFRi (-21%) in one of the studies. Increased plasma Pi levels were first detected 12h post dosing with MEKi (+21%) or FGFRi (+14%) and 24h post dosing with ERKi (+50%). Plasma Pi levels were further increased at d3 of ERKi (+104%) treatment and at d4 and d7 of MEKi (+55-63%) or FGFRi (+55-114%) treatments.

Plasma Ca^{2+} levels remained mostly unchanged during the course of the studies. Nevertheless, plasma Ca^{2+} levels showed slight, but significant decreases following the administration of ERKi (-8%) or FGFRi (-9%) for 2h and increases following the administration of ERKi for 3d (+11%) or FGFRi for 24h (+5%) or 4d (+5%).

Plasma levels of Mg^{2+} remained mostly unchanged during the course of the studies. However, plasma Mg^{2+} levels showed a slight, but significant decrease in animals treated with FGFRi for 2h (-7%) and increase in animals treated with FGFRi for 12h (+11%).

Plasma levels of Pi were increased from 12h post-dosing with MEKi or 24h post-dosing with ERKi or FGFRi until the end of the study period (d7).

Plasma levels of Ca^{2+} and Mg^{2+} remained mostly unchanged during the course of the treatments with ERKi, MEKi or FGFRi.
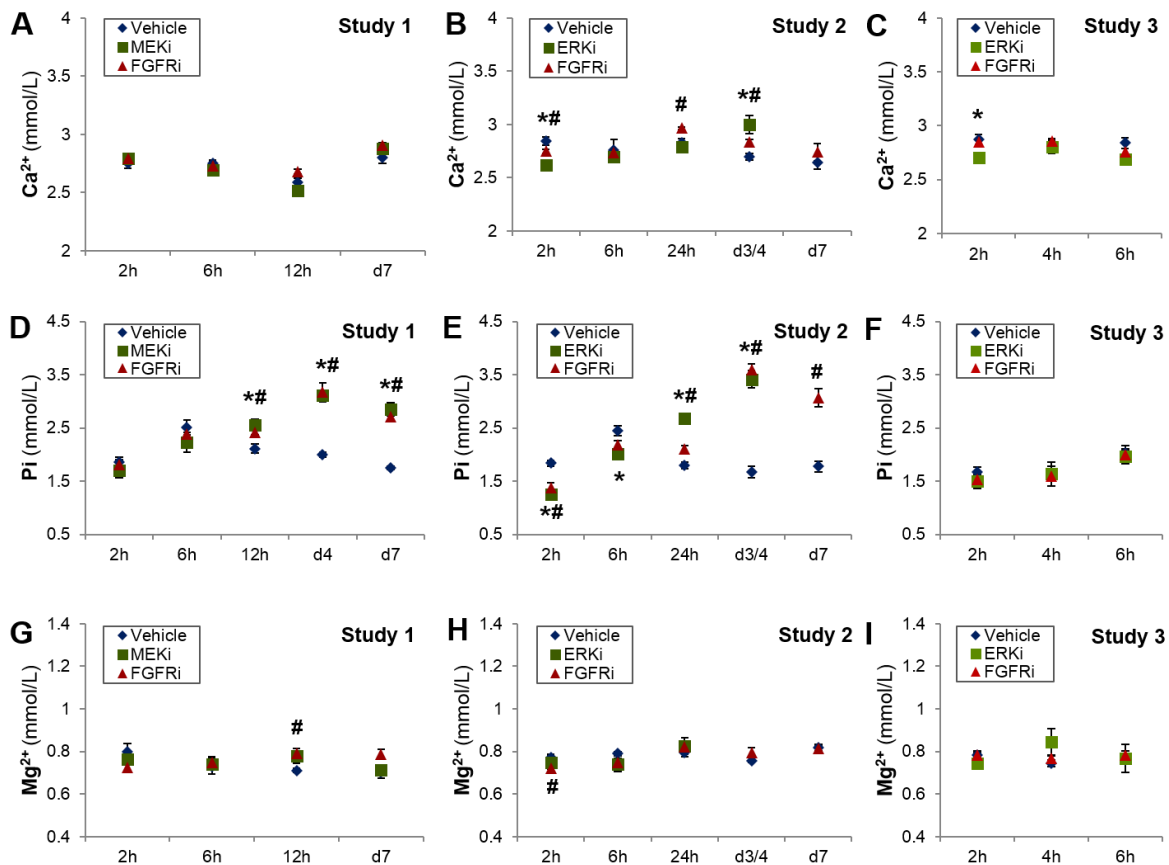
Figure 3.4: Plasma concentrations of Ca²⁺, Pi and Mg²⁺ in animals treated with 150 mg/kg/day of ERKi, 1.4 mg/kg/day of MEKi or 20 mg/kg/day FGFRi. Plasma Ca²⁺ (A-C), Pi (D-F) and Mg²⁺ (G-I) concentrations in animals from Study 1 (A,D,G), Study 2 (B,E,H) and Study 3 (C,F,I). Data representative of *N* = 3-6 rats + SEM. * # p<0.05 vs vehicle (Mann-Whitney, * vehicle vs MEKi/ERKi, # vehicle vs FGFRi). Plasma concentrations of Ca²⁺, Pi and Mg²⁺ were analysed by the Clinical Pathology department at AstraZeneca UK.

3.4.3 Effect of ERK, MEK and FGFR inhibition on the production of 1,25-dihydroxyvitamin D₃

In the previous 28d study with MEKi, the plasma levels of $1,25D_3$ had been analysed at different time points using a commercial radioimmunoassay (Figure 3.5). In that study, MEKi did not induce any significant changes in plasma levels of $1,25D_3$. Nevertheless, the levels of $1,25D_3$ showed a high variability likely associated with the low sensitivity of the assay. This variability may have contributed to the lack of statistical significance in the analysis of those samples ($N = 5$ animals per group). In fact, a power analysis estimated that an $N = 22$ would be required to obtain statistical significance for the quantification of $1,25D_3$ using this assay. The $1,25D_3$ radioimmunoassay required a large sample volume, which, due to the strict home office license regulations of plasma collection, would have precluded the analysis of $1,25D_3$ and other analytes such as Pi, Ca^{2+} and FGF 23 in the same samples. In the light of the sample limitations and the high variability of the assay, the quantification of $1,25D_3$ was not performed in animals from the remaining dosing groups. Recently, mass spectroscopy methods have been reported to yield more sensitive results in the quantification of $1,25D_3$ than radioimmunoassays (Strathmann et al. 2011). For this reason, a collaborator at Astrazeneca tried to develop an in house assay to quantify $1,25D_3$ by mass spectroscopy, however this attempt was not successful.

As an alternative to the detection of plasma $1,25D_3$, the expression of the enzymes responsible for its production, Cyp27b1, and degradation, Cyp24a1, were analysed. Also, the activity of $1,25D_3$ was indirectly analysed through the assessment of the expression of its receptor, VDR, which is susceptible to regulation by $1,25D_3$ (Healy et al. 2003). The expression of Cyp27b1, Cyp24a1 and VDR was analysed in the kidney, since the kidney is the organ where $1,25D_3$ is primarily produced and one of the organs where $1,25D_3$ signalling contributes to mineral ion homeostasis. The expression of Cyp27b1 and Cyp24a1 mRNA was assessed by qPCR and the expression of VDR mRNA and protein was quantified by qPCR, IHC and Western blotting.

By qPCR, Cyp27b1 mRNA expression was increased in animals treated with ERKi (25-fold) or FGFRi (10-fold) for 6h (Figure 3.6 A) or ERKi (103-fold) for 3d (Figure 3.6 C). Conversely, no significant increases in Cyp27b1 mRNA expression were observed in animals treated with FGFRi for 8d (Figure 3.6 C).

Cyp24a1 mRNA expression was decreased in animals treated with ERKi (31-fold) or FGFRi (18-fold) for 6h (Figure 3.6 B) or with ERKi (23-fold) for 3d (Figure 3.6 D). Conversely, no significant decreases in Cyp24a1 mRNA expression were observed in animals treated with FGFRi for 8d (Figure 3.6 D).

By IHC, VDR protein was detected in glomerular podocytes, PT, DT and CD in and cytoplasm of DT (Figure 3.7 D,G). By qPCR, IHC and Western blotting, decreases in both VDR mRNA and protein expression were observed in animals treated with ERKi (-35% mRNA, -50% protein) or FGFRi (-40% mRNA, -50% protein) for 6h (Figure 3.7 An mRNA; Figure 3.7 C,E-F protein) or with ERKi (-40% mRNA, -65% protein) for 3d (Figure 3.7 B mRNA; Table 7.10 protein). Animals treated with FGFRi for 8d showed a small decrease in mRNA (-19%, Figure 3.7 B), but not in protein expression (Table 7.10). By IHC, no changes in VDR protein expression were observed in animals dosed MEKi for 8d (Table 7.10). Conversely, increases in VDR protein expression were observed in animals treated with MEKi (150%) or FGFRi (43%) for 25/28d (Figure 3.7 H-I).

No changes in $1,25D_3$ were detected following MEKi treatment – However it was observed that the $1,25D_3$ radioimmunoassay displayed a high variability.

Treatment with ERKi for 6h or 3d or FGFRi for 3d resulted in the increase of Cyp27b1 and decrease of Cyp24a1 mRNA expression, consistent with the increased production of $1,25D_3$ – these effects were not observed following the 8d treatment with FGFRi

Treatment with ERKi for 6h or 3d or FGFRi for 3d resulted in a decrease in VDR expression. Conversely, VDR expression remained unchanged following 8d with MEKi or FGFRi and increased following 28d treatment with these inhibitors.
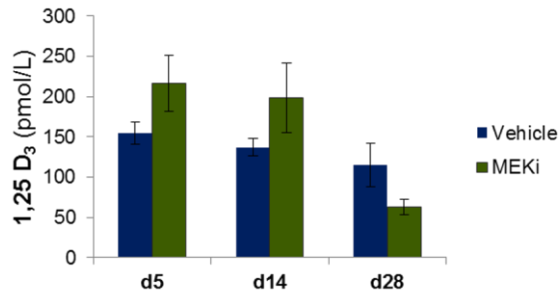
Figure 3.5: Plasma concentrations of 1,25D$_3$ in animals treated for 5, 14 or 28 days with 1.4 mg/kg/day of MEKi. Plasma 1,25D$_3$ concentrations in animals from study 1. Data representative of $N = 5$ rats + SEM. Plasma concentrations of Ca^{2+}, Pi and Mg^{2+} were analysed by the Clinical Pathology department at AstraZeneca UK
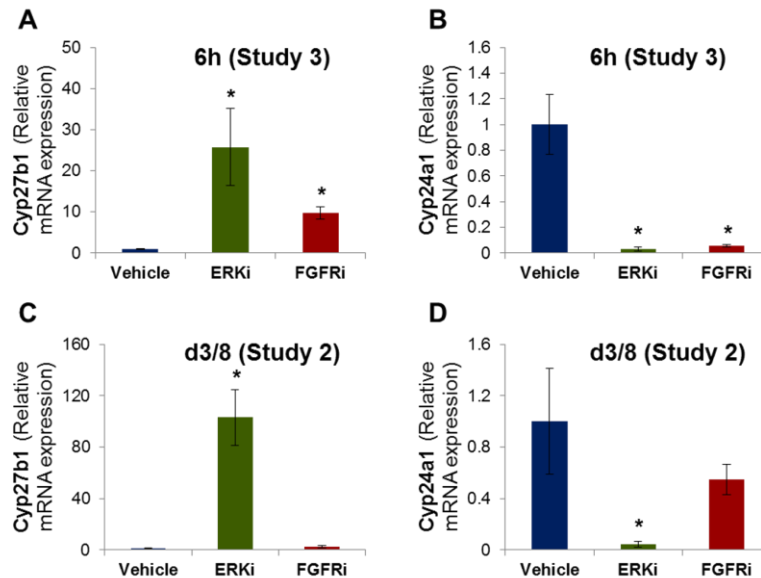
Figure 3.6: Expression of Cyp27b1 and Cyp24a1 mRNA in kidneys from rats treated with 150 mg/kg/day of ERKi or 20 mg/kg/day of FGFRi. Cyp27b1 (A, C) and Cyp24a1 (B,D) mRNA quantified by qPCR in kidney extracts of rats from the studies 3 (A,B) and 2 (C,D), dosed with vehicle, ERKi or FGFRi for respectively 3/8d or 6h. Data representative of $N = 3$-6 rats + SEM. * $p < 0.05$ vs the vehicle control (Mann-Whitney).
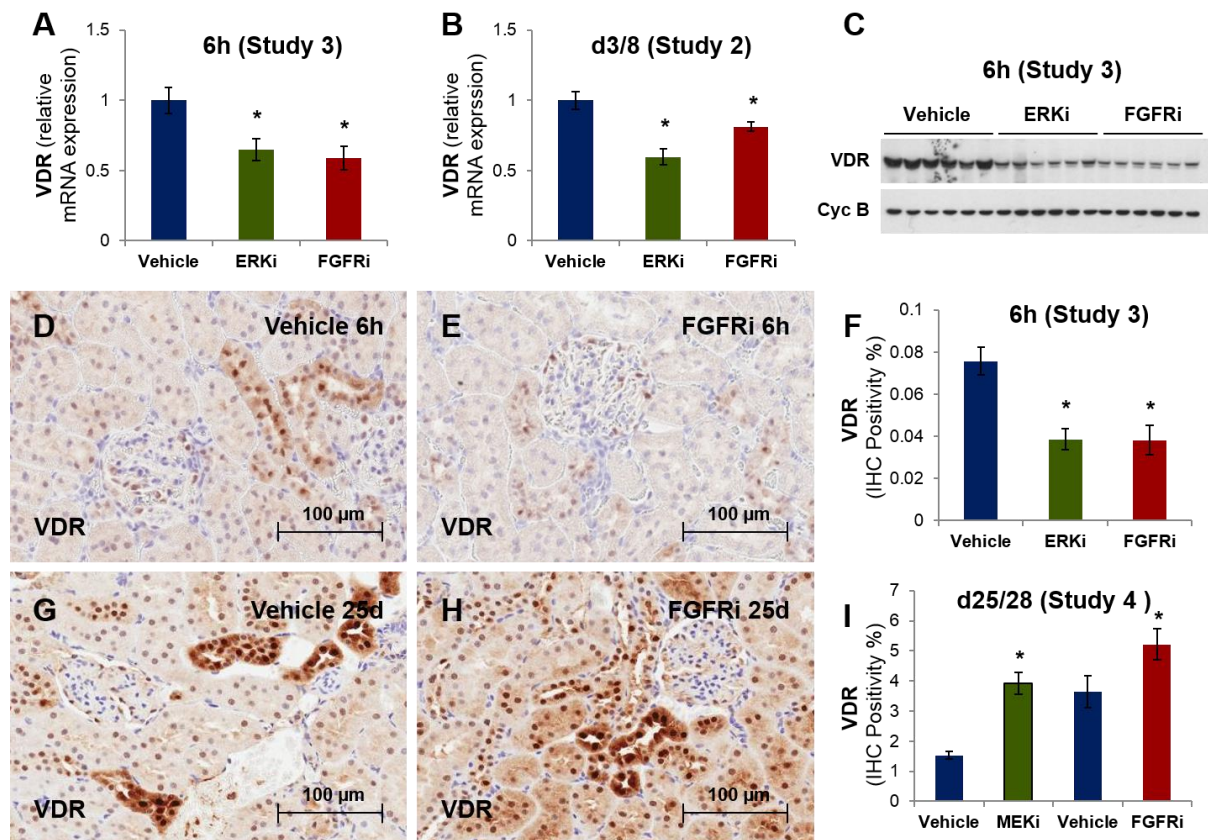
Figure 3.7: Expression of VDR mRNA and protein in kidneys from rats treated with 150 mg/kg/day of ERKi or 20 mg/kg/day of FGFRi. VDR mRNA was quantified by qPCR in kidney extracts of rats from the studies 3 (A) and 2 (B), dosed with vehicle, ERKi or FGFRi for respectively 6h or 3/8d. VDR protein analysed by Western blotting in animals from Study 3 (C). Photomicrographs of VDR immunostaining in sections of rats from study 3, dosed with vehicle (D) and FGFRi (E) for 6h; and study 4, dosed with vehicle (G) or FGFRi (H) for 25d. Positive signal in immunohistochemistry corresponds to the brown staining. Histograms represent the quantification of VDR expression (immunohistochemically stained area) in animals from the studies 3 (F) and 4 (I). Data representative of $N = 3$-6 rats + SEM. * $p < 0.05$ vs the vehicle control (Mann-Whitney). Scale bar = 100 μm.

3.4.4 Effect of ERK, MEK and FGFR inhibition on the plasma levels of FGF23 and PTH

Plasma levels of FGF23 were analysed at different time points in animals treated with ERKi for 6h or 3d, MEKi for 8d or FGFRi for 6h or 8d (Figure 3.8) using an enzyme-linked immunosorbent (ELISA) assay. All the compounds caused an initial decrease in FGF23, reaching a 3-fold decrease around 6h after dosing. FGF23 levels remained decreased after 3d dosing with ERKi. Conversely, longer dosing periods with MEKi (7d) and FGFRi (4/7d) induced a 4-10 fold increase in FGF23 levels.

Plasma levels of PTH were analysed in terminal samples from animals dosed for 8d with MEKi or FGFRi (Figure 3.9) using a multiplex assay. No changes in PTH were observed following treatment with either of the inhibitors. Nevertheless, it was observed that the results showed high variability within each group, which suggests that the assay may have a low sensitivity or samples were not adequately processed. For these reasons, the assay was not performed in samples from animals treated with ERKi (samples from animals treated with ERKi were processed using a similar protocol as samples from animals treated with MEKi or FGFRi).

Plasma FGF23 levels initially decrease (2-6h) following the administration of ERKi, MEKi or FGFRi. Conversely, following repeated dosing (>4d) with MEKi or FGFRi, FGF23 levels increase.

PTH remained unchanged in animals treated with MEKi or FGFRi
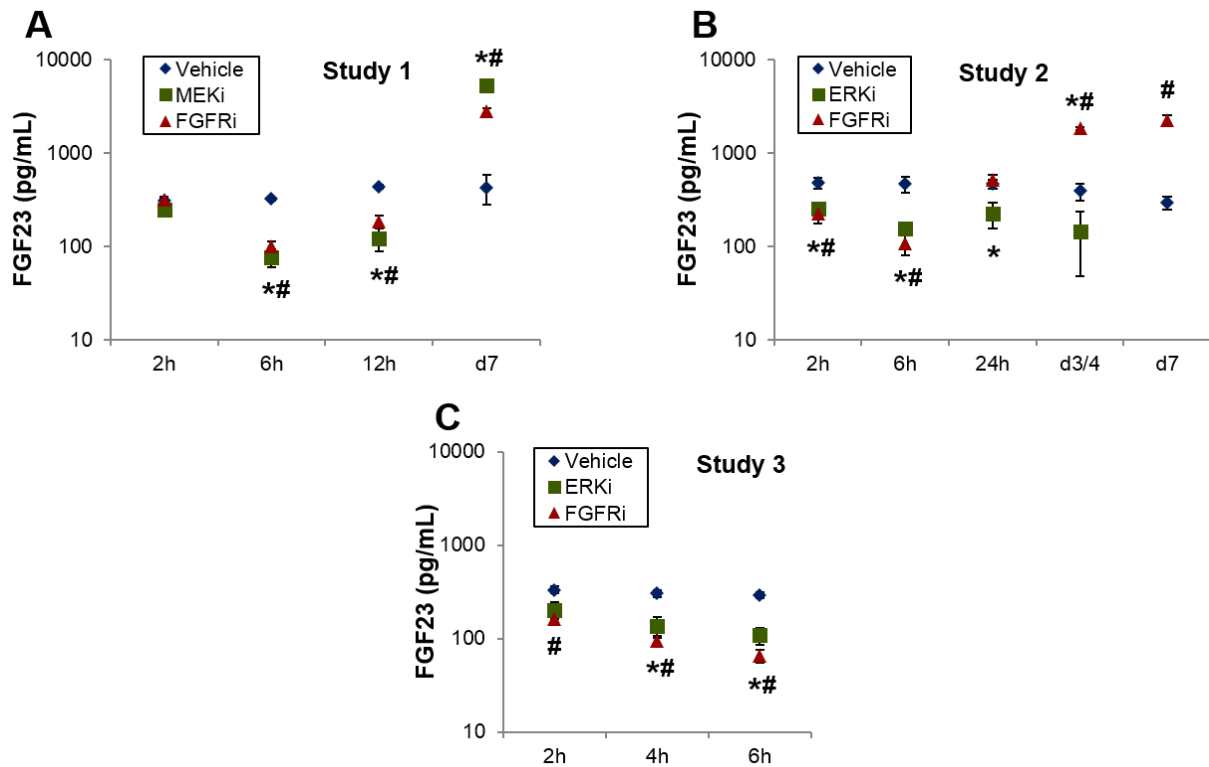
Figure 3.8: Plasma concentrations of FGF23 in animals treated with 150 mg/kg/day of ERKi, 1.4 mg/kg/day of MEKi or 20 mg/kg/day FGFRi. Plasma FGF23 concentrations in animals from the Studies 1 (A), 2 (B) and 3 (C). Data representative of N = 3-6 rats + SEM. * # $p<0.05$ (Mann Whitney - * vehicle vs MEKi/ERKi, # vehicle vs FGFRi). Plasma concentrations of FGF23 were analysed by the Clinical Pathology department at AstraZeneca UK.
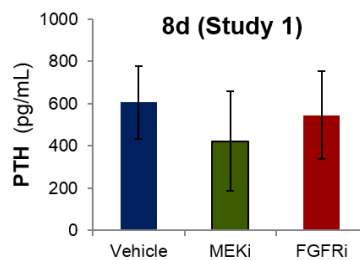
Figure 3.9: Plasma concentrations of PTH in animals treated for 8 days with 1.4 mg/kg/day of MEKi or 20 mg/kg/day FGFRi. Plasma PTH concentrations in animals from study 1. Data representative of N = 3-6 rats + SEM. Plasma concentrations of PTH were analysed by the Clinical Pathology department at AstraZeneca UK.

3.4.5 Summary

Treatment with ERKi, MEKi and FGFRi resulted in soft-tissue mineralization in rats. In addition, these inhibitors induced an increase in plasma levels of Pi and affected the production/expression of the hormones $1,25D_3$ and FGF23. The effects of ERKi, MEKi and FGFRi in mineral homeostasis were dependent upon the duration of the treatment, as evidenced by the differences in the expression of Pi, $1,25D_3$ and FGF23 following the first dose (>6h) and during the repeated-dosing phase (>3d) of the studies. At 6h post-dosing, ERKi, MEKi and FGFRi induced a decrease in plasma levels of FGF23 and an increase in the production of $1,25D_3$ (estimated in animals treated with ERKi and FGFRi through the assessment of the expression of Cyp27b1 and Cyp24a1). These effects preceded the increase in Pi, which was only observed at 12h/24h post-dosing. Opposite to the effects observed at 6-12h post-dosing, the administration of MEKi or FGFRi for >4d induced an increase in the plasma levels of FGF23 and in no changes in the expression of Cyp27b1 and Cyp24a1.

Table 3.5 shows the common effects of ERKi, MEKi and FGFRi in plasma levels of Pi and FGF23 and the effects of ERKi or FGFRi in the renal expression of Cyp27b1 and Cyp24a1 at 6h, 12/24h, 3d/4d and 7d/8d of the treatment period.

Table 3.6 summarizes the effects of ERKi, MEKi and FGFRi in the mineralization of soft-tissues, plasma levels of the ions Ca^{2+}, Pi, Mg^{2+}, plasma levels of the hormones $1,25D_3$, FGF23 and PTH and renal expression of the genes/proteins Cyp27b1, Cyp24a1 and VDR.

Table 3.5: Summary of the effects of ERKi, MEKi and FGFRi on Pi, FGF23, Cyp27b1 and Cyp24a1 following different treatment periods with the inhibitors.

	Drug	6h	12h/24h	3d/4d	7d/8d
Pi	ERKi, MEKi or FGFRi	=	+	+	+
FGF23		-	-	+[1]	+
Cyp27b1	ERKi or FGFRi	+	NA	+ (ERKi)	+ (FGFRi)
Cyp24a1		-	NA	- (ERKi)	- (FGFRi)

1 – FGF23 levels were remained unchanged in animals treated with ERKi for 24h

Table 3.6: Summary of the effects of ERKi, MEKi and FGFRi in the occurrence of soft-tissue mineralization and mineral homeostasis.

	Method	Dosing	ERKi	MEKi	FGFRi
Mineralization	von Kossa	6h	-	-	-
		d3/8[1]	+	+	+
Calcium	Roche P analyser	6h	=	=	=
		d3/8	=	=	=
Phosphate	Roche P analyser	6h	=	=	=
		d3/8	+	+	+
Magnesium	Roche P analyser	6h	=	=	=
		d3/8	=	=	=
1,25D$_3$	RIA	6h	NA	NA	NA
		d3/8	NA	=[2]	NA
Cyp27b1	qPCR	6h	+	NA	+
		d3/8	+	NA	=
Cyp24a1	qPCR	6h	-	NA	-
		d3/8	-	NA	=
VDR	qPCR / IHC / Western	6h	-	NA	-
		d3/8	-	=	=
FGF23	ELISA	6h	-	-	-
		d3/8	=	+	+
PTH	Luminex	6h	NA	NA	NA
		d3/8	NA	=	=

1 – At this time point, mineralization is observed in other organs than kidney in animals treated with ERKi and MEKi.

2 – 1,25D$_3$ values showed high variability between animals of the same group, suggesting a low sensitivity of the method

3.5 Results - Effects of ERKi, MEKi and FGFRi in the activation of cell signalling pathways in the kidney

3.5.1 *Expression of Fibroblast Growth Factor Receptors*

As described in the introduction, the kidney likely has a key role in the mineralization induced by MEK/ERK or FGFR inhibition, since it is the organ where $1,25D_3$ is mainly produced and where Ca^{2+} and Pi are reabsorbed from urine. Moreover, these processes are susceptible of regulation by FGF23 signalling through the FGFRs and MEK/ERK pathway (Andrukhova et al. 2012, Andrukhova et al. 2014). Hence, it is possible that MEK/ERK or FGFR inhibition affect the production of $1,25D_3$ and reabsorption of Ca^{2+} and Pi by preventing the regulatory effects of FGF23 in these processes.

The intra-renal distributions of ERK, MEK, FGFR1-4 and Klotho are currently unclear as the reports of the localization of these proteins available in the literature are inconsistent. In order to identify which parts of the nephron could be directly affected by ERKi, MEKi or FGFRi, the distribution patterns of ERK, FGFR 1-4 and Klotho mRNA and protein and MEK protein were analysed in rat kidney by *in situ* hybridization and immunohistochemistry.

Generally, a comparable expression pattern was detected with both techniques. FGFR 1 (Figure 3.10 A-B) was detected throughout the nephron, showing strong apical membrane expression in PT, DT and CD and weak staining in the glomerulus. FGFR 2 (Figure 3.10 C-D) and FGFR 3 (Figure 3.10 E-F) were detected in the basolateral membrane of DT and CD and to a lower extent in the apical membrane of PT and in the glomerulus. FGFR4 (Figure 3.10 G-H) was detected in the PT and DT, displaying a punctuate pattern in the cytoplasm. Klotho was detected in the cytoplasm, basolateral and apical membrane of PT, DT and CD, with the stronger expression observed in a population of DT cells (Figure 3.11). ERK (Figure 3.12 A,C) and MEK (Figure 3.12 E) were detected throughout the nephron, showing a cytoplasmic and nuclear (ERK) staining pattern. Conversely, phospho-ERK (Figure 3.12 D) and phospho-MEK (Figure 3.12 F) were detected predominantly in nuclei from DT and CDs, and, in very low levels in the PT. These results show a broad distribution of FGFR 1-4, Klotho, ERK and MEK in the kidney. A summary of the mRNA and protein

distribution of FGFR1-4, ERK, phospho-ERK, MEK and phospho-MEK is shown on Table 3.7.

The FGF receptors, Klotho, MEK and ERK are expressed throughout the nephron.

Some expression differences are evident between the different FGFRs such as the polarity and intensity of the immunoreactivity in the different nephron segments.
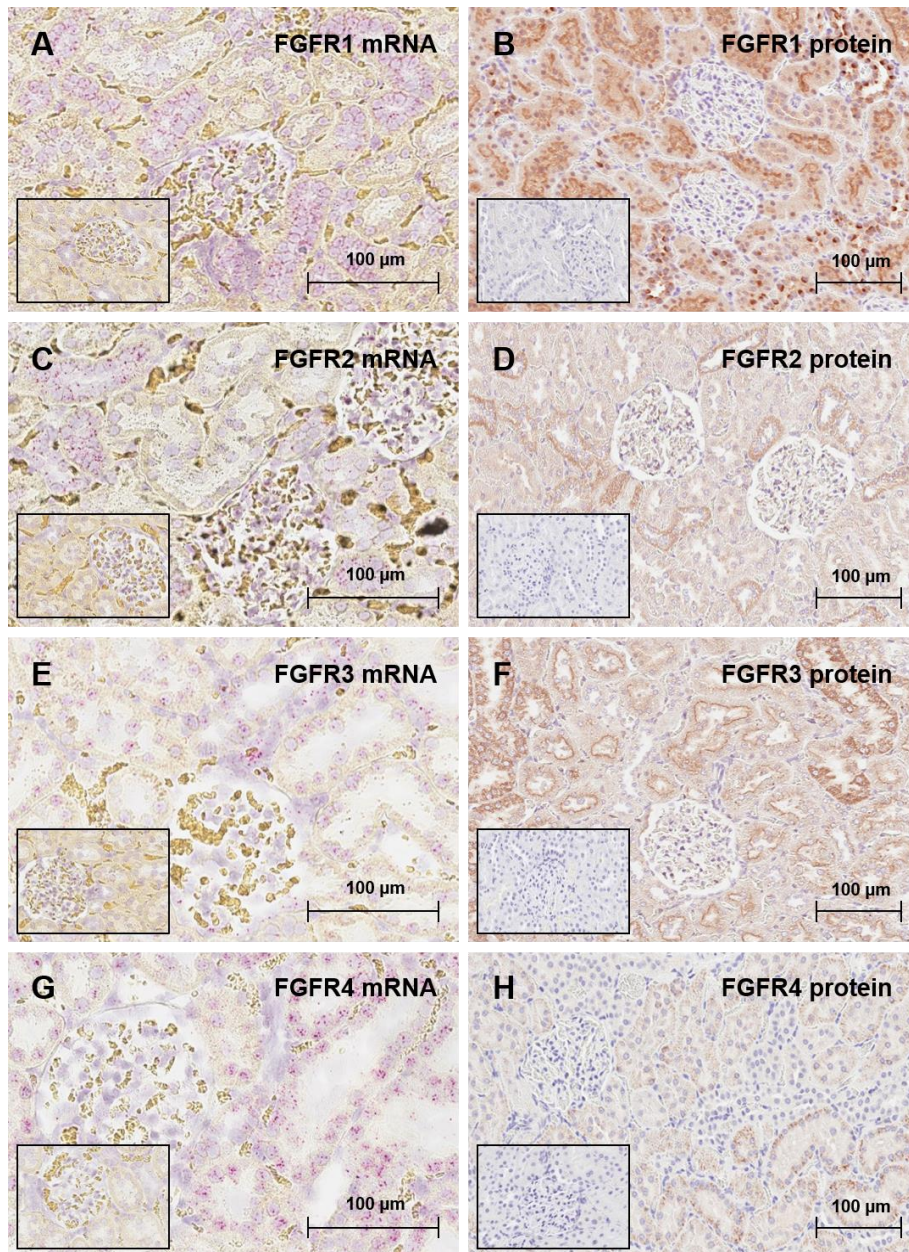
Figure 3.10: Expression of FGFRs 1-4 in the kidney cortex of control rats detected by *in situ* hybridization and immunohistochemistry. mRNA (A,C,E,G) and protein (B,D,F,H) expression patterns of FGFR 1 (A,B), FGFR 2 (C,D), FGFR 3 (E,F) and FGFR4 (G,H). Positive signal is indicated by the purple (FGFRs) staining in *in situ* hybridization and by the brown staining in immunohistochemistry. The square in the bottom left corner of each image shows the negative control. Scale bar = 100 µm**.**
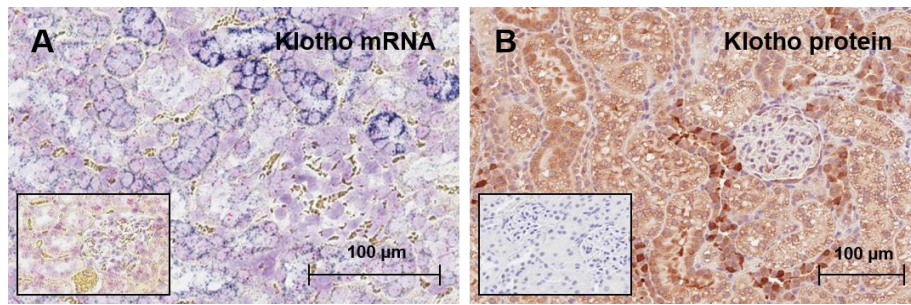
Figure 3.11: Expression of Klotho in the kidney cortex of control rats detected by *in situ* hybridization and immunohistochemistry. Positive signal is indicated by the purple staining by *in situ* hybridization (A) and by the brown staining in immunohistochemistry (B). The square in the bottom left corner shows the negative control. Scale bar = 100 μm.
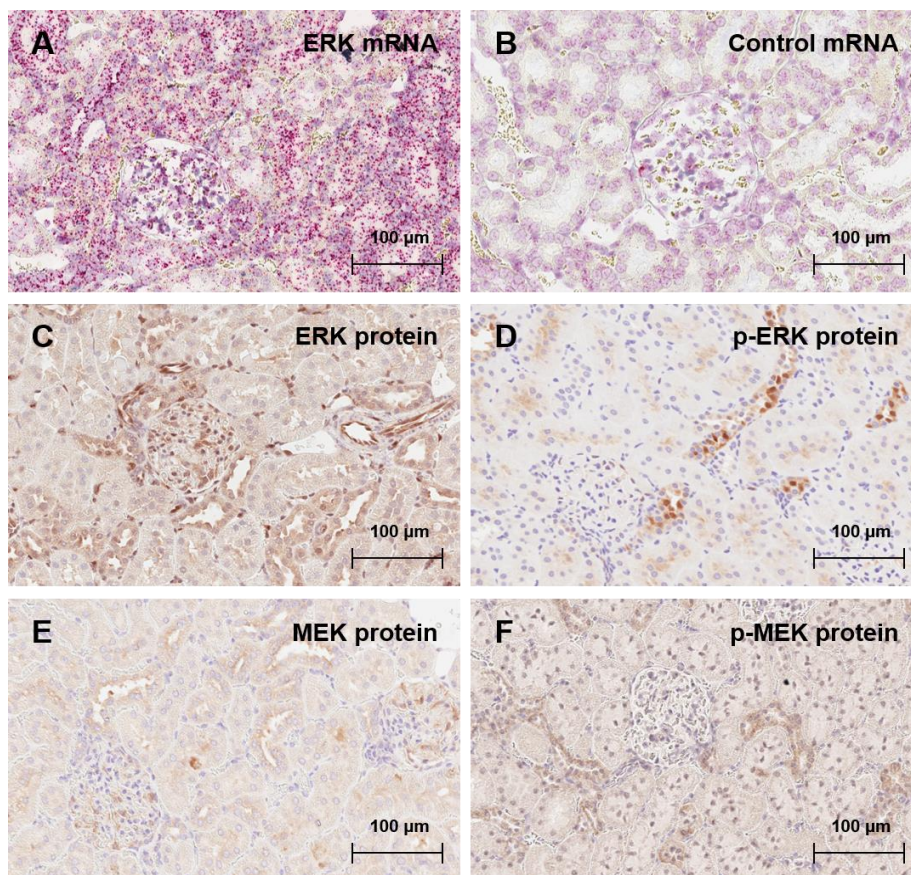
Figure 3.12: Expression of phospho- and total ERK and MEK in the kidney cortex of control rats detected by *in situ* hybridization and immunohistochemistry. mRNA (A,B) and protein (C,D,E,F) expression patterns of total ERK (A,C), control (B), phospho-ERK (p-ERK, D), total MEK (E) and phospho-MEK (p-MEK, F). Positive signal is indicated by the purple (FGFRs) staining in *in situ* hybridization and by the brown staining in immunohistochemistry. Scale bar = 100 μm**.**

Table 3.7: Summary of the distribution of FGFR1-4, Klotho, ERK, phospho-ERK, MEK and phospho-MEK mRNA and/or protein.

		Glomerulus	PT	TAL	DT	CD
FGFR1	ISH	+	++	++	++	++
	IHC	+	++ / a	++ / a	++ / a	++ / a
FGFR2	ISH	+	+	++	++	++
	IHC	+	+ / a	++ / b	++ / b	++ / b
FGFR3	ISH	-	+	++	++	++
	IHC	-	+ / a	++ / b	++ / b	++ / b
FGFR4	ISH	-	+	++	++	-
	IHC	-	+ / c	++ / c	++ / c	-
Klotho	ISH	-	+	++	++	+
	IHC	-	+/ a,b,c	++ / a,b,c	++ / a,b,c	+ / a,b,c
ERK	ISH	++	++	++	++	++
	IHC	++	++ / c, n	++ / c, n	++ / c, n	++ / c, n
phospho -ERK	IHC	-	+ / n	++ / n	++ / n	++ / n
MEK	IHC	++	++ / c, n	++ / c, n	++ / c, n	++ / c, n
phospho -MEK	IHC	-	+ / n	++ / n	++ / n	++ / n

Apical (a), basolateral (b), cytoplasmic (c) or nuclear (n) immunoreactivity.

3.5.2 Effect of ERK, MEK and FGFR inhibition on the activation of the MEK/ERK signalling pathway

The activation of the ERK pathway was analysed in animals treated with ERKi and MEKi in order to confirm that both compounds effectively target the kidney. In addition, ERK activation was also analysed in animals treated with FGFRi in order to assess if this compound also inhibited the MEK/ERK pathway in the kidney. Phopho-ERK was not a suitable biomarker to assess ERK activation in animals treated with ERKi, since this compound does not prevent ERK from becoming phosphorylated. For this reason, in addition to phospho-ERK, the downstream proteins in the MEK/ERK pathway p90 ribosomal S6 kinase (RSK) and early growth response protein 1 (EGR1) were used as biomarkers to assess ERK activation.

By IHC and Western blotting, ERK phosphorylation was increased in animals dosed with ERKi for 6h (+15-fold, Table 7.13) or 3d (+15-fold, Figure 3.13 E-F,L), decreased in animals dosed with MEKi for 8d (-92%, Figure 3.13 B-C,K) or 28d (-61%, Table 7.13) and remained unchanged in animals treated with FGFRi for 6h (Table 7.13), 8d (Figure 3.13 C,F,K-L) or 25d (Table 7.13).

By IHC and Western blotting, total ERK levels were reduced in animals treated with ERKi for 3d (-87%, Figure 3.13 H,J,L). Also, by IHC total ERK levels were reduced in animals treated with FGFRi for 8d (-72%, Figure 3.13 I,J) in Study 2, however this effect was not evident by Western blotting (Figure 3.13 L). By IHC and Western blotting total ERK levels remained unchanged in animals treated with ERKi for 6h or MEKi or FGFRi for 6h, 8d (Study 1) or 25/28d (Figure 3.13 K, Table 7.14).

By IHC, phospho and total RSK were detected in glomeruli, TAL, DT, blood vessels smooth muscle and to less extent PT. Phospho-RSK (Figure 3.14 A) was expressed predominantly in the nucleus, with some cells also showing membrane and cytoplasmic expression. Total RSK (Figure 3.14 D) was detected mainly in the cytoplasm. The expression of both phospho- (Figure 3.14 A-C, Table 7.15) and total RSK (Figure 3.14 D-F, Table 7.16) was highly variable from animal to animal and although it appears to be generally decreased in animals treated with ERKi, MERKi or FGFRi, due to the high variability between samples it was not possible to obtain any meaningful conclusions. These data suggests that phospho-RSK is not a sensitive biomarker for ERK activation.

By IHC, EGR1 was detected in the nuclei of cells from glomeruli, distal nephron and blood vessels (Figure 3.15 A,D). Expression of EGR1 was strongly decreased in animals treated with ERKi for 6h (-84%, Table 7.17) or 3d (-74%, Figure 3.15 E-F) or MEKi for 8d (-70%, Figure 3.15 B-C). Conversely, EGR1 expression remained unchanged in animals treated with FGFRi for 6h (Table 7.17) and it was increased in animals treated for 8d with FGFRi (+84%, Figure 3.15 F).

The results obtained for the expression/activation of ERK, RSK and EGR1 suggest that FGFRi treatment does not result in the inhibition of the MEK/ERK pathway in the kidney. As FGFR inhibition has been previously described to reduce the phosphorylation of ERK in the kidney (Yanochko et al. 2013), I aimed to assess if the administration of FGFRi was able to effectively inhibit FGFR signalling in the kidney. Previous studies carried out at AstraZeneca UK have shown that the FGFRi treatment is able to prevent the phosphorylation of the FGFRs and the phosphorylation of the downstream signalling protein FRS2 in to tumour cell models (AstraZeneca UK unpublished data). Since no methods to detect phospho-FGFR and phospho-FRS2 in rat kidney were previously reported, I evaluated the suitability of three antibodies against phospho-FGFR (pan), phospho-FGFR3 and phospho-FRS2 alpha using IHC and Western blotting techniques in control rat kidney tissue. No immunoreactivity was detected for the phospho-FGFR (pan) and phospho-FRS2 alpha antibodies with either of the methods and for the phospho-FGFR3 antibody with Western blotting (not shown). Conversely, weak immunoreactivity was detected mainly in the DT by IHC with the phospho-FGFR3 antibody (Figure 3.16). Unfortunately, this method showed high variability between samples and high background signal, which resulted in a low signal/background ratio. The low sensitivity of the IHC and the inability to confirm the identity of the detected proteins by Western blotting deemed this method unsuitable to assess the activation of FGFRs. Due to the lack of a suitable method to detect the expression of phospho-FGFR or phospho-FRS2 in rat kidney, it was not possible to confirm the inhibition of the FGFRs by FGFRi.

ERK pathway signalling is inhibited by ERKi and MEKi, but not FGFRi.

Total ERK expression is reduced by ERKi, but not MEKi or FGFRi.

It was not possible to obtain a method to assess FGFR activation.
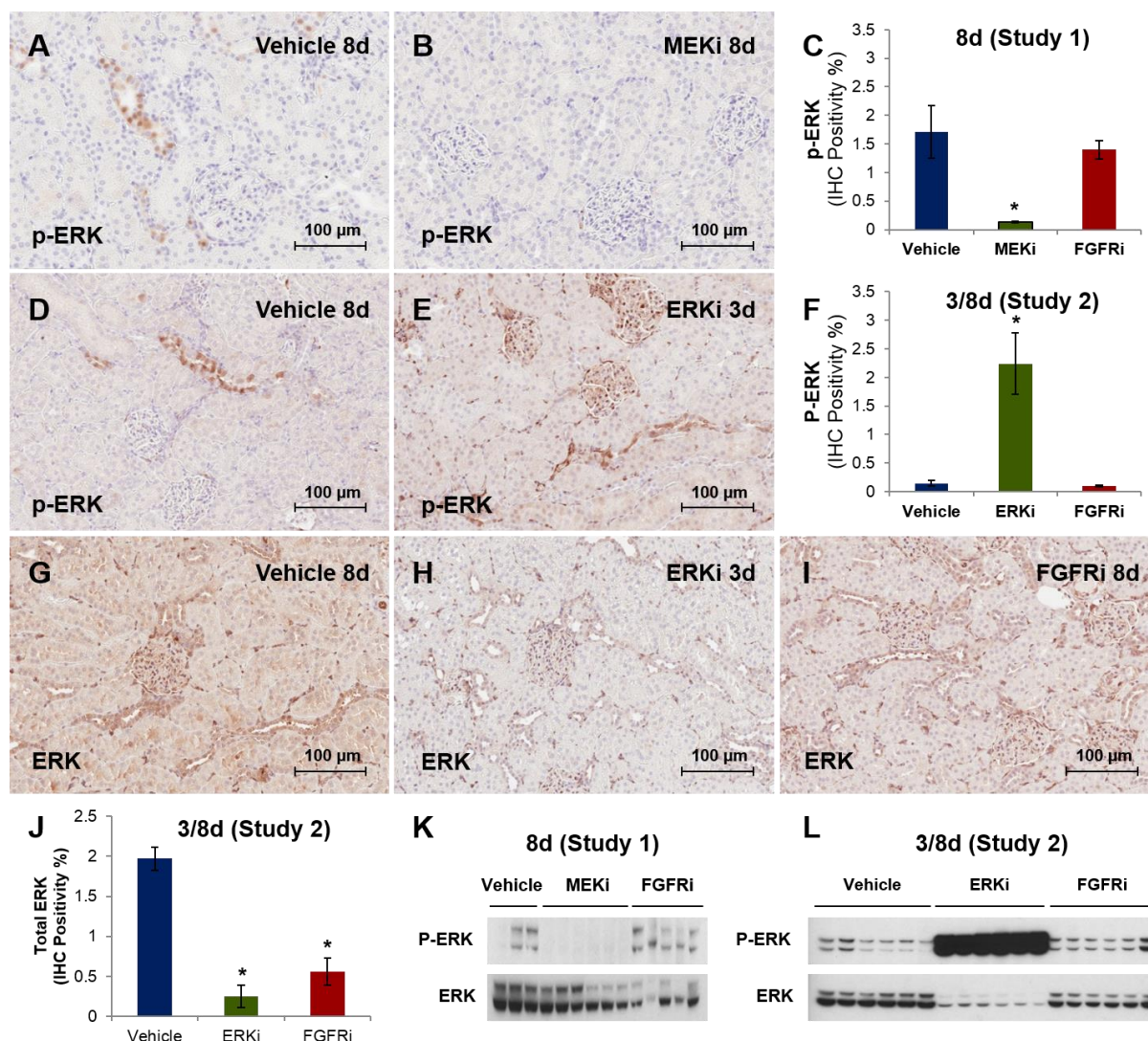
Figure 3.13: Expression of phospho-ERK and ERK protein in kidneys from rats treated with 150 mg/kg/day of ERKi, 1.4 mg/kg/day of MEKi or 20 mg/kg/day of FGFRi. Photomicrographs of phospho-ERK (p-ERK) immunostaining in sections of rats from study 1 dosed with vehicle (A) or MEKi (B) for 8d; and study 2, dosed with vehicle (D) for 8d or ERKi (E) for 3d. Photomicrographs of total ERK immunostaining in sections of rats from study 2 dosed with vehicle (G) for 8d, ERKi (H) for 3d or FGFRi for 8d (I). Positive signal in immunohistochemistry is visible as brown staining. Histograms represent the quantification of phospho-ERK expression (immunohistochemically stained area) in animals from the studies 1 (C) and 2 (F) and the expression of total ERK in the study 2 (J). Phospho-ERK and ERK analysed by Western blotting in animals from the studies 2 (K) and 3 (L). Data representative of N = 3-6 rats + SEM. * p<0.05 vs the vehicle control (Mann-Whitney test). Scale bar = 100 μm.
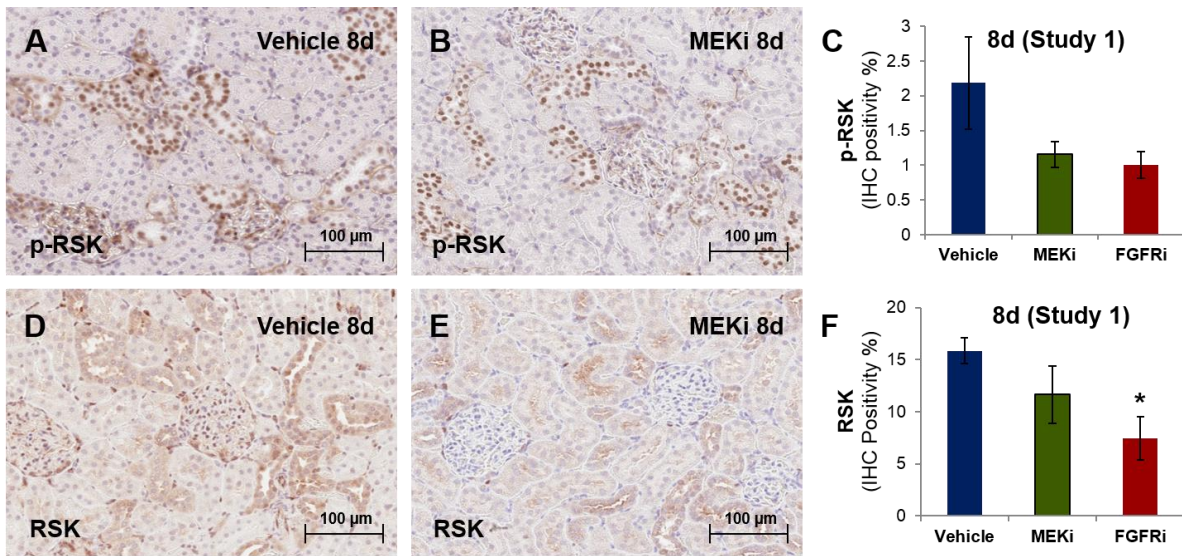
Figure 3.14: Expression of phospho-RSK and RSK protein in kidneys from rats treated with 150 mg/kg/day of ERKi or 20 mg/kg/day of FGFRi. Photomicrographs of phospho-RSK (p-RSK) immunostaining in sections of rats from study 1 dosed with vehicle (A) or MEKi (B) for 8d. Photomicrographs of total RSK immunostaining in sections of rats from study 1 dosed with vehicle (D) or MEKi (E) for 8d. Positive signal in immunohistochemistry corresponds to the brown staining. Histograms represent the quantification of phospho-RSK (C) and total RSK (F) expression (immunohistochemically stained area) in animals from study 1. Data representative of $N = 3\text{-}6$ rats + SEM. * $p < 0.05$ vs the vehicle control (Mann-Whitney test). Scale bar = 100 µm.
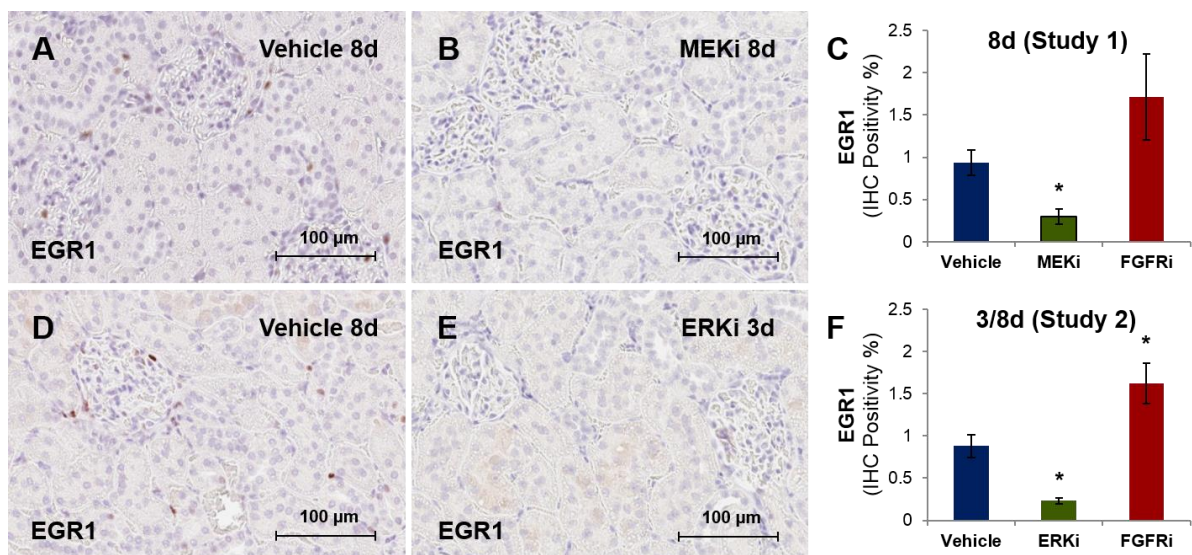
Figure 3.15: Expression of EGR1 in cortical kidney sections from rats treated with 150 mg/kg/day of ERKi, 1.4 mg/kg/day of MEKi or 20 mg/kg/day of FGFRi. Photomicrograph of EGR1 immunostaining in sections of rats from study 1 dosed with vehicle (A) or FGFRi (B) for 8d; and from study 2 dosed with vehicle (D) for 8d or ERKi (E) for 3d. Positive signal in immunohistochemistry corresponds to the brown staining. Histograms represent the quantification of EGR1 expression (immunohistochemically stained area) in animals from the studies 1 (C) and 2 (F). Data representative of N = 3-6 rats + SEM. * $p<0.05$ vs the vehicle control (Mann-Whitney test). Scale bar = 100 µm.
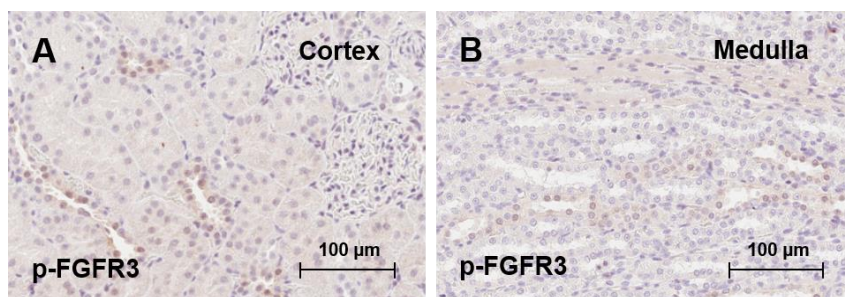
Figure 3.16: Expression of phospho-FGFR3 in control rat kidney. Photomicrographs of phospho-FGFR3 (p-FGFR3) immunostaining in cortical (A) and medullary (B) rat kidney sections. Positive signal in immunohistochemistry corresponds to the brown staining. Scale bar = 100 µm.

3.5.3 Effects of ERK and FGFR inhibition on cell signalling in the kidney.

Although treatment with FGFRi did not result in the inhibition of ERK signalling, it resulted in similar effects in mineral homeostasis as treatments with ERKi and MEKi. It is plausible that the three inhibitors induce these effects through the activation or inhibition of common downstream cell signalling pathways. In order to identify signalling pathways affected by ERKi and FGFRi that may contribute to the process of soft-tissue mineralization, the expression of 60 cell signalling pathway proteins was analysed by RPPA using kidneys of animals treated for 6h with these inhibitors (Table 3.8).

By RPPA, phospho-ERK expression was increased in animals treated with ERKi (+331%) and remained unchanged in animals treated with FGFRi, whilst total ERK expression remained unchanged in animals treated with either of the inhibitors. These results are consistent with the expression of phospho-ERK and ERK observed by IHC and Western blotting. Besides the mentioned increase in phospho-ERK, all the alterations in protein expression and/or activation were small (<40% expression change), which suggests that this assay may have failed to identify the key pathways contributing to process of ERKi and FGFRi induced mineralization. Nevertheless, the noteworthy findings of this assay are described below. In order to ensure that the common effects of ERKi and FGFRi on cell signalling are identified by this assay despite their small nature, two different thresholds were considered in the statistical analysis, $p < 0.05$ and $p < 0.10$.

- The downstream MEK/ERK pathway proteins MNK1 and cAMP response element-binding protein (CREB) show decreased activation following treatment with ERKi ($p < 0.1$) and FGFRi ($p < 0.05$).

- The downstream FGFR signalling protein PLC gamma shows decreased activation following treatment with ERKi ($p < 0.1$) and FGFRi ($p < 0.05$).

- FGFRi increased the expression ($p < 0.05$) and both inhibitors increased inhibitory phosphorylations ($p < 0.05$) of beta-catenin – a downstream component of the WNT signalling pathway previously described to be involved in soft-tissue mineralization processes.

- FGFRi increased the expression of poly ADP ribose polymerase (PARP) ($p < 0.05$) and both inhibitors increased the expression of B-cell lymphoma-x (Bcl-x) ($p < 0.05$). These two proteins are key regulators of the apoptotic process.

- FGFRi, but not ERKi prevents the activation of a number of downstream proteins in FGFR signalling including Src ($p < 0.05$) (Li et al. 2004) and mitogen-activated protein kinase-activated protein kinase 2 (MAPKAPK-2) ($p < 0.05$) (Tan et al. 1996).

Neither of the inhibitors affected the activation of a number cell signalling proteins including c-Jun N-terminal kinase (JNK), AKT, nuclear factor kappa-light-chain-enhancer of activated B cells (NFkB) and p38 – most likely these proteins are not involved in the process of mineralization induced by ERKi and FGFRi.

RPPA showed similar results as IHC and Western blotting for the expression and phosphorylation of ERK in animals treated with ERKi and FGFRi

With the exception of phospho-ERK, the proteins analysed by RPPA showed small expression changes (<40% expression) in animals treated with ERKi and FGFRi, which suggests that the key pathways leading to soft-tissue mineralization were not identified by this assay.

By RPPA, ERKi and FGFRi were found to induce similar effects in the expression and/or phosphorylation of a number of proteins involved in different pathways including MEK/ERK, PLC and WNT.

By RPPA, FGFRi but not ERKi was found to decrease the activation of a number of downstream proteins in FGFR signalling

Table 3.8: RPPA performed in total kidney homogenate samples from rats treated for 6h with 150 mg/kg of ERKi or 20 mg/kg FGFRi.

	Akt	p-Akt	Bcl-x	β-Cat	p-β-Cat	Calpain2	CC3	p-Chk1	c-Jun	p-c-Jun	CREB	p-CREB	p-EGFR	EGFR	GSK-3β
ERKi	117*	100	112*	106	108*	103	104	102	95	101	88	88#	101	95	103
FGFRi	114	92#	125*	112*	126*	109	100	96	110	103	70*	86*	102	88*	107

	p-GSK-3β	p-IGF-1Rβ	p-IKK α/β	IRS-1	p-IRS-1	JAK1	MAPKAPK-2	p-MAPKA PK-2	MEK1/2	p-MEK1/2	p-MNK1	p-MSK1	mTOR	p-NFkB	p-p21
ERKi	111*	105	112#	101	100	104	92	95	91	105	91#	89	99	99	112
FGFRi	111#	114	105	106	98	119*	99	89*	91	91	91*	82#	100	98	119#

	p38	p-p38	ERK	p-ERK	PARP	p-PDGFR	p-PDK-1	PI3 K α	PKA	PKC-α	p-PKC	p-VEGFR	PLC-γ1	p-PLC-γ1	PTEN
ERKi	100	99	90#	431*	113	98	98	99	97	100	91	98	94	92#	99
FGFRi	105	81	96	90	123*	103	105	96	88#	94	89*	95	95	82*	99

	p-Raf 259	p-Raf 338	Raf1	Rap1	p-S6 Rib	JNK	p-JNK	p-Smad1/5	Src	P-Src	P-Tyk2	Ubiquitin	-	-	-
ERKi	92	113*	105	100	66	103	105	101	94	94	93	93	-	-	-
FGFRi	86*	110*	116*	95	61	113*	108	90	95	85*	98	95	-	-	-

Array results are presented as relative protein expression (%) versus the vehicle group, after normalization to beta actin expression. Data representative of $N = 6$ rats + SEM. * $p<0.05$ vs the vehicle control; # $p<0.10$ vs the vehicle control (Mann-Whitney test, expression increase in green and decrease in red). RPPA was performed at the Edinburgh Cancer Research Centre.

3.5.4 Effects of ERK, MEK and FGFR inhibition on WNT signalling.

The modest protein expression effects of ERKi and FGFRi detected by RPPA may develop into more pronounced effects at later timepoints and/or in the activation of downstream signalling proteins. Nevertheless, it is important to ensure that the effects observed are consistent and evident by other methods such as IHC and Western blotting. With the aim of validating the RPPA assay, IHC was carried out to analyse the expression of beta-catenin in samples from animals treated with ERKi or FGFRi. Beta-catenin was selected to perform this assay since in addition to showing increased expression by RPPA following treatment with FGFRi, this protein has been previously associated with the process of soft-tissue calcification (Gu et al. 2014).

By IHC, beta-catenin expression was observed with stronger intensity in TAL, DT and CD and with weaker intensity in PT and glomeruli (Figure 3.17 A,D). In all segments beta-catenin expression was detected mainly in the basolateral membrane and / or cytoplasm, but not in the nucleus. Treatment with ERKi, MEKi or FGFRi during 6h (Figure 3.17 A-C), 3/8d (Figure 3.17 D-F, Table 7.20) or 25/28d (Table 7.20) did not induce any evident changes in the expression or localization of beta-catenin. Nevertheless, the intensity of the immunoreactivity showed great differences between animals of the same groups, which may have prevented the detection of subtle protein expression changes.

By IHC, animals treated with ERKi, MEKi or FGFRi showed no evident alterations of the expression or cellular localization of beta catenin.

103
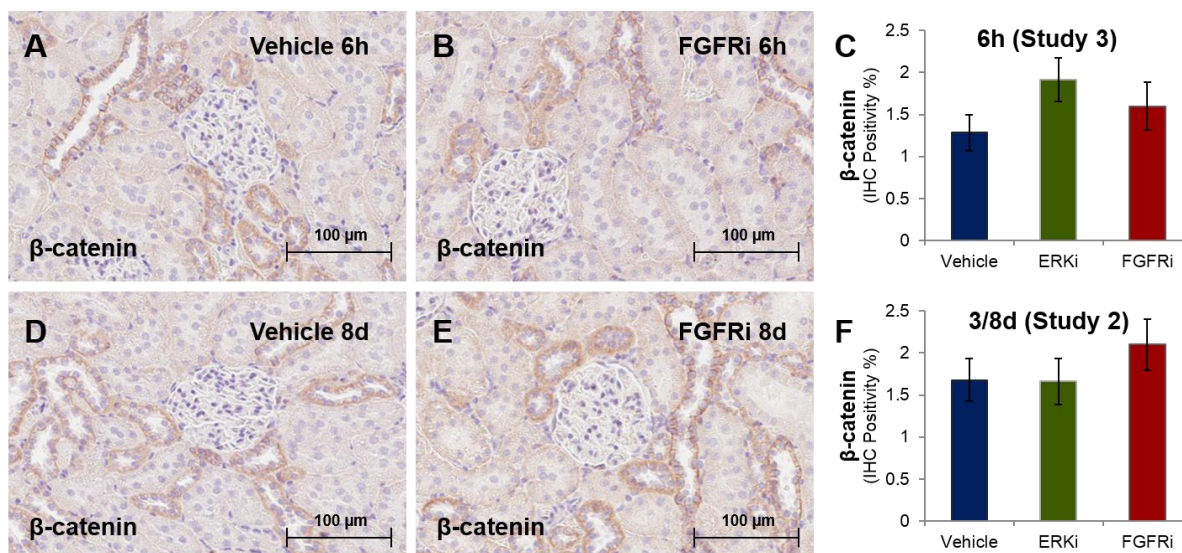
Figure 3.17: Expression of beta-catenin in cortical kidney sections from rats treated with 150 mg/kg/day of ERKi, 1.4 mg/kg/day of MEKi or 20 mg/kg/day of FGFRi. Photomicrographs of beta-catenin immunostaining in sections of rats from studies 3 dosed with vehicle (A) or FGFRi (B) for 6h; and from study 3 dosed with vehicle (D) or FGFRi (E) for 8d. Positive signal in immunohistochemistry corresponds to the brown staining. Histograms represent the quantification of beta-catenin expression (immunohistochemically stained area) in animals from the studies 3 (C) and 2 (F). Data representative of $N = 3$-6 rats + SEM. * $p < 0.05$ vs the vehicle control (Mann-Whitney test). Scale bar = 100 μm.

3.5.5 Summary

The targets of ERKi, MEKi and FGFRi, respectively ERK, MEK and the FGFRs, showed a broad intra-renal distribution, thus suggesting that these drugs may be able to directly affect different parts of the nephron. Analysis of ERK phosphorylation and EGR1 expression showed that the activation of the ERK pathway is effectively prevented by ERKi and MEKi but not by FGFRi. A RPPA used to identify downstream pathways that may contribute in soft-tissue mineralization showed small expression changes (<40% expression) in proteins involved in different signalling pathways including MEK/ERK, PLC and WNT. The effects of ERKi, MEKi and FGFRi in the activation of cell signalling pathways described in this subchapter are summarized in Table 3.9.

Table 3.9: Summary of the effects of ERKi, MEKi and FGFRi in the expression of phospho-ERK, ERK, phospho-RSK, RSK, EGR1, beta catenin.

	Method	Dosing	ERKi	MEKi	FGFRi
phospho-ERK	IHC / Western	6h	+	NA	=
		d3/8	+	-	=
ERK	IHC / Western	6h	=	NA	=
		d3/8	-	=	=
phospho-RSK[1]	IHC	6h	=	NA	=
		d3/8	=	=	=
RSK[1]	IHC	6h	=	NA	=
		d3/8	=	=	-
EGR1	IHC	6h	-	NA	=
		d3/8	-	-	=
Beta-catenin	IHC	6h	=	=	=
		d3/8	=	=	=

[1]The expression of phospho-RSK and RSK displayed a high variability.

3.6 Results - Effects of ERKi, MEKi and FGFRi on the expression of proteins involved in renal Ca^{2+} and Pi reabsorption

3.6.1 Effect of ERK, MEK and FGFR inhibition on the expression of proteins involved in renal Pi reabsorption

The expression of NaPi-IIa, the transporter that accounts for 60-70% of the renal Pi reabsorption (Wagner et al. 2008), was analysed by immunohistochemistry in rat kidney sections of animals treated with ERKi, MEKi or FGFRi in order to assess if the increase in plasma Pi induced by the administration of these inhibitors is associated with alterations in renal Pi reabsorption.

NaPi-IIa was detected in cytoplasmic vesicles and in the brush border of PT, with a comparable expression observed in the outer and inner cortical regions (A,D). ERKi, MEKi or FGFRi induced distinct effects in the expression pattern of NaPi-IIa, depending in the length of the treatment. Treatment with ERKi (Figure 3.18 B) or FGFRi (Figure 3.18 C) for 6h induced an increase a shift in NaPi-IIa expression from cytoplasmic vesicles to the brush border membrane. These effects correspond to changes in the protein expression pattern rather than pronounced changes in protein expression levels. Hence, although evident by observation of the immunostainings, these effects were not easily detected by image analysis. A slight decrease in NaPi-IIa expression was observed in rats treated with ERKi for 3d (Figure 3.18 G) or with FGFRi for 8d in Study 2 (Figure 3.18 E,G) or 25d (Figure 3.18 H). In these treatment groups, the expression decrease was detected in the outer cortex, with inner cortical immunoreactivity remaining unchanged or even slightly increased. Conversely, NaPi-IIa expression remained unchanged in animals treated with MEKi or FGFRi for 8d in Study 1 (Table 7.21) and was increased in the inner cortex of animals treated with MEKi for 8d (Figure 3.18 H). Nevertheless, animals from the vehicle group of the 28d study with MEKi showed a significantly lower outer cortical expression of NaPi-IIa when compared to the 8d study, which may have contributed for the discrepancies between the treatment groups.

Treatment with ERKi and FGFRi for 6h results in shift of NaPi-IIa expression from the cytoplasmic vesicles to the brush border membrane, consistent with increased reabsorption of Pi

Treatment with ERKi, MEKi and FGFR for >3d results in no changes or slight alterations of NaPiIIa expression pattern (decreased outer cortical expression and/or increased inner cortical expression), depending on the studies.

Figure 3.18: Expression of NaPi-IIa in cortical kidney sections from rats treated with 150 mg/kg/day of ERKi, 1.4 mg/kg/day of MEKi or 20 mg/kg/day of FGFRi. Higher magnification photomicrographs of NaPi-IIa immunostaining in sections of rats from study 3 dosed with vehicle (A), ERKi (B) or FGFRi (C) for 6h. Lower magnification photomicrographs of NaPi-IIa immunostaining in animals from study 2 dosed with vehicle (D) or FGFRi (E) for 8d. Positive signal in immunohistochemistry corresponds to the brown staining. Histograms represent the quantification of NaPi-IIa expression (immunohistochemically stained area) in animals from the studies 3 (F), 2 (G) and 4 (H). Data representative of $N = 3$-6 rats + SEM. * $p < 0.05$ vs the vehicle control (Mann-Whitney test). Scale bar = 100 μm.

3.6.2 Effect of ERK, MEK and FGFR inhibition on the expression of proteins involved in renal Ca^{2+} reabsorption

Renal Ca^{2+} reabsorption is induced by $1,25D_3$ (Johnson and Kumar 1994) and FGF23 (Andrukhova et al. 2014). In this study, despite the effects of ERKi, MEKi and FGFRi in the production of these hormones, plasma levels of Ca^{2+} remained mostly unaffected during the course of the treatments. Plasma Ca^{2+} levels are strictly regulated at a systemic level by different hormones including PTH and calcitonin (Felsenfeld et al. 2013) and by local actions of the CaSR in different organs such as such as bone (Theman and Collins 2009) and intestine (Garg 2013). For this reason, it is possible that $1,25D_3$ and/or FGF23 induce an increase in renal reabsorption and local Ca^{2+} levels whilst having little effects on the plasma Ca^{2+} levels. In order to assess if the inhibition of MEK/ERK pathway or FGFR signalling affects Ca^{2+} reabsorption, the expression of three proteins involved in the process (TRPV5, calbindin-D28k and PMCA) were analysed by IHC in animals treated with ERKi, MEKi or FGFRi.

By IHC, TRPV5 was detected in the apical membrane of DT (Figure 3.19 A,D,F). A decrease in TRPV5 expression was observed in animals dosed with ERKi (-51%, Figure 3.19 C) or FGFRi (-75%, Figure 3.19 B,C) for 6h or animals dosed with ERKi (60%,Figure 3.19 I) for 3d. Conversely, an increase in TRPV5 expression was observed in animals treated with MEKi (+10-fold, Figure 3.19 E-F) or FGFRi (+3-fold/4-fold, Figure 3.19 F,H-I) for 8d or animals treated with MEKi (+42%,Table 7.22) or FGFRi (+73%,Table 7.22) for 25/28d.

By IHC, calbindin-D28k was detected in the cytoplasm of DT (Figure 3.20 A,D). No changes in calbindin-D28k expression were found in animals treated with ERKi or FGFRi for 6h or ERKi for 3d (Table 7.23). Conversely, an increase in calbindin-D28k expression was observed in animals treated with MEKi (+182%, Figure 3.20 B,C) or FGFRi (+184%, Figure 3.20 E,F) for 8d or with MEKi (+89%, Table 7.23) or FGFRi (+57%, Table 7.23) for 25/28d.

By IHC, PMCA was detected in the basolateral membrane of DT (Figure 3.21 A). Expression of PMCA was unchanged in animals treated with ERKi or FGFRi for 6h, ERKi for 3d or FGFRi for 25d (Table 7.24) Conversely, expression of PMCA was

increased in animals treated with MEKi (+7.5-fold, Figure 3.21 B,C) or FGFRi (+3.5-fold, Figure 3.21 C) for 8d or with MEKi for 28d (+68%, Table 7.24)

Treatment with MEKi and FGFRi for >8d resulted in increased expression of the proteins involved in Ca^{2+} reabsorption TRPV5, calbindin-D28k and PMCA.

Treatment with ERKi for 6h or 3d or with FGFR for 6h resulted in a decrease in the expression of TRPV5.
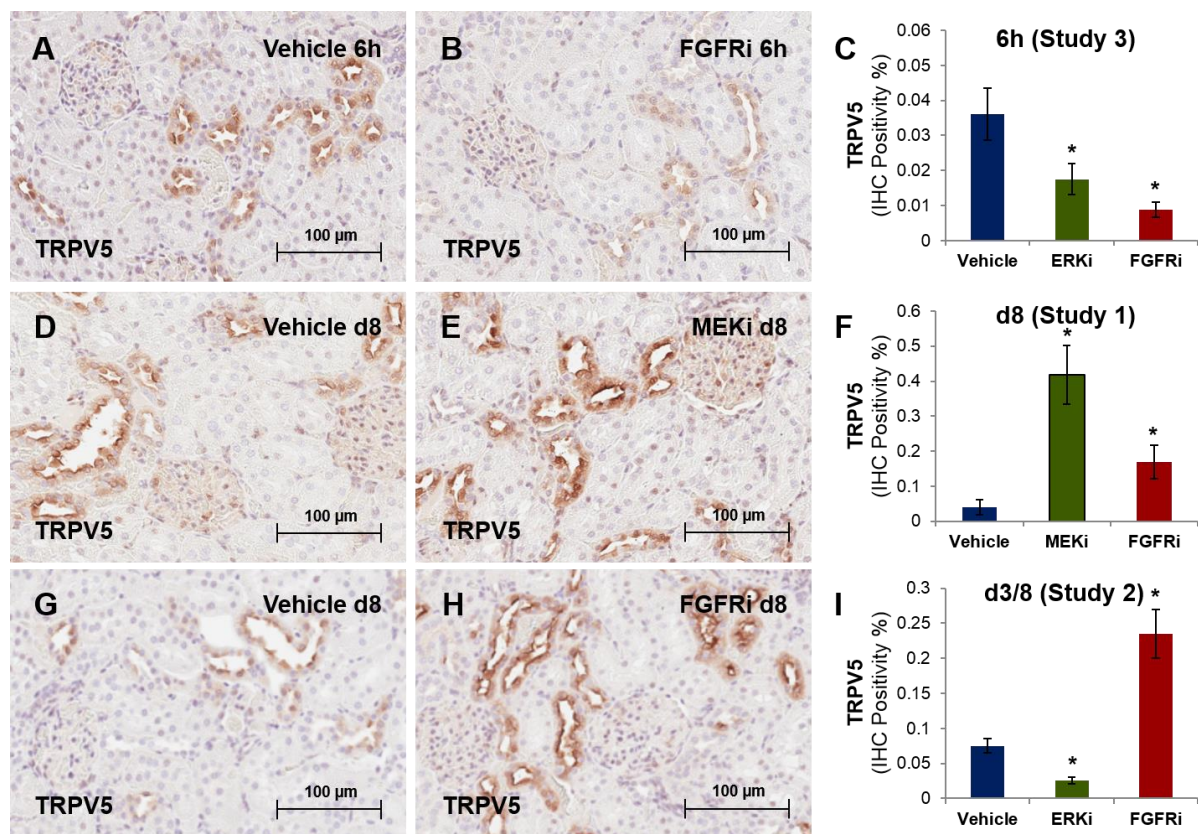
Figure 3.19: Expression of TRPV5 in cortical kidney sections from rats treated with 150 mg/kg/day of ERKi, 1.4 mg/kg/day of MEKi or 20 mg/kg/day of FGFRi. Photomicrographs of TRPV5 immunostaining in sections of rats from Study 3 dosed with vehicle (A) or FGFRi (B) for 6h; Study 1 dosed with vehicle (D) or MEKi (E) for 8d; and Study 2 dosed with vehicle (G) or FGFRi (H) for 8d. Positive signal in immunohistochemistry corresponds to the brown staining. Histograms represent the quantification of TRPV5 expression (immunohistochemically stained area) in animals from the studies S3 (C), S1 (F) and S2 (I). Data representative of $N = 3$-6 rats + SEM. * $p < 0.05$ vs the vehicle control (Mann-Whitney test). Scale bar = 100 μm.
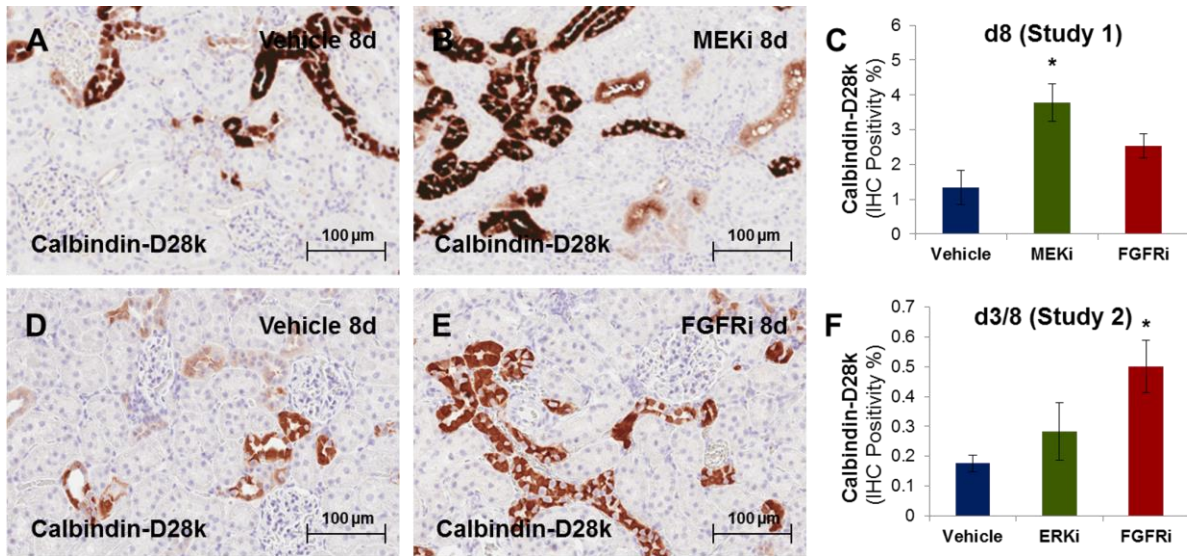
Figure 3.20: Expression of calbindin-D28k in cortical kidney sections from rats treated with 150 mg/kg/day of ERKi, 1.4 mg/kg/day of MEKi or 20 mg/kg/day of FGFRi. Photomicrographs of calbindin-D28k immunostaining in sections of rats from Study 1 dosed with vehicle (A) or MEKi (B) for 8d; and Study 2 dosed with vehicle (D) or FGFRi (E) for 8d. Positive signal in immunohistochemistry corresponds to the brown staining. Histograms represent the quantification of calbindin-D28k expression (immunohistochemically stained area) in animals from the studies 1 (C) and S2 (F). Data representative of $N = 3$-6 rats + SEM. * $p < 0.05$ vs the vehicle control (Mann-Whitney test). Scale bar = 100 µm.
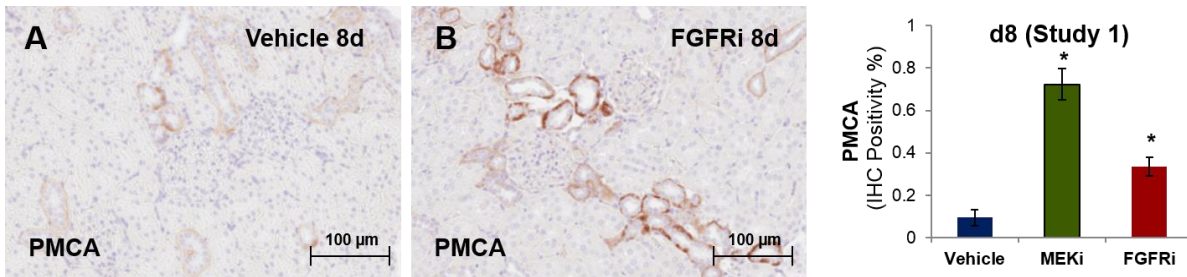
Figure 3.21: Expression of PMCA in cortical kidney sections from rats treated with 150 mg/kg/day of ERKi, 1.4 mg/kg/day of MEKi or 20 mg/kg/day of FGFRi. Photomicrographs of PMCA immunostaining in sections of rats from the study S1 dosed with vehicle (A), MEKi (B) or FGFRi (C) for 8d. Positive signal in immunohistochemistry corresponds to the brown staining. Histograms represent the quantification of PMCA expression (immunohistochemically stained area) in animals from the studies S1 (D), S2 (E) and S4 (F). Data representative of $N = 3$-6 rats + SEM. * $p < 0.05$ vs the vehicle control (Mann-Whitney test). Scale bar = 100 µm.

3.6.3 Effect of ERK, MEK and FGFR inhibition on the expression of Klotho

Another key protein for the renal reabsorption of Ca^{2+} and Pi is Klotho. Klotho regulates the expression of NaPi-IIa and TRPV5, not only by acting as a co-receptor for FGF23 but also through FGF-23 independent effects, which are mediated by its secreted form (Huang 2010). Given that the expression of Klotho can be induced by $1,25D_3$ (Wang et al. 2005) and inhibited by FGF23 (Dai et al. 2012), it is plausible that perturbations in the expression of Klotho may contribute to the altered expression of NaPi-IIa or TRPV5. In order to investigate if the expression of the Klotho is affected by treatment with ERKi, MEKi or FGFRi, renal expression and plasma levels of Klotho were analysed by IHC and ELISA, respectively, in samples from animals treated with these inhibitors.

By IHC, no changes in renal Klotho expression were detected in animals treated with ERKi or FGFRi for 6h (Table 7.25); ERKi, MEKi or FGFRi for 3/8d (Figure 3.22 B-C, Table 7.25); or MEKi or FGFRi for 25/28d (Table 7.25). Plasma levels of Klotho were analysed in terminal samples from animals dosed with MEKi or FGFRi for 8d (Figure 3.23). Plasma Klotho levels were increased (+12%) in animals treated with MEKi and decreased (-14%) in animals treated with FGFRi.

Kidney expression of Klotho remained unchanged.

Plasma Klotho was increased in animals treated with MEKi and decreased in animals treated with FGFRi.
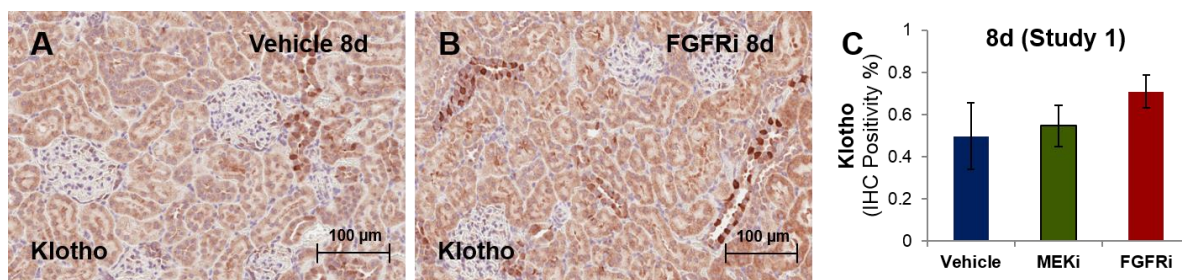
Figure 3.22: Expression of Klotho in cortical kidney sections from rats treated with 1.4 mg/kg/day of MEKi or 20 mg/kg/day of FGFRi. Photomicrographs of Klotho immunostaining in sections of rats from Study 1 dosed with vehicle (A) or FGFRi (C) for 8d. Positive signal in immunohistochemistry corresponds to the brown staining. Histograms represent the quantification of Klotho expression (immunohistochemically stained area) in animals from Study 1 (D). Data representative of $N = 3$-6 rats + SEM. * $p < 0.05$ vs the vehicle control (Mann-Whitney test). Scale bar = 100 μm.
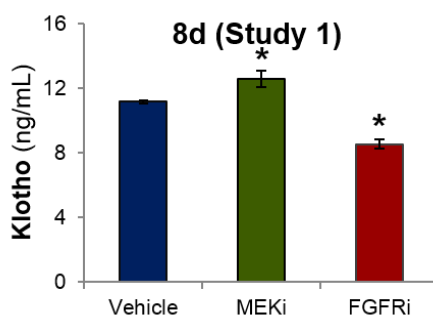
Figure 3.23: Plasma concentrations of Klotho in animals treated for 8 days with 1.4 mg/kg/day of MEKi or 20 mg/kg/day FGFRi. Plasma levels of Klotho in animals from Study 1. Data representative of $N = 3$-6 rats + SEM. * $p < 0.05$ vs the vehicle control (Mann-Whitney test). Plasma concentrations of Klotho were analysed by the Clinical Pathology department at AstraZeneca UK.

3.6.4 Summary

The effects of ERKi, MEKi and FGFRi in Ca^{2+} and Pi reabsorption were conditioned by the type/length of the treatment. Acute (6h) dosing with ERKi and FGFRi induced an increase in brush border membrane expression of NaPi-IIa, consistent with increased Pi reabsorption. Additionally, it induced a decrease in TRPV5, consistent with decreased distal Ca^{2+} reabsorption. Conversely, repeated dosing with ERKi, MEKi or FGFRi for >3d induced change in NaPi-IIa expression pattern in some of the treatment groups. These consisted in a decrease in NaPi-IIa expression in the outer cortex and/or an increase in the inner cortex. Also, repeated dosing with MEKi or FGFRi for >8d induced an increase in the expression of TRPV5, calbindin-D28k and PMCA, consistent with an increase in distal Ca^{2+} reabsorption. Table 3.10 summarizes the effects of ERKi, MEKi and FGFRi in the renal expression of NaPi-IIa, TRPV5, calbindin-D28k, PMCA and Klotho and plasma levels of Klotho.

Table 3.10: Summary of the effects of ERKi, MEKi and FGFRi in the expression of key proteins involved in the reabsorption of Ca^{2*} and Pi or in the regulation of this process.

	Method	Dosing	ERKi	MEKi	FGFRi
NaPi-IIa[1]	IHC	6h	=	NA	+
		d3/8	-	=/+	=/-
TRPV5	IHC	6h	=	NA	-
		d3/8	-	+	+
Calbindin-D28k	IHC	6h	=	NA	=
		d3/8	=	+	+
PMCA	IHC	6h	=	NA	=
		d3/8	=	+	+
Klotho (plasma)	ELISA	6h	NA	NA	NA
		d3/8	NA	-	+
Klotho (kidney)	IHC	6h	=	NA	=
		d3/8	=	=	=

1 – In NaPi-IIa, there was a shift in the localization of the immunoreactivity. Shorter treatments (6h) with ERKi or FGFRi induced a shift of the immunoreactivity from cytoplasmic vesicles to the brush border membrane that could not be easily quantified by image analysis. Conversely longer treatments (>3d) resulted in expression pattern changes in some of the treatment groups.

3.7 Results - Effects of ERKi, MEKi and FGFRi in the expression of calcification modulator proteins

3.7.1 Effect of ERK, MEK and FGFR inhibition on the expression of alkaline phosphatase and Pit-1

As an active and regulated process, soft-tissue mineralization is modulated by multiple factors including the expression of proteins that promote or inhibit calcification. Alkaline phosphatase and Pit-1 are two pro-calcifying proteins susceptible to regulation by $1,25D_3$ (Jono et al. 1998, Tatsumi et al. 1998). It is plausible that besides affecting Pi and Ca^{2+} reabsorption, $1,25D_3$ contributes to the occurrence of soft-tissue mineralization in rats treated with ERKi, MEKi or FGFRi by promoting the expression of alkaline phosphatase and Pit-1. In order to investigate if the expression of alkaline phosphatase and Pit-1 is affected by ERKi, MEKi and FGFRi treatment, IHC was carried out on kidney sections from animals treated with these inhibitors.

By IHC, alkaline phosphatase was detected at extremely low levels in the distal tubule, where it displayed a vesicular pattern (Figure 3.24 A,D). No differences in alkaline phosphatase expression were observed in animals treated with ERKi or FGFRi for 6h (Table 7.27). Conversely, alkaline phosphatase expression was increased at in animals treated with ERKi (+2-fold, Figure 3.24 D) for 3d or with FGFRi for 8d (+2-fold, Study 2). An increase in alkaline phosphatase expression was also evident by microscopic observation of the slides of animals treated with MEKi (Figure 3.24 B) or FGFRi (not shown) for 8d in Study 1. However, these changes were not deemed significant by image analysis (MEKi, $p=0.077$; FGFRi, $p=0.070$), likely due to the fact that the alkaline phosphatase immunostainings from Study 1 showed a low IHC signal/background ratio which prevented a specific detection of the positive IHC signal by the image analysis software.

By IHC, Pit-1 was broadly detected in the kidney, with the strongest expression observed in glomeruli and blood vessels and a weaker and variable expression observed in the PT and CD (Figure 3.25 A-D). Treatment with ERKi, or FGFRi for 6h (Figure 3.25 B-C) or ERKi, MEKi and FGFRi for 3/8d (Figure 3.25 E-F, Table 7.28) did not induce any evident changes in the expression of Pit-1.

Expression of alkaline phosphatase was increased in animals treated for longer periods (>3d) with ERKi, MEKi or FGFRi.

No changes in the expression pattern of Pit-1 were observed following treatment with ERKi, MEKi or FGFRi
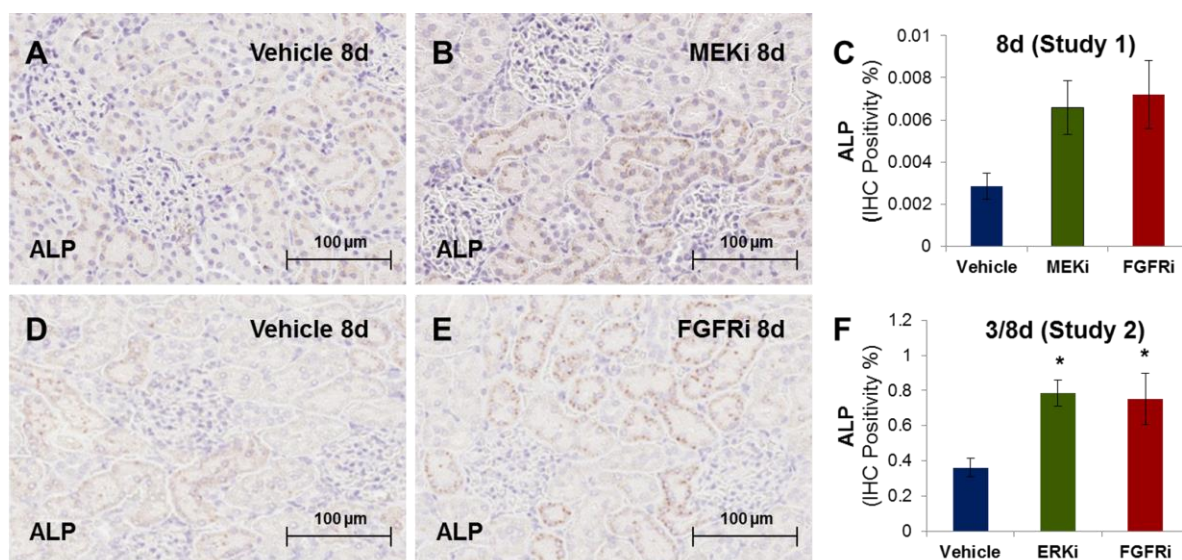
Figure 3.24: Expression of the alkaline phosphatase in cortical kidney sections from rats treated with 150 mg/kg/day of ERKi, 1.4 mg/kg/day of MEKi or 20 mg/kg/day of FGFRi. Photomicrographs of alkaline phosphatase (ALP) immunostaining in sections of rats from study 1 dosed with vehicle (A) or MEKi (B) for 8d; and study 2 dosed with vehicle (D) or FGFRi (E) for 3d. Positive signal in immunohistochemistry corresponds to the brown staining. Histograms represent the quantification of alkaline phosphatase expression (immunohistochemically stained area) in animals from the studies 1 (C) and 2 (F). Data representative of $N = 3$-6 rats + SEM. * $p < 0.05$ vs the vehicle control (Mann-Whitney test). Scale bar = 100 µm.
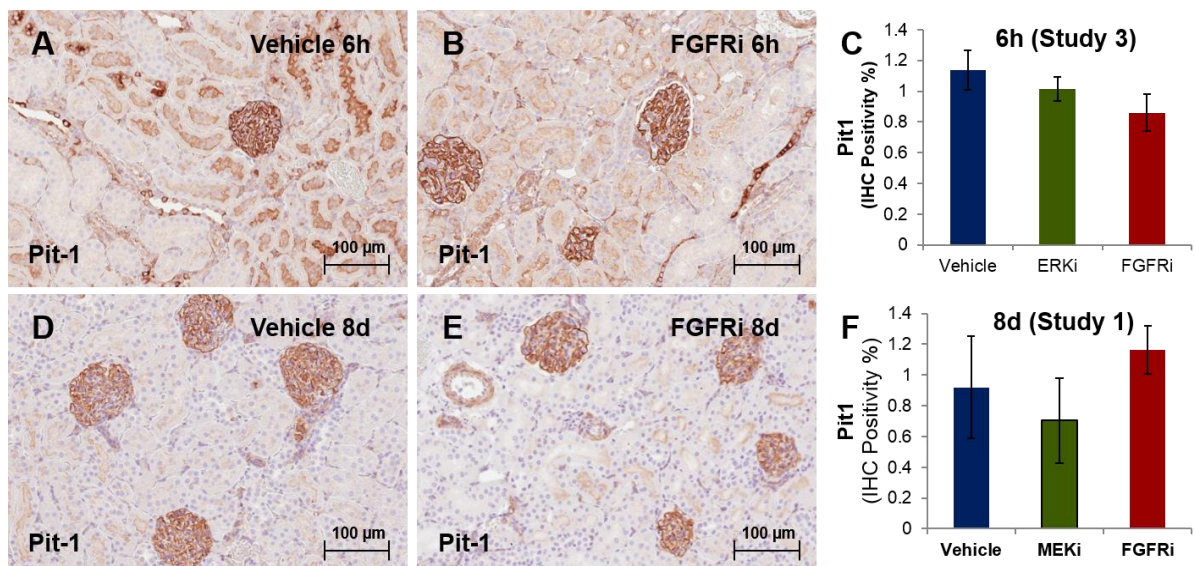
Figure 3.25: Expression of Pit-1 in cortical kidney sections from rats treated with 150 mg/kg/day of ERKi, 1.4 mg/kg/day of MEKi or 20 mg/kg/day of FGFRi. Photomicrographs of Pit-1 immunostaining in sections of rats from Study 3 dosed with vehicle (A) or FGFRi (B) for 6h and in animals from Study 1 dosed with vehicle (D) or FGFRi (E) for 8d. Positive signal in immunohistochemistry corresponds to the brown staining. Histograms represent the quantification of Pit-1 expression (immunohistochemically stained area) in animals from Study 3 (C) and Study 1 (F). Data representative of N = 3-6 rats + SEM. * p<0.05 vs the vehicle control (Mann-Whitney test). Scale bar = 100 µm.

3.7.2 Effect of ERK, MEK and FGFR inhibition on the expression of osteopontin, osteoprotegerin, sclerostin and DKK1

Different studies have shown that soft-tissue mineralization is accompanied by an increase in local and/or plasma expression of various calcification inhibitors including osteopontin (Kwon et al. 2000, Yu et al. 2009), osteoprotegerin (Schoppet et al. 2004, Abedin et al. 2007), sclerostin (Koos et al. 2013, Kuipers et al. 2015) and DKK1 (Ueland et al. 2009, Kim et al. 2011). Although the mechanisms are not completely clear, the expression of such proteins may be induced by calcifying cells with the aim of preventing the occurrence of further calcification. In order to investigate if the soft-tissue mineralization induced by ERKi, MEKi and FGFRi is associated with the upregulation of calcification inhibitor proteins, renal expression of osteopontin was analysed by IHC and plasma expression of osteoprotegerin, DKK1 and sclerostin was analysed by a multiplex assay using samples from rats treated with these inhibitors.

By IHC, the expression of osteopontin was detected in the thin limbs of the renal medulla and not in the cortex of vehicle-treated animals (Figure 3.26 A). Some of the animals treated with FGFRi for 8d (Figure 3.26 B-C) or 25d or with MEKi for 28d (not shown) showed cortical expression of osteopontin in distal tubules, blood vessels and glomeruli. Moreover, the animals that displayed cortical immunoreactivity of ostepontin also evidenced calcium deposition by von Kossa (Figure 3.3). Conversely, no kidney cortical osteopontin expression was observed in animals from the remaining groups, which also did not show evidence of soft-tissue mineralization in the kidney (not shown).

By multiplex assay, ERKi or FGFRi dosing for 6h did not induce any changes in the plasma levels of osteoprotegerin (Figure 3.27 A), DKK1 (Figure 3.27 B) and sclerostin (Figure 3.27 C). Conversely, ERKi dosing for 3d induced and increase in plasma levels of osteoprotegerin (+58%, Figure 3.27 A) and DKK1 (+68%, Figure 3.27 B), but not sclerostin (Figure 3.27 C) whilst FGFRi dosing for 8d induced an increase in plasma levels of osteoprotegerin (+39%, Figure 3.27 A), DKK1 (+60%, Figure 3.27 B) and sclerostin (+200%, Figure 3.27 C). Due to limited availability of plasma samples, it was not possible to perform this assay using animals treated with MEKi.

Cortical expression of osteopontin was induced in animals treated for 8d with FGFRi or 28d with MEKi or FGFRi (consistent with the presence of mineralization).

Treatment for with ERKi for 3d or FGFRi for 8d induced an increase in DKK1 and osteoprotegerin.

Treatment with FGFRi for 8d induced an increase in sclerostin.
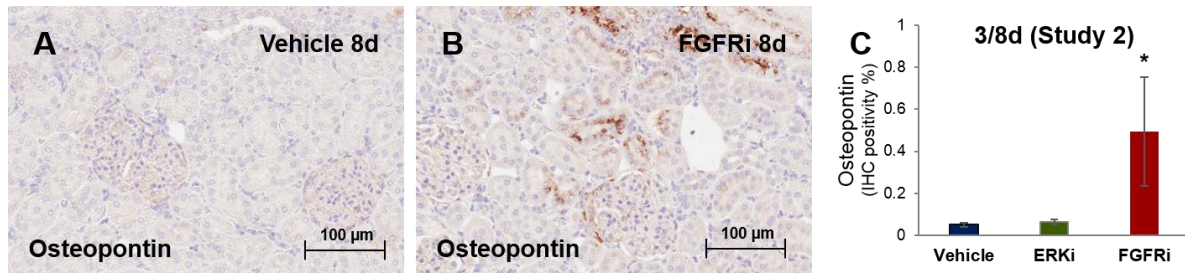
Figure 3.26: Expression of the osteopontin in cortical kidney sections from rats treated with 150 mg/kg/day of ERKi or 20 mg/kg/day of FGFRi. Photomicrograhs of osteopontin immunostaining in sections of rats from study 2 dosed with vehicle (A) or FGFRi (B) for 8d. Positive signal in immunohistochemistry corresponds to the brown staining. Histogram represents the quantification of osteopontin expression (immunohistochemically stained area) in animals from study 2 (C). Data representative of $N = 4$-6 rats + SEM. * $p < 0.05$ vs the vehicle control (Mann-Whitney test). Scale bar = 100 μm.
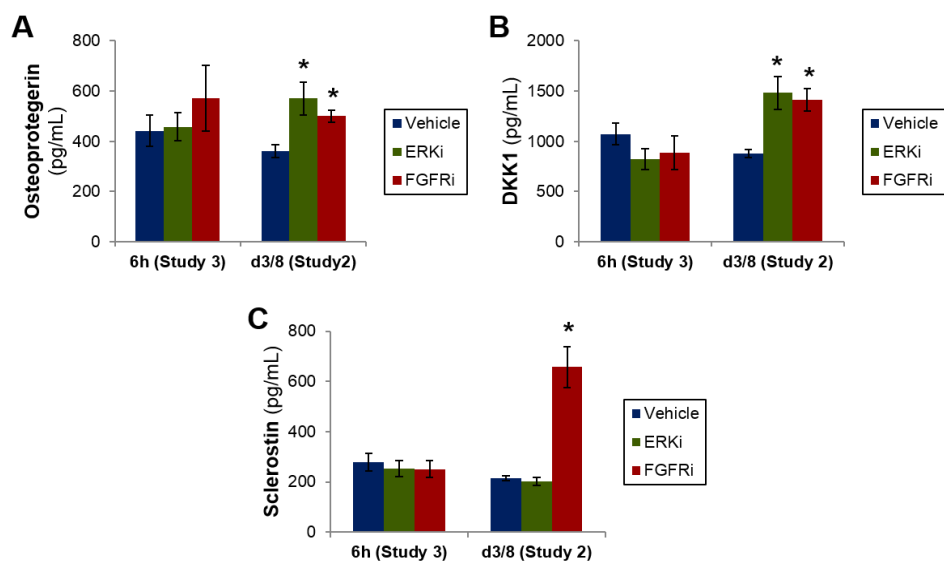
Figure 3.27: Plasma concentrations of osteoprotegerin, DKK1 and sclerostin in animals treated for 6h or 3/8d with 150 mg/kg/day of ERKi or 20 mg/kg/day FGFRi. Plasma osteoprotegerin (A), DKK1 (B), and sclerostin (C) levels in animals from the studies 2 and 3. Data representative of $N = 4$-6 rats + SEM. * $p < 0.05$ vs the vehicle control (Mann-Whitney test). The quantification of the plasma concentrations of osteoprotegerin, DKK1 and sclerostin was carried out by the Clinical Pathology department at AstraZeneca UK.

3.7.3 Summary table

Animals treated with ERKi, MEKi or FGFRi for >3d showed increased expression of the calcification inducer alkaline phosphatase. Associated with the presence of kidney mineralization, renal cortical expression of ostepontin was observed in animals treated with MEK for 28d or FGFRi for >8d. Besides, plasma levels of DKK1 and osteoprotegerin were increased in animals treated with ERKi for 3d or FGFRi for 8d and plasma levels of sclerostin were increased in animals treated with FGFRi for 8d (DKK1, osteoprotegerin and sclerostin were not assessed in animals treated with MEKi). The increases in renal expression of osteopontin and plasma levels of DKK1, osteoprotegerin and sclerostin are consistent with previous studies that show increased expression of these calcification inhibitors in calcifying tissue (Kwon et al. 2000, Schoppet et al. 2004, Abedin et al. 2007, Ueland et al. 2009, Yu et al. 2009, Kim et al. 2011, Koos et al. 2013, Kuipers et al. 2015). Table 3.11 summarizes the effects of ERKi, MEKi and FGFRi in the renal expression of alkaline phosphatase, Pit-1 and osteopontin and plasma levels of osteoprotegerin, DKK1 and sclerostin.

Table 3.11: Summary of the effects of ERKi, MEKi and FGFRi in the expression of calcification modulators

	Method	Dosing	ERKi	MEKi	FGFRi
Alkaline phosphatase	IHC	6h	=	NA	=
		d3/8	+	+	+
Pit-1	IHC	6h	=	NA	=
		d3/8	=	=	=
Osteopontin[1]	IHC	6h	=	NA	=
		d3/8	=	+	+
Osteoprotegerin	Luminex	6h	=	NA	=
		d3/8	+	NA	+
DKK1	Luminex	6h	=	NA	=
		d3/8	+	NA	+
Sclerostin	Luminex	6h	=	NA	=
		d3/8	=	NA	+

1 – Osteopontin immunoreactivity in the cortex – no change in osteopontin immunoreactivity was observed in the medulla.

3.8 Discussion

Study execution

This study assessed the mechanisms of soft-tissue mineralization following the administration of an ERK 1/2 inhibitor (ERKi), a MEK 1/2 inhibitor (MEKi) or an FGFR 1-3 inhibitor (FGFRi) to rats. The effects of these inhibitors in mineral homeostasis and soft-tissue mineralization were analysed following a single dose (6h post-dose) or following a 3/8d repeated dosing period. Also, the effects of MEKi and FGFRi were analysed in samples available from a previous 25/28d study carried out at AstraZeneca. ERKi, MEKi and FGFRi were administrated at the maximum tolerated dose (MTD), with a dosing regimen designed to keep effective plasma drug concentrations during the whole study. Moreover, the animals were terminated 2h after the last dosing, a time where these inhibitors were expected to reach maximal concentrations in blood (C_{max}). The drug dosages, dosing regimens and length of the treatments used in this study aimed to prevent and/or address differences in drug exposure, which may have contributed to the discrepant biological effects previously observed in animals treated with MEK and FGFR inhibitors (Brown et al. 2005, Wohrle et al. 2011, Diaz et al. 2012, Wohrle et al. 2013, Yanochko et al. 2013).

Toxicokinetic analysis

The toxicokinetic analysis has shown that plasma ERKi and FGFRi concentrations remained high during the course of the study, as planned. Conversely, MEKi concentrations may have dropped to low levels between dosing intervals since this compound was only administered once a day due to its toxicity and its C_{12h} corresponded to 9% of its C_{max}. Nevertheless, the toxicokinetic analysis also confirmed that ERKi, MEKi and FGFRi reached the C_{max} at 2h post dosing, suggesting that the animals were terminated and the biological tissues were collected at the a period when the effects of the inhibitors should be detectable.

Effects of ERKi, MEKi and FGFRi in soft-tissue mineralization and mineral homeostasis

Soft-tissue mineralization

In this study, the administration of ERKi, MEKi or FGFRi to rats resulted in soft-tissue mineralization in different organs including stomach, heart and kidney (the latter not observed with ERKi) and increased plasma Pi. Analogous findings were reported in rats treated with the MEK inhibitors PD352901 and GEN-A (Brown and Gad 2010, Diaz et al. 2012, Yanochko et al. 2013) and the FGFR inhibitors PD176067 or PD0330361 (Brown et al. 2005, Yanochko et al. 2013). The observation that soft-tissue mineralization is induced by treatment with different MEK and FGFR inhibitors strongly suggests that this effect is a consequence of the primary pharmacology (class effect) of these compounds, rather than an off-target effect. Moreover, the observation for the first time that an ERK inhibitor treatment is also able to induce soft-tissue calcification further supports a role for the MEK/ERK pathway in this process.

Bone, kidney and parathyroid axis

I aimed to analyse the expression of FGF23, $1,25D_3$ and PTH in animals treated with ERKi, MEKi and FGFRi since these molecules are key hormones for mineral homeostasis, susceptible to regulation by FGFR and MEK/ERK signalling (Ben-Dov et al. 2007, Chanakul et al. 2013, Xiao et al. 2014).

$1,25D_3$

Since it was not possible to find a sensitive assay to quantify plasma levels of $1,25D_3$, I analysed the expression of the genes that encode the proteins responsible for its production, Cyp27b1, and degradation, Cyp24a1, in the kidney. The expression of Cyp27b1 was increased and the expression of Cyp24a1 was decreased in animals treated with ERKi or FGFRi for 6h or ERKi for 3d, consistent with an increase in $1,25D_3$ production. These changes precede the increase in plasma Pi, which is only observed at 12h/24h post-dosing. Since $1,25D_3$ is able to induce renal reabsorption and intestinal absorption of Pi, most likely the increase in $1,25D_3$ production contributes to

122

the increase in plasma Pi levels (Dusso et al. 2005, Kido et al. 2013). The increase in Cyp27b1 and decrease in Cyp24a1 was not statistically significant in animals treated with FGFRi for 8d. This may be the result of a negative feedback mechanism in which $1,25D_3$ induces a downregulation of Cyp27b1 (Murayama et al. 1998) and an upregulation of Cyp24a1 (Vaisanen et al. 2005) to prevent a further increase in its levels. In addition to the renal effects in $1,25D_3$ production, it is possible that inhibitors of ERK, MEK and FGFR induce increased production of $1,25D_3$ in extra-renal tissues since extra-renal Cyp27b1 is normally inhibited by FGF23 signalling through the FGF receptors and the MEK/ERK pathway (Chanakul et al. 2013). The effects of ERKi, MEKi and FGFRi in $1,25D_3$ production support previous studies that report that MEK (Brown and Gad 2010, Diaz et al. 2012, Yanochko et al. 2013) or FGFR (Wohrle et al. 2011, Yanochko et al. 2013) inhibitors induce an upregulation of Cyp27b1, a downregulation of Cyp24a1 and/or an increase in $1,25D_3$ detectable from 4h-12h post dosing. In addition to the effects on the production of $1,25D_3$, ERKi, MEKi and FGFRi also affected the expression of its receptor, VDR. VDR expression was markedly decreased in animals treated with ERKi or FGFRi for 6h or ERKi for 3d. Conversely, this effect was reversed in animals treated with MEKi or FGFRi for 8d and an increase in VDR expression was observed in the 25d/28d studies. VDR mediates the genomic actions of $1,25D_3$ (Haussler et al. 1998). Consequently the presence and expression levels of VDR condition the susceptibility of different tissues to $1,25D_3$- induced gene regulation. The expression of VDR can be regulated by different factors including the inducers $1,25D_3$ (Healy et al. 2003) and FGF23 (Canalejo et al. 2010) and the inhibitor PTH (Reinhardt and Horst 1990). It is plausible that the inhibition of signalling through the FGFRs or through the MEK/ERK pathway blocks FGF23-induced VDR expression, leading to an initial decrease in VDR levels. Conversely, following longer treatment periods, the increased levels of $1,25D_3$ may signal through the VDR molecules and gradually increase the expression of this receptor. This way, shorter dosing periods with ERKi, MEKi and FGFRi may result in increased production of $1,25D_3$ but also in some limitations in the genomic actions of this hormone. Conversely, following longer treatment periods, VDR levels are normalized and $1,25D_3$ is able to carry out its genomic actions to the full extent.

FGF23

FGF23 was measured in different time points following the administration of ERKi, MEKi or FGFRi. All compounds induced an initial decrease (2-12h post dose) in plasma FGF23. This decrease is observed at the same time as the alterations in the expression of Cyp27b1 and Cyp24b1 mRNA, and precedes the increase in Pi. Considering that the expression of FGF23 can be induced by activated FGF receptors signalling through the MEK/ERK or PLC gamma pathways (Xiao et al. 2014), it is probable that this initial decrease in FGF23 is the consequence of a blockage in the FGFR-induced FGF23 expression in bone, either at the FGFR or MEK/ERK pathway level. Animals treated with MEKi or FGFRi for >4 days showed increased plasma levels of FGF23. This increase may be the consequence of an enhanced induction of FGF23 gene expression by the high levels of $1,25D_3$ (Prie and Friedlander 2010) or Pi (Arai-Nunota et al. 2014). The observation that the effects of ERKi and MEKi in plasma levels of FGF23 differ with the duration of the treatment explains some of the discrepancies previously reported. To be exact, in previous studies mice treated with a FGFR inhibitor for <7h showed a decrease in the production and plasma levels of FGF23 (Wohrle et al. 2011) whilst rats treated with a MEK or an FGFR inhibitor for >24h showed increased plasma levels of FGF23 (Diaz et al. 2012, Yanochko et al. 2013).

PTH

No changes in PTH were observed following treatment with MEKi or FGFRi for 8d. Nevertheless, the variability of the results was very high, possibly due to a low sensitivity of the method. PTH is not an easy analyte to detect due to the existence of different fragments of this hormone (Martin and González 2007). Previously, some studies have successfully detected intact PTH in rodents treated with MEKi or FGFRi using ELISA methods (Brown and Gad 2010, Wohrle et al. 2011, Diaz et al. 2012), while others have failed to detect this analyte using similar methods (Yanochko et al. 2013). In the studies where PTH was detected successfully, this analyte was assessed using an N = 4-6 animals per group, a number comparable to what was used in this study. Nevertheless, the values of PTH measured in these studies were associated with high values for the standard error of the mean, thus suggesting that the methods

employed also attain low sensitivities. For instance, some of the treatments shown in these studies evidenced PTH values with a 2-3 fold difference in comparison to the vehicle, which was not deemed significant. A factor that may contribute to the variability of the PTH results is the processing of the sample. Previous studies indicate that freeze-thawing the samples may decrease the stability of PTH, therefore leading to an increased variability in PTH results (Brinc et al. 2012). Accordingly, PTH variability is decreased when samples are collected in EDTA, stored at 4°C and analysed within 48h (Hanon et al. 2013). Due to the low sensitivity of the available assays and to also due the nature (frozen) and limited availability of the plasma samples, the detection of PTH by ELISA was not carried out in animals treated with ERKi, MEKi or FGFRi. Since $1,25D_3$ (Kugai et al. 1984) and FGF23 (Ben-Dov et al. 2007) are able to inhibit the production and secretion of PTH in the parathyroid, it is plausible that the altered levels of FGF23 and $1,25D_3$ associated with ERKi, MEKi or FGFRi treatment affect the expression of PTH. In fact, the previous studies have shown that the plasma levels of PTH were increased in mice treated with an FGF receptor inhibitor for <7h (Wohrle et al. 2011) and decreased in rats treated with MEK inhibitor for >24h (Brown and Gad 2010, Diaz et al. 2012).

The involvement of PTH in the mechanism of soft-tissue mineralization induced by the inhibition of the FGFRs or the inhibition of the MEK/ERK pathway should be addressed when more sensitive PTH detection methods become available or by using the PTH ELISA methods currently available with an optimized sample processing and a larger number of animals in each treatment group.

Effects of ERKi, MEKi and FGFRi in the activation of cell signalling pathways in the kidney

MEK/ERK inhibitors and FGFR inhibitors induce analogous perturbations in mineral ion homeostasis, however there is no direct evidence to support that these perturbations are induced by similar molecular mechanisms. It is plausible that these perturbations are induced by analogous mechanisms involving the kidney since FGF23 signalling through FGFRs via the MEK/ERK pathway was previously described to regulate different processes involved in mineral homeostasis including the

production of 1,25D$_3$ (Chanakul et al. 2013) and the expression of NaPi-IIa (Andrukhova et al. 2012) and TRPV5 (Andrukhova et al. 2014). Nevertheless, the uncertainty of the distribution of the FGFRs 1-4, Klotho, MEK and ERK along the nephron generated some controversy regarding the role of FGF23 in these processes. In order to clarify the intra-renal distribution of FGFRs 1-4, Klotho, MEK and ERK these proteins and assess which nephron segments could be directly affected by ERKi, MEKi and FGFRi, the expression these proteins was analysed in the kidney using ISH and IHC.

FGFRs and Klotho

Whilst the FGFRs, MEK and ERK are direct targets of FGFRi, MEKi and ERKi, Klotho is a co-receptor required for the interaction between endocrine FGFs such as FGF23 and the FGFRs (Urakawa et al. 2006). FGFRs 1-4 were detected throughout the nephron including the PT, DT and CD (not FGFR4) segments. The results shown in this study are partially in agreement with a study performed by Cancilla and coworkers, which reported a similar expression pattern for FGFR1, FGFR2 and for FGFR3, with the exception of CD in FGFR3 and PT in FGFR3 (Cancilla et al. 2001). Klotho was observed with stronger intensity in DT and CD and weaker intensity in PT, in agreement with recent reports (Hu et al. 2010, Andrukhova et al. 2012). The detection of the FGFRs and Klotho in the PT strongly support that FGF23 regulates the production of 1,25D$_3$ (Chanakul et al. 2013) and expression of NaPi-IIa (Andrukhova et al. 2012) by directly targeting this nephron segment. The direct targeting of the PT by FGF23 is a more plausible explanation for the effects of FGF23 in this nephron segment than a paracrine regulation elicited by the DCT, which was suggested in previous studies that detected the expression of Klotho in the DCT but not in the PT (Farrow et al. 2009).

ERK and MEK

ERK and MEK were also detected throughout the nephron including the PT, DT and CD segments. The phosphorylated forms of these proteins were mainly observed in DT and only to a smaller extent in the PT. Previous studies had reported expression of ERK by IHC in the DT and CD, but not in PT (Omori et al. 2000, Fujita et al. 2004).

Conversely, functional studies carried out in cell cultures suggest the expression and functional roles for ERK in the proximal tubule including cytokine production and angiotensin signalling (Sengul et al. 2003, Su et al. 2006). The observation of the expression of MEK and ERK in the PT supports these functional studies.

The discrepancies in the IHC patterns of the FGFRs between this study and previous studies may be explained by the use of antibodies that recognize different isoforms of the same FGFR. On the other hand, the differences in the IHC patterns of Klotho, MEK and ERK detected in this study and the patterns reported in previous studies may be ascribed to the sensitivity of the IHC methods or to deficient tissue processing that may have prevented antigen recognition in the previous studies.

The co-localization of the FGF receptors, Klotho, MEK and ERK in the PT and DT support previous studies that described that FGF23 regulates the expression of NaPi-IIa (Andrukhova et al. 2012), Cyp27b1 (Chanakul et al. 2013) and TRPV5 (Andrukhova et al. 2014) by signalling through the FGFRs and through the MEK/ERK pathway in these nephron segments. These observations are consistent with FGFRi, MEKi and ERKi inducing the production of $1,25D_3$ and Pi reabsorption in the kidney by a common mechanism involving in the inhibition of FGF23 signalling, either at the level of the FGFRs or at the level of the MEK/ERK pathway.

MEK/ERK signalling pathway activation

The inhibition of MEK/ERK signalling by ERKi or MEKi was confirmed through the analysis of the phosphorylation of ERK and expression of its downstream target EGR1. ERKi induced an increase in the phospho-ERK, consistent with the drug mode of action, which prevents the binding of phospho-ERK to its targets, but not its phosphorylation, thus leading to an accumulation of phospho-ERK (AstraZeneca unpublished data). Conversely, MEKi induced a decrease in phospho-ERK and both compounds induced a decrease in the expression of the transcription factor EGR1, consistent with the inhibition of the MEK/ERK pathway. ERK phosphorylation and EGR1 expression remained mostly unchanged in animals treated with FGFRi.

Previous studies have shown that the MEK/ERK pathway is a downstream component of the renal FGFR signalling, involved in the FGF23-induced regulation of the proteins NaPi-IIa (Andrukhova et al. 2012), Cyp27b1 (Chanakul et al. 2013) and TRPV5

(Andrukhova et al. 2014). Moreover, FGF23 administration was found to induce ERK activation in mouse kidney (Farrow et al. 2009) and FGFRi treatment was found to decrease ERK phosphorylation in tumour cell models displaying high FGF receptor signalling (Astrazeneca unpublished work). The observation that FGFRi had no effects in ERK phosphorylation and EGR1 expression suggests that this compound is not able to prevent the activation of the MEK/ERK pathway and therefore may induce soft-tissue mineralization by a different mechanism than ERKi and MEKi. Nevertheless, the MEK/ERK pathway can be activated by different receptors including vascular endothelial growth factor receptor (VEGFR), epidermal growth factor receptor (EGFR) and CaSR (Kifor et al. 2001, Adams et al. 2004, Narasimhan et al. 2009). Since the activation of ERK by FGF23 is low under basal conditions (Farrow et al. 2010), it is possible that FGFRi effectively prevents the FGFR-mediated activation of MEK/ERK signalling whilst having little changes in the overall activation of this pathway. This assumption is supported by the observation that ERK phosphorylation was not increased following treatment with FGFRi for >8d, despite the presence of increased levels of phosphate and FGF23, which were previously found to induce ERK activation by signalling through the FGFRs (Yamazaki et al. 2010). Conversely to FGFRi, the administration of the pan-FGFR inhibitor PD-0330361 to rats resulted in a significant decrease in ERK phosphorylation in the kidney in a previous study (Yanochko et al. 2013). Due to the high degree of homology between the different tyrosine kinases, FGFR inhibitors may inhibit to a lower degree other kinases (Broekman et al. 2011). This way, it is possible that inhibition of ERK by PD-0330361 in that study is a result of the drug hitting other kinases that signal through the MEK/ERK pathway. This is supported by the observation that PD-0330361 was administered in a very high dose, which led to marked toxicity effects and earlier termination of the study. Another explanation is that FGFRi is does not reach the kidney in effective concentrations and the mineral homeostasis perturbations are induced by the effects of FGFRi in other organs. Nevertheless, this hypothesis would not explain why the ERK phosphorylation levels are not increased by the high FGF23 levels observed in animals treated with FGFRi for >8d.

FGFR signalling activation

I aimed to confirm the inhibition of the FGFRs by analysing the expression of phospho-FGFR and/or phospho-FRS2 (target of FGFR) in kidney sections from animals treated with FGFRi. Unfortunately, it was not possible to carry out this analysis since none of the three antibodies assessed for this purpose was able to specifically detect is corresponding target in rat kidney. Other targets of the FGFRs include PLC-gamma (Rhee 2001) and different signalling pathways such as Src (Sandilands et al. 2007) and Janus kinase (JAK) / signal transducer and activator of transcription (STAT) (Dudka et al. 2010). Nevertheless, PLC-gamma and the components of these signalling pathways are likely not good biomarkers for FGFR activation, since these proteins are also targets of other receptors (Rhee 2001, Parsons and Parsons 2004, Johnston and Grandis 2011).

RPPA evaluation of the effects of ERKi and FGFRi on cell signalling

An RPPA assay was carried out in rats treated for 6h with ERKi or FGFRi with the aim of identifying the pathways that are affected within hours of the administration of these inhibitors and may contribute to the occurrence of soft-tissue mineralization. This method showed similar results as IHC and Western blotting for the expression of phospho and total ERK, which were included in the analysis as controls. Besides phospho-ERK, all the effects of ERKi and FGFRi in protein expression detected by RPPA were small (<40% expression change). This observation suggests that RPPA failed to identify the key proteins contributing to soft-tissue mineralization, however it may not be the case as some of the small expression changes identified may increase following longer treatment periods with the inhibitors. The expression changes induced by ERKi include slight decreases in the activation of MNK1 and CREB, downstream proteins of MEK/ERK signalling. These effects were also observed in animals treated with FGFRi, which additionally attained slight decreases in the activation of MAPKAPK-2, Src and PLC gamma, downstream proteins in FGFR signalling. These observations support that FGFRi effectively inhibits the FGFRs and the FGFR-mediated ERK activation in the kidney. Other proteins that showed small expression changes following treatment with ERKi and FGFRi include beta-catenin and GSK3-beta, components of the WNT pathway; and PARP1 (only FGFRi) and Bcl-x, two

proteins involved in regulation of the apoptotic process. Although the expression changes observed by RPPA are too small to indicate a clear role for these processes in mineralization induced by ERKi or FGFRi, activation of WNT signalling (Zeadin et al. 2012, Guerrero et al. 2014, Yao et al. 2015) and apoptosis (You et al. 2009) were previously associated with the induction of soft-tissue mineralization. As validation for the RPPA assay, beta-catenin expression was also analysed by IHC. Beta-catenin showed a variable expression between animals and the treatment with ERKi or FGFRi did not induce any evident changes in the expression or localization of this protein. The discrepancy between both methods suggests that the small expression changes observed by RPPA may not be real. Nevertheless, this may not hold true since RPPA may be more sensitive than IHC to detect beta-catenin. In fact, consistent with a dysregulation of the WNT pathway, animals treated with ERKi for 3d or FGFRi for 8d showed an increase in the plasma levels of the WNT pathway inhibitors DKK1 and sclerostin (only FGFRi).

Effects of ERKi, MEKi and FGFRi on the expression of proteins involved in renal Ca^{2+} and Pi reabsorption

Pi reabsorption in the PT

The contribution of the renal Pi reabsorption to the increased plasma Pi levels was investigated. Due to the strict home office license regulations it was not possible to conciliate the experimental design used in this study with the collection of urine using metabolic cages. As an alternative, the expression of NaPi-IIa, the transporter that accounts for 70% of the renal Pi reabsorption (Wagner et al. 2008), was analysed. Treatment with ERKi or FGFRi for 6h promoted a shift of NaPi-IIa expression from cytoplasmic vesicles to the brush border membrane. Conversely, longer (>3d/8d) treatment with ERKi or FGFRi the inhibitors resulted in a slight decrease in NaPi-IIa expression in the outer cortex, and no changes or even a slight increase in NaPi-IIa expression in the inner cortex. Besides, treatment with MEKi for 8d did not affect NaPi-IIa expression, whilst treatment with this inhibitor for 28d resulted in a slight increase in NaPi-IIa expression in the inner cortex. These results suggest that NaPi-IIa may contribute to the initial increase in plasma Pi levels, but not to the sustained high Pi

levels following longer treatments with ERKi, MEKi or FGFRi. Previous studies have shown that FGF23 promotes the internalization of NaPi-IIa mainly through Klotho-dependent processes (Andrukhova et al. 2012) involving signalling through FGFR1 and ERK (Yan et al. 2005, Gattineni et al. 2009). To a lesser extent, FGF23 also promotes the internalization of NaPi-IIa by Klotho-independent processes (Andrukhova et al. 2012) and signalling through FGFR4 (Gattineni et al. 2009). Most likely, the regulation of NaPi-IIa by FGF23 can also occur independently of ERK, since the Klotho-independent actions of FGF23 were previously shown to involve other pathways than ERK (Faul et al. 2011, Olauson et al. 2013). Opposite to FGF23, 1,25D$_3$ induces the of expression of NaPi-IIa in the inner cortex, whilst having no effects in the outer cortical expression of this protein (Taketani et al. 1998). The increase in the brush border expression of NaPi-IIa observed 6h post dosing with ERKi or FGFRi is likely the effect of a decrease in the internalization of this protein promoted by the low levels of FGF23. Conversely, the slight alterations in the expression pattern of NaPi-IIa observed following longer treatment periods with ERKi, MEKi and FGFRi may be the outcome of opposite regulatory signals of FGF23 and 1,25D$_3$. Whilst 1,25D$_3$ induces the expression of NaPi-IIa in the inner cortex of the kidney, FGF23, possibly by signalling through FGFR4 and pathways other than ERK, inhibits NaPi-IIa expression throughout the kidney cortex. In three different studies with rodents, treatment with a FGFR or a MEK inhibitor for <12h did not affect NaPi-IIa mRNA or protein expression (Wohrle et al. 2011, Diaz et al. 2012, Wohrle et al. 2013). Conversely, one study showed that NaPi-IIa expression decreased in rats treated during 4d with an FGFR inhibitor and remained unchanged in rats treated during 6d with a MEK inhibitor (Yanochko et al. 2013). A different study showed that NaPi-IIa expression decreased in rats treated for 3d treatment with a MEK inhibitor (Diaz et al. 2012). The discrepancies in NaPi-IIa expression between the various studies may be associated with different drug exposures. Whilst in this study plasma drug concentrations were high at the time that the animals were killed, this may have not occurred in the other studies. For instance, a low exposure to the drug would explain the decrease in NaPi-IIa expression observed in rats treated for 4d with a FGFR inhibitor or for 3d with a MEK inhibitor, since these effects are consistent with the compensatory response of the organism to the high levels of Pi or FGF23. Renal reabsorption of Pi can also be mediated by other transporters than NaPi-IIa, including NaPi-IIc and sodium-dependent phosphate transporter 2 (Pit-2). The expression of

these two receptors is regulated by plasma Pi levels (Ohkido et al. 2003, Villa-Bellosta et al. 2009). Also, similarly to NaPi-IIa, the expression of NaPi-IIc can be induced by 1,25D$_3$ (Masuda et al. 2010) and inhibited by FGF23 (Gattineni et al. 2009). Further studies should clarify if NaPi-IIc and Pit-2 are involved in the increase in Pi induced by ERKi, MEKi and FGFRi.

Besides the increase in renal Pi reabsorption, a factor that may contribute to the elevated plasma Pi levels is a decrease in renal function (McMillan 2013). Although renal function could not be accurately analysed in this study due to the lack of urinary data, it was observed that treatment with ERKi for 3d or FGFRi for 8d or 28d induced an increase plasma creatinine levels (Table 7.33), which is consistent with a decrease in renal function. Further studies should accurately assess if the administration of ERKi, MEKi and FGFRi to rats decreases the renal function and evaluate how this impairment contributes to the elevated levels of Pi.

Ca^{2+} reabsorption in the DCT

Treatment with ERKi or FGFRi for 6h or ERKi for 3d resulted in the decreased expression of TRPV5. Conversely, treatment with MEKi or FGFRi for >8d resulted in the increased expression of TRPV5, calbindin-D28k and PMCA in the kidney, consistent with an increased reabsorption of Ca^{2+} in the DCT. FGF23 is able to induce the expression of TRPV5 by signalling through the FGFRs and through the MEK/ERK pathway (Andrukhova et al. 2014). Also, 1,25D$_3$ is able to induce the expression of TRPV5, calbindin-D28k and PMCA (Huang and Christakos 1988, Hoenderop et al. 2001, Kip and Strehler 2004). Most likely, the initial decrease in TRPV5 following the administration of ERKi or FGFRi is induced by the low FGF23 levels and/or inhibition of FGF23 signalling. Conversely, the increased expression of TRPV5, PMCA and calbindin-D28k following longer treatments (>8d) with MEKi or FGFRi is likely induced by the high levels of 1,25D$_3$. These results suggest that long term treatment with MEKi or FGFRi results in increased Ca^{2+} reabsorption in the kidney, despite the lack of changes in plasma Ca^{2+}. Nevertheless, these two situations are not incompatible since the Ca^{2+} is strictly regulated at a systemic level through the activation of processes such as resorption from bone or absorption from intestine. Even without affecting plasma Ca^{2+} levels, an increase in renal Ca^{2+} reabsorption could promote kidney

mineralization by increasing the Ca^{2+} x Pi product locally. Consistent with this hypothesis, kidney mineralization was mainly detected in connective tissue contiguous to distal tubules in animals treated with MEKi or FGFRi.

Effects of ERKi, MEKi and FGFRi in the expression of calcification modulator proteins

Calcification inducers

Soft-tissue mineralization is not the simple deposition of Ca^{2+} and Pi but rather an active and regulated process (Giachelli 2004). This way, in addition to the high Ca^{2+} x Pi product, the induction of soft-tissue mineralization is generally associated with an increased expression of calcification inducers and / or a decreased expression of calcification inhibitors (Giachelli 2004).

Alkaline phosphatase

Treatment with ERKi for 3d or MEKi or FGFRi for 8d induced an increase in kidney expression of the calcification inducer protein alkaline phosphatase, mainly in the DCT. The observation of high alkaline phosphatase expression in treatment groups where kidney mineralization was not observed (eg. animals treated with ERKi for 3d or MEKi for 8d) suggests that the increase in alkaline phosphatase expression precedes the occurrence of soft-tissue mineralization. Likely, alkaline phosphatase contributes to the initiation of the mineralization process following treatment with ERKi, MEKi or FGFRi, as this protein is able to hydrolyse the calcification inhibitor pyrophosphate, generating Pi and creating suitable conditions to the occurrence of mineralization (Schoppet and Shanahan 2008). Alkaline phosphatase expression can be induced by $1,25D_3$ (Jono et al. 1998) and Pi (Orimo and Shimada 2008) and inhibited by FGF23 (Shalhoub et al. 2011). Moreover, regulation of alkaline phosphatase by Pi and FGF23 involves at least partially signalling through the MEK/ERK (Shalhoub et al. 2011) pathways, respectively. This way, the increase in alkaline phosphatase expression following treatment with ERKi, MEKi or FGFRi may

be induced by the high levels 1,25D$_3$ and/or Pi or by the blockage in the FGF23-mediated inhibition of alkaline phosphatase.

Pit-1

Pit-1, a transporter with a key role in the induction of soft-tissue calcification (Chavkin et al. 2015) and possibly involved in renal Pi reabsorption (Tenenhouse et al. 1998) was also analysed. Strong Pit-1 expression was observed in kidney blood vessels and glomeruli and weaker expression was observed throughout the nephron including the PT, DCT and CD segments. To my knowledge, this is the first description of the expression pattern of Pit-1 in rat kidney. This description is consistent with the expression pattern previously reported for Pit-1 mRNA in mouse kidney (Tenenhouse et al. 1998). Treatment with ERKi, MEKi or FGFRi did not affect the expression or distribution of Pit-1, which suggests that this transporter is not involved in the mineralization or increased plasma Pi levels observed in animals treated with these inhibitors.

Calcification inhibitors

Soft-tissue mineralization is generally accompanied by a phenotype transition and induction of different calcification inhibitors (Kwon et al. 2000, Schoppet et al. 2004, Abedin et al. 2007, Ueland et al. 2009, Yu et al. 2009, Kim et al. 2011, Koos et al. 2013, Kuipers et al. 2015), possibly elicited to prevent the occurrence of further calcification.

Osteopontin

Osteopontin, a calcification inhibitor normally detected in the renal medulla, was also expressed in the cortex of the animals treated with MEKi and FGFRi that displayed kidney mineralization. The expression of osteopontin in these animals showed a similar pattern as the mineral deposition detected by von Kossa, which suggests that this protein is expressed in calcifying tissue.

Osteoprotegerin, DKK1 and sclerostin

Also, the plasma levels of the calcification inhibitors osteoprotegerin, DKK1 and sclerostin were increased by treatment with ERKi for 3d (only osteoprotegerin and DDK1) and FGFRi for 8d. Conversely, no changes in the expression of osteoprotegerin, DKK1 and sclerostin were observed in animals treated with these inhibitors for 6h. These observations suggest that the increase in osteopontin, osteoprotegerin, DKK1 and sclerostin succeed the settling of mineralization. Consistent with these observations, the expression of osteopontin (Mohler et al. 1997), osteoprotegerin (Schoppet et al. 2004), DKK1 (Kim et al. 2011) and sclerostin (Kuipers et al. 2015) was previously found to be upregulated in calcifying tissue. Also, the plasma levels of these proteins were found to be increased in patients showing evidences of vascular calcification (Abedin et al. 2007, Ueland et al. 2009, Abdel-Azeez and Al-Zaky 2010, Brandenburg et al. 2013).

Osteopontin, osteoprotegerin, DKK1 and sclerostin inhibit soft-mineralization through distinct processes. Osteopontin inhibits mineralization by releasing a peptide that binds to hydroxyapatite and prevents the development of the crystals (Addison et al. 2010); DKK1 and sclerostin inhibit mineralization by preventing the activation of the WNT signalling pathway, which regulates the expression of pro-calcifying proteins such as BMP2 and alkaline phosphatase (Martinez-Moreno et al. 2012, Guerrero et al. 2014); Osteoprotegerin inhibits mineralization by acting as a decoy-receptor for the pro-calcifying protein RANK (Boyce and Xing 2007) and the pro-apoptotic protein TNF-related apoptosis-inducing ligand (TRAIL) (Sandra et al. 2006). The activation of such diverse processes illustrates the complexity of the mechanism of mineralization induced by ERKi, MEKi and FGFRi.

3.9 Conclusion

In summary, administration of ERKi, MEKi and FGFRi to rats resulted in soft-tissue mineralization of different organs including kidney, stomach and heart. Associated with soft-tissue mineralization, the three inhibitors induced similar perturbations in mineral homeostasis including increased plasma levels of Pi and altered production of $1,25D_3$ and FGF23. The kidney appears to have a key role in the process of soft-tissue mineralization induced by ERKi, MEKi and FGFRi since the treatment with these inhibitors affected the renal expression of genes/proteins involved in the production of $1,25D_3$, reabsorption of Ca^{2+} and Pi and modulation of mineralization. In addition, bone is also expected to have an important role in this process since ERKi, MEKi and FGFRi induced alterations in the plasma levels of FGF23, which is mainly produced in this organ.

Most likely, the process of soft-tissue mineralization is initially triggered by the inhibition of FGF23 signalling, either at the FGFR or at the MEK/ERK pathway levels. Supporting this conjecture, the perturbations in mineral homeostasis observed 6h post-dosing with these inhibitors are direct effects of FGF23 inhibition. These include increased expression of Cyp27b1 and NaPi-IIa and decreased expression of Cyp24a1, TRPV5, VDR and decreased plasma levels of FGF23. Furthermore, following longer treatment periods, the altered expression of Cyp27b1 and Cyp24a1 likely promotes an increased production of $1,25D_3$, which may be the driving factor for soft-tissue mineralization. Supporting with this view, the biological effects observed following MEKi and FGFRi treatment for >8d are consistent with $1,25D_3$ toxicity. These effects include increased plasma levels of FGF23 and Pi and increased expression of proteins involved in Ca^{2+} reabsorption in the DCT and pro-calcifying proteins such as alkaline phosphatase. Finally, the tissues undergoing soft-tissue mineralization resulting from the high $Ca^{2+}xPi$ product and increased expression of pro-calcifying proteins promote the expression calcification inhibitors such as sclerostin, DKK1, osteoprotegerin and osteopontin in order to prevent the occurrence of further calcification. The model of soft-tissue mineralization induced by treatment with ERKi, MEKi or FGFRi that I hypothesized is represented in Figure 3.28.
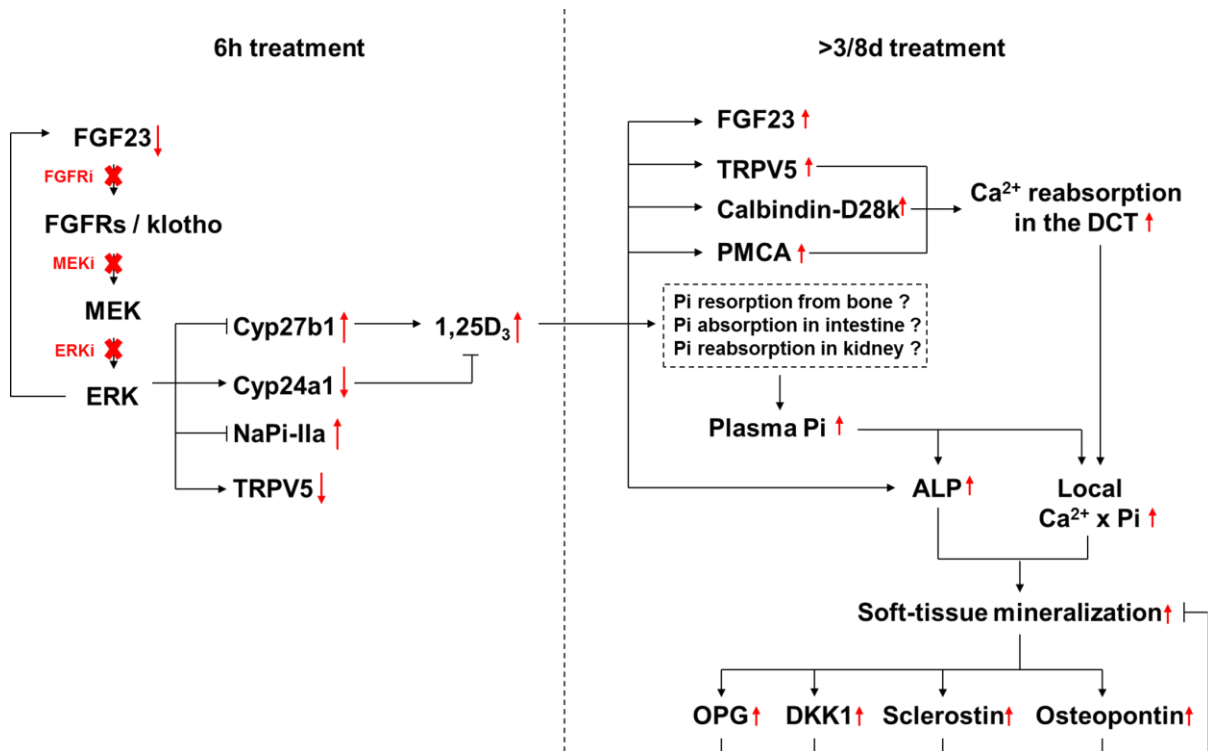
Figure 3.28: Model of the soft-tissue mineralization induced by administration of ERKi, MEKi or FGFR to rats. The model hypothesises the effects of ERKi, MEKi and FGFRi 6h after dosing (left) and following >3d/8d treatment with these inhibitors (right). ALP, alkaline phosphatase; OPG, osteoprotegerin.

4 Evaluation of an ex vivo kidney tissue slice model

4.1 Introduction

In the previous chapters I have addressed the renal mechanisms by which ERK 1/2 (ERKi), MEK 1/2 (MEKi) or FGFR 1-3 (FGFRi) induce soft-tissue mineralization by carrying out *in vivo* studies with rats. Rats treated with these inhibitors evidenced soft-tissue mineralization associated with alterations in the renal expression of key genes/proteins for mineral homeostasis including Cyp27b1, TRPV5 and alkaline phosphatase. In addition, these animals evidenced alterations in plasma levels of different hormones including FGF23, osteoprotegerin and DKK1. Moreover, these biological effects were different in animals dosed acutely (6h) or repeatedly (>3d) with ERKi, MEKi or FGFRi. Due to the systemic character, such complex mechanisms are difficult to unravel using only *in vivo* studies. *In vitro* or *ex vivo* models allow the assessment of drug effects in specific organs, tissues or cell types and therefore these models are often used as alternatives or complements to *in vivo* studies. There is a range of kidney cell lines currently available, which were originated from different nephron segments including proximal tubule (opossum kidney, OK; human renal proximal tubular epithelial cell, hRPTEC; human kidney 2, HK-2), distal tubule (mouse distal convoluted tubule, MDCT; murine distal convoluted tubule 4, mpkDCT4) and collecting duct (human collecting duct, HCD) (Bens and Vandewalle 2008). Some of these cell lines have been used for studies of mineral homeostasis. For instance, OK cells have been used to study the effects of hormones and drugs on phosphate reabsorption (Nashiki et al. 2005, Patzer et al. 2006). Also, MDCT (Gesek and White 1997, Magyar et al. 2002) and mpkDCT4 (Diepens et al. 2004) cells have been used to study the physiological processes associated with calcium reabsorption. In addition to the established cell lines, human primary kidney cells have been described as a suitable model to study mineral ion homeostasis. Work carried out by Dr. Rebecca Wadey at Cardiff University has shown these cells express key proteins for mineral homeostasis including FGF receptors, TRPV5 and NaPi-IIa and retain responses to known physiological stimuli including FGF23 induced ERK phosphorylation and modulation of NaPi-IIa expression by phosphate. Nevertheless, the use of cell models for studies of mineral homeostasis has severe limitations. Established cell lines consist

of a specific cell type, thus not truly representing the nephron, which is composed by different segments, each containing different cell types. Also, most of the available kidney cell lines consist in cells that have de-differentiated to some extent, lacking the ability to polarize and the expression of kidney-specific proteins. Primary kidney cells may be a more representative model of the nephron since these show a lower level of de-differentiation than established cultures and can be composed of different cell types. Nevertheless primary cells encompass other limitations including more difficult culture protocols, higher variability and the loss of a kidney-like phenotype when the cells are cultured for >7d (Ekwall et al. 1990). In addition to primary cells and established cell lines, organotypic slice cultures have been used to study the kidney *ex vivo*. Precision microtomes (Krumdieck et al. 1980) allow the cutting of thin tissue slices that preserve key characteristics of *in vivo* tissue including tissue architecture, interactions between different cells and interactions between cells and matrix. Organotypic kidney slices were previously shown to retain kidney-specific characteristics after a few days in culture and to be suitable for toxicology studies (Vickers et al. 2004). In this chapter I aimed to establish an *ex vivo* kidney model that would allow the study of the mechanisms of mineralization induced by ERKi, MEKi or FGFRi. In order to accomplish this, kidney slices cultured for 1h, 1d and 3d were evaluated for cellular morphology, viability and expression of key proteins involved in mineral homeostasis. Also, these slices were evaluated for responses to known physiological stimuli including Pi changes and MEK inhibition. The results from this chapter suggest that this kidney slice model is suitable for studies of mineral homeostasis only up to 1d, deeming it an unsuitable model to study the effects of ERKi, MEKi and FGFRi in the process of soft-tissue mineralization.

4.2 Methods

4.2.1 Tissue slice preparation and culture

Animal kidney tissue was obtained from Han Wistar rats, supplied by Harlan (Hillcrest, UK) or Charles River (Harlow, UK). Han Wistar rats aged between 1 and 3 months were killed by CO_2 inhalation and kidneys were collected. The kidney capsule and surrounding fat were removed and the kidneys were washed in PBS. Kidneys were cut in half along the transverse plane, mounted to the jig of an Integraslice 7550 PSDS (Campden Instruments, Loughborough, UK) and embedded in 1.8% low melting point agarose (Life Technologies, Carlsbad, USA) in PBS. The jig was screwed into the Integraslice chamber, which was then filled with PBS at 4ºC. Slices were cut at a 200 µm thickness with 0.25 mm/s speed and 1.5 mm slicing amplitude. Slices were stored in a dish filled with sterile PBS at 4°C for up to 2h until all slices had been cut. Slices were transferred to individual wells of a 12-well-plate containing Dulbecco's modified Eagle medium (DMEM) / nutrient mixture F-12 (DMEM/F12) medium (Life Technologies, Carlsbad, USA), supplemented with 10% fetal bovine serum (GE Healthcare, Little Chalfont, UK) and 2% penicillin/streptomycin (Life Technologies, Carlsbad, USA). The plate was incubated at 37°C in a 5% CO_2 / 95% air atmosphere and culture media was changed once daily. At the end of the incubation time, slices were either snap frozen in liquid nitrogen or fixed in neutrally buffered formalin for 1h and embedded in paraffin.

4.2.2 Western blotting

Rat kidney slices were homogenized in modified RIPA buffer (25 mM Tris HCl pH 7.6, 150 mM NaCl, 1% NP40, 0.1% sodium dodecyl sulfate, 1% sodium deoxycholate, 1 mM n-ethylmaleimide, 1 mM phenylmethanesulfonylfluoride) containing Halt protease and phosphatase inhibitors (Pierce, Rockford, USA). Cell lysis was carried out using a Dounce homogenizer (Wheaton, Rochdale, UK). Following lysis, homogenates were centrifuged at 10,000 x g for 5 min to remove insoluble debris. Protein extracts were quantified using a BCA protein assay (Pierce, Rockford, USA). Twenty micrograms of each extract were electrophoresed on NuPage® 10% or BisTris polyacrylamide gels (Invitrogen, Paisley, UK). Gels were transferred to nitrocellulose membranes and stained with Ponceau S to confirm even protein loading of wells. Non-specific protein binding was blocked using 5% low-fat dried milk in Tris-buffered saline containing

0.1%Tween (TBST) for 1h at room temperature. Phospho-ERK (CST4376, Cell Signaling Technology, Danvers, USA) or total-ERK (CST4695, Cell Signaling Technology) primary antibodies were added at a concentration of 1:2000 in 5% milk/TBST overnight at 4ºC. An HRP-conjugated anti-mouse or anti-rabbit secondary antibody (Promega, Madison, USA) was added appropriately at a concentration of 1:20,000 or 1:6,000 in 5% milk/TBST before detection of immunoreactivity with ECL prime and development on a ChemiDoc MP (Biorad, Hercules, USA).

4.2.3 *Immunohistochemistry*

Kidneys were fixed for 24 to 48h in 10% neutral-buffered formalin, embedded in paraffin, and 4µm sections were cut. Sections were de-waxed using xylene and rehydrated using 100% and 95% ethanol. Heat-mediated antigen retrieval was performed by incubating the sections in 10 mM Citrate buffer, pH 6 at 100°C for 10 min. Endogenous peroxidase activity was blocked with 3% (aq) hydrogen peroxide for 10 min. Nonspecific binding of the antibody was prevented by incubating slides with blocking solution (phosphate buffered saline containing 0.5% Tween 20, 1% bovine serum albumin and 3% of Seablock blocking buffer (EastCoast Bio, North Berwick, USA) for 20 min. Slides were incubated with primary antibodies (Table 4.1) diluted at 1:200 in blocking solution for 1h at room temperature. Goat anti-mouse or goat anti-rabbit secondary antibody (DAKO, Glostrup, Denmark) diluted at 1:800 in blocking solution was applied to the slides, and peroxidase was visualized with diamino benzidine (DAKO, Glostrup, Denmark). Sections were counterstained using hematoxylin (Carazzi's) for 1min before dehydrating in 95% and 100% ethanol, clearing in xylene, and mounting using Hystomount (TAAB Labs, Aldermaston, UK). Negative controls were performed using isotype controls or omission of the primary antibodies.

Whole slide images were scanned in a Scanscope® scanner (Aperio Technologies Incorporated, Vista, USA). Positive Pixel Count Algorithm of the ImageScope software (Aperio Technologies Incorporated, Vista, USA), was used to quantify the positive signal in whole kidney. Detection thresholds were manually set in order to obtain the best signal/noise ratio for NaPi-IIa. The percentage of positive staining (relative stained area) was calculated as the sum of all stained pixels divided by the sum of all stained and unstained pixels.

Table 4.1: Antibodies used for immunohistochemistry

Protein	Supplier/Code	Raised in
CaSR	Thermo / MA1-934	Mouse
Klotho	Alpha Diagnostic / KL11-A	Rabbit
NaPi-IIa	Alpha Diagnostic / NPT27-A	Rabbit
PMCA	Santa Cruz / sc-20028	Mouse
TRPV5	Alomone / ACC-035	Rabbit
VDR	Santa Cruz / sc-13133	Mouse

4.2.4 ATP assay

Kidney slices were cultured for 1h, 1d or 3d, snap frozen in liquid nitrogen and stored at -80 C. On the day of the assay, slices were removed from the -80ºC, weighted and a previously described phenolic extraction method (Chida et al. 2012) was used to extract ATP. The phenolic extracts were quantified using a luminescent ATP determination kit (Life Technologies, Carlsbad, USA), according to the manufacturer's instructions.

4.2.5 Phosphate response assay

After slicing, kidney slices were acclimatized at 37°C for 1h in DMEM/F12 medium (Life Technologies, Carlsbad, USA), supplemented with 10% fetal bovine serum (GE Healthcare, Little Chalfont, UK) and 2% penicillin/streptomycin (Life Technologies, Carlsbad, USA). After 1h, slices were transferred into DMEM medium containing no Pi (Life Technologies, Carlsbad, USA), supplemented with 10% fetal bovine serum (GE Healthcare, Little Chalfont, UK), 2% penicillin/streptomycin (Life Technologies, Carlsbad, USA) and either 0 or 2 mM sodium phosphate. After 4h slices were fixed in 10% neutrally buffered formalin for 1h and embedded in paraffin. Response to phosphate was assessed by analysing NaPi-IIa expression by IHC as described above.

4.2.6 ERK inhibition assay

After slicing, kidney slices were acclimatized at 37°C for 1h in DMEM/F12 medium (Life Technologies, Carlsbad, USA), supplemented with 10% fetal bovine serum (GE Healthcare, Little Chalfont, UK) and 2% penicillin/streptomycin (Life Technologies, Carlsbad, USA). After 1h, slices were transferred into DMEM/F12 medium containing

no serum and were incubated for 1h in a thermal block at 37°C. After 1h, the MEK inhibitor U0126 (Sigma, St Louis, USA) was added at a concentration of 0 or 15 nM, along with 50 ng/mL of epidermal growth factor (Lonza, Basel, Switzerland), used to induce ERK activation. After 10 min slices were snap frozen with liquid nitrogen. ERK inhibition was then analysed by Western blotting as described above.

4.2.7 Statistics

All data shown represents mean ± standard error of the mean. Statistical analysis was carried out with Microsoft Office Excel (Microsoft, Redmond, USA) using the Real Statistics Resource Pack. A two-tailed, Mann Whitney U test was employed and p values lower that 0.05 were considered to be significant.

4.3 Results

4.3.1 Morphology and viability of cultured kidney slices

By H&E (Figure 4.1 A-D), no differences in morphology were observed in control kidney and in slices cultured for 1h. The morphology was mostly preserved in slices cultured for 1d, however there was some evidence of tissue damage including nuclear pleomorphism, vacuolation and loss of PT brush border. Tissue damage was increased in slices cultured for 3d, which showed evidences of tubular necrosis including homogeneous eosinophilic cytoplasm and absence of nuclei.

The cellular ATP levels (Figure 4.2) measured in kidney slices cultured for 1h (50.36 ± 5.09 nmol ATP/mg wet weight) were comparable to the ATP levels previously reported for freshly cut kidney tissue (53.85 ± 3.34 nmol ATP/mg wet weight) (Jaramillo-Juárez et al. 2005). The ATP values remained unchanged in slices cultured for 1d and reduced by 98% in slices cultured for 3d. These data suggests that kidney slices are viable up to 1d in culture.

Kidney slices cultured for 1h show a similar morphology as control kidney tissue. Conversely, tissue damage is evident in slices cultured for >1d.

ATP contents were similar in slices cultured for 1h and 1d, but strongly reduced in slices cultured for 3d, suggesting that kidney slices are viable up to 1d in culture.
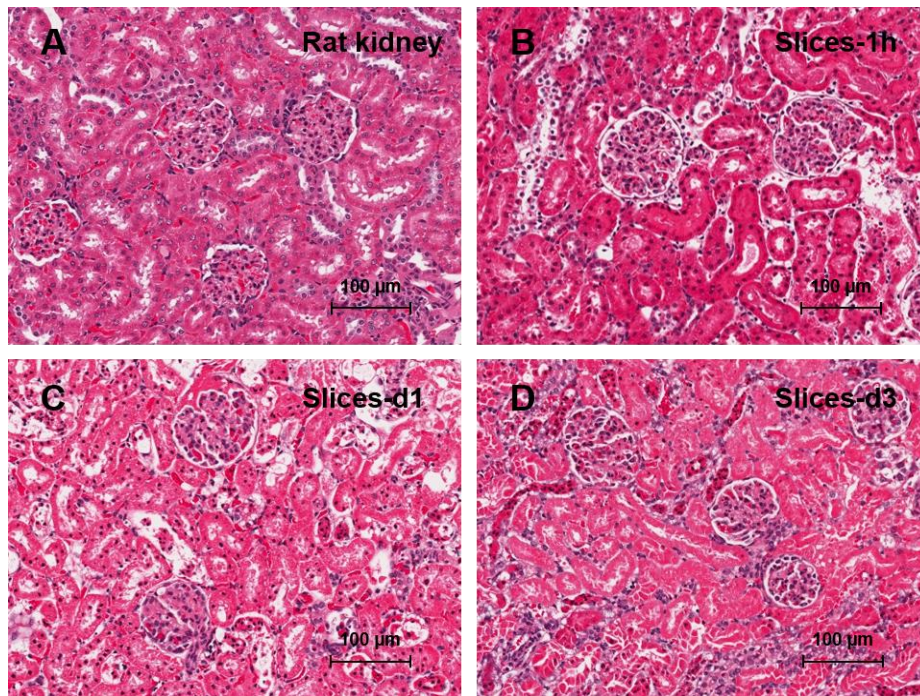
Figure 4.1: Morphology of rat kidney slices cultured for 1h, 1d and 3d.
Photomicrographs of hematoxylin and eosin staining in sections from control rat kidney (A) and kidney slices cultured for 1h (B), 1d (C) and 3d (D). Data representative of N = 3 rats. Scale bar = 100 µm.
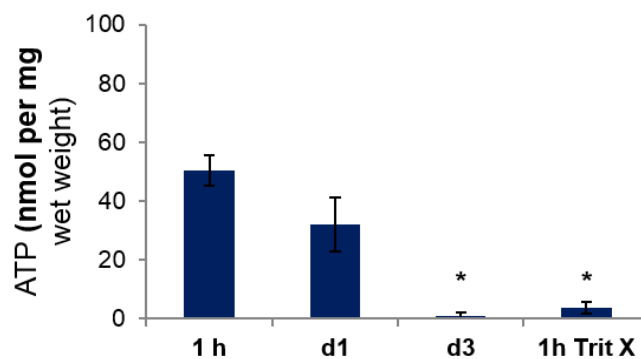
Figure 4.2: Viability of rat kidney slices cultured for 1h, 1d and 3d. Viability analysed by assessing the ATP contents of kidney slices cultured for 1h, 1d and 3d (E). Negative control for viability performed by incubating the kidney slices for 1h with 1% Triton X. Data representative of N = 3 rats + SEM. * $p < 0.05$ vs slices incubated for 1h (Mann-Whitney test).

4.3.2 Kidney slices cultured for up to 3 days express CaSR, Klotho, NaPi-IIa, TRPV5, calbindin-D28k and PMCA.

A problem that may be associated with *ex vivo* models is the de-differentiation of cells and loss of expression of cell type specific proteins. In order to confirm that the expression of key proteins for mineral homeostasis is not lost in cultured kidney slices, the expression of CaSR (Figure 4.3 A,D,G,J), Klotho (Figure 4.3 B,E,H,K), NaPi-IIa (Figure 4.3 C,F,I,L), TRPV5 (Figure 4.4 A,D,G,J), calbindin-D28k (Figure 4.4 B,E,H,K) and PMCA (Figure 4.4 C,F,I,L) was analysed by IHC in slices cultured for 1h, 1d and 3d and compared to the expression of these proteins in control kidney tissue. No changes in protein distribution were observed between control kidney and slices cultured for 1h and 1d for all proteins. Moreover, all the analysed proteins were still expressed in slices cultured for 3d, however it was difficult to assess if the protein distribution is similar due to the poor morphology observed at these time points.

Expression of key proteins for mineral homeostasis is maintained in kidney slices cultured up to 3 days.
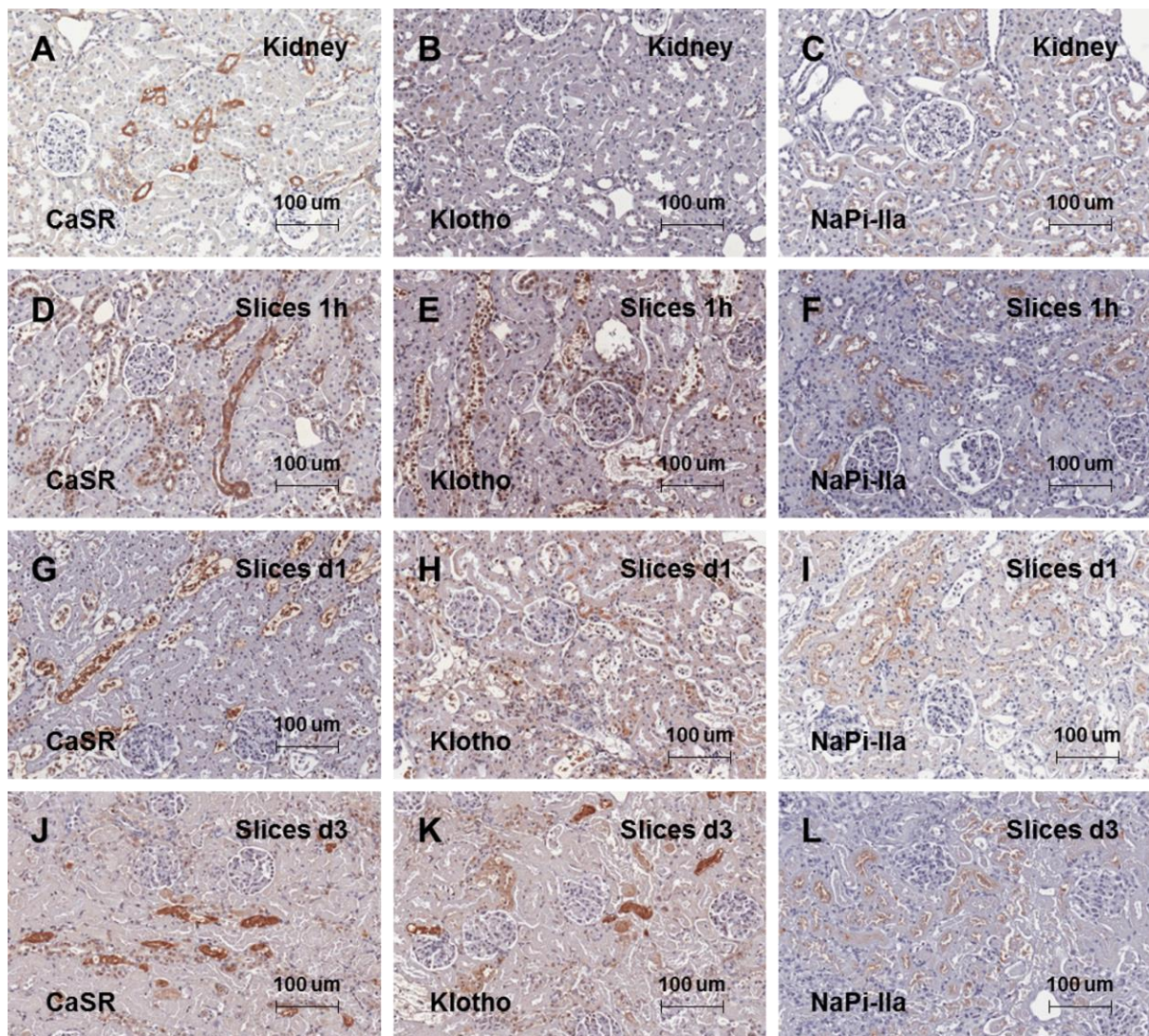
Figure 4.3: Expression of CaSR, Klotho and NaPi-IIa in rat kidney slices cultured for 1h, 1d and 3d. High magnification photographs of CaSR (A,D,G,J), Klotho (B,E,H,K) and NaPi-IIa (C,F,I,L) in sections from control rat kidney (A-C) and kidney slices cultured for 1h (D-F), 1d (G-I) and 3d (J-L). Data representative of $N = 3$. Scale bar = 100 μm.
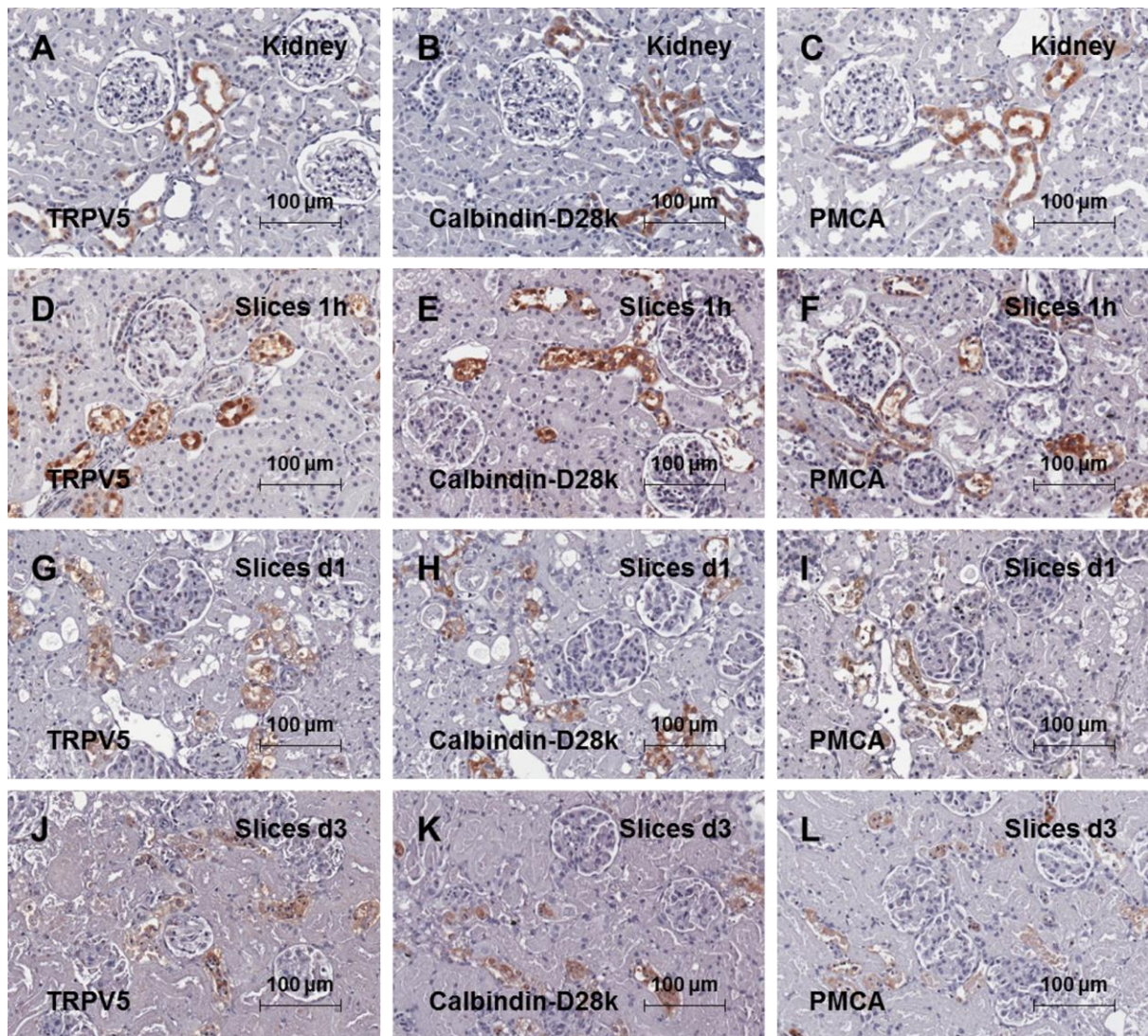
Figure 4.4: Expression of TRPV5, calbindin-D28k and PMCA in rat kidney slices cultured for 1h, 1d and 3d. Photomicrographs of TRPV5 (A,D,G,J), calbindin-D28k (B,E,H,K) and PMCA (C,F,I,L) in sections from control rat kidney (A-C) and kidney slices cultured for 1h (D-F), 1d (G-I) and 3d (J-L). Data representative of $N = 3$ rats. Scale bar = 100 µm.

4.3.3 Kidney slices retain functional characteristics of the kidney tissue

The functionality of the cultured kidney slices was analysed through the assessment of responses to known physiological stimuli. Namely, the expression of NaPi-IIa was assessed by IHC in kidney slices incubated for 4h in media containing 0 mM or 2 mM of Pi (Figure 49). A 24% increase in NaPi-IIa expression was observed in slices incubated with 0 mM Pi versus 2 mM Pi. Also, the phosphorylation and expression of ERK were analysed by Western blotting in kidney slices incubated for 20 min with 50 ng/mL EGF and 0 nM or 15 nM of the MEK inhibitor U0126 (Figure 50). ERK phosphorylation was strongly decreased in slices treated with U0126, whilst total ERK expression remained unchanged. These results show that this kidney slice model retains functional responses to extracellular Pi changes and MEK inhibition.

Expression of NaPi-IIa in cultured kidney slices was modulated by the levels of Pi in the medium.

Inhibition of MEK resulted in a reduction of EGF-induced ERK phosphorylation, but not total ERK expression in cultured kidney slices.
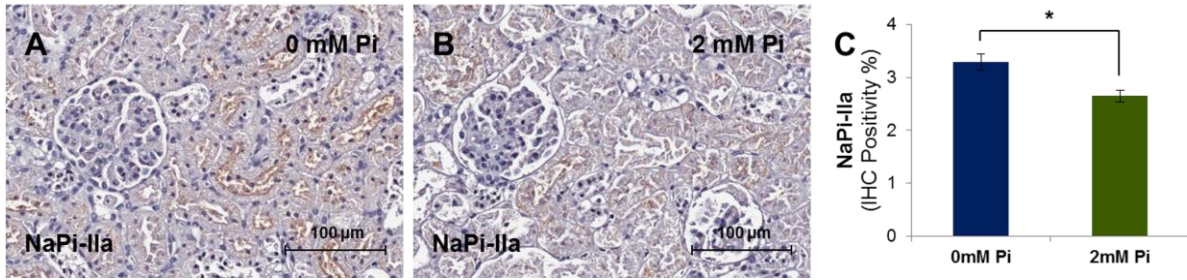
Figure 4.5: Functional characterization of rat kidney slices – response to Pi. Photomicrographs of NaPi-IIa immunostaining in sections of rat kidney slices incubated for 4h in culture media containing 0 mM (A) or 2 mM (B) of Pi. Positive signal in immunohistochemistry corresponds to the brown staining. Histogram represent the quantification of NaPi-IIa expression (immunohistochemically stained area) in animals from the study S1 (C). Data representative of N = 4 rats + SEM. * p<0.05 (Mann-Whitney test). Scale bar = 100 µm.
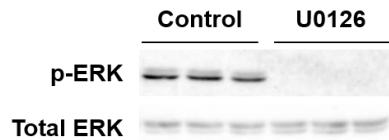
Figure 4.6: Functional characterization of rat kidney slices – response to a MEK inhibitor. Western blotting to assess the expression of phospho-ERK (p-ERK) and total ERK in rat kidney sections incubated for 20m with 50ng/mL of EGF in the presence or absence of 15 nM of the MEK inhibitor U0126. Data representative of N = 3 rats.

4.4 Discussion

The results from Chapter 3 show that MEK/ERK or FGFR inhibition affect the renal expression of genes/proteins involved in processes that contribute to mineral ion homeostasis, such as production of $1,25D_3$ and Ca^{2+} reabsorption. Since these processes take place in different nephron segments, the *ex vivo* study of the effects of MEK/ERK or FGFR inhibition at the organ level requires the use of models that preserve the identity and function of the cells from each of the nephron segments. Kidney slices were previously shown to retain renal cell architecture and kidney-specific characteristics after a few days in culture (Vickers et al. 2004). Hence, I decided to evaluate the suitability of using kidney slice cultures as a model to study processes associated with Ca^{2+} and Pi homeostasis. If deemed a suitable model, I aimed to use kidney slice cultures to assess the process of mineralization induced by MEKi and FGFRi. The initial experiments that I intended to carry out using the kidney slice cultures are described in Chapter 5.3 / Table 5.5.

In this study, kidney slices cultured up to 1d were viable and showed similar features as control kidney tissue including cellular morphology and expression of six key proteins for mineral homeostasis (TRPV5, calbindin-D28k, PMCA, NaPi-IIa, CaSR and Klotho). Besides, the kidney slices retained functional aspects of the kidney including responses to extracellular Pi and to MEK inhibition. These findings suggest that the kidney slice cultures assessed in this study are a suitable model for short-term (<1d) studies of Ca^{2+} and Pi homeostasis. Consistent with this observation, a previous study has shown that uncultured kidney slices show a decrease in Pi reabsorption following a 30-min incubation with FGF23 and/or PTH (Weinman et al. 2011). Although kidney slice cultures have not been commonly used for studies of mineral homeostasis, these have been widely used to study other topics including drug efficacy (Poosti et al. 2015) and drug toxicity (Vickers et al. 2004). A limitation of the kidney slice culture model analysed in this study is the large decrease in viability and pronounced tissue damage observed in slices cultured for 3d, which deems the model unsuitable for studies longer than 1d. Considering that most of the renal effects of MEKi and FGFRi *in vivo*, including soft-tissue mineralization, were only observed following treatments longer that 1d, this model may not be suitable to study the

biological effects induced by the treatment with these inhibitors. The quality and survival of tissue slices is depends on three main factors: slice thickness (Parrish et al. 1995), which should be low in order to allow the exchange of nutrients and oxygen; culture media (Obatomi et al. 1998), which should contain a suitable chemical and nutrient composition; and culture conditions, which should provide an adequate exposure of the slices to culture media and to oxygen (Toutain et al. 1998). The thickness of the slices (200 µm) and the culture media (DMEM/F12) used in this study were previously reported to be suitable for kidney slice culture (Obatomi et al. 1998). Nevertheless, the culture conditions (static multi-well plate) used in this study may have not been the most suitable for the proper aeration of the kidney slices, which possibly contributed to a rapid loss of viability. Previous studies have shown that kidney slices can be cultured up to at least 5 days by using a dynamic culture method (Parrish et al. 1995). This method consists of loading the kidney slices into titanium inserts, which are placed inside vials containing a small volume of culture media. Then, the vials are incubated in a rotator in order to alternately expose the slices to oxygen and culture media. Further studies should address if the kidney slices cultured for 5d with the dynamic culture method are a suitable model for studies of Ca^{2+} and Pi homeostasis. During the assessment of the maximum tolerated dose that preceded the studies presented in Chapter 3, soft-tissue mineralization and increased plasma Pi were observed in rats treated with MEKi for 3d or FGFRi for 2d (data not shown). Hence, by increasing the viability of the slices to 5 days with the use of a culture method such as dynamic culture method, kidney slice cultures may become a suitable model to assess the mineralization induced by MEKi and FGFRi.

4.5 Conclusions

In summary, kidney slices cultured up to 1d retain key features of kidney tissue including cellular morphology, expression of key proteins for mineral homeostasis and functionality. Conversely, slices incubated for longer than 1d show pronounced tissue damage and severely decreased viability. These results suggest that the kidney slices are usable for studies of mineral ion homeostasis only up to 1d. This limitation deems this model unsuitable to study the mechanisms of mineralization induced by treatment with ERKi, MEKi and FGFRi.

5 Key findings and future directions

Over the course of this thesis I have assessed the renal mechanisms of soft-tissue mineralization induced by the inhibition of the MEK/ERK pathway or the inhibition of FGF receptors. Below, I describe the key findings of each chapter and suggest experiments that would clarify or further explore some of the aspects associated with these mechanisms.

5.1 Intra-renal distribution and role of the CaSR in the mineralization induced by inhibition of MEK/ERK pathway and FGF receptors

I set out to assess the role of the renal CaSR in the mineralization induced by MEK/ERK or FGFR inhibition, since this receptor has been previously described to regulate key processes for mineral ion homeostasis including $1,25D_3$ production (Bland et al. 2002) and Ca^{2+} (Loupy et al. 2012) and Pi (Ba et al. 2003) reabsorption.

Since the intra-renal distribution of the CaSR is a controversial topic, I first analysed the renal expression of this receptor using ISH, IHC and PLA techniques. The CaSR was detected throughout the nephron including the glomerulus, PT, TAL, DCT, CNT and CD segments. This distribution supports previous roles reported for the CaSR in different processes associated with mineral homeostasis including $1,25D_3$ production and Pi reabsorption in the PT (Bland et al. 2002, Ba and Friedman 2004), calcium reabsorption in the TAL (Loupy et al. 2012) and DCT (Topala et al. 2009) and acid secretion in the CD (Renkema et al. 2009). Moreover, the clarification of the renal CaSR expression pattern allows further physiological roles to be determined in the kidney. A straightforward way of studying such roles is the assessment of the phenotype of nephron segment specific CaSR knockout mice models.

Having the CaSR intra-renal distribution clarified, I analysed the effects of the administration of a MEK 1/2 inhibitor (MEKi) or an FGFR 1-3 inhibitor (FGFRi) to rats on the occurrence of soft-tissue mineralization, plasma levels of Ca^{2+} and Pi in the renal expression of the CaSR. Both inhibitors induced an increase in plasma Pi and the occurrence of soft-tissue mineralization of different organs including kidney,

stomach and heart. Conversely, none of the inhibitors had any effect in plasma levels of Ca^{2+} or in the expression or cellular distribution of the CaSR. Although these results may suggest that the renal CaSR is not a key protein for the soft-tissue mineralization induced by MEKi or FGFRi, this conclusion cannot be drawn without assessing the effect of these inhibitors in the activation and downstream signalling of the CaSR.

5.2 Effects of the inhibition of the MEK/ERK pathway or the FGF receptors in mineral homeostasis and soft-tissue mineralization

Further analysis carried out in rats treated with ERKi, MEKi and FGFRi have shown that acute (6h) and repeated (>3/8d) dosing with these compounds resulted in different biological effects. Acute dosing with the ERKi and FGFRi resulted in the following effects:

-        Decrease in plasma FGF23;

-        Upregulation of Cyp27b1 and a downregulation of Cyp24a1 in the kidney, which are consistent with an increase in the production of $1,25D_3$;

-        Shift in NaPi-IIa expression from cytoplasmic vesicles to the brush border membrane.

Conversely, following repeated dosing, ERKi/MEKi and FGFRi induced the following effects:

-        Increase in plasma Pi

-        Increase in plasma FGF23;

-        Attenuation of the expression changes in Cyp27b1 and Cyp24a1;

-        Alteration of the NaPi-IIa expression pattern in the kidney: decreased NaPiIIa expression in the outer kidney cortex in animals treated with ERKi (3d) or FGFRi (8d); increased NaPiIIa expression in the inner cortex in animals treated with MEKi (28d);

-        Increase in the renal expression of TRPV5, calbindin-D28k and PMCA, consistent with an increased reabsorption of Ca^{2+} in the DCT;

-        Increase in the renal expression of the mineralization inducer alkaline phosphatase;

- Increase in the renal expression of osteopontin and plasma expression of DKK1, osteoprotegerin and sclerostin, which are mineralization inhibitors normally expressed in mineralized tissue.

Most of the effects observed following >3/8d treatment with the inhibitors are consistent with the toxicity of 1,25D$_3$. Unfortunately, it was not possible to accurately quantify 1,25D$_3$ in animals treated with ERKi, MEKi and FGFRi. This impediment is associated with the fact that the assays available for 1,25D$_3$ attain a low sensitivity which would not allow an accurate quantification of this hormone in the samples from this study (N = 3-6 animals per group). The number of animals used in this study was selected by carrying out power analysis for different parameters including soft-tissue mineralization and serum levels of Pi and FGF23 but not serum levels of 1,25D$_3$. A power analysis estimated that a much larger number of animals than what was used in this study (N > 22 per group) would be needed to obtain significance from the 1,25D$_3$ quantification. Also due to the low sensitivity of the assay and/or inadequate sample processing, it was not possible to accurately quantify PTH in animals from this study. PTH may be involved in the process of mineralization induced by ERKi, MEKi and FGFRi since it is a key hormone for mineral homeostasis, susceptible to regulation by FGF23 and 1,25D$_3$. The plasma levels of 1,25D$_3$ and PTH should be addressed in future studies by developing better assays to quantify these hormones or by carrying out *in vivo* studies using a larger number of animals.

Other limitations of this study include problems with the licensing of MEKi, which precluded the performance of studies comprising the acute administration of this compound; and the impossibility of analysing urinary function and urinary Ca^{2+} and Pi levels, since the experimental design used in this study was not compatible with the collection of urine using metabolic cages due to the home office license regulations. The acute effects of MEK inhibition should be addressed in further studies using MEKi, in case the licensing problems with this compound are solved, or alternatively in studies using a commercially available MEK inhibitor. Also, future studies should comprise the collection of urine to assess urinary function and urinary Ca^{2+} and Pi levels. Table 5.1 summarizes the limitations of this study.

Table 5.1: Limitations of the *in vivo* studies with ERKi, MEKi and FGFRi.

Parameter		Comment
Plasma 1,25D$_3$		Assay used attained low sensitivity. Only tested in animals treated with MEKi
Plasma PTH		Assay used attained low sensitivity. Only tested in animals treated with MEKi and FGFRi
Urinary function		Assay not carried out because urine could not be collected
Urine Ca^{2+}		Assay not carried out because urine could not be collected
Urine Pi		Assay not carried out because urine could not be collected
FGFR pathway activation		Different phospho-FGFR and phospho-FRS2 assays were tested, however these did not allow a sensitive detection of their intended targets
MEKi experiments	6h treatment	The licensing of MEKi did not allow to carry out the study
	Cyp27b1 / Cyp24a1	No frozen tissue samples were available to carry out mRNA extractions
	Sclerostin	No plasma samples were available to perform these assays
	Osteoprotegerin	
	DKK1	

In order to assess which nephron segments could be directly affected by the treatment with ERKi, MEKi or FGFRi, the intra-renal distributions of their targets ERK, MEK and FGFRs 1-4 were assessed in control rat kidney. The expression of these proteins was detected throughout the nephron including the PT, DT and CD (not FGFR4) segments. These findings are consistent with ERKi, MEKi and FGFRi regulating renal processes such as 1,25D$_3$ production and Pi reabsorption by analogous mechanisms involving the inhibition of FGF23 signalling at the MEK/ERK pathway or at the FGFRs level.

The administration of ERKi and MEKi to rats resulted in the inhibition of ERK signalling in the kidney, thus confirming the intended inhibitory effects of both inhibitors. Conversely, ERK activation was unaffected in rats treated with FGFRi. Since the MEK/ERK pathway is activated by different receptors, it is possible that FGFRi is able

to inhibit the FGFR-induced ERK activation, whilst having little effect on the overall activation of this pathway. An RPPA assay was carried out to identify cell signalling pathways affected by the administration of ERKi and FGFRi that might contribute to the occurrence of soft-tissue mineralization. With the exception of phospho-ERK upregulation by ERKi, the proteins analysed by the RPPA assay only showed small expression changes (<40% expression) in animals treated with ERKi or FGFRi, which suggests that the key pathways leading to soft-tissue mineralization were not identified by this assay. Since the experiments carried out in this study did not show any strong evidence that FGFRi directly targets the kidney, I aimed to analyse the activation of FGFR pathway. As no methods to detect FGFR activation in rat kidney had been described, I assessed the suitability of carrying out IHC or Western blotting using two different phospho-FGFR and a phospho-FRS antibodies for this purpose. Unfortunately, none of these methods allowed a sensitive detection of the intended targets. This issue should be addressed in further studies.

Table 5.2, Table 5.3 and Table 5.4 show key future studies that can be performed to further the understanding of the mechanisms of mineralization induced by ERKi, MEKi or FGFRi. These include the confirmation of the role of $1,25D_3$, Ca^{2+} reabsorption and alkaline phosphatase in the mechanism of soft-tissue mineralization; the identification of the origin of the increased plasma Pi; and the assessment of the roles of FGF23 and bone hormonal production in the mechanisms of soft-tissue mineralization.

Table 5.2: Future experiments using *in vivo* studies to further unravel the mechanisms of mineralization induced by ERKi, MEKi or FGFRi - 1

Parameter	Rationale / Assays
Origin of increased Pi	*Rationale* – The results obtained in this study show that Pi is increased in animals treated with ERKi, MEKi or FGFRi. Since NaPi-IIa was not markedly upregulated in animals treated with these inhibitors, the increase in Pi is likely induced by increased expression of other Pi transport proteins in kidney or intestine, by increased Pi resorption from bone or by a decrease in urinary function. *Assay* - Dose animals with ERKi, MEKi or FGFRi and analyse the following parameters: *Bone resorption* - Analyse serum markers of bone resorption (eg. carboxy-terminal collagen crosslinks, CTX (Rosen et al. 2000)) and analyse bone expression of proteins involved in the resorption process *Intestinal absorption* - Analyse the expression of the type IIb sodium-phosphate co-transporter (NaPi-IIb) in the intestine and the Pi content in the faeces *Renal reabsorption* - Analyse the renal expression of NaPi-IIc and Pit2 and the levels of Pi in the urine *Urinary function* – Analyse creatinine clearance

Table 5.3: Future experiments using *in vivo* studies to further unravel the mechanisms of mineralization induced by ERKi, MEKi or FGFRi - 2

Parameter	Rationale / Assays
Role of 1,25D$_3$	***Rationale*** – The results obtained in this study suggest that an increase in 1,25D$_3$ is the factor that drives the mineral homeostasis perturbations and soft-tissue mineralization in animals treated with ERKi, MEKi and FGFRi. If this holds true, the inhibition of 1,25D$_3$ production or the inhibition of its genomic actions of should prevent these effects ***Assay*** - Dose animals with ERKi, MEKi or FGFRi in combination with an inhibitor of Cyp27b1 such as SDZ88-357 (Lou et al. 2010) or an inhibitor of VDR such as PS121912 (Sidhu et al. 2014) and assess the following parameters: *Mineralization* - Assess mineralization by von Kossa assay *Pi and Ca^{2+}*- Assess plasma levels of Pi and Ca^{2+} and assess the expression of proteins involved in the renal reabsorption of these ions *FGF23* - Assess the plasma levels of FGF23 *Alkaline phosphatase* - Assess protein expression of alkaline phosphatase in kidney.
Role of renal Ca^{2+} reabsorption	***Rationale*** – The results obtained in this study suggest that renal Ca^{2+} reabsorption is increased in the DCT of rats treated with MEKi or FGFRi, which leads to a high local Ca^{2+}xPi product that favours the occurrence of renal soft-tissue mineralization. If this holds true, soft-tissue mineralization should be prevented by the administration of an inhibitor of TRPV5 such as ruthenium red (Nilius et al. 2001). ***Assay*** - Dose animals with ERKi, MEKi or FGFRi in combination with an inhibitor of TRPV5 and assess the following parameters: *Mineralization* - Assess mineralization by von Kossa assay *Pi and Ca^{2+}*- Assess plasma levels of Pi and Ca^{2+} and assess the expression of proteins involved in the renal reabsorption of these ions
Role of alkaline phosphatase	***Rationale*** – The results obtained in this study suggest that alkaline phosphatase expression is increased in kidneys of rats treated with ERKi, MEKi or FGFRi, favouring the occurrence of renal soft-tissue mineralization. If this holds true, soft-tissue mineralization should be prevented by the administration of an alkaline phosphatase inhibitor such as SBI-425 (Sheen et al. 2015). ***Assay*** - Dose animals with ERKi, MEKi or FGFRi in combination with an alkaline phosphatase inhibitor and assess the following parameters: *Mineralization* - Assess mineralization by von Kossa assay. *Pi and Ca^{2+}*- Assess plasma levels of Pi and Ca^{2+} and assess the expression of proteins involved in the renal reabsorption of these ions

Table 5.4: Future experiments using *in vivo* studies to further unravel the mechanisms of mineralization induced by ERKi, MEKi or FGFRi - 3

Parameter	Rationale / Assays
Role of FGF23	***Rationale*** – The results from this study suggest that the increased production of 1,25D$_3$, mineral homeostasis perturbations and soft-tissue mineralization observed in animals treated with ERKi, MEKi and FGFRi are consequences of the inhibition of FGF23 signalling. If this holds true, treatment with an FGF23-neutralizing antibody alone should result in similar biological effects. Besides, the results from this study indicate that the plasma levels of FGF23 increase following >4d treatment with MEKi/FGFRi. The administration of ERKi, MEKi or ERKi in combination with an FGF23 neutralizing antibody aims to assess if the increase in FGF23 plays any role in the occurrence of soft-tissue mineralization. ***Assay*** - Dose animals with an FGF23 neutralizing antibody alone in combination with ERKi, MEKi and FGFRi and analyse the following parameters: *ERK activation* – Assess the phosphorylation of ERK in the kidney *Mineralization* - Assess mineralization by von Kossa assay *Pi and Ca^{2+}* - Assess plasma levels of Pi and Ca^{2+} and assess the expression of proteins involved in the renal reabsorption of these ions *FGF23* - Assess the plasma levels of FGF23 *Alkaline phosphatase* - Assess protein expression of alkaline phosphatase in kidney
Bone effects	***Rationale*** – The results from this study suggest that treatment with ERKi for >8d increased the plasma levels of different bone proteins including FGF23, DKK1, sclerostin and osteoprotegerin. FGF23 is a key protein for mineral homeostasis, DKK1 and sclerostin are inhibitors of Wnt signalling pathway and osteoprotegerin is a key protein for bone resorption. In addition to bone, these four proteins were previously detected in soft-tissue calcified under pathological conditions (Ueland et al. 2009, van Venrooij et al. 2014). Previous studies have reported a crosstalk between FGF23 and Wnt signalling (Farrow et al. 2010), and also roles for both pathways in the process of bone resorption (Sapir-Koren and Livshits 2014). This study aims to assess if the increased expression of the proteins involved in FGF23, Wnt and RANK/osteoprotegerin signalling is originated from bone or from calcifying soft-tissue. Also, it aims to assess if bone resorption contributes to the soft-tissue mineralization induced by ERKi, MEKi or FGFRi. ***Assay*** - Dose animals with ERKi, MEKi or FGFRi and analyse the following parameters: *FGF23* - Assess plasma levels and expression in bone and calcifying tissue *Sclerostin* - Assess plasma levels and expression in bone and calcifying tissue *DKK1* - Assess plasma levels and expression in bone and calcifying tissue *RANKL* - Assess plasma levels and expression in bone and calcifying tissue *Osteoprotegerin* - Assess plasma levels and expression in bone and calcifying tissue *Beta-catenin* - Assess expression in bone and calcifying tissue *Bone resorption markers*- Analyse serum markers of bone resorption (as described above)

5.3 Evaluation of an ex vivo kidney tissue slice model

I evaluated the suitability of using kidney slice cultures to study the soft-tissue mineralization induced by MEK/ERK or FGFR inhibition, since the kidney *in vitro* models described in the literature encompass limitations that preclude an accurate assessment of some of the key processes associated with mineral ion homeostasis. Kidney slices cultured for <1d retained key features of kidney tissue including cellular morphology, expression of key proteins for mineral homeostasis and functionality, whilst slices cultured for >1d showed pronounced tissue damage and severely decreased viability. These results suggest that the kidney slice cultures may be a suitable model for studies of mineral ion homeostasis lasting only up to 1d, which might not be sufficient to study some of the biological effects induced by ERKi, MEKi and FGFRi including soft-tissue mineralization. Previous studies have shown that by using a dynamic culture method, kidney slices remain viable up to at least 5d in culture (Parrish et al. 1995). Further studies should assess if kidney slices cultured with the dynamic culture method are a suitable model for longer term (5-7d) studies of mineral ion homeostasis. If deemed a suitable model, the kidney slices should be used to further investigate the mechanism of mineralization induced by ERKi, MEKi or FGFRi. The initial experiments planned using the kidney slices are described in Table 5.5.

Table 5.5: Future experiments using kidney slice cultures to further unravel the mechanisms of mineralization induced by ERKi, MEKi or FGFRi

Parameter	Experimental aims
Model validation	Assess if kidney slices cultured with the dynamic culture method retain high viability and characteristics of kidney cells (eg. expression of proteins involved in mineral ion homeostasis and functionality) for 5-7d.
Target inhibition	Assess if treatment with ERKi, MEKi or FGFRi results in the inhibition of the MEK/ERK pathway. Assess if treatment with FGFRi results in the inhibition of FGFR signalling.
Mineralization	Assess if treatment with ERKi, MEKi or FGFRi results in mineralization *ex vivo*.
Ca^{2+} and Pi reabsorption	Assess if the expression of the proteins involved in the reabsorption of Ca^{2+} and Pi is affected by the treatment with ERKi, MEKi or FGFRi. Assess if the inhibition of the uptake of Ca^{2+} with a drug such as ruthenium red (Nilius et al. 2001) or Pi with a drug such as phosphonoformic acid (Brooks et al. 1997) prevents the occurrence of soft-tissue mineralization induced by ERKi, MEKi or FGFRi.
$1,25D_3$ production	Assess if the production of $1,25D_3$ is affected treatment with ERKi, MEKi or FGFRi. Assess if it is possible to prevent the mineralization induced by ERKi, MEKi or FGFRi through the inhibition of Cyp27b1 with a drug such as SDZ88-357 (Lou et al. 2010) .
Pro-calcifying proteins	Assess if the expression of alkaline phosphatase and/or other pro-calcifying proteins is affected by the treatment with ERKi, MEKi or FGFRi. Assess if it possible to prevent the mineralization induced by with ERKi, MEKi or FGFRi by inhibiting the activity of alkaline phosphatase with a drug such as such as SBI-425 (Sheen et al. 2015).

6 References

Abdel-Azeez, H. A.-H. and M. Al-Zaky (2010). "Plasma osteopontin as a predictor of coronary artery disease: association with echocardiographic characteristics of atherosclerosis." Journal of Clinical Laboratory Analysis **24**(3): 201-206.

Abedin, M., T. Omland, T. Ueland, A. Khera, P. Aukrust, S. A. Murphy, T. Jain, U. Gruntmanis, D. K. McGuire and J. A. de Lemos (2007). "Relation of osteoprotegerin to coronary calcium and aortic plaque (from the Dallas Heart Study)." American Journal Cardiology **99**(4): 513-518.

Absi, M. and D. T. Ward (2013). "Increased Endothelin-1 Responsiveness in Human Coronary Artery Smooth Muscle Cells Exposed to 1,25-Dihydroxyvitamin D3." American Journal of Physiology Cell Physiology.

Adams, J. S. and M. Hewison (2012). "Extrarenal expression of the 25-hydroxyvitamin D-1-hydroxylase." Archives of Biochemistry and Biophysics **523**(1): 95-102.

Adams, T. E., N. M. McKern and C. W. Ward (2004). "Signalling by the type 1 insulin-like growth factor receptor: Interplay with the epidermal growth factor receptor." Growth Factors **22**(2): 89-95.

Addison, W. N., D. L. Masica, J. J. Gray and M. D. McKee (2010). "Phosphorylation-dependent inhibition of mineralization by osteopontin ASARM peptides is regulated by PHEX cleavage." Journal of Bone and Mineral Research **25**(4): 695-705.

Addison, W. N., Y. Nakano, T. Loisel, P. Crine and M. D. McKee (2008). "MEPE-ASARM peptides control extracellular matrix mineralization by binding to hydroxyapatite: an inhibition regulated by PHEX cleavage of ASARM." Journal of Bone and Mineral Research **23**(10): 1638-1649.

Almaden, Y., A. Canalejo, A. Hernandez, E. Ballesteros, S. Garcia-Navarro, A. Torres and M. Rodriguez (1996). "Direct effect of phosphorus on PTH secretion from whole rat parathyroid glands in vitro." Journal of Bone and Mineral Research **11**(7): 970-976.

Anderson, H. C. (1969). "Vesicles associated with calcification in the matrix of epiphyseal cartilage." Journal of Cell Biology **41**(1): 59-72.

Anderson, H. C. (2003). "Matrix vesicles and calcification." Current Rheumatology Reports **5**(3): 222-226.

Anderson, H. C., J. B. Sipe, L. Hessle, R. Dhanyamraju, E. Atti, N. P. Camacho and J. L. Millan (2004). "Impaired calcification around matrix vesicles of growth plate and bone in alkaline phosphatase-deficient mice." American Journal of Pathology **164**(3): 841-847.

Andrukhova, O., A. Smorodchenko, M. Egerbacher, C. Streicher, U. Zeitz, R. Goetz, V. Shalhoub, M. Mohammadi, E. E. Pohl, B. Lanske and R. G. Erben (2014). "FGF23 promotes renal calcium reabsorption through the TRPV5 channel." EMBO Journal **33**(3): 229-246.

Andrukhova, O., U. Zeitz, R. Goetz, M. Mohammadi, B. Lanske and R. G. Erben (2012). "FGF23 acts directly on renal proximal tubules to induce phosphaturia through activation of the ERK1/2-SGK1 signaling pathway." Bone **51**(3): 621-628.

Anour, R., O. Andrukhova, E. Ritter, U. Zeitz and R. G. Erben (2012). "Klotho lacks a vitamin D independent physiological role in glucose homeostasis, bone turnover, and steady-state PTH secretion in vivo." PloS One **7**(2): e31376.

Arai-Nunota, N., M. Mizobuchi, H. Ogata, A. Yamazaki-Nakazawa, C. Kumata, F. Kondo, N. Hosaka, F. Koiwa, E. Kinugasa, T. Shibata and T. Akizawa (2014). "Intravenous Phosphate Loading Increases Fibroblast Growth Factor 23 in Uremic Rats." PloS One **9**(3): e91096.

Armbrecht, H. J., M. A. Boltz and T. L. Hodam (2003). "PTH increases renal 25(OH)D3-1alpha -hydroxylase (CYP1alpha) mRNA but not renal 1,25(OH)2D3 production in adult rats." American Journal of Physiology: Renal Physiology **284**(5): F1032-1036.

Armbrecht, H. J., K. Okuda, N. Wongsurawat, R. K. Nemani, M. L. Chen and M. A. Boltz (1992). "Characterization and regulation of the vitamin D hydroxylases." The Journal of Steroid Biochemistry and Molecular Biology **43**(8): 1073-1081.

Askew, F. A., R. B. Bourdillon, H. M. Bruce, R. G. C. Jenkins and T. A. Webster (1930). "The Distillation of Vitamin D." Proceedings of the Royal Society of London. Series B, Containing Papers of a Biological Character **107**(748): 76-90.

Atchison, D. K., M. C. Ortiz-Capisano and W. H. Beierwaltes (2010). "Acute activation of the calcium-sensing receptor inhibits plasma renin activity in vivo." American Journal of Physiology - Regulatory, Integrative and Comparative Physiology **299**(4): R1020-R1026.

Awata, H., C. Huang, M. E. Handlogten and R. T. Miller (2001). "Interaction of the Calcium-sensing Receptor and Filamin, a Potential Scaffolding Protein." Journal of Biological Chemistry **276**(37): 34871-34879.

Ba, J., D. Brown and P. A. Friedman (2003). "Calcium-sensing receptor regulation of PTH-inhibitable proximal tubule phosphate transport." American Journal of Physiology: Renal Physiology **285**(6): F1233-1243.

Ba, J. and P. A. Friedman (2004). "Calcium-sensing receptor regulation of renal mineral ion transport." Cell Calcium **35**(3): 229-237.

Bai, M., S. Quinn, S. Trivedi, O. Kifor, S. H. Pearce, M. R. Pollak, K. Krapcho, S. C. Hebert and E. M. Brown (1996). "Expression and characterization of inactivating and activating mutations in the human Ca2+o-sensing receptor." Journal of Biological Chemistry **271**(32): 19537-19545.

Bai, M., S. Trivedi and E. M. Brown (1998). "Dimerization of the extracellular calcium-sensing receptor (CaR) on the cell surface of CaR-transfected HEK293 cells." Journal of Biological Chemistry **273**(36): 23605-23610.

Bajwa, A., M. N. Forster, A. Maiti, B. L. Woolbright and M. J. Beckman (2008). "Specific regulation of CYP27B1 and VDR in proximal versus distal renal cells." Archives of Biochemistry and Biophysics **477**(1): 33-42.

Barthel, T. K., D. R. Mathern, G. K. Whitfield, C. A. Haussler, H. A. t. Hopper, J. C. Hsieh, S. A. Slater, G. Hsieh, M. Kaczmarska, P. W. Jurutka, O. I. Kolek, F. K. Ghishan and M. R. Haussler (2007). "1,25-Dihydroxyvitamin D3/VDR-mediated induction of FGF23 as well as transcriptional control of other bone anabolic and catabolic genes that orchestrate the regulation of phosphate and calcium mineral metabolism." Journal of Steroid Biochemistry and Molecular Biology **103**(3-5): 381-388.

Ben-Dov, I. Z., H. Galitzer, V. Lavi-Moshayoff, R. Goetz, M. Kuro-o, M. Mohammadi, R. Sirkis, T. Naveh-Many and J. Silver (2007). "The parathyroid is a target organ for FGF23 in rats." Journal of Clinical Investigation **117**(12): 4003-4008.

Bens, M. and A. Vandewalle (2008). "Cell models for studying renal physiology." Pflügers Archiv. European Journal of Physiology **457**(1): 1-15.

Bergwitz, C. and H. Juppner (2010). "Regulation of phosphate homeostasis by PTH, vitamin D, and FGF23." Annual Review of Medicine **61**: 91-104.

Bethke, R. M., C. H. Kick and W. Wilder (1932). "THE EFFECT OF THE CALCIUM-PHOSPHORUS RELATIONSHIP ON GROWTH, CALCIFICATION, AND BLOOD COMPOSITION OF THE RAT." Journal of Biological Chemistry **98**(2): 389-403.

Bikle, Daniel D. (2014). "Vitamin D Metabolism, Mechanism of Action, and Clinical Applications." Chemistry & Biology **21**(3): 319-329.

Bindels, R. J., A. Hartog, J. Timmermans and C. H. Van Os (1991). "Active Ca2+ transport in primary cultures of rabbit kidney CCD: stimulation by 1,25-dihydroxyvitamin D3 and PTH." American Journal of Physiology **261**(5 Pt 2): F799-807.

Blaine, J., M. Chonchol and M. Levi (2015). "Renal Control of Calcium, Phosphate, and Magnesium Homeostasis." Clinical Journal of the American Society of Nephrology **10**(7): 1257-1272.

Blanchard, A., X. Jeunemaitre, P. Coudol, M. Dechaux, M. Froissart, A. May, R. Demontis, A. Fournier, M. Paillard and P. Houillier (2001). "Paracellin-1 is critical for magnesium and calcium reabsorption in the human thick ascending limb of Henle." Kidney International **59**(6): 2206-2215.

Bland, R., D. Zehnder, S. Hughes, A. Rao, P. Stewart and M. Hewison (2002). Modification of calcium sensing receptor expression modulates 25-hydroxyvitamin D3-1alpha-hydroxylase activity in a human proximal tubule cell line. 21st Joint Meeting of the British Endocrine Societies., Harrogate, UK.

Blankenship, K. A., J. J. Williams, M. S. Lawrence, K. R. McLeish, W. L. Dean and J. M. Arthur (2001). "The calcium-sensing receptor regulates calcium absorption in MDCK cells by inhibition of PMCA." American Journal of Physiology: Renal Physiology **280**(5): F815-822.

Block, G. A., K. J. Martin, A. L. de Francisco, S. A. Turner, M. M. Avram, M. G. Suranyi, G. Hercz, J. Cunningham, A. K. Abu-Alfa, P. Messa, D. W. Coyne, F. Locatelli, R. M. Cohen, P. Evenepoel, S. M. Moe, A. Fournier, J. Braun, L. C. McCary, V. J. Zani, K. A. Olson, T. B. Drueke and W. G. Goodman (2004). "Cinacalcet for secondary hyperparathyroidism in patients receiving hemodialysis." New England Journal of Medicine **350**(15): 1516-1525.

Bobryshev, Y. V., A. N. Orekhov, I. Sobenin and D. A. Chistiakov (2014). "Role of bone-type tissue-nonspecific alkaline phosphatase and PHOSPO1 in vascular calcification." Current Pharmaceutical Design **20**(37): 5821-5828.

Bonewald, L. F. and M. J. Wacker (2013). "FGF23 production by osteocytes." Pediatric Nephrology **28**(4): 563-568.

Bonucci, E. (2013). The Mineralization of Bone and Its Analogues with Other Hard Tissues.

Boros, S., R. J. Bindels and J. G. Hoenderop (2009). "Active Ca(2+) reabsorption in the connecting tubule." Pflügers Archiv. European Journal of Physiology **458**(1): 99-109.

Boyce, B. F. and L. Xing (2007). "Biology of RANK, RANKL, and osteoprotegerin." Arthritis Research & Therapy **9 Suppl 1**: S1.

Brandenburg, V. M., R. Kramann, R. Koos, T. Kruger, L. Schurgers, G. Muhlenbruch, S. Hubner, U. Gladziwa, C. Drechsler and M. Ketteler (2013). "Relationship between sclerostin and cardiovascular calcification in hemodialysis patients: a cross-sectional study." BMC Nephrology **14**: 219.

Brinc, D., M. K. Chan, A. A. Venner, M. D. Pasic, D. Colantonio, L. Kyriakopolou and K. Adeli (2012). "Long-term stability of biochemical markers in pediatric serum specimens stored at -80 degrees C: a CALIPER Substudy." Clinical Biochemistry **45**(10-11): 816-826.

Broekman, F., E. Giovannetti and G. J. Peters (2011). "Tyrosine kinase inhibitors: Multi-targeted or single-targeted?" World Journal of Clinical Oncology **2**(2): 80-93.

Brooks, A. N., E. Kilgour and P. D. Smith (2012). "Molecular Pathways: Fibroblast Growth Factor Signaling: A New Therapeutic Opportunity in Cancer." Clinical Cancer Research **18**(7): 1855-1862.

Brooks, D. P., S. M. Ali, L. C. Contino, E. Stack, T. A. Fredrickson, J. Feild and R. M. Edwards (1997). "Phosphate excretion and phosphate transporter messenger RNA in uremic rats treated with phosphonoformic acid." Journal of Pharmacology and Experimental Therapeutics **281**(3): 1440-1445.

Brown, A. P., C. L. Courtney, L. M. King, S. C. Groom and M. J. Graziano (2005). "Cartilage Dysplasia and Tissue Mineralization in the Rat Following Administration of a FGF Receptor Tyrosine Kinase Inhibitor." Toxicologic Pathology **33**(4): 449-455.

Brown, A. P. and S. C. Gad (2010). Development of Serum Calcium and Phosphorus as Clinical Biomarkers for Drug-Induced Systemic Mineralization: Case Study with a MEK Inhibitor. Pharmaceutical Sciences Encyclopedia, John Wiley & Sons, Inc.

Brown, E. M., G. Gamba, D. Riccardi, M. Lombardi, R. Butters, O. Kifor, A. Sun, M. A. Hediger, J. Lytton and S. C. Hebert (1993). "Cloning and characterization of an extracellular Ca(2+)-sensing receptor from bovine parathyroid." Nature **366**(6455): 575-580.

Bucay, N., I. Sarosi, C. R. Dunstan, S. Morony, J. Tarpley, C. Capparelli, S. Scully, H. L. Tan, W. Xu, D. L. Lacey, W. J. Boyle and W. S. Simonet (1998). "osteoprotegerin-deficient mice develop early onset osteoporosis and arterial calcification." Genes and Development **12**(9): 1260-1268.

Bustamante, M., U. Hasler, V. Leroy, S. de Seigneux, M. Dimitrov, D. Mordasini, M. Rousselot, P.-Y. Martin and E. Féraille (2008). "Calcium-sensing Receptor Attenuates AVP-induced Aquaporin-2 Expression via a Calmodulin-dependent Mechanism." Journal of the American Society of Nephrology **19**(1): 109-116.

Canaff, L. and G. N. Hendy (2002). "Human calcium-sensing receptor gene. Vitamin D response elements in promoters P1 and P2 confer transcriptional responsiveness to 1,25-dihydroxyvitamin D." Journal of Biological Chemistry **277**(33): 30337-30350.

Canalejo, R., A. Canalejo, J. M. Martinez-Moreno, M. E. Rodriguez-Ortiz, J. C. Estepa, F. J. Mendoza, J. R. Munoz-Castaneda, V. Shalhoub, Y. Almaden and M. Rodriguez (2010). "FGF23 Fails to Inhibit Uremic Parathyroid Glands." Journal of the American Society of Nephrology **21**(7): 1125-1135.

Cancilla, B., A. Davies, J. A. Cauchi, G. P. Risbridger and J. F. Bertram (2001). "Fibroblast growth factor receptors and their ligands in the adult rat kidney." Kidney International **60**(1): 147-155.

Cantley, L. K., J. Russell, D. Lettieri and L. M. Sherwood (1985). "1,25-Dihydroxyvitamin D3 Suppresses Parathyroid Hormone Secretion from Bovine Parathyroid Cells in Tissue Culture." Endocrinology **117**(5): 2114-2119.

Capasso, G., P. J. Geibel, S. Damiano, P. Jaeger, W. G. Richards and J. P. Geibel (2013). "The calcium sensing receptor modulates fluid reabsorption and acid secretion in the proximal tubule." Kidney International **84**(2): 277-284.

Cardus, A., S. Panizo, E. Parisi, E. Fernandez and J. M. Valdivielso (2007). "Differential effects of vitamin D analogs on vascular calcification." Journal of Bone and Mineral Research **22**(6): 860-866.

Caride, A. J., E. N. Chini, S. Homma, T. P. Dousa and J. T. Penniston (1998). "mRNAs coding for the calcium-sensing receptor along the rat nephron: effect of a low-phosphate diet." Kidney and Blood Pressure Research **21**(5): 305-309.

Caudrillier, A., R. Mentaverri, M. Brazier, S. Kamel and Z. A. Massy (2010). "Calcium-sensing receptor as a potential modulator of vascular calcification in chronic kidney disease." Journal Of Nephrology **23**(1): 17-22.

Cavanaugh, A., Y. Huang and G. E. Breitwieser (2012). "Behind the curtain: cellular mechanisms for allosteric modulation of calcium-sensing receptors." British Journal of Pharmacology **165**(6): 1670-1677.

Chanakul, A., M. Y. Zhang, A. Louw, H. J. Armbrecht, W. L. Miller, A. A. Portale and F. Perwad (2013). "FGF-23 regulates CYP27B1 transcription in the kidney and in extra-renal tissues." PloS One **8**(9): e72816.

Chang, Q., S. Hoefs, A. W. van der Kemp, C. N. Topala, R. J. Bindels and J. G. Hoenderop (2005). "The beta-glucuronidase klotho hydrolyzes and activates the TRPV5 channel." Science **310**(5747): 490-493.

Chang, W. T., B. Radin and M. T. McCurdy (2014). "Calcium, magnesium, and phosphate abnormalities in the emergency department." Emergency Medicine Clinics of North America **32**(2): 349-366.

Chattopadhyay, N., I. Cheng, K. Rogers, D. Riccardi, A. Hall, R. Diaz, S. C. Hebert, D. I. Soybel and E. M. Brown (1998). "Identification and localization of extracellular Ca(2+)-sensing receptor in rat intestine." American Journal of Physiology **274**(1 Pt 1): G122-130.

Chavkin, N. W., J. J. Chia, M. H. Crouthamel and C. M. Giachelli (2015). "Phosphate uptake-independent signaling functions of the type III sodium-dependent phosphate transporter, PiT-1, in vascular smooth muscle cells." Experimental Cell Research **333**(1): 39-48.

Chen, C. D., S. Podvin, E. Gillespie, S. E. Leeman and C. R. Abraham (2007). "Insulin stimulates the cleavage and release of the extracellular domain of Klotho by ADAM10

and ADAM17." Proceedings of the National Academy of Sciences of the United States of America **104**(50): 19796-19801.

Chen, N. X. and S. M. Moe (2003). "Arterial calcification in diabetes." Curr Diab Rep **3**(1): 28-32.

Chen, N. X., K. D. O'Neill, X. Chen and S. M. Moe (2008). "Annexin-mediated matrix vesicle calcification in vascular smooth muscle cells." Journal of Bone and Mineral Research **23**(11): 1798-1805.

Chen, R. A. and W. G. Goodman (2004). "Role of the calcium-sensing receptor in parathyroid gland physiology." American Journal of Physiology: Renal Physiology **286**(6): F1005-1011.

Cheng, S. X., J. P. Geibel and S. C. Hebert (2004). "Extracellular polyamines regulate fluid secretion in rat colonic crypts via the extracellular calcium-sensing receptor." Gastroenterology **126**(1): 148-158.

Chida, J., K. Yamane, T. Takei and H. Kido (2012). "An efficient extraction method for quantitation of adenosine triphosphate in mammalian tissues and cells." Analytica Chimica Acta **727**: 8-12.

Civitelli, R. and K. Ziambaras (2011). "Calcium and phosphate homeostasis: concerted interplay of new regulators." Journal of Endocrinological Investigation **34**(7 Suppl): 3-7.

Clapham, D. E. (2007). "Calcium signaling." Cell **131**(6): 1047-1058.

Collip, J. B. (1925). "The Extraction Of A Parathyroid Hormone Which Will Prevent Or Control Parathyroid Tetany And Which Regulates The Level Of Blood Calcium." Journal of Biological Chemistry **63**(2): 395-438.

Conigrave, A. and V. C. Avlani, A.

Mun, H. (2012). Modulation of cAMP and cAMP-sensitive signaling by the calcium-sensing receptor. 1st CaSR symposium, Vienna, Bone.

Conigrave, A. D. and E. M. Brown (2006). "Taste receptors in the gastrointestinal tract. II. L-amino acid sensing by calcium-sensing receptors: implications for GI physiology." American Journal of Physiology: Gastrointestinal and Liver Physiology **291**(5): G753-761.

Conigrave, A. D., H. C. Mun, L. Delbridge, S. J. Quinn, M. Wilkinson and E. M. Brown (2004). "L-amino acids regulate parathyroid hormone secretion." Journal of Biological Chemistry **279**(37): 38151-38159.

Crosier, M. D., S. L. Booth, I. Peter, B. Dawson-Hughes, P. A. Price, C. J. O'Donnell, U. Hoffmann, M. K. Williamson and J. M. Ordovas (2009). "Matrix Gla protein polymorphisms are associated with coronary artery calcification in men." Journal of Nutritional Science and Vitaminology **55**(1): 59-65.

Dai, B., V. David, A. Martin, J. Huang, H. Li, Y. Jiao, W. Gu and L. D. Quarles (2012). "A comparative transcriptome analysis identifying FGF23 regulated genes in the kidney of a mouse CKD model." PloS One **7**(9): e44161.

de Groot, T., K. Lee, M. Langeslag, Q. Xi, K. Jalink, R. J. Bindels and J. G. Hoenderop (2009). "Parathyroid hormone activates TRPV5 via PKA-dependent phosphorylation." Journal of the American Society of Nephrology **20**(8): 1693-1704.

Deuell, K. A., A. Callegari, C. M. Giachelli, M. E. Rosenfeld and M. Scatena (2012). "RANKL enhances macrophage paracrine pro-calcific activity in high phosphate-treated smooth muscle cells: dependence on IL-6 and TNF-alpha." Journal of Vascular Research **49**(6): 510-521.

Di Bartolo, B. A. and M. M. Kavurma (2014). "Regulation and function of rankl in arterial calcification." Current Pharmaceutical Design **20**(37): 5853-5861.

Di Mise, A., G. Tamma, M. Ranieri, M. Svelto, B. van den Heuvel, E. N. Levtchenko and G. Valenti (2015). "Conditionally Immortalized Human Proximal-Tubular Epithelial Cells isolated from the urine of a healthy subject express functional Calcium Sensing Receptor." American Journal of Physiology: Renal Physiology: ajprenal.00352.02014.

Diaz, D., K. Allamneni, J. M. Tarrant, S. C. Lewin-Koh, R. Pai, P. Dhawan, G. R. Cain, C. Kozlowski, H. Hiraragi, N. La, D. P. Hartley, X. Ding, B. J. Dean, S. Bheddah and D. M. Dambach (2012). "Phosphorous dysregulation induced by MEK small molecule inhibitors in the rat involves blockade of FGF-23 signaling in the kidney." Toxicological Sciences **125**(1): 187-195.

Diepens, R. J., E. den Dekker, M. Bens, A. F. Weidema, A. Vandewalle, R. J. Bindels and J. G. Hoenderop (2004). "Characterization of a murine renal distal convoluted tubule cell line for the study of transcellular calcium transport." American Journal of Physiology: Renal Physiology **286**(3): F483-489.

Dudka, A. A., S. M. M. Sweet and J. K. Heath (2010). "STAT3 BINDING TO THE FGF RECEPTOR IS ACTIVATED BY RECEPTOR AMPLIFICATION." Cancer Research **70**(8): 3391-3401.

Dusso, A. S., A. J. Brown and E. Slatopolsky (2005). "Vitamin D." American Journal of Physiology - Renal Physiology **289**(1): F8-F28.

Ea, H.-K., C. Nguyen, D. Bazin, A. Bianchi, J. Guicheux, P. Reboul, M. Daudon and F. Lioté (2011). "Articular cartilage calcification in osteoarthritis: Insights into crystal-induced stress." Arthritis & Rheumatism **63**(1): 10-18.

Eisman, J. A. and R. Bouillon (2014). "Vitamin D: direct effects of vitamin D metabolites on bone: lessons from genetically modified mice." BoneKEy Rep **3**.

Ekwall, B., V. Silano, A. Paganuzzi-Stammati and F. Zucco (1990). Toxicity Tests with Mammalian Cell Cultures. Short-Term Toxicity Tests For Non-Genotoxic Effects. P. Bourdeau, E. Somers, G. M. Richardson and J. R. Hickman. Chichester, New York, Brisbane, Toronto, Singapore, John Wiley & Sons.

El-Maadawy, S., M. T. Kaartinen, T. Schinke, M. Murshed, G. Karsenty and M. D. McKee (2003). "Cartilage formation and calcification in arteries of mice lacking matrix Gla protein." Connective Tissue Research **44 Suppl 1**: 272-278.

Evenepoel, P. and M. Wolf (2013). "A balanced view of calcium and phosphate homeostasis in chronic kidney disease." Kidney International **83**(5): 789-791.

Farrow, E. G., S. I. Davis, L. J. Summers and K. E. White (2009). "Initial FGF23-Mediated Signaling Occurs in the Distal Convoluted Tubule." Journal of the American Society of Nephrology **20**(5): 955-960.

Farrow, E. G., L. J. Summers, S. C. Schiavi, J. A. McCormick, D. H. Ellison and K. E. White (2010). "Altered renal FGF23-mediated activity involving MAPK and Wnt: effects of the Hyp mutation." Journal of Endocrinology **207**(1): 67-75.

Faul, C., A. P. Amaral, B. Oskouei, M.-C. Hu, A. Sloan, T. Isakova, Guti, xE, O. M. rrez, R. Aguillon-Prada, J. Lincoln, J. M. Hare, P. Mundel, A. Morales, J. Scialla, M. Fischer, E. Z. Soliman, J. Chen, A. S. Go, S. E. Rosas, L. Nessel, R. R. Townsend, H. I. Feldman, M. St. John Sutton, A. Ojo, C. Gadegbeku, G. S. Di Marco, S. Reuter, D. Kentrup, K. Tiemann, M. Brand, J. A. Hill, O. W. Moe, M. Kuro-o, J. W. Kusek, M. G. Keane and M. Wolf (2011). "FGF23 induces left ventricular hypertrophy." The Journal of Clinical Investigation **121**(11): 4393-4408.

Felsenfeld, A., M. Rodriguez and B. Levine (2013). "New insights in regulation of calcium homeostasis." Current Opinion in Nephrology and Hypertension **22**(4): 371-376.

Felsenfeld, A. J., M. Rodriguez and E. Aguilera-Tejero (2007). "Dynamics of parathyroid hormone secretion in health and secondary hyperparathyroidism." Clinical Journal of the American Society of Nephrology **2**(6): 1283-1305.

Fleisch, H. (1981). "Diphosphonates: History and mechanisms of action." Metabolic Bone Disease and Related Research **3**(4–5): 279-287.

Floege, J., K. L. Hudkins, F. Eitner, Y. Cui, R. S. Morrison, M. A. Schelling and C. E. Alpers (1999). "Localization of fibroblast growth factor-2 (basic FGF) and FGF receptor-1 in adult human kidney." Kidney International **56**(3): 883-897.

Forster, R. E., P. W. Jurutka, J.-C. Hsieh, C. A. Haussler, C. L. Lowmiller, I. Kaneko, M. R. Haussler and G. Kerr Whitfield (2011). "Vitamin D receptor controls expression of the anti-aging klotho gene in mouse and human renal cells." Biochemical and Biophysical Research Communications **414**(3): 557-562.

Fox, J., S. H. Lowe, R. L. Conklin, B. A. Petty and E. F. Nemeth (1999). "Calcimimetic compound NPS R-568 stimulates calcitonin secretion but selectively targets parathyroid gland Ca(2+) receptor in rats." Journal of Pharmacology and Experimental Therapeutics **290**(2): 480-486.

Fraser, J. D. and P. A. Price (1988). "Lung, heart, and kidney express high levels of mRNA for the vitamin K-dependent matrix Gla protein. Implications for the possible functions of matrix Gla protein and for the tissue distribution of the gamma-carboxylase." Journal of Biological Chemistry **263**(23): 11033-11036.

Fuhrmann, V., N. Kinkl, T. Leveillard, J. Sahel and D. Hicks (1999). "Fibroblast growth factor receptor 4 (FGFR4) is expressed in adult rat and human retinal photoreceptors and neurons." Journal of Molecular Neuroscience **13**(1-2): 187-197.

Fujita, H., S. Omori, K. Ishikura, M. Hida and M. Awazu (2004). "ERK and p38 mediate high-glucose-induced hypertrophy and TGF-beta expression in renal tubular cells." American Journal of Physiology: Renal Physiology **286**(1): F120-126.

Fukumoto, S. (2014). "Phosphate metabolism and vitamin D." BoneKEy Rep **3**.

Garg, M. K. (2013). "The intestinal calcistat." Indian Journal of Endocrinology and Metabolism **17**(Suppl 1): S25-28.

Gattineni, J., C. Bates, K. Twombley, V. Dwarakanath, M. L. Robinson, R. Goetz, M. Mohammadi and M. Baum (2009). "FGF23 decreases renal NaPi-2a and NaPi-2c expression and induces hypophosphatemia in vivo predominantly via FGF receptor 1." American Journal of Physiology: Renal Physiology **297**(2): F282-291.

Gattineni, J., K. Twombley, R. Goetz, M. Mohammadi and M. Baum (2011). "Regulation of serum 1,25(OH)2Vitamin D3 levels by fibroblast growth factor 23 is mediated by FGF receptors 3 and 4." American Journal of Physiology - Renal Physiology **301**(2): F371-F377.

Geibel, J. P. (2010). "The calcium-sensing receptor." Journal Of Nephrology **23 Suppl 16**: S130-S135.

Gesek, F. A. and K. E. White (1997). "Molecular and functional identification of beta-adrenergic receptors in distal convoluted tubule cells." American Journal of Physiology **272**(6 Pt 2): F712-720.

Giachelli, C. M. (2004). "Vascular Calcification Mechanisms." Journal of the American Society of Nephrology **15**(12): 2959-2964.

Giachelli, C. M., S. Jono, A. Shioi, Y. Nishizawa, K. Mori and H. Morii (2001). "Vascular calcification and inorganic phosphate." American Journal of Kidney Diseases **38**(4 Suppl 1): S34-37.

Godwin, S. L. and S. P. Soltoff (2002). "Calcium-sensing receptor-mediated activation of phospholipase C-gamma1 is downstream of phospholipase C-beta and protein kinase C in MC3T3-E1 osteoblasts." Bone **30**(4): 559-566.

Goetz, R., Y. Nakada, M. C. Hu, H. Kurosu, L. Wang, T. Nakatani, M. Shi, A. V. Eliseenkova, M. S. Razzaque, O. W. Moe, M. Kuro-o and M. Mohammadi (2010). "Isolated C-terminal tail of FGF23 alleviates hypophosphatemia by inhibiting FGF23-FGFR-Klotho complex formation." Proceedings of the National Academy of Sciences of the United States of America **107**(1): 407-412.

Golub, E. E. (2009). "Role of Matrix Vesicles in Biomineralization." Biochimica et Biophysica Acta **1790**(12): 1592-1598.

Gong, S.-G. (2014). "Isoforms of Receptors of Fibroblast Growth Factors." Journal of Cellular Physiology **229**(12): 1887-1895.

Gong, Y. and J. Hou (2014). "Claudin-14 Underlies Ca++-Sensing Receptor–Mediated Ca++ Metabolism via NFAT-microRNA–Based Mechanisms." Journal of the American Society of Nephrology **25**(4): 745-760.

Gowen, L. C., D. N. Petersen, A. L. Mansolf, H. Qi, J. L. Stock, G. T. Tkalcevic, H. A. Simmons, D. T. Crawford, K. L. Chidsey-Frink, H. Z. Ke, J. D. McNeish and T. A. Brown (2003). "Targeted disruption of the osteoblast/osteocyte factor 45 gene (OF45) results in increased bone formation and bone mass." Journal of Biological Chemistry **278**(3): 1998-2007.

Gu, G. J., T. Chen, H. M. Zhou, K. X. Sun and J. Li (2014). "Role of Wnt/beta-catenin signaling pathway in the mechanism of calcification of aortic valve." Journal of Huazhong University of Science and Technology Medical Sciences **34**(1): 33-36.

Guerrero, F., C. Herencia, Y. Almaden, J. M. Martinez-Moreno, A. Montes de Oca, M. E. Rodriguez-Ortiz, J. M. Diaz-Tocados, A. Canalejo, M. Florio, I. Lopez, W. G. Richards, M. Rodriguez, E. Aguilera-Tejero and J. R. Munoz-Castaneda (2014). "TGF-beta prevents phosphate-induced osteogenesis through inhibition of BMP and Wnt/beta-catenin pathways." PloS One **9**(2): e89179.

Gupta, A., K. Winer, M. J. Econs, S. J. Marx and M. T. Collins (2004). "FGF-23 is elevated by chronic hyperphosphatemia." Journal of Clinical Endocrinology and Metabolism **89**(9): 4489-4492.

Gustafsdottir, S. M., E. Schallmeiner, S. Fredriksson, M. Gullberg, O. Söderberg, M. Jarvius, J. Jarvius, M. Howell and U. Landegren (2005). "Proximity ligation assays for sensitive and specific protein analyses." Analytical Biochemistry **345**(1): 2-9.

Habener, J. F., M. Amherdt, M. Ravazzola and L. Orci (1979). "Parathyroid hormone biosynthesis. Correlation of conversion of biosynthetic precursors with intracellular protein migration as determined by electron microscope autoradiography." Journal of Cell Biology **80**(3): 715-731.

Hanon, E. A., C. M. Sturgeon and E. J. Lamb (2013). "Sampling and storage conditions influencing the measurement of parathyroid hormone in blood samples: a systematic review." Clinical Chemistry and Laboratory Medicine **51**(10): 1925-1941.

Haussler, M., G. Whitfield, I. Kaneko, R. Forster, R. Saini, J.-C. Hsieh, C. Haussler and P. Jurutka (2012). "The role of vitamin D in the FGF23, klotho, and phosphate bone-kidney endocrine axis." Reviews in Endocrine & Metabolic Disorders: 1-13.

Haussler, M. R., C. A. Haussler, P. W. Jurutka, P. D. Thompson, J. C. Hsieh, L. S. Remus, S. H. Selznick and G. K. Whitfield (1997). "The vitamin D hormone and its nuclear receptor: molecular actions and disease states." Journal of Endocrinology **154 Suppl**: S57-73.

Haussler, M. R., G. K. Whitfield, C. A. Haussler, J. C. Hsieh, P. D. Thompson, S. H. Selznick, C. E. Dominguez and P. W. Jurutka (1998). "The nuclear vitamin D receptor: biological and molecular regulatory properties revealed." Journal of Bone and Mineral Research **13**(3): 325-349.

Haut, L. L., A. C. Alfrey, S. Guggenheim, B. Buddington and N. Schrier (1980). "Renal toxicity of phosphate in rats." Kidney International **17**(6): 722-731.

Healy, K. D., J. B. Zella, J. M. Prahl and H. F. DeLuca (2003). "Regulation of the murine renal vitamin D receptor by 1,25-dihydroxyvitamin D3 and calcium." Proceedings of the National Academy of Sciences of the United States of America **100**(17): 9733-9737.

Herrmann, S. M., C. Whatling, E. Brand, V. Nicaud, J. Gariepy, A. Simon, A. Evans, J. B. Ruidavets, D. Arveiler, G. Luc, L. Tiret, A. Henney and F. Cambien (2000). "Polymorphisms of the human matrix gla protein (MGP) gene, vascular calcification, and myocardial infarction." Arteriosclerosis, Thrombosis, and Vascular Biology **20**(11): 2386-2393.

Hesse, M., L. F. Frohlich, U. Zeitz, B. Lanske and R. G. Erben (2007). "Ablation of vitamin D signaling rescues bone, mineral, and glucose homeostasis in Fgf-23 deficient mice." Matrix Biology **26**(2): 75-84.

Hessle, L., K. A. Johnson, H. C. Anderson, S. Narisawa, A. Sali, J. W. Goding, R. Terkeltaub and J. L. Millan (2002). "Tissue-nonspecific alkaline phosphatase and plasma cell membrane glycoprotein-1 are central antagonistic regulators of bone mineralization." Proceedings of the National Academy of Sciences of the United States of America **99**(14): 9445-9449.

Heyeraas, K. J., S. R. Haug, R. D. Bukoski and E. M. Awumey (2008). "Identification of a Ca2+-sensing receptor in rat trigeminal ganglia, sensory axons, and tooth dental pulp." Calcified Tissue International **82**(1): 57-65.

Hjälm, G., R. J. MacLeod, O. Kifor, N. Chattopadhyay and E. M. Brown (2001). "Filamin-A Binds to the Carboxyl-terminal Tail of the Calcium-sensing Receptor, an Interaction That Participates in CaR-mediated Activation of Mitogen-activated Protein Kinase." Journal of Biological Chemistry **276**(37): 34880-34887.

Ho, A. M., M. D. Johnson and D. M. Kingsley (2000). "Role of the mouse ank gene in control of tissue calcification and arthritis." Science **289**(5477): 265-270.

Hobaus, J., U. Thiem, D. M. Hummel and E. Kallay (2013). "Role of calcium, vitamin D, and the extrarenal vitamin D hydroxylases in carcinogenesis." Anti-Cancer Agents in Medicinal Chemistry **13**(1): 20-35.

Hoenderop, J. G. J., D. Muller, A. W. C. M. Van der Kemp, A. Hartog, M. Suzuki, K. Ishibashi, M. Imai, F. Sweep, P. H. G. M. Willems, C. H. v. Os and R. J. M. Bindels (2001). "Calcitriol Controls the Epithelial Calcium Channel in Kidney." Journal of the American Society of Nephrology **12**(7): 1342-1349.

Hough, T. A., D. Bogani, M. T. Cheeseman, J. Favor, M. A. Nesbit, R. V. Thakker and M. F. Lyon (2004). "Activating calcium-sensing receptor mutation in the mouse is associated with cataracts and ectopic calcification." Proceedings of the National Academy of Sciences of the United States of America **101**(37): 13566-13571.

Hu, M. C., M. Shi, J. Zhang, J. Pastor, T. Nakatani, B. Lanske, M. S. Razzaque, K. P. Rosenblatt, M. G. Baum, M. Kuro-o and O. W. Moe (2010). "Klotho: a novel phosphaturic substance acting as an autocrine enzyme in the renal proximal tubule." The FASEB Journal **24**(9): 3438-3450.

Huang, B., Y. Sun, I. Maciejewska, D. Qin, T. Peng, B. McIntyre, J. Wygant, W. T. Butler and C. Qin (2008). "Distribution of SIBLING proteins in the organic and inorganic phases of rat dentin and bone." European Journal of Oral Sciences **116**(2): 104-112.

Huang, C.-L. (2010). "Regulation of ion channels by secreted Klotho: mechanisms and implications." Kidney International **77**(10): 855-860.

Huang, C., A. Sindic, C. E. Hill, K. M. Hujer, K. W. Chan, M. Sassen, Z. Wu, Y. Kurachi, S. Nielsen, M. F. Romero and R. T. Miller (2007). "Interaction of the Ca2+-sensing receptor with the inwardly rectifying potassium channels Kir4.1 and Kir4.2 results in inhibition of channel function." American Journal of Physiology: Renal Physiology **292**(3): F1073-1081.

Huang, Y. C. and S. Christakos (1988). "Modulation of rat calbindin-D28 gene expression by 1,25-dihydroxyvitamin D3 and dietary alteration." Molecular Endocrinology **2**(10): 928-935.

Jaramillo-Juárez, F., M. L. Rodríguez-Vázquez, J. Muñoz-Martínez, T. Quezada-Tristán, F. A. Posadas del Río, J. Llamas-Viramontes, G. G. Ortíz, A. Feria-Velasco and J. L. Reyes (2005). "The ATP levels in kidneys and blood are mainly decreased by acute ingestion of tullidora (Karwinskia humboldtiana)." Toxicon **46**(1): 99-103.

Johnson, J. A. and R. Kumar (1994). "Vitamin D and renal calcium transport." Current Opinion in Nephrology and Hypertension **3**(4): 424-429.

Johnson, K., A. Jung, A. Murphy, A. Andreyev, J. Dykens and R. Terkeltaub (2000). "Mitochondrial oxidative phosphorylation is a downstream regulator of nitric oxide effects on chondrocyte matrix synthesis and mineralization." Arthritis and Rheumatism **43**(7): 1560-1570.

Johnson, K., S. Vaingankar, Y. Chen, A. Moffa, M. B. Goldring, K. Sano, P. Jin-Hua, A. Sali, J. Goding and R. Terkeltaub (1999). "Differential mechanisms of inorganic pyrophosphate production by plasma cell membrane glycoprotein-1 and B10 in chondrocytes." Arthritis and Rheumatism **42**(9): 1986-1997.

Johnsson, M. S. and G. H. Nancollas (1992). "The role of brushite and octacalcium phosphate in apatite formation." Critical Reviews in Oral Biology and Medicine **3**(1-2): 61-82.

Johnston, P. A. and J. R. Grandis (2011). "STAT3 SIGNALING: Anticancer Strategies and Challenges." Molecular Interventions **11**(1): 18-26.

Jono, S., M. D. McKee, C. E. Murry, A. Shioi, Y. Nishizawa, K. Mori, H. Morii and C. M. Giachelli (2000). "Phosphate regulation of vascular smooth muscle cell calcification." Circulation Research **87**(7): E10-17.

Jono, S., Y. Nishizawa, A. Shioi and H. Morii (1998). "1,25-Dihydroxyvitamin D3 increases in vitro vascular calcification by modulating secretion of endogenous parathyroid hormone-related peptide." Circulation **98**(13): 1302-1306.

Jüppner, H. and M. Wolf (2012). "αKlotho: FGF23 coreceptor and FGF23-regulating hormone." The Journal of Clinical Investigation **122**(12): 4336-4339.

Kameda, T., H. Mano, Y. Yamada, H. Takai, N. Amizuka, M. Kobori, N. Izumi, H. Kawashima, H. Ozawa, K. Ikeda, A. Kameda, Y. Hakeda and M. Kumegawa (1998). "Calcium-sensing receptor in mature osteoclasts, which are bone resorbing cells." Biochemical and Biophysical Research Communications **245**(2): 419-422.

Kanatani, M., T. Sugimoto, M. Fukase and T. Fujita (1991). "Effect of elevated extracellular calcium on the proliferation of osteoblastic MC3T3-E1 cells:its direct and indirect effects via monocytes." Biochemical and Biophysical Research Communications **181**(3): 1425-1430.

Kartsogiannis, V., H. Zhou, N. J. Horwood, R. J. Thomas, D. K. Hards, J. M. W. Quinn, P. Niforas, K. W. Ng, T. J. Martin and M. T. Gillespie (1999). "Localization of RANKL (receptor activator of NFκB ligand) mRNA and protein in skeletal and extraskeletal tissues." Bone **25**(5): 525-534.

Katsumata, S., H. Matsuzaki, R. Katsumata-Tsuboi, M. Uehara and K. Suzuki (2014). "Effects of high phosphorus diet on bone metabolism-related gene expression in young and aged mice." J Nutr Metab **2014**: 575932.

Kido, S., I. Kaneko, S. Tatsumi, H. Segawa and K. Miyamoto (2013). "Vitamin D and type II sodium-dependent phosphate cotransporters." Contributions to Nephrology **180**: 86-97.

Kifor, O., R. J. MacLeod, R. Diaz, M. Bai, T. Yamaguchi, T. Yao, I. Kifor and E. M. Brown (2001). "Regulation of MAP kinase by calcium-sensing receptor in bovine parathyroid and CaR-transfected HEK293 cells." American Journal of Physiology: Renal Physiology **280**(2): F291-302.

Kim, K. I., K. U. Park, E. J. Chun, S. I. Choi, Y. S. Cho, T. J. Youn, G. Y. Cho, I. H. Chae, J. Song, D. J. Choi and C. H. Kim (2011). "A novel biomarker of coronary atherosclerosis: serum DKK1 concentration correlates with coronary artery calcification and atherosclerotic plaques." <u>Journal of Korean Medical Science</u> **26**(9): 1178-1184.

Kip, S. N. and E. E. Strehler (2004). "Vitamin D3 upregulates plasma membrane Ca2+-ATPase expression and potentiates apico-basal Ca2+ flux in MDCK cells." <u>American Journal of Physiology: Renal Physiology</u> **286**(2): F363-369.

Kirsch, T. (2006). "Determinants of pathological mineralization." <u>Current Opinion in Rheumatology</u> **18**(2): 174-180.

Kirsch, T., W. Wang and D. Pfander (2003). "Functional differences between growth plate apoptotic bodies and matrix vesicles." <u>Journal of Bone and Mineral Research</u> **18**(10): 1872-1881.

Kitazawa, S., K. Kajimoto, T. Kondo and R. Kitazawa (2003). "Vitamin D3 supports osteoclastogenesis via functional vitamin D response element of human RANKL gene promoter." <u>Journal of Cellular Biochemistry</u> **89**(4): 771-777.

Knights, V. and S. J. Cook (2010). "De-regulated FGF receptors as therapeutic targets in cancer." <u>Pharmacology & Therapeutics</u> **125**(1): 105-117.

Kolek, O. I., E. R. Hines, M. D. Jones, L. K. LeSueur, M. A. Lipko, P. R. Kiela, J. F. Collins, M. R. Haussler and F. K. Ghishan (2005). "1alpha,25-Dihydroxyvitamin D3 upregulates FGF23 gene expression in bone: the final link in a renal-gastrointestinal-skeletal axis that controls phosphate transport." <u>American Journal of Physiology: Gastrointestinal and Liver Physiology</u> **289**(6): G1036-1042.

Koos, R., V. Brandenburg, A. H. Mahnken, R. Schneider, G. Dohmen, R. Autschbach, N. Marx and R. Kramann (2013). "Sclerostin as a potential novel biomarker for aortic valve calcification: an in-vivo and ex-vivo study." <u>Journal of Heart Valve Disease</u> **22**(3): 317-325.

Kroll, M. H. (2000). "Parathyroid hormone temporal effects on bone formation and resorption." <u>Bulletin of Mathematical Biology</u> **62**(1): 163-188.

Krumdieck, C. L., J. dos Santos and K.-J. Ho (1980). "A new instrument for the rapid preparation of tissue slices." <u>Analytical Biochemistry</u> **104**(1): 118-123.

Kugai, N., Y. Koide, S. Kimura and K. Yamashita (1984). "Inhibitory effects of active vitamin D preparations on PTH secretion in rats." <u>Endocrinologia Japonica</u> **31**(2): 151-158.

Kuipers, A. L., I. Miljkovic, J. J. Carr, J. G. Terry, C. S. Nestlerode, Y. Ge, C. H. Bunker, A. L. Patrick and J. M. Zmuda (2015). "Association of circulating sclerostin with vascular calcification in Afro-Caribbean men." <u>Atherosclerosis</u> **239**(1): 218-223.

Kumar, R., P. J. Tebben and J. R. Thompson (2012). "Vitamin D and the kidney." <u>Archives of Biochemistry and Biophysics</u> **523**(1): 77-86.

Kuro-o, M. (2008). "Endocrine FGFs and Klothos: emerging concepts." <u>Trends in Endocrinology and Metabolism</u> **19**(7): 239-245.

Kuro-o, M. (2010). "Overview of the FGF23-Klotho axis." <u>Pediatric Nephrology</u> **25**(4): 583-590.

Kuro-o, M., Y. Matsumura, H. Aizawa, H. Kawaguchi, T. Suga, T. Utsugi, Y. Ohyama, M. Kurabayashi, T. Kaname, E. Kume, H. Iwasaki, A. Iida, T. Shiraki-Iida, S. Nishikawa, R. Nagai and Y. I. Nabeshima (1997). "Mutation of the mouse klotho gene leads to a syndrome resembling ageing." Nature **390**(6655): 45-51.

Kurosu, H., Y. Ogawa, M. Miyoshi, M. Yamamoto, A. Nandi, K. P. Rosenblatt, M. G. Baum, S. Schiavi, M. C. Hu, O. W. Moe and M. Kuro-o (2006). "Regulation of fibroblast growth factor-23 signaling by klotho." Journal of Biological Chemistry **281**(10): 6120-6123.

Kwon, H. M., B. K. Hong, T. S. Kang, K. Kwon, H. K. Kim, Y. Jang, D. Choi, H. Y. Park, S. M. Kang, S. Y. Cho and H. S. Kim (2000). "Expression of osteopontin in calcified coronary atherosclerotic plaques." Journal of Korean Medical Science **15**(5): 485-493.

Lassiter, W. and R. Colindres (1982). Phosphate Reabsorption in the Distal Convoluted Tubule. Regulation of Phosphate and Mineral Metabolism. S. Massry, J. Letteri and E. Ritz, Springer US. **151:** 21-32.

Lavi-Moshayoff, V., G. Wasserman, T. Meir, J. Silver and T. Naveh-Many (2010). "PTH increases FGF23 gene expression and mediates the high-FGF23 levels of experimental kidney failure: a bone parathyroid feedback loop." American Journal of Physiology: Renal Physiology **299**(4): F882-889.

Leach, K., P. M. Sexton, A. Christopoulos and A. D. Conigrave (2014). "Engendering biased signalling from the calcium-sensing receptor for the pharmacotherapy of diverse disorders." British Journal of Pharmacology **171**(5): 1142-1155.

Lebart, M. C., C. Mejean, D. Casanova, E. Audemard, J. Derancourt, C. Roustan and Y. Benyamin (1994). "Characterization of the actin binding site on smooth muscle filamin." Journal of Biological Chemistry **269**(6): 4279-4284.

Leclercq-Meyer, V., J. Marchand, R. Leclercq and W. J. Malaisse (1981). "Calcium Deprivation Enhances Glucagon Release in the Presence of 2-Ketoisocaproate." Endocrinology **108**(6): 2093-2097.

Lederer, E. D., S. S. Sohi and K. R. McLeish (2000). "Parathyroid hormone stimulates extracellular signal-regulated kinase (ERK) activity through two independent signal transduction pathways: role of ERK in sodium-phosphate cotransport." Journal of the American Society of Nephrology **11**(2): 222-231.

Li, X., V. G. Brunton, H. R. Burgar, L. M. Wheldon and J. K. Heath (2004). "FRS2-dependent SRC activation is required for fibroblast growth factor receptor-induced phosphorylation of Sprouty and suppression of ERK activity." Journal of Cell Science **117**(Pt 25): 6007-6017.

Lin, K. I., N. Chattopadhyay, M. Bai, R. Alvarez, C. V. Dang, J. M. Baraban, E. M. Brown and R. R. Ratan (1998). "Elevated extracellular calcium can prevent apoptosis via the calcium-sensing receptor." Biochemical and Biophysical Research Communications **249**(2): 325-331.

Liu, S., L. Vierthaler, W. Tang, J. Zhou and L. D. Quarles (2008). "FGFR3 and FGFR4 Do not Mediate Renal Effects of FGF23." Journal of the American Society of Nephrology **19**(12): 2342-2350.

Lou, Y. R., F. Molnar, M. Perakyla, S. Qiao, A. V. Kalueff, R. St-Arnaud, C. Carlberg and P. Tuohimaa (2010). "25-Hydroxyvitamin D(3) is an agonistic vitamin D receptor ligand." Journal of Steroid Biochemistry and Molecular Biology **118**(3): 162-170.

Loupy, A., S. K. Ramakrishnan, B. Wootla, R. Chambrey, R. de la Faille, S. Bourgeois, P. Bruneval, C. Mandet, E. I. Christensen, H. Faure, L. Cheval, K. Laghmani, C. Collet, D. Eladari, R. H. Dodd, M. Ruat and P. Houillier (2012). "PTH-independent regulation of blood calcium concentration by the calcium-sensing receptor." Journal of Clinical Investigation **122**(9): 3355-3367.

Luo, G., P. Ducy, M. D. McKee, G. J. Pinero, E. Loyer, R. R. Behringer and G. Karsenty (1997). "Spontaneous calcification of arteries and cartilage in mice lacking matrix GLA protein." Nature **386**(6620): 78-81.

Mackenzie, N. C., D. Zhu, E. M. Milne, R. van 't Hof, A. Martin, L. Darryl Quarles, J. L. Millan, C. Farquharson and V. E. MacRae (2012). "Altered bone development and an increase in FGF-23 expression in Enpp1(-/-) mice." PloS One **7**(2): e32177.

Magyar, C. E., K. E. White, R. Rojas, G. Apodaca and P. A. Friedman (2002). "Plasma membrane Ca2+-ATPase and NCX1 Na+/Ca2+ exchanger expression in distal convoluted tubule cells." American Journal of Physiology: Renal Physiology **283**(1): F29-40.

Mahon, M. J. (2012). "The parathyroid hormone receptorsome and the potential for therapeutic intervention." Current Drug Targets **13**(1): 116-128.

Maillard, M. P., A. Tedjani, C. Perregaux and M. Burnier (2009). "Calcium-sensing receptors modulate renin release in vivo and in vitro in the rat." Journal of Hypertension **27**(10): 1980-1987.

Maldonado-Perez, D., G. E. Breitwieser, L. Gama, A. C. Elliott, D. T. Ward and D. Riccardi (2003). "Human calcium-sensing receptor can be suppressed by antisense sequences." Biochemical and Biophysical Research Communications **311**(3): 610-617.

Mansfield, K., R. Rajpurohit and I. M. Shapiro (1999). "Extracellular phosphate ions cause apoptosis of terminally differentiated epiphyseal chondrocytes." Journal of Cellular Physiology **179**(3): 276-286.

Marsell, R., T. Krajisnik, H. Goransson, C. Ohlsson, O. Ljunggren, T. E. Larsson and K. B. Jonsson (2008). "Gene expression analysis of kidneys from transgenic mice expressing fibroblast growth factor-23." Nephrology, Dialysis, Transplantation **23**(3): 827-833.

Martin, K. and E. González (2007). "Parathyroid hormone assay: problems and opportunities." Pediatric Nephrology **22**(10): 1651-1654.

Martinez-Moreno, J. M., J. R. Munoz-Castaneda, C. Herencia, A. M. Oca, J. C. Estepa, R. Canalejo, M. E. Rodriguez-Ortiz, P. Perez-Martinez, E. Aguilera-Tejero, A. Canalejo, M. Rodriguez and Y. Almaden (2012). "In vascular smooth muscle cells paricalcitol prevents phosphate-induced Wnt/beta-catenin activation." American Journal of Physiology: Renal Physiology **303**(8): F1136-1144.

Masi, L. and M. L. Brandi (2007). "Calcitonin and calcitonin receptors." Clinical Cases in Mineral and Bone Metabolism **4**(2): 117-122.

Masi, L., A. Gozzini, A. Franchi, D. Campanacci, A. Amedei, A. Falchetti, F. Franceschelli, G. Marcucci, A. Tanini, R. Capanna and M. L. Brandi (2009). "A novel recessive mutation of fibroblast growth factor-23 in tumoral calcinosis." Journal of Bone and Joint Surgery (American Volume) **91**(5): 1190-1198.

Masuda, M., H. Yamamoto, M. Kozai, S. Tanaka, M. Ishiguro, Y. Takei, O. Nakahashi, S. Ikeda, T. Uebanso, Y. Taketani, H. Segawa, K. Miyamoto and E. Takeda (2010). "Regulation of renal sodium-dependent phosphate co-transporter genes (Npt2a and Npt2c) by all-trans-retinoic acid and its receptors." Biochemical Journal **429**(3): 583-592.

Matsuzaki, H., Y. Kajita and M. Miwa (2013). "Magnesium deficiency increases serum fibroblast growth factor-23 levels in rats." Magnesium Research **26**(1): 18-23.

McClare, C. W. (1975). "How does ATP act as an energy source?" Ciba Foundation Symposium(31): 301-325.

McCollum, E. V., N. Simmonds, J. E. Becker and P. G. Shipley (1922). "Studies on experimental rickets: Xxi. An experimental demonstration of the existence of a vitamin which promotes calcium deposition." Journal of Biological Chemistry **53**(2): 293-312.

McCubrey, J. A., L. S. Steelman, S. L. Abrams, W. H. Chappell, S. Russo, R. Ove, M. Milella, A. Tafuri, P. Lunghi, A. Bonati, F. Stivala, F. Nicoletti, M. Libra, A. M. Martelli, G. Montalto and M. Cervello (2010). "Emerging MEK inhibitors." Expert Opinion on Emerging Drugs **15**(2): 203-223.

McLarnon, S., D. Holden, D. Ward, M. Jones, A. Elliott and D. Riccardi (2002). "Aminoglycoside antibiotics induce pH-sensitive activation of the calcium-sensing receptor." Biochemical and Biophysical Research Communications **297**(1): 71-77.

McMillan, J. (2013). Acute Kidney Injury (AKI). Merck Manuals. M. Co. Kenilworth, USA, Merck & Co.

McNeil, S. E., S. A. Hobson, V. Nipper and K. D. Rodland (1998). "Functional Calcium-sensing Receptors in Rat Fibroblasts Are Required for Activation of SRC Kinase and Mitogen-activated Protein Kinase in Response to Extracellular Calcium." Journal of Biological Chemistry **273**(2): 1114-1120.

Meister, M., A. Tomasovic, A. Banning and R. Tikkanen (2013). "Mitogen-Activated Protein (MAP) Kinase Scaffolding Proteins: A Recount." International Journal of Molecular Sciences **14**(3): 4854-4884.

Memon, F., M. El-Abbadi, T. Nakatani, T. Taguchi, B. Lanske and M. S. Razzaque (2008). "Does Fgf23-klotho activity influence vascular and soft tissue calcification through regulating mineral ion metabolism?" Kidney International **74**(5): 566-570.

Mohler, E. R., 3rd, L. P. Adam, P. McClelland, L. Graham and D. R. Hathaway (1997). "Detection of osteopontin in calcified human aortic valves." Arteriosclerosis, Thrombosis, and Vascular Biology **17**(3): 547-552.

Montes de Oca, A., F. Guerrero, J. M. Martinez-Moreno, J. A. Madueno, C. Herencia, A. Peralta, Y. Almaden, I. Lopez, E. Aguilera-Tejero, K. Gundlach, J. Buchel, M. E. Peter, J. Passlick-Deetjen, M. Rodriguez and J. R. Munoz-Castaneda (2014). "Magnesium inhibits Wnt/beta-catenin activity and reverses the osteogenic transformation of vascular smooth muscle cells." PloS One **9**(2): e89525.

Montessuit, C., J. P. Bonjour and J. Caverzasio (1995). "Expression and regulation of Na-dependent P(i) transport in matrix vesicles produced by osteoblast-like cells." Journal of Bone and Mineral Research **10**(4): 625-631.

Moochhala, S. H. (2012). "Extracellular Pyrophosphate in the Kidney: How Does It Get There and What Does It Do?" Nephron Physiology **120**(4): p33-p38.

Morava, E., J. Kuhnisch, J. M. Drijvers, J. H. Robben, C. Cremers, P. van Setten, A. Branten, S. Stumpp, A. de Jong, K. Voesenek, S. Vermeer, A. Heister, H. L. Claahsen-van der Grinten, C. W. O'Neill, M. A. Willemsen, D. Lefeber, P. M. Deen, U. Kornak, H. Kremer and R. A. Wevers (2011). "Autosomal recessive mental retardation, deafness, ankylosis, and mild hypophosphatemia associated with a novel ANKH mutation in a consanguineous family." Journal of Clinical Endocrinology and Metabolism **96**(1): E189-198.

Moreno, J. A., M. C. Izquierdo, M. D. Sanchez-Niño, B. Suárez-Alvarez, C. Lopez-Larrea, A. Jakubowski, J. Blanco, R. Ramirez, R. Selgas, M. Ruiz-Ortega, J. Egido, A. Ortiz and A. B. Sanz (2011). "The Inflammatory Cytokines TWEAK and TNFα Reduce Renal Klotho Expression through NFκB." Journal of the American Society of Nephrology : JASN **22**(7): 1315-1325.

Morris, H. A. and P. H. Anderson (2010). "Autocrine and Paracrine Actions of Vitamin D." The Clinical Biochemist Reviews **31**(4): 129-138.

Motoyama, H. I. and P. A. Friedman (2002). "Calcium-sensing receptor regulation of PTH-dependent calcium absorption by mouse cortical ascending limbs." Am J Physiol Renal Physiol. **283**(3): F399-F406.

Mozar, A., N. Haren, M. Chasseraud, L. Louvet, C. Maziere, A. Wattel, R. Mentaverri, P. Morliere, S. Kamel, M. Brazier, J. C. Maziere and Z. A. Massy (2008). "High extracellular inorganic phosphate concentration inhibits RANK-RANKL signaling in osteoclast-like cells." Journal of Cellular Physiology **215**(1): 47-54.

Munroe, P. B., R. O. Olgunturk, J. P. Fryns, L. Van Maldergem, F. Ziereisen, B. Yuksel, R. M. Gardiner and E. Chung (1999). "Mutations in the gene encoding the human matrix Gla protein cause Keutel syndrome." Nature Genetics **21**(1): 142-144.

Murayama, A., K. Takeyama, S. Kitanaka, Y. Kodera, T. Hosoya and S. Kato (1998). "The promoter of the human 25-hydroxyvitamin D3 1 alpha-hydroxylase gene confers positive and negative responsiveness to PTH, calcitonin, and 1 alpha,25(OH)2D3." Biochemical and Biophysical Research Communications **249**(1): 11-16.

Nancollas, G. H. (1992). The involvement of calcium phosphates in biological mineralization and demineralization processes. Pure and Applied Chemistry. **64:** 1673.

Narasimhan, P., J. Liu, Y. S. Song, J. L. Massengale and P. H. Chan (2009). "VEGF Stimulates the ERK 1/2 Signaling Pathway and Apoptosis in Cerebral Endothelial Cells After Ischemic Conditions." Stroke **40**(4): 1467-1473.

Nashiki, K., Y. Taketani, T. Takeichi, N. Sawada, H. Yamamoto, M. Ichikawa, H. Arai, K. Miyamoto and E. Takeda (2005). "Role of membrane microdomains in PTH-mediated down-regulation of NaPi-IIa in opossum kidney cells." Kidney International **68**(3): 1137-1147.

Naveh-Many, T. and J. Silver (1990). "Regulation of parathyroid hormone gene expression by hypocalcemia, hypercalcemia, and vitamin D in the rat." Journal of Clinical Investigation **86**(4): 1313-1319.

Nemeth, E. F. and D. Shoback (2013). "Calcimimetic and calcilytic drugs for treating bone and mineral-related disorders." Best Practice & Research: Clinical Endocrinology & Metabolism **27**(3): 373-384.

Nilius, B., J. Prenen, R. Vennekens, J. G. Hoenderop, R. J. Bindels and G. Droogmans (2001). "Pharmacological modulation of monovalent cation currents through the epithelial Ca2+ channel ECaC1." British Journal of Pharmacology **134**(3): 453-462.

Obatomi, D. K., S. Brant, V. Anthonypillai, D. A. Early and P. H. Bach (1998). "Optimizing preincubation conditions for precision-cut rat kidney and liver tissue slices: effect of culture media and antioxidants." Toxicology in Vitro **12**(6): 725-737.

Ogbureke, K. U. and L. W. Fisher (2004). "Expression of SIBLINGs and their partner MMPs in salivary glands." Journal of Dental Research **83**(9): 664-670.

Ogbureke, K. U. and L. W. Fisher (2005). "Renal expression of SIBLING proteins and their partner matrix metalloproteinases (MMPs)." Kidney International **68**(1): 155-166.

Oh, J., J. Beckmann, J. Bloch, V. Hettgen, J. Mueller, L. Li, M. Hoemme, M. L. Gross, R. Penzel, P. Mundel, F. Schaefer and C. P. Schmitt (2011). "Stimulation of the calcium-sensing receptor stabilizes the podocyte cytoskeleton, improves cell survival, and reduces toxin-induced glomerulosclerosis." Kidney International **80**(5): 483-492.

Ohkido, I., H. Segawa, R. Yanagida, M. Nakamura and K. Miyamoto (2003). "Cloning, gene structure and dietary regulation of the type-IIc Na/Pi cotransporter in the mouse kidney." Pflügers Archiv. European Journal of Physiology **446**(1): 106-115.

Ohnishi, M., T. Nakatani, B. Lanske and M. S. Razzaque (2009). "Reversal of mineral ion homeostasis and soft-tissue calcification of klotho knockout mice by deletion of vitamin D 1alpha-hydroxylase." Kidney International **75**(11): 1166-1172.

Ohsu, T., Y. Amino, H. Nagasaki, T. Yamanaka, S. Takeshita, T. Hatanaka, Y. Maruyama, N. Miyamura and Y. Eto (2010). "Involvement of the calcium-sensing receptor in human taste perception." Journal of Biological Chemistry **285**(2): 1016-1022.

Olauson, H., K. Lindberg, R. Amin, T. Sato, T. Jia, R. Goetz, M. Mohammadi, G. Andersson, B. Lanske and T. E. Larsson (2013). "Parathyroid-specific deletion of Klotho unravels a novel calcineurin-dependent FGF23 signaling pathway that regulates PTH secretion." PLoS Genetics **9**(12): e1003975.

Omori, S., M. Hida, K. Ishikura, S. Kuramochi and M. Awazu (2000). "Expression of mitogen-activated protein kinase family in rat renal development." Kidney International **58**(1): 27-37.

Orimo, H. (2010). "The mechanism of mineralization and the role of alkaline phosphatase in health and disease." Journal of Nippon Medical School **77**(1): 4-12.

Orimo, H. and T. Shimada (2008). "The role of tissue-nonspecific alkaline phosphatase in the phosphate-induced activation of alkaline phosphatase and mineralization in SaOS-2 human osteoblast-like cells." Molecular and Cellular Biochemistry **315**(1-2): 51-60.

Ortiz-Capisano, M. C., P. A. Ortiz, J. L. Garvin, P. Harding and W. H. Beierwaltes (2007). "Expression and function of the calcium-sensing receptor in juxtaglomerular cells." Hypertension **50**(4): 737-743.

Ortiz-Capisano, M. C., M. Reddy, M. Mendez, J. L. Garvin and W. H. Beierwaltes (2013). "Juxtaglomerular cell CaSR stimulation decreases renin release via activation of the PLC/IP(3) pathway and the ryanodine receptor." American Journal of Physiology: Renal Physiology **304**(3): F248-256.

Parrish, A. R., A. J. Gandolfi and K. Brendel (1995). "Precision-cut tissue slices: Applications in pharmacology and toxicology." Life Sciences **57**(21): 1887-1901.

Parsons, S. J. and J. T. Parsons (2004). "Src family kinases, key regulators of signal transduction." Oncogene **23**(48): 7906-7909.

Patzer, L., N. Hernando, U. Ziegler, B. Beck-Schimmer, J. Biber and H. Murer (2006). "Ifosfamide metabolites CAA, 4-OH-Ifo and Ifo-mustard reduce apical phosphate transport by changing NaPi-IIa in OK cells." Kidney International **70**(10): 1725-1734.

Perwad, F., M. Y. Zhang, H. S. Tenenhouse and A. A. Portale (2007). "Fibroblast growth factor 23 impairs phosphorus and vitamin D metabolism in vivo and suppresses 25-hydroxyvitamin D-1alpha-hydroxylase expression in vitro." American Journal of Physiology: Renal Physiology **293**(5): F1577-1583.

Phillips, C. G., M. T. Harnett, W. Chen and S. M. Smith (2008). "Calcium-sensing receptor activation depresses synaptic transmission." Journal of Neuroscience **28**(46): 12062-12070.

Player, A. N., L.-P. Shen, D. Kenny, V. P. Antao and J. A. Kolberg (2001). "Single-copy Gene Detection Using Branched DNA (bDNA) In Situ Hybridization." Journal of Histochemistry and Cytochemistry **49**(5): 603-611.

Polidoro, L., G. Properzi, F. Marampon, G. L. Gravina, C. Festuccia, E. Di Cesare, L. Scarsella, C. Ciccarelli, B. M. Zani and C. Ferri (2013). "Vitamin D Protects Human Endothelial Cells from H2O 2 Oxidant Injury Through the Mek/Erk-Sirt1 Axis Activation." Journal of Cardiovascular Translational Research **6**(2): 221-231.

Poosti, F., B. T. Pham, D. Oosterhuis, K. Poelstra, H. van Goor, P. Olinga and J. L. Hillebrands (2015). "Precision-cut kidney slices (PCKS) to study development of renal fibrosis and efficacy of drug targeting ex vivo." Disease Models & Mechanisms.

Prasad, M., W. T. Butler and C. Qin (2010). "Dentin sialophosphoprotein in biomineralization." Connective Tissue Research **51**(5): 404-417.

Prasad, N. and D. Bhadauria (2013). "Renal phosphate handling: Physiology." Indian Journal of Endocrinology and Metabolism **17**(4): 620-627.

Preuss, H. G. (1993). "Basics of renal anatomy and physiology." Clinics in Laboratory Medicine **13**(1): 1-11.

Price, P. A., G. R. Thomas, A. W. Pardini, W. F. Figueira, J. M. Caputo and M. K. Williamson (2002). "Discovery of a high molecular weight complex of calcium, phosphate, fetuin, and matrix gamma-carboxyglutamic acid protein in the serum of etidronate-treated rats." Journal of Biological Chemistry **277**(6): 3926-3934.

Prie, D. and G. Friedlander (2010). "Reciprocal control of 1,25-dihydroxyvitamin D and FGF23 formation involving the FGF23/Klotho system." Clinical Journal of the American Society of Nephrology **5**(9): 1717-1722.

Procino, G., L. Mastrofrancesco, G. Tamma, D. R. Lasorsa, M. Ranieri, G. Stringini, F. Emma, M. Svelto and G. Valenti (2012). "Calcium-sensing receptor and aquaporin 2 interplay in hypercalciuria-associated renal concentrating defect in humans. An in vivo and in vitro study." PloS One **7**(3): e33145.

Proudfoot, D., J. N. Skepper, L. Hegyi, M. R. Bennett, C. M. Shanahan and P. L. Weissberg (2000). "Apoptosis regulates human vascular calcification in vitro: evidence

for initiation of vascular calcification by apoptotic bodies." Circulation Research **87**(11): 1055-1062.

Proudfoot, D., J. N. Skepper, L. Hegyi, A. Farzaneh-Far, C. M. Shanahan and P. L. Weissberg (2001). "The role of apoptosis in the initiation of vascular calcification." Zeitschrift für Kardiologie **90 Suppl 3**: 43-46.

Quinn, S. J., A. R. B. Thomsen, O. I. Egbuna, J. Pang, K. Baxi, D. Goltzman, M. R. Pollak and E. M. Brown (2013). "CaSR-mediated Interactions Between Calcium and Magnesium Homeostasis in Mice." American Journal of Physiology - Endocrinology And Metabolism.

Ranch, D., M. Y. Zhang, A. A. Portale and F. Perwad (2011). "Fibroblast growth factor 23 regulates renal 1,25-dihydroxyvitamin D and phosphate metabolism via the MAP kinase signaling pathway in Hyp mice." Journal of Bone and Mineral Research **26**(8): 1883-1890.

Raue, F., J. Pichl, H. G. Dorr, D. Schnabel, P. Heidemann, G. Hammersen, C. Jaursch-Hancke, R. Santen, C. Schofl, M. Wabitsch, C. Haag, E. Schulze and K. Frank-Raue (2011). "Activating mutations in the calcium-sensing receptor: genetic and clinical spectrum in 25 patients with autosomal dominant hypocalcaemia - a German survey." Clinical Endocrinology **75**(6): 760-765.

Ray, K., P. Clapp, P. K. Goldsmith and A. M. Spiegel (1998). "Identification of the sites of N-linked glycosylation on the human calcium receptor and assessment of their role in cell surface expression and signal transduction." Journal of Biological Chemistry **273**(51): 34558-34567.

Razzaque, M. S., D. Sitara, T. Taguchi, R. St-Arnaud and B. Lanske (2006). "Premature aging-like phenotype in fibroblast growth factor 23 null mice is a vitamin D-mediated process." FASEB Journal **20**(6): 720-722.

Reilly, M. P., N. Iqbal, M. Schutta, M. L. Wolfe, M. Scally, A. R. Localio, D. J. Rader and S. E. Kimmel (2004). "Plasma leptin levels are associated with coronary atherosclerosis in type 2 diabetes." Journal of Clinical Endocrinology and Metabolism **89**(8): 3872-3878.

Reinhardt, T. A. and R. L. Horst (1990). "Parathyroid hormone down-regulates 1,25-dihydroxyvitamin D receptors (VDR) and VDR messenger ribonucleic acid in vitro and blocks homologous up-regulation of VDR in vivo." Endocrinology **127**(2): 942-948.

Renkema, K. Y., A. Velic, H. B. Dijkman, S. Verkaart, A. W. van der Kemp, M. Nowik, K. Timmermans, A. Doucet, C. A. Wagner, R. J. Bindels and J. G. Hoenderop (2009). "The calcium-sensing receptor promotes urinary acidification to prevent nephrolithiasis." Journal of the American Society of Nephrology **20**(8): 1705-1713.

Revelli, A., M. Massobrio and J. Tesarik (1998). "Nongenomic Effects of 1α,25-Dihydroxyvitamin D3." Trends in Endocrinology and Metabolism **9**(10): 419-427.

Rhee, S. G. (2001). "Regulation of phosphoinositide-specific phospholipase C." Annual Review of Biochemistry **70**: 281-312.

Riccardi, D. and E. M. Brown (2010). "Physiology and pathophysiology of the calcium-sensing receptor in the kidney." American Journal of Physiology - Renal Physiology **298**(3): F485-F499.

Riccardi, D., A. E. Hall, N. Chattopadhyay, J. Z. Xu, E. M. Brown and S. C. Hebert (1998). "Localization of the extracellular Ca2+/polyvalent cation-sensing protein in rat kidney." American Journal of Physiology - Renal Physiology **274**(3): F611-F622.

Riccardi, D. and P. J. Kemp (2012). "The calcium-sensing receptor beyond extracellular calcium homeostasis: conception, development, adult physiology, and disease." Annual Review of Physiology **74**: 271-297.

Riccardi, D., W. S. Lee, K. Lee, G. V. Segre, E. M. Brown and S. C. Hebert (1996). "Localization of the extracellular Ca(2+)-sensing receptor and PTH/PTHrP receptor in rat kidney." American Journal of Physiology **271**(4 Pt 2): F951-956.

Riccardi, D., J. Park, W. S. Lee, G. Gamba, E. M. Brown and S. C. Hebert (1995). "Cloning and functional expression of a rat kidney extracellular calcium/polyvalent cation-sensing receptor." Proceedings of the National Academy of Sciences of the United States of America **92**(1): 131-135.

Riccardi, D., M. Traebert, D. T. Ward, B. Kaissling, J. Biber, S. C. Hebert and H. Murer (2000). "Dietary phosphate and parathyroid hormone alter the expression of the calcium-sensing receptor (CaR) and the Na+-dependent Pi transporter (NaPi-2) in the rat proximal tubule." Pflügers Archiv. European Journal of Physiology **441**(2-3): 379-387.

Roberts, S., S. Narisawa, D. Harmey, J. L. Millan and C. Farquharson (2007). "Functional involvement of PHOSPHO1 in matrix vesicle-mediated skeletal mineralization." Journal of Bone and Mineral Research **22**(4): 617-627.

Ronchetti, I., F. Boraldi, G. Annovi, P. Cianciulli and D. Quaglino (2013). "Fibroblast involvement in soft connective tissue calcification." Front Genet **4**: 22.

Rosen, H. N., A. C. Moses, J. Garber, I. D. Iloputaife, D. S. Ross, S. L. Lee and S. L. Greenspan (2000). "Serum CTX: a new marker of bone resorption that shows treatment effect more often than other markers because of low coefficient of variability and large changes with bisphosphonate therapy." Calcified Tissue International **66**(2): 100-103.

Rossini, M., B. Cheunsuchon, E. Donnert, L. J. Ma, J. W. Thomas, E. G. Neilson and A. B. Fogo (2005). "Immunolocalization of fibroblast growth factor-1 (FGF-1), its receptor (FGFR-1), and fibroblast-specific protein-1 (FSP-1) in inflammatory renal disease." Kidney International **68**(6): 2621-2628.

Ryan, Z. C., H. Ketha, M. S. McNulty, M. McGee-Lawrence, T. A. Craig, J. P. Grande, J. J. Westendorf, R. J. Singh and R. Kumar (2013). "Sclerostin alters serum vitamin D metabolite and fibroblast growth factor 23 concentrations and the urinary excretion of calcium." Proceedings of the National Academy of Sciences of the United States of America **110**(15): 6199-6204.

Sandilands, E., S. Akbarzadeh, A. Vecchione, D. G. McEwan, M. C. Frame and J. K. Heath (2007). "Src kinase modulates the activation, transport and signalling dynamics of fibroblast growth factor receptors." EMBO Reports **8**(12): 1162-1169.

Sandra, F., L. Hendarmin and S. Nakamura (2006). "Osteoprotegerin (OPG) binds with Tumor Necrosis Factor-Related Apoptosis-Inducing Ligand (TRAIL): Suppression of TRAIL-induced apoptosis in ameloblastomas." Oral Oncology **42**(4): 415-420.

Sands, J. M., M. Naruse, M. Baum, I. Jo, S. C. Hebert, E. M. Brown and H. W. Harris (1997). "Apical extracellular calcium/polyvalent cation-sensing receptor regulates

vasopressin-elicited water permeability in rat kidney inner medullary collecting duct." Journal of Clinical Investigation **99**(6): 1399-1405.

Sapir-Koren, R. and G. Livshits (2014). "Bone mineralization is regulated by signaling cross talk between molecular factors of local and systemic origin: the role of fibroblast growth factor 23." Biofactors **40**(6): 555-568.

Schoppet, M., N. Al-Fakhri, F. E. Franke, N. Katz, P. J. Barth, B. Maisch, K. T. Preissner and L. C. Hofbauer (2004). "Localization of osteoprotegerin, tumor necrosis factor-related apoptosis-inducing ligand, and receptor activator of nuclear factor-kappaB ligand in Monckeberg's sclerosis and atherosclerosis." Journal of Clinical Endocrinology and Metabolism **89**(8): 4104-4112.

Schoppet, M., N. Al-Fakhri, F. E. Franke, N. Katz, P. J. Barth, B. Maisch, K. T. Preissner and L. C. Hofbauer (2004). "Localization of Osteoprotegerin, Tumor Necrosis Factor-Related Apoptosis-Inducing Ligand, and Receptor Activator of Nuclear Factor-κB Ligand in Mönckeberg's Sclerosis and Atherosclerosis." The Journal of Clinical Endocrinology & Metabolism **89**(8): 4104-4112.

Schoppet, M. and C. M. Shanahan (2008). "Role for alkaline phosphatase as an inducer of vascular calcification in renal failure?" Kidney International **73**(9): 989-991.

Sengul, S., C. Zwizinski and V. Batuman (2003). "Role of MAPK pathways in light chain-induced cytokine production in human proximal tubule cells." American Journal of Physiology: Renal Physiology **284**(6): F1245-1254.

Shalhoub, V., S. Ward, B. Sun, J. Stevens, L. Renshaw, N. Hawkins and W. Richards (2011). "Fibroblast Growth Factor 23 (FGF23) and Alpha-Klotho Stimulate Osteoblastic MC3T3.E1 Cell Proliferation and Inhibit Mineralization." Calcified Tissue International **89**(2): 140-150.

Sharma, U., D. Pal and R. Prasad (2014). "Alkaline Phosphatase: An Overview." Indian Journal of Clinical Biochemistry **29**(3): 269-278.

Sheen, C. R., P. Kuss, S. Narisawa, M. C. Yadav, J. Nigro, W. Wang, T. N. Chhea, E. A. Sergienko, K. Kapoor, M. R. Jackson, M. F. Hoylaerts, A. B. Pinkerton, W. C. O'Neill and J. L. Millan (2015). "Pathophysiological role of vascular smooth muscle alkaline phosphatase in medial artery calcification." Journal of Bone and Mineral Research **30**(5): 824-836.

Shimada, T., H. Hasegawa, Y. Yamazaki, T. Muto, R. Hino, Y. Takeuchi, T. Fujita, K. Nakahara, S. Fukumoto and T. Yamashita (2004). "FGF-23 is a potent regulator of vitamin D metabolism and phosphate homeostasis." Journal of Bone and Mineral Research **19**(3): 429-435.

Shimada, T., M. Kakitani, Y. Yamazaki, H. Hasegawa, Y. Takeuchi, T. Fujita, S. Fukumoto, K. Tomizuka and T. Yamashita (2004). "Targeted ablation of Fgf23 demonstrates an essential physiological role of FGF23 in phosphate and vitamin D metabolism." Journal of Clinical Investigation **113**(4): 561-568.

Shimada, T., I. Urakawa, Y. Yamazaki, H. Hasegawa, R. Hino, T. Yoneya, Y. Takeuchi, T. Fujita, S. Fukumoto and T. Yamashita (2004). "FGF-23 transgenic mice demonstrate hypophosphatemic rickets with reduced expression of sodium phosphate cotransporter type IIa." Biochemical and Biophysical Research Communications **314**(2): 409-414.

Shinki, T., C. H. Jin, A. Nishimura, Y. Nagai, Y. Ohyama, M. Noshiro, K. Okuda and T. Suda (1992). "Parathyroid hormone inhibits 25-hydroxyvitamin D3-24-hydroxylase mRNA expression stimulated by 1 alpha,25-dihydroxyvitamin D3 in rat kidney but not in intestine." Journal of Biological Chemistry **267**(19): 13757-13762.

Sidhu, P. S., N. Nassif, M. M. McCallum, K. Teske, B. Feleke, N. Y. Yuan, P. Nandhikonda, J. M. Cook, R. K. Singh, D. D. Bikle and L. A. Arnold (2014). "Development of Novel Vitamin D Receptor–Coactivator Inhibitors." ACS Medicinal Chemistry Letters **5**(2): 199-204.

Silver, J. and T. Naveh-Many (2009). "Phosphate and the parathyroid." Kidney International **75**(9): 898-905.

Speer, M. Y. and C. M. Giachelli (2004). "Regulation of cardiovascular calcification." Cardiovascular Pathology **13**(2): 63-70.

Staines, K. A., V. E. MacRae and C. Farquharson (2012). "The importance of the SIBLING family of proteins on skeletal mineralisation and bone remodelling." Journal of Endocrinology **214**(3): 241-255.

Steitz, S. A., M. Y. Speer, G. Curinga, H. Y. Yang, P. Haynes, R. Aebersold, T. Schinke, G. Karsenty and C. M. Giachelli (2001). "Smooth muscle cell phenotypic transition associated with calcification: upregulation of Cbfa1 and downregulation of smooth muscle lineage markers." Circulation Research **89**(12): 1147-1154.

Steitz, S. A., M. Y. Speer, M. D. McKee, L. Liaw, M. Almeida, H. Yang and C. M. Giachelli (2002). "Osteopontin inhibits mineral deposition and promotes regression of ectopic calcification." American Journal of Pathology **161**(6): 2035-2046.

Strathmann, F. G., T. J. Laha and A. N. Hoofnagle (2011). "Quantification of 1alpha,25-dihydroxy vitamin D by immunoextraction and liquid chromatography-tandem mass spectrometry." Clinical Chemistry **57**(9): 1279-1285.

Su, Z., J. Zimpelmann and K. D. Burns (2006). "Angiotensin-(1-7) inhibits angiotensin II-stimulated phosphorylation of MAP kinases in proximal tubular cells." Kidney International **69**(12): 2212-2218.

Suda, T., Y. Ueno, K. Fujii and T. Shinki (2003). "Vitamin D and bone." Journal of Cellular Biochemistry **88**(2): 259-266.

Sweatt, A., D. C. Sane, S. M. Hutson and R. Wallin (2003). "Matrix Gla protein (MGP) and bone morphogenetic protein-2 in aortic calcified lesions of aging rats." Journal of Thrombosis and Haemostasis **1**(1): 178-185.

Taketani, Y., H. Segawa, M. Chikamori, K. Morita, K. Tanaka, S. Kido, H. Yamamoto, Y. Iemori, S. Tatsumi, N. Tsugawa, T. Okano, T. Kobayashi, K.-i. Miyamoto and E. Takeda (1998). "Regulation of Type II Renal Na+-dependent Inorganic Phosphate Transporters by 1,25-Dihydroxyvitamin D3 : IDENTIFICATION OF A VITAMIN D-RESPONSIVE ELEMENT IN THE HUMAN NAPI-3 GENE." Journal of Biological Chemistry **273**(23): 14575-14581.

Takeyama, K.-i., S. Kitanaka, T. Sato, M. Kobori, J. Yanagisawa and S. Kato (1997). "25-Hydroxyvitamin D3 1α-Hydroxylase and Vitamin D Synthesis." Science **277**(5333): 1827-1830.

Tan, Y., J. Rouse, A. Zhang, S. Cariati, P. Cohen and M. J. Comb (1996). "FGF and stress regulate CREB and ATF-1 via a pathway involving p38 MAP kinase and MAPKAP kinase-2." EMBO Journal **15**(17): 4629-4642.

Tartaix, P. H., M. Doulaverakis, A. George, L. W. Fisher, W. T. Butler, C. Qin, E. Salih, M. Tan, Y. Fujimoto, L. Spevak and A. L. Boskey (2004). "In Vitro Effects of Dentin Matrix Protein-1 on Hydroxyapatite Formation Provide Insights into in Vivo Functions." Journal of Biological Chemistry **279**(18): 18115-18120.

Tatsumi, S., H. Segawa, K. Morita, H. Haga, T. Kouda, H. Yamamoto, Y. Inoue, T. Nii, K. Katai, Y. Taketani, K. I. Miyamoto and E. Takeda (1998). "Molecular cloning and hormonal regulation of PiT-1, a sodium-dependent phosphate cotransporter from rat parathyroid glands." Endocrinology **139**(4): 1692-1699.

Tenenhouse, H. S., C. Gauthier, J. Martel, F. A. Gesek, B. A. Coutermarsh and P. A. Friedman (1998). "Na+ -phosphate cotransport in mouse distal convoluted tubule cells: evidence for Glvr-1 and Ram-1 gene expression." Journal of Bone and Mineral Research **13**(4): 590-597.

Tenenhouse, H. S., S. Roy, J. Martel and C. Gauthier (1998). Differential expression, abundance, and regulation of Na+-phosphate cotransporter genes in murine kidney.

Terkeltaub, R. (2006). "Physiologic and pathologic functions of the NPP nucleotide pyrophosphatase/phosphodiesterase family focusing on NPP1 in calcification." Purinergic Signal **2**(2): 371-377.

Theman, T. A. and M. T. Collins (2009). "The role of the calcium-sensing receptor in bone biology and pathophysiology." Current Pharmaceutical Biotechnology **10**(3): 289-301.

Toka, H. R., K. Al-Romaih, J. M. Koshy, S. DiBartolo, C. H. Kos, S. J. Quinn, G. C. Curhan, D. B. Mount, E. M. Brown and M. R. Pollak (2012). "Deficiency of the Calcium-Sensing Receptor in the Kidney Causes Parathyroid Hormone–Independent Hypocalciuria." Journal of the American Society of Nephrology **23**(11): 1879-1890.

Topala, C. N., J. P. H. Schoeber, L. E. Searchfield, D. Riccardi, J. G. J. Hoenderop and R. J. M. Bindels (2009). "Activation of the Ca2+-sensing receptor stimulates the activity of the epithelial Ca2+ channel TRPV5." Cell Calcium **45**(4): 331-339.

Toutain, H. J., V. Moronvalle-Halley, J. P. Sarsat, C. Chelin, D. Hoet and D. Leroy (1998). "Morphological and functional integrity of precision-cut rat liver slices in rotating organ culture and multiwell plate culture: Effects of oxygen tension." Cell Biology and Toxicology **14**(3): 175-190.

Tsujikawa, H., Y. Kurotaki, T. Fujimori, K. Fukuda and Y. Nabeshima (2003). "Klotho, a gene related to a syndrome resembling human premature aging, functions in a negative regulatory circuit of vitamin D endocrine system." Molecular Endocrinology **17**(12): 2393-2403.

Turunen, M. M., T. W. Dunlop, C. Carlberg and S. Väisänen (2007). "Selective use of multiple vitamin D response elements underlies the 1 α,25-dihydroxyvitamin D(3)-mediated negative regulation of the human CYP27B1 gene." Nucleic Acids Research **35**(8): 2734-2747.

Ueland, T., K. Otterdal, T. Lekva, B. Halvorsen, A. Gabrielsen, W. J. Sandberg, G. Paulsson-Berne, T. M. Pedersen, L. Folkersen, L. Gullestad, E. Oie, G. K. Hansson and P. Aukrust (2009). "Dickkopf-1 enhances inflammatory interaction between

platelets and endothelial cells and shows increased expression in atherosclerosis." Arteriosclerosis, Thrombosis, and Vascular Biology **29**(8): 1228-1234.

Ueland, T., K. Otterdal, T. Lekva, B. Halvorsen, A. Gabrielsen, W. J. Sandberg, G. Paulsson-Berne, T. M. Pedersen, L. Folkersen, L. Gullestad, E. Øie, G. K. Hansson and P. Aukrust (2009). "Dickkopf-1 Enhances Inflammatory Interaction Between Platelets and Endothelial Cells and Shows Increased Expression in Atherosclerosis." Arteriosclerosis, Thrombosis, and Vascular Biology **29**(8): 1228-1234.

Urakawa, I., Y. Yamazaki, T. Shimada, K. Iijima, H. Hasegawa, K. Okawa, T. Fujita, S. Fukumoto and T. Yamashita (2006). "Klotho converts canonical FGF receptor into a specific receptor for FGF23." Nature **444**(7120): 770-774.

Vaisanen, S., T. W. Dunlop, L. Sinkkonen, C. Frank and C. Carlberg (2005). "Spatio-temporal activation of chromatin on the human CYP24 gene promoter in the presence of 1alpha,25-Dihydroxyvitamin D3." Journal of Molecular Biology **350**(1): 65-77.

van Abel, M., J. G. Hoenderop, A. W. van der Kemp, M. M. Friedlaender, J. P. van Leeuwen and R. J. Bindels (2005). "Coordinated control of renal Ca(2+) transport proteins by parathyroid hormone." Kidney International **68**(4): 1708-1721.

van de Graaf, S. F., I. Boullart, J. G. Hoenderop and R. J. Bindels (2004). "Regulation of the epithelial Ca2+ channels TRPV5 and TRPV6 by 1alpha,25-dihydroxy Vitamin D3 and dietary Ca2+." Journal of Steroid Biochemistry and Molecular Biology **89-90**(1-5): 303-308.

van Venrooij, N. A., R. C. Pereira, Y. Tintut, M. C. Fishbein, N. Tumber, L. L. Demer, I. B. Salusky and K. Wesseling-Perry (2014). "FGF23 protein expression in coronary arteries is associated with impaired kidney function." Nephrology, Dialysis, Transplantation **29**(8): 1525-1532.

Vervloet, M. G., F. J. van Ittersum, R. M. Buttler, A. C. Heijboer, M. A. Blankenstein and P. M. ter Wee (2011). "Effects of dietary phosphate and calcium intake on fibroblast growth factor-23." Clinical Journal of the American Society of Nephrology **6**(2): 383-389.

Vickers, A. E., K. Rose, R. Fisher, M. Saulnier, P. Sahota and P. Bentley (2004). "Kidney slices of human and rat to characterize cisplatin-induced injury on cellular pathways and morphology." Toxicologic Pathology **32**(5): 577-590.

Villa-Bellosta, R., S. Ravera, V. Sorribas, G. Stange, M. Levi, H. Murer, J. Biber and I. C. Forster (2009). "The Na+-Pi cotransporter PiT-2 (SLC20A2) is expressed in the apical membrane of rat renal proximal tubules and regulated by dietary Pi." American Journal of Physiology: Renal Physiology **296**(4): F691-699.

von Ahlfen, S., A. Missel, K. Bendrat and M. Schlumpberger (2007). "Determinants of RNA quality from FFPE samples." PloS One **2**(12): e1261.

Wada, T., T. Nakashima, N. Hiroshi and J. M. Penninger (2006). "RANKL–RANK signaling in osteoclastogenesis and bone disease." Trends in Molecular Medicine **12**(1): 17-25.

Wagner, C. A., J. Biber and H. Murer (2008). "Of Men and Mice: Who Is in Control of Renal Phosphate Reabsorption?" Journal of the American Society of Nephrology **19**(9): 1625-1626.

Wang, H. W., M. Lu and S. C. Hebert (1996). "Cytochrome P-450 metabolites mediate extracellular Ca^{2+}-induced inhibition of apical K^+ channels in the TAL." American Journal of Physiology: Cell Physiology **271**: C103-C111.

Wang, J., H. Y. Zhou, E. Salih, L. Xu, L. Wunderlich, X. Gu, J. G. Hofstaetter, M. Torres and M. J. Glimcher (2006). "Site-specific in vivo calcification and osteogenesis stimulated by bone sialoprotein." Calcified Tissue International **79**(3): 179-189.

Wang, T.-T., L. E. Tavera-Mendoza, D. Laperriere, E. Libby, N. B. MacLeod, Y. Nagai, V. Bourdeau, A. Konstorum, B. Lallemant, R. Zhang, S. Mader and J. H. White (2005). "Large-Scale in Silico and Microarray-Based Identification of Direct 1,25-Dihydroxyvitamin D3 Target Genes." Molecular Endocrinology **19**(11): 2685-2695.

Ward, D. T., E. M. Brown and H. W. Harris (1998). "Disulfide Bonds in the Extracellular Calcium-Polyvalent Cation-sensing Receptor Correlate with Dimer Formation and Its Response to Divalent Cations in Vitro." Journal of Biological Chemistry **273**(23): 14476-14483.

Ward, D. T., S. K. Yau, A. P. Mee, E. B. Mawer, C. A. Miller, H. O. Garland and D. Riccardi (2001). "Functional, Molecular, and Biochemical Characterization of Streptozotocin-Induced Diabetes." Journal of the American Society of Nephrology **12**(4): 779-790.

Weber, K., R. G. Erben, A. Rump and J. Adamski (2001). "Gene structure and regulation of the murine epithelial calcium channels ECaC1 and 2." Biochemical and Biophysical Research Communications **289**(5): 1287-1294.

Weiner, S. (2003). "An Overview of Biomineralization Processes and the Problem of the Vital Effect." Reviews in Mineralogy & Geochemistry **54**(1): 1-29.

Weinman, E. J., D. Steplock, S. Shenolikar and R. Biswas (2011). "Fibroblast growth factor-23-mediated inhibition of renal phosphate transport in mice requires sodium-hydrogen exchanger regulatory factor-1 (NHERF-1) and synergizes with parathyroid hormone." Journal of Biological Chemistry **286**(43): 37216-37221.

Weston, A. H., M. Absi, D. T. Ward, J. Ohanian, R. H. Dodd, P. Dauban, C. Petrel, M. Ruat and G. Edwards (2005). "Evidence in favor of a calcium-sensing receptor in arterial endothelial cells: studies with calindol and Calhex 231." Circulation Research **97**(4): 391-398.

Wexler, L., B. Brundage, J. Crouse, R. Detrano, V. Fuster, J. Maddahi, J. Rumberger, W. Stanford, R. White, K. Taubert and A. Staff (1996). "Coronary Artery Calcification: Pathophysiology, Epidemiology, Imaging Methods, and Clinical Implications: A Statement for Health Professionals From the American Heart Association." Circulation **94**(5): 1175-1192.

White, K. E., W. E. Evans, J. L. H. O'Riordan, M. C. Speer, M. J. Econs, B. Lorenz-Depiereux, M. Grabowski, T. Meitinger and T. M. Strom (2000). "Autosomal dominant hypophosphataemic rickets is associated with mutations in FGF23." Nature Genetics **26**(3): 345-348.

Windaus, A. and F. Bock (1937). Über das Provitamin aus dem Sterin der Schweineschwarte. Hoppe-Seyler´s Zeitschrift für physiologische Chemie. **245:** 168.

Wohrle, S., O. Bonny, N. Beluch, S. Gaulis, C. Stamm, M. Scheibler, M. Muller, B. Kinzel, A. Thuery, J. Brueggen, N. E. Hynes, W. R. Sellers, F. Hofmann and D. Graus-Porta (2011). "FGF receptors control vitamin D and phosphate homeostasis by

mediating renal FGF-23 signaling and regulating FGF-23 expression in bone." Journal of Bone and Mineral Research **26**(10): 2486-2497.

Wohrle, S., C. Henninger, O. Bonny, A. Thuery, N. Beluch, N. E. Hynes, V. Guagnano, W. R. Sellers, F. Hofmann, M. Kneissel and D. Graus Porta (2013). "Pharmacological inhibition of fibroblast growth factor (FGF) receptor signaling ameliorates FGF23-mediated hypophosphatemic rickets." Journal of Bone and Mineral Research **28**(4): 899-911.

Wranicz, J. and D. Szostak-Wegierek (2014). "Health outcomes of vitamin D. Part I. characteristics and classic role." Roczniki Panstwowego Zakladu Higieny **65**(3): 179-184.

Wu, A. L., B. Feng, M. Z. Chen, G. Kolumam, J. Zavala-Solorio, S. K. Wyatt, V. D. Gandham, R. A. Carano and J. Sonoda (2013). "Antibody-Mediated Activation of FGFR1 Induces FGF23 Production and Hypophosphatemia." PloS One **8**(2): e57322.

Wysolmerski, J. J. (2012). "Parathyroid hormone-related protein: an update." Journal of Clinical Endocrinology and Metabolism **97**(9): 2947-2956.

Xiao, Z., J. Huang, L. Cao, Y. Liang, X. Han and L. D. Quarles (2014). "Osteocyte-specific deletion of Fgfr1 suppresses FGF23." PloS One **9**(8): e104154.

Yamashita, T., M. Yoshioka and N. Itoh (2000). "Identification of a novel fibroblast growth factor, FGF-23, preferentially expressed in the ventrolateral thalamic nucleus of the brain." Biochemical and Biophysical Research Communications **277**(2): 494-498.

Yamazaki, M., K. Ozono, T. Okada, K. Tachikawa, H. Kondou, Y. Ohata and T. Michigami (2010). "Both FGF23 and extracellular phosphate activate Raf/MEK/ERK pathway via FGF receptors in HEK293 cells." Journal of Cellular Biochemistry **111**(5): 1210-1221.

Yan, X., H. Yokote, X. Jing, L. Yao, T. Sawada, Y. Zhang, S. Liang and K. Sakaguchi (2005). "Fibroblast growth factor 23 reduces expression of type IIa Na+/Pi co-transporter by signaling through a receptor functionally distinct from the known FGFRs in opossum kidney cells." Genes to Cells **10**(5): 489-502.

Yang, D., J. Guo, P. Divieti and F. R. Bringhurst (2006). "Parathyroid hormone activates PKC-delta and regulates osteoblastic differentiation via a PLC-independent pathway." Bone **38**(4): 485-496.

Yang, H., G. Curinga and C. M. Giachelli (2004). "Elevated extracellular calcium levels induce smooth muscle cell matrix mineralization in vitro." Kidney International **66**(6): 2293-2299.

Yang, T., S. Hassan, Y. G. Huang, A. M. Smart, J. P. Briggs and J. B. Schnermann (1997). "Expression of PTHrP, PTH/PTHrP receptor, and Ca(2+)-sensing receptor mRNAs along the rat nephron." American Journal of Physiology **272**(6 Pt 2): F751-758.

Yanochko, G. M., A. Vitsky, J. R. Heyen, B. Hirakawa, J. L. Lam, J. May, T. Nichols, F. Sace, D. Trajkovic and E. Blasi (2013). "Pan-FGFR inhibition leads to blockade of FGF23 signaling, soft tissue mineralization, and cardiovascular dysfunction." Toxicological Sciences **135**(2): 451-464.

Yao, L., Y. T. Sun, W. Sun, T. H. Xu, C. Ren, X. Fan, L. Sun, L. L. Liu, J. M. Feng, J. F. Ma and L. N. Wang (2015). "High phosphorus level leads to aortic calcification via beta-catenin in chronic kidney disease." American Journal of Nephrology **41**(1): 28-36.

Yasuoka, Y., Y. Sato, J. Healy, H. Nonoguchi and K. Kawahara (2014). "pH-sensitive expression of calcium-sensing receptor (CaSR) in type-B intercalated cells of the cortical collecting ducts (CCD) in mouse kidney." Clinical and Experimental Nephrology: 1-12.

You, H., H. Yang, Q. Zhu, M. Li, J. Xue, Y. Gu, S. Lin and F. Ding (2009). "Advanced oxidation protein products induce vascular calcification by promoting osteoblastic trans-differentiation of smooth muscle cells via oxidative stress and ERK pathway." Renal Failure **31**(4): 313-319.

Yu, P.-J., A. Skolnick, G. Ferrari, K. Heretis, P. Mignatti, G. Pintucci, B. Rosenzweig, J. Diaz-Cartelle, I. Kronzon, G. Perk, H. I. Pass, A. C. Galloway, E. A. Grossi and J. B. Grau (2009). "Correlation between plasma osteopontin levels and aortic valve calcification: Potential insights into the pathogenesis of aortic valve calcification and stenosis." The Journal of Thoracic and Cardiovascular Surgery **138**(1): 196-199.

Yu, X., O. A. Ibrahimi, R. Goetz, F. Zhang, S. I. Davis, H. J. Garringer, R. J. Linhardt, D. M. Ornitz, M. Mohammadi and K. E. White (2005). "Analysis of the biochemical mechanisms for the endocrine actions of fibroblast growth factor-23." Endocrinology **146**(11): 4647-4656.

Zeadin, M. G., M. K. Butcher, S. G. Shaughnessy and G. H. Werstuck (2012). "Leptin promotes osteoblast differentiation and mineralization of primary cultures of vascular smooth muscle cells by inhibiting glycogen synthase kinase (GSK)-3β." Biochemical and Biophysical Research Communications **425**(4): 924-930.

Zehnder, D., R. Bland, R. S. Chana, D. C. Wheeler, A. J. Howie, M. C. Williams, P. M. Stewart and M. Hewison (2002). "Synthesis of 1,25-dihydroxyvitamin D(3) by human endothelial cells is regulated by inflammatory cytokines: a novel autocrine determinant of vascular cell adhesion." Journal of the American Society of Nephrology **13**(3): 621-629.

Zehnder, D., R. Bland, M. C. Williams, R. W. McNinch, A. J. Howie, P. M. Stewart and M. Hewison (2001). "Extrarenal expression of 25-hydroxyvitamin d(3)-1 alpha-hydroxylase." Journal of Clinical Endocrinology and Metabolism **86**(2): 888-894.

Zoidis, E., C. Ghirlanda-Keller, M. Gosteli-Peter, J. Zapf and C. Schmid (2004). "Regulation of phosphate (Pi) transport and NaPi-III transporter (Pit-1) mRNA in rat osteoblasts." Journal of Endocrinology **181**(3): 531-540.

7 Appendix

The tables presented in this appendix contain the raw data for the experiments presented in this thesis.

Table 7.1: Image analysis of CaSR IHC carried out in sections from rats treated with 1.4 mg/kg/day of MEKi, 20 mg/kg/day of FGFRi or the respective vehicles.

Group	Study	Time point	N	IHC positivity (%)	P
Vehicle	4	28d	10	3.58 ± 0.29	-
MEKi	4	28d	10	2.91 ± 0.22	0.15
Vehicle	4	25d	7	3.72 ± 0.26	-
FGFRi	4	25d	6	3.38 ± 0.08	0.20

Table 7.2: Plasma drug concentrations during a 12h period following the administration of 150 mg/kg of ERKi, 1.4 mg/kg of MEKi or 10 mg/kg of FGFRi to rats by oral gavage.

Group	Study	Time point	N	Drug concentration (µmol/L)
ERKi	2	d1, 2h	6	155 ± 15
ERKi	2	d1, 6h	6	111 ± 7
ERKi	2	d1, 12h	6	53 ± 8
MEKi	1	d1, 2h	6	1.17 ± 0.22
MEKi	1	d1, 4h	6	0.39 ± 0.06
MEKi	1	d1, 6h	6	0.19 ± 0.01
MEKi	1	d1, 12h	6	0.11 ± 0.01
MEKi	1	d7, 2h	6	1.77 ± 0.37
MEKi	1	d7, 4h	6	0.72 ± 0.17
MEKi	1	d7, 6h	6	0.41 ± 0.08
MEKi	1	d7, 12h	6	0.11 ± 0.03
FGFRi	1	d1, 2h	6	2.94 ± 0.27
FGFRi	1	d1, 4h	6	1.80 ± 0.33
FGFRi	1	d1, 6h	6	0.76 ± 0.07
FGFRi	1	d1, 12h	6	0.07 ± 0.03
FGFRi	1	d7, 2h	6	2.00 ± 0.38
FGFRi	1	d7, 4h	6	1.69 ± 0.37
FGFRi	1	d7, 6h	6	1.32 ± 0.39
FGFRi	1	d7, 12h	6	0.39 ± 0.11

Table 7.3: Plasma concentrations of Ca^{2+} in animals treated with 150 mg/kg/day of ERKi, 1.4 mg/kg/day of MEKi, 20 mg/kg/day FGFRi or the respective vehicles.

Group	Study	Time point	N	Plasma Ca^{2+} (mmol/L)	P
Vehicle	1	d1, 2h	3	2.75 ± 0.04	-
MEKi	1	d1, 2h	6	2.79 ± 0.03	0.438
FGFRi	1	d1, 2h	6	2.79 ± 0.01	0.366
Vehicle	1	d1, 6h	3	2.75 ± 0.03	-
MEKi	1	d1, 6h	6	2.69 ± 0.02	0.197
FGFRi	1	d1, 6h	6	2.73 ± 0.04	0.519
Vehicle	1	d1, 12h	3	2.59 ± 0.04	-
MEKi	1	d1, 12h	6	2.52 ± 0.04	0.366
FGFRi	1	d1, 12h	6	2.68 ± 0.02	0.071
Vehicle	1	d7, 2h	3	2.80 ± 0.05	-
MEKi	1	d7, 2h	6	2.88 ± 0.04	0.439
FGFRi	1	d7, 2h	4	2.91 ± 0.02	0.077
Vehicle	2	d1, 2h	6	2.84 ± 0.04	**-**
ERKi	2	d1, 2h	6	2.62 ± 0.03	**0.004**
FGFRi	2	d1, 2h	6	2.75 ± 0.02	**0.045**
Vehicle	2	d1, 6h	6	2.76 ± 0.10	-
ERKi	2	d1, 6h	5	2.70 ± 0.03	0.144
FGFRi	2	d1, 6h	5	2.74 ± 0.02	0.200
Vehicle	2	d1, 24h	6	2.83 ± 0.04	-
ERKi	2	d1, 24h	6	2.79 ± 0.05	0.601
FGFRi	2	d1, 24h	6	2.97 ± 0.01	**0.036**
Vehicle	2	d4, 2h	6	2.70 ± 0.03	**-**
ERKi	2	d4, 2h	6	3.00 ± 0.08	**0.008**
FGFRi	2	d4, 2h	6	2.84 ± 0.03	**0.02**
Vehicle	2	d7, 2h	5	2.64 ± 0.06	-
FGFRi	2	d7, 2h	5	2.74 ± 0.08	0.465
Vehicle	3	d1, 2h	6	2.87 ± 0.05	-
ERKi	3	d1, 2h	6	2.70 ± 0.04	**0.025**
FGFRi	3	d1, 2h	6	2.85 ± 0.03	0.872
Vehicle	3	d1, 6h	5	2.80 ± 0.03	-
ERKi	3	d1, 6h	6	2.80 ± 0.06	0.584
FGFRi	3	d1, 6h	5	2.86 ± 0.02	0.143
Vehicle	3	d1, 24h	6	2.84 ± 0.05	-
ERKi	3	d1, 24h	6	2.69 ± 0.04	**0.037**
FGFRi	3	d1, 24h	4	2.76 ± 0.03	0.241

Table 7.4: Plasma concentrations of Pi in animals treated with 150 mg/kg/day of ERKi, 1.4 mg/kg/day of MEKi, 20 mg/kg/day FGFRi or the respective vehicles.

Group	Study	Time point	N	Plasma Pi (mmol/L)	P
Vehicle	1	d1, 2h	3	1.86 ± 0.09	-
MEKi	1	d1, 2h	6	1.71 ± 0.14	0.438
FGFRi	1	d1, 2h	6	1.81 ± 0.09	0.606
Vehicle	1	d1, 6h	3	2.51 ± 0.14	-
MEKi	1	d1, 6h	6	2.23 ± 0.19	0.302
FGFRi	1	d1, 6h	6	2.38 ± 0.12	0.698
Vehicle	1	d1, 12h	3	2.11 ± 0.09	-
MEKi	1	d1, 12h	6	2.55 ± 0.10	**0.028**
FGFRi	1	d1, 12h	6	2.41 ± 0.03	**0.020**
Vehicle	1	d4, 2h	3	2.00 ± 0.04	-
MEKi	1	d4, 2h	6	3.11 ± 0.04	**0.020**
FGFRi	1	d4, 2h	6	3.18 ± 0.18	**0.020**
Vehicle	1	d7, 2h	3	1.75 ± 0.04	-
MEKi	1	d7, 2h	6	2.85 ± 0.12	**0.020**
FGFRi	1	d7, 2h	5	2.71 ± 0.09	**0.025**
Vehicle	2	d1, 2h	6	1.84 ± 0.05	-
ERKi	2	d1, 2h	6	1.26 ± 0.06	**0.004**
FGFRi	2	d1, 2h	6	1.38 ± 0.10	**0.004**
Vehicle	2	d1, 6h	6	2.45 ± 0.09	-
ERKi	2	d1, 6h	6	2.02 ± 0.09	**0.006**
FGFRi	2	d1, 6h	6	2.19 ± 0.08	**0.065**
Vehicle	2	d1, 24h	6	1.80 ± 0.06	-
ERKi	2	d1, 24h	6	2.68 ± 0.09	**0.004**
FGFRi	2	d1, 24h	6	2.11 ± 0.06	**0.008**
Vehicle	2	d4, 2h	6	1.68 ± 0.11	-
ERKi	2	d4, 2h	5	3.41 ± 0.16	**0.006**
FGFRi	2	d4, 2h	6	3.59 ± 0.11	**0.005**
Vehicle	2	d7, 2h	6	1.78 ± 0.10	-
FGFRi	2	d7, 2h	6	3.07 ± 0.17	**0.004**
Vehicle	3	d1, 2h	6	1.68 ± 0.09	-
ERKi	3	d1, 2h	6	1.49 ± 0.12	0.262
FGFRi	3	d1, 2h	6	1.54 ± 0.09	0.173
Vehicle	3	d1, 6h	5	1.65 ± 0.14	-
ERKi	3	d1, 6h	6	1.64 ± 0.22	0.361
FGFRi	3	d1, 6h	5	1.59 ± 0.07	0.346
Vehicle	3	d1, 24h	6	2.04 ± 0.13	-
ERKi	3	d1, 24h	6	1.97 ± 0.14	0.810
FGFRi	3	d1, 24h	4	2.00 ± 0.08	1.00

Table 7.5: Plasma concentrations of Mg^{2+} in animals treated with 150 mg/kg/day of ERKi, 1.4 mg/kg/day of MEKi, 20 mg/kg/day FGFRi or the respective vehicles.

Group	Study	Time point	N	Plasma Mg^{2+} (mmol/L)	P
Vehicle	1	d1, 2h	3	0.80 ± 0.04	-
MEKi	1	d1, 2h	6	0.76 ± 0.03	0.301
FGFRi	1	d1, 2h	6	0.72 ± 0.02	0.093
Vehicle	1	d1, 6h	3	0.73 ± 0.04	-
MEKi	1	d1, 6h	6	0.74 ± 0.03	0.897
FGFRi	1	d1, 6h	6	0.75 ± 0.03	0.698
Vehicle	1	d1, 12h	3	0.71 ± 0.01	-
MEKi	1	d1, 12h	6	0.78 ± 0.04	0.366
FGFRi	1	d1, 12h	6	0.79 ± 0.01	**0.020**
Vehicle	1	d7, 2h	3	0.70 ± 0.03	-
MEKi	1	d7, 2h	6	0.71 ± 0.02	0.060
FGFRi	1	d7, 2h	4	0.79 ± 0.02	0.077
Vehicle	2	d1, 2h	6	0.77 ± 0.01	-
ERKi	2	d1, 2h	6	0.75 ± 0.03	0.078
FGFRi	2	d1, 2h	6	0.72 ± 0.01	**0.025**
Vehicle	2	d1, 6h	5	0.79 ± 0.01	-
ERKi	2	d1, 6h	5	0.74 ± 0.04	0.210
FGFRi	2	d1, 6h	5	0.75 ± 0.02	0.117
Vehicle	2	d1, 24h	6	0.80 ± 0.02	-
ERKi	2	d1, 24h	5	0.83 ± 0.04	0.201
FGFRi	2	d1, 24h	6	0.82 ± 0.01	0.149
Vehicle	2	d4, 2h	6	0.76 ± 0.01	-
FGFRi	2	d4, 2h	6	0.80 ± 0.02	0.078
Vehicle	2	d7, 2h	6	0.82 ± 0.02	-
FGFRi	2	d7, 2h	5	0.81 ± 0.01	0.855
Vehicle	3	d1, 2h	6	0.78 ± 0.01	-
ERKi	3	d1, 2h	6	0.74 ± 0.01	0.055
FGFRi	3	d1, 2h	6	0.79 ± 0.02	0.872
Vehicle	3	d1, 6h	5	0.74 ± 0.01	-
ERKi	3	d1, 6h	6	0.84 ± 0.06	0.273
FGFRi	3	d1, 6h	5	0.77 ± 0.02	0.347
Vehicle	3	d1, 24h	6	0.76 ± 0.02	-
ERKi	3	d1, 24h	6	0.77 ± 0.06	0.173
FGFRi	3	d1, 24h	4	0.78 ± 0.02	0.522

Table 7.6: Plasma concentrations of 1,25D$_3$ in animals treated with 1.4 mg/kg/day of MEKi.

Group	Study	Time point	N	Plasma 1,25D$_3$ (pmol/L)	P
Vehicle	4	d5	5	154 ± 13	-
MEKi	4	d5	5	216 ± 34	0.076
Vehicle	4	d14	5	137 ± 11	-
MEKi	4	d14	5	199 ± 44	0.531
Vehicle	4	d28	5	115 ± 27	-
MEKi	4	d28	5	63 ± 10	0.174

Table 7.7: Cyp27b1 mRNA quantification by qPCR in samples from rats treated with 150 mg/kg/day of ERKi, 20 mg/kg/day of FGFRi or vehicle.

Group	Study	Time point	N	Cyp27b1 (relative mRNA expression)	P
Vehicle	3	6h	6	1.00 ± 0.13	-
ERKi	3	6h	6	25.76 ± 9.33	**0.004**
FGFRi	3	6h	6	9.72 ± 1.51	**0.004**
Vehicle	2	d8	6	1.00 ± 0.21	**-**
ERKi	2	d8	6	103.03 ± 21.66	**0.004**
FGFRi	2	d8	6	2.47 ± 0.72	0.109

Table 7.8: Cyp24a1 mRNA quantification by qPCR in samples from rats treated with 150 mg/kg/day of ERKi, 20 mg/kg/day of FGFRi or vehicle.

Group	Study	Time point	N	Cyp24a1 (relative mRNA expression)	P
Vehicle	3	6h	6	1.00 ± 0.24	-
ERKi	3	6h	6	0.03 ± 0.02	**0.004**
FGFRi	3	6h	6	0.05 ± 0.00	**0.004**
Vehicle	2	d8	6	1.00 ± 0.41	-
ERKi	2	d8	6	0.04 ± 0.02	**0.006**
FGFRi	2	d8	6	0.55 ± 0.12	0.631

Table 7.9: VDR mRNA quantification by qPCR in samples from rats treated with 150 mg/kg/day of ERKi, 20 mg/kg/day of FGFRi or vehicle.

Group	Study	Time point	N	VDR (relative mRNA expression)	P
Vehicle	3	6h	6	1.00 ± 0.09	-
ERKi	3	6h	6	0.65 ± 0.08	**0.025**
FGFRi	3	6h	6	0.59 ± 0.08	**0.006**
Vehicle	2	d8	6	1.00 ± 0.06	-
ERKi	2	d8	6	0.60 ± 0.06	**0.004**
FGFRi	2	d8	6	0.81 ± 0.03	**0.016**

Table 7.10: Image analysis of VDR IHC carried out in sections from rats treated with 150 mg/kg/day of ERKi, 1.4 mg/kg/day of MEKi, 20 mg/kg/day of FGFRi or the respective vehicles.

Group	Study	Time point	N	IHC positivity (%)	P
Vehicle	1	8d	3	0.332 ± 0.103	-
MEKi	1	8d	4	0.439 ± 0.087	0.470
FGFRi	1	8d	6	0.161 ± 0.032	0.121
Vehicle	2	8d	6	0.091 ± 0.019	-
ERKi	2	3d	4	0.030 ± 0.008	**0.033**
FGFRi	2	8d	3	0.094 ± 0.030	1.00
Vehicle	3	6h	6	0.076 ± 0.006	-
ERKi	3	6h	6	0.039 ± 0.005	**0.004**
FGFRi	3	6h	6	0.038 ± 0.007	**0.010**
Vehicle	4	28d	10	1.53 ± 0.12	-
MEKi	4	28d	10	3.92 ± 0.35	**<0.001**
Vehicle	4	25d	10	3.64 ± 0.53	-
FGFRi	4	25d	10	5.21 ± 0.51	**0.016**

Table 7.11: Plasma concentrations of FGF23 in animals treated with 150 mg/kg/day of ERKi, 1.4 mg/kg/day of MEKi, 20 mg/kg/day FGFRi or the respective vehicles.

Group	Study	Time point	N	Plasma FGF23 (pg/mL)	P
Vehicle	1	d1, 2h	3	306 ± 23	-
MEKi	1	d1, 2h	5	245 ± 36	0.297
FGFRi	1	d1, 2h	6	312 ± 25	0.897
Vehicle	1	d1, 6h	3	319 ± 13	-
MEKi	1	d1, 6h	6	76 ± 17	**0.020**
FGFRi	1	d1, 6h	6	100 ± 12	**0.020**
Vehicle	1	d1, 12h	3	435 ± 24	-
MEKi	1	d1, 12h	5	121 ± 33	**0.025**
FGFRi	1	d1, 12h	5	182 ± 28	**0.025**
Vehicle	1	d7, 2h	3	427 ± 149	-
MEKi	1	d7, 2h	3	5307 ± 479	**0.049**
FGFRi	1	d7, 2h	4	2802 ± 215	**0.033**
Vehicle	2	d1, 2h	6	476 ± 63	-
ERKi	2	d1, 2h	6	250 ± 21	**0.025**
FGFRi	2	d1, 2h	6	226 ± 52	**0.025**
Vehicle	2	d1, 6h	4	464 ± 89	-
ERKi	2	d1, 6h	5	153 ± 13	**0.014**
FGFRi	2	d1, 6h	6	107 ± 28	**0.010**
Vehicle	2	d1, 24h	6	462 ± 52	-
ERKi	2	d1, 24h	6	222 ± 68	0.055
FGFRi	2	d1, 24h	6	518 ± 58	0.378
Vehicle	2	d4, 2h	6	388 ± 82	-
ERKi	2	d4, 2h	6	142 ± 94	**0.037**
FGFRi	2	d4, 2h	6	1823 ± 63	**0.004**
Vehicle	2	d7, 2h	6	292 ± 48	-
FGFRi	2	d7, 2h	6	2225 ± 291	**0.004**
Vehicle	3	d1, 2h	6	332 ± 28	-
ERKi	3	d1, 2h	6	203 ± 42	0.055
FGFRi	3	d1, 2h	6	164 ± 12	**0.004**
Vehicle	3	d1, 4h	6	304 ± 25	-
ERKi	3	d1, 4h	5	138 ± 32	**0.006**
FGFRi	3	d1, 4h	5	93 ± 8	**0.006**
Vehicle	3	d1, 6h	6	294 ± 23	-
ERKi	3	d1, 6h	6	108 ± 23	**0.004**
FGFRi	3	d1, 6h	5	65 ± 11	**0.006**

Table 7.12: Plasma concentrations of PTH in animals treated with 150 mg/kg/day of ERKi, 1.4 mg/kg/day of MEKi, 20 mg/kg/day FGFRi or the respective vehicles.

Group	Study	Time point	N	Plasma PTH (pg/mL)	P
Vehicle	1	d8	3	606 ± 172	-
MEKi	1	d8	6	523 ± 235	0.197
FGFRi	1	d8	5	544 ± 208	0.881

Table 7.13: Image analysis of phospho-ERK IHC carried out in sections from rats treated with 150 mg/kg/day of ERKi, 1.4 mg/kg/day of MEKi, 20 mg/kg/day of FGFRi or the respective vehicles.

Group	Study	Time point	N	IHC positivity (%)	P
Vehicle	1	8d	3	1.716 ± 0.460	-
MEKi	1	8d	4	0.133 ± 0.010	**0.034**
FGFRi	1	8d	6	1.397 ± 0.155	0.605
Vehicle	2	8d	6	0.142 ± 0.049	-
ERKi	2	3d	4	2.239 ± 0.541	**0.010**
FGFRi	2	8d	4	0.093 ± 0.015	1.000
Vehicle	3	6h	6	0.046 ± 0.009	-
ERKi	3	6h	6	0.708 ± 0.104	**0.004**
FGFRi	3	6h	6	0.035 ± 0.008	0.200
Vehicle	4	28d	10	0.243 ± 0.025	-
MEKi	4	28d	10	0.093 ± 0.016	**<0.001**
Vehicle	4	25d	10	0.119 ± 0.020	-
FGFRi	4	25d	10	0.140 ± 0.026	0.705

Table 7.14: Image analysis of ERK IHC carried out in sections from rats treated with 150 mg/kg/day of ERKi, 1.4 mg/kg/day of MEKi, 20 mg/kg/day of FGFRi or the respective vehicles.

Group	Study	Time point	N	IHC positivity (%)	P
Vehicle	1	8d	3	0.390 ± 0.09	-
MEKi	1	8d	4	0.406 ± 0.05	1.00
FGFRi	1	8d	6	0.414 ± 0.03	1.00
Vehicle	2	8d	4	1.97 ± 0.14	-
ERKi	2	3d	4	0.25 ± 0.14	**0.021**
FGFRi	2	8d	4	0.56 ± 0.17	**0.021**
Vehicle	3	6h	6	0.83 ± 0.16	-
ERKi	3	6h	6	0.87 ± 0.06	0.749
FGFRi	3	6h	6	1.08 ± 0.10	0.262
Vehicle	4	28d	10	4.21 ± 0.52	-
MEKi	4	28d	10	4.90 ± 0.43	0.290
Vehicle	4	25d	9	2.67 ± 0.32	-
FGFRi	4	25d	9	2.42 ± 0.38	0.566

Table 7.15: Image analysis of phospho-RSK IHC carried out in sections from rats treated with 150 mg/kg/day of ERKi, 1.4 mg/kg/day of MEKi, 20 mg/kg/day of FGFRi or the respective vehicles.

Group	Study	Time point	N	IHC positivity (%)	P
Vehicle	1	8d	3	2.184 ± 0.660	-
MEKi	1	8d	4	1.155 ± 0.187	0.158
FGFRi	1	8d	6	1.002 ± 0.192	0.121
Vehicle	2	8d	6	0.370 ± 0.065	-
ERKi	2	3d	4	0.279 ± 0.019	0.522
FGFRi	2	8d	4	0.370 ± 0.019	0.831
Vehicle	3	6h	6	0.232 ± 0.055	-
ERKi	3	6h	6	0.131 ± 0.016	0.200
FGFRi	3	6h	6	0.164 ± 0.021	0.631

Table 7.16: Image analysis of RSK IHC carried out in sections from rats treated with 150 mg/kg/day of ERKi, 1.4 mg/kg/day of MEKi, 20 mg/kg/day of FGFRi or the respective vehicles.

Group	Study	Time point	N	IHC positivity (%)	P
Vehicle	1	8d	3	15.85 ± 1.21	-
MEKi	1	8d	4	11.64 ± 2.72	0.157
FGFRi	1	8d	6	7.44 ± 2.09	**0.039**
Vehicle	2	8d	5	9.94 ± 1.52	-
ERKi	2	3d	4	4.24 ± 1.03	**0.014**
FGFRi	2	8d	4	7.04 ± 1.15	0.327
Vehicle	3	6h	6	5.80 ± 0.94	-
ERKi	3	6h	6	4.06 ± 0.33	0.055
FGFRi	3	6h	6	4.59 ± 0.86	0.423

Table 7.17: Image analysis of EGR1 IHC carried out in sections from rats treated with 150 mg/kg/day of ERKi, 1.4 mg/kg/day of MEKi, 20 mg/kg/day of FGFRi or the respective vehicles.

Group	Study	Time point	N	IHC positivity (%)	P
Vehicle	1	8d	3	0.93 ± 0.15	-
MEKi	1	8d	4	0.30 ± 0.09	**0.034**
FGFRi	1	8d	6	1.71 ± 0.51	0.197
Vehicle	2	8d	6	0.88 ± 0.13	-
ERKi	2	3d	4	0.23 ± 0.03	**0.010**
FGFRi	2	8d	4	1.62 ± 0.24	**0.033**
Vehicle	3	6h	6	1.14 ± 0.18	-
ERKi	3	6h	6	0.19 ± 0.01	**0.004**
FGFRi	3	6h	6	1.12 ± 0.11	0.873

Table 7.18: RPPA performed in total kidney homogenate samples from rats treated for 6h with 150 mg/kg of ERKi or 20 mg/kg FGFRi – 1.

	Akt		p-Akt		Bcl-x		β-Catenin	
	Expression	P	Expression	P	Expression	P	Expression	P
Vehicle	1.04 ± 0.04	-	0.72 ± 0.02	-	3.28 ± 0.11	-	5.54 ± 0.11	-
ERKi	1.21 ± 0.05	**0.016**	0.71 ± 0.04	1.000	3.66 ± 0.16	**0.025**	5.86 ± 0.15	0.150
FGFRi	1.18 ± 0.09	0.150	0.66 ± 0.02	0.078	4.10 ± 0.01	**0.004**	6.189 ± 0.13	**0.006**

	p-β-Catenin		Calpain2		CC3		p-Chk1	
	Expression	P	Expression	P	Expression	P	Expression	P
Vehicle	0.47 ± 0.01	-	1.67 ± 0.07	-	0.47 ± 0.02	-	0.61 ± 0.02	-
ERKi	0.51 ± 0.01	**0.025**	1.72 ± 0.04	0.522	0.49 ± 0.02	0.522	0.62 ± 0.01	0.262
FGFRi	0.60 ± 0.03	**0.025**	1.82 ± 0.08	0.200	0.47 ± 0.03	1.000	0.59 ± 0.02	0.423

	c-Jun		p-c-Jun		CREB		p-CREB	
	Expression	P	Expression	P	Expression	P	Expression	P
Vehicle	0.41 ± 0.02	-	0.36 ± 0.02	-	1.52 ± 0.13	-	1.69 ± 0.08	-
ERKi	0.39 ± 0.02	0.749	0.37 ± 0.01	0.873	1.33 ± 0.09	0.262	1.49 ± 0.06	0.078
FGFRi	0.45 ± 0.02	0.631	0.38 ± 0.02	0.631	1.06 ± 0.08	**0.010**	1.44 ± 0.04	**0.037**

	p-EGFR		EGFR		GSK-3-β		p-GSK-3-β	
	Expression	P	Expression	P	Expression	P	Expression	P
Vehicle	2.12 ± 0.10	-	0.70 ± 0.03	-	1.74 ± 0.06	-	0.52 ± 0.02	-
ERKi	2.14 ± 0.09	0.873	0.67 ± 0.02	0.631	1.79 ± 0.05	0.423	0.58 ± 0.02	**0.037**
FGFRi	2.16 ± 0.05	1.000	0.62 ± 0.02	**0.037**	1.87 ± 0.05	0.200	0.58 ± 0.03	0.078

	p-IGF-1R β		p-IKK α/β		IRS-1		p-IRS-1	
	Expression	P	Expression	P	Expression	P	Expression	P
Vehicle	4.23 ± 0.18	-	0.70 ± 0.03	-	0.31 ± 0.02	-	0.49 ± 0.02	-
ERKi	4.47 ± 0.20	0.423	0.79 ± 0.02	0.078	0.31 ± 0.01	0.749	0.49 ± 0.03	1.00
FGFRi	4.83 ± 0.25	0.109	0.74 ± 0.02	0.522	0.32 ± 0.02	0.522	0.48 ± 0.03	0.749

	JAK1		MAPKAPK-2		p-MAPKAPK-2		MEK1/2	
	Expression	P	Expression	P	Expression	P	Expression	P
Vehicle	0.54 ± 0.02	-	5.96 ± 0.27	-	0.66 ± 0.02	-	1.10 ± 0.06	-
ERKi	0.56 ± 0.02	0.631	5.49 ± 0.11	0.109	0.63 ± 0.03	0.522	1.00 ± 0.03	0.423
FGFRi	0.64 ± 0.03	**0.010**	5.89 ± 0.18	0.631	0.59 ± 0.02	0.037	1.00 ± 0.05	0.262

	p-MEK1/2		p-MNK1		p-MSK1		mTOR	
	Expression	P	Expression	P	Expression	P	Expression	P
Vehicle	1.12 ± 0.06	-	1.07 ± 0.03	-	0.40 ± 0.02	-	2.07 ± 0.08	-
ERKi	1.17 ± 0.04	0.423	0.98 ± 0.02	0.055	0.36 ± 0.01	0.109	2.05 ± 0.06	0.522
FGFRi	1.02 ± 0.04	0.200	0.97 ± 0.04	0.037	0.33 ± 0.01	0.055	2.08 ± 0.05	0.873

	p-NFkB		p-p21		p38		p-p38	
	Expression	P	Expression	P	Expression	P	Expression	P
Vehicle	0.37 ± 0.01	-	4.51 ± 0.26	-	15.24 ± 0.33	-	2.47 ± 0.27	-
ERKi	0.37 ± 0.02	0.749	5.07 ± 0.29	0.200	15.17 ± 0.59	0.873	2.44 ± 0.20	0.631
FGFRi	0.36 ± 0.02	0.109	5.37 ± 0.25	0.055	15.99 ± 0.46	0.337	2.00 ± 0.19	0.262

Table 7.19: RPPA performed in total kidney homogenate samples from rats treated for 6h with 150 mg/kg of ERKi or 20 mg/kg FGFRi – 2.

	ERK1/2		p-ERK1/2		PARP		p-PDGFR	
	Expression	P	Expression	P	Expression	P	Expression	P
Vehicle	10.99 ± 0.43	-	4.637 ± 0.38	-	1.13 ± 0.03	-	4.57 ± 0.11	-
ERKi	9.91 ± 0.26	0.055	19.96 ± 2.03	**0.004**	1.28 ± 0.08	0.109	4.48 ± 0.17	0.522
FGFRi	10.54 ± 0.20	0.337	4.18 ± 0.28	0.522	1.389 ± 0.04	**0.004**	4.71 ± 0.12	0.423

	p-PDK-1		PI3K α		PKA		p-PKC	
	Expression	P	Expression	P	Expression	P	Expression	P
Vehicle	2.08 ± 0.08	-	0.90 ± 0.02	-	2.88 ± 0.16	-	3.19 ± 0.13	-
ERKi	2.04 ± 0.06	0.873	0.89 ± 0.03	0.522	2.78 ± 0.09	0.522	2.89 ± 0.10	0.109
FGFRi	2.20 ± 0.08	0.423	0.87 ± 0.03	0.423	2.53 ± 0.08	0.078	2.84 ± 0.05	**0.037**

	p-VEGFR		PLC-γ		p-PLC-γ		PTEN	
	Expression	P	Expression	P	Expression	P	Expression	P
Vehicle	0.45 ± 0.01	-	0.48 ± 0.02	-	0.43 ± 0.01	-	1.83 ± 0.04	-
ERKi	0.44 ± 0.02	0.749	0.45 ± 0.01	0.262	0.40 ± 0.01	0.055	1.81 ± 0.06	0.873
FGFRi	0.43 ± 0.01	0.150	0.45 ± 0.01	0.337	0.35 ± 0.01	**0.004**	1.82 ± 0.03	0.631

	p-Raf (259)		p-Raf (338)		Raf1		Rap1	
	Expression	P	Expression	P	Expression	P	Expression	P
Vehicle	0.72 ± 0.03	-	1.67 ± 0.05	-	1.84 ± 0.06	-	0.41 ± 0.02	-
ERKi	0.66 ± 0.03	0.262	1.88 ± 0.05	**0.010**	1.93 ± 0.07	0.337	0.41 ± 0.02	0.873
FGFRi	0.62 ± 0.02	**0.025**	1.84 ± 0.05	0.055	2.14 ± 0.05	**0.006**	0.39 ± 0.02	0.631

	p-S6 Rib		JNK		p-JNK		p-Smad1/5	
	Expression	P	Expression	P	Expression	P	Expression	P
Vehicle	1.04 ± 0.21	-	1.15 ± 0.05	-	0.57 ± 0.03	-	0.79 ± 0.04	-
ERKi	0.69 ± 0.04	0.522	1.18 ± 0.04	0.522	0.60 ± 0.02	0.522	0.80 ± 0.04	0.873
FGFRi	0.64 ± 0.06	0.150	1.30 ± 0.04	0.078	0.61 ± 0.07	0.873	0.71 ± 0.02	0.109

	Src		p-Src		p-Tyk2		Ubiquitin	
	Expression	P	Expression	P	Expression	P	Expression	P
Vehicle	47.46 ± 2.25	-	0.70 ± 0.033	-	1.00 ± 0.04	-	13.79 ± 0.73	-
ERKi	44.63 ± 1.68	0.337	0.66 ± 0.036	0.423	0.93 ± 0.02	0.337	12.81 ± 0.58	0.337
FGFRi	45.04 ± 1.46	0.337	0.59 ± 0.023	**0.025**	0.98 ± 0.03	0.631	13.13 ± 0.51	0.631

	PKC-α	
	Expression	P
Vehicle	1.08 ± 0.06	-
ERKi	1.08 ± 0.05	0.749
FGFRi	1.01 ± 0.05	0.200

Table 7.20: Image analysis of β-catenin IHC carried out in sections from rats treated with 150 mg/kg/day of ERKi, 1.4 mg/kg/day of MEKi, 20 mg/kg/day of FGFRi or the respective vehicles.

Group	Study	Time point	N	IHC positivity (%)	P
Vehicle	1	8d	3	2.00 ± 0.26	-
MEKi	1	8d	4	1.59 ± 0.28	0.480
FGFRi	1	8d	6	1.75 ± 0.22	0.302
Vehicle	2	8d	6	1.68 ± 0.25	-
ERKi	2	3d	4	1.66 ± 0.27	1.009
FGFRi	2	8d	4	2.10 ± 0.30	0.522
Vehicle	3	6h	6	1.28 ± 0.21	-
ERKi	3	6h	6	1.91 ± 0.26	0.078
FGFRi	3	6h	6	1.60 ± 0.29	0.337
Vehicle	4	28d	10	2.27 ± 0.33	-
MEKi	4	28d	10	2.37 ± 0.24	0.701

Table 7.21: Image analysis of NaPi-IIa IHC carried out in sections from rats treated with 150 mg/kg/day of ERKi, 1.4 mg/kg/day of MEKi, 20 mg/kg/day of FGFRi or the respective vehicles.

Group	Study	Time point	N	IHC positivity (%)	P
Vehicle	1	8d	3	0.911 ± 0.204	-
MEKi	1	8d	4	1.020 ± 0.249	0.724
FGFRi	1	8d	6	1.041 ± 0.242	0.439
Vehicle	2	8d	6	1.176 ± 0.284	-
ERKi	2	3d	4	0.290 ± 0.134	**0.033**
FGFRi	2	8d	4	0.318 ± 0.082	**0.033**
Vehicle	3	6h	6	0.741 ± 0.197	-
ERKi	3	6h	6	0.996 ± 0.187	0.149
FGFRi	3	6h	6	1.832 ± 0.312	**0.016**
Vehicle	4	28d	10	3.856 ± 0.406	-
MEKi	4	28d	10	5.573 ± 0.564	**0.023**
Vehicle	4	25d	10	2.479 ± 0.361	-
FGFRi	4	25d	10	1.241 ± 0.136	**0.010**

Table 7.22: Image analysis of TRPV5 IHC carried out in sections from rats treated with 150 mg/kg/day of ERKi, 1.4 mg/kg/day of MEKi, 20 mg/kg/day of FGFRi or the respective vehicles.

Group	Study	Time point	N	IHC positivity (%)	P
Vehicle	1	8d	3	0.039 ± 0.021	-
MEKi	1	8d	4	0.418 ± 0.083	**0.034**
FGFRi	1	8d	6	0.170 ± 0.047	**0.034**
Vehicle	2	8d	6	0.075 ± 0.010	-
ERKi	2	3d	4	0.026 ± 0.004	**0.019**
FGFRi	2	8d	4	0.235 ± 0.034	**0.011**
Vehicle	3	6h	6	0.036 ± 0.008	-
ERKi	3	6h	6	0.017 ± 0.004	**0.046**
FGFRi	3	6h	6	0.009 ± 0.002	**0.016**
Vehicle	4	28d	10	1.537 ± 0.163	-
MEKi	4	28d	10	2.189 ± 0.166	**0.016**
Vehicle	4	25d	10	0.560 ± 0.110	-
FGFRi	4	25d	10	0.955 ± 0.111	**0.023**

Table 7.23: Image analysis of calbindin-D28k IHC carried out in sections from rats treated with 150 mg/kg/day of ERKi, 1.4 mg/kg/day of MEKi, 20 mg/kg/day of FGFRi or the respective vehicles.

Group	Study	Time point	N	IHC positivity (%)	P
Vehicle	1	8d	3	1.34 ± 0.50	-
MEKi	1	8d	4	3.78 ± 0.53	**0.034**
FGFRi	1	8d	6	2.54 ± 0.34	0.071
Vehicle	2	8d	6	0.18 ± 0.03	-
ERKi	2	3d	4	0.28 ± 0.10	0.394
FGFRi	2	8d	4	0.50 ± 0.09	**0.011**
Vehicle	3	6h	6	0.18 ± 0.04	-
ERKi	3	6h	6	0.15 ± 0.05	0.631
FGFRi	3	6h	6	0.21 ± 0.04	0.631
Vehicle	4	28d	10	0.73 ± 0.07	-
MEKi	4	28d	10	1.37 ± 0.09	**<0.001**
Vehicle	4	25d	10	1.11 ± 0.16	-
FGFRi	4	25d	10	1.74 ± 0.18	**0.034**

Table 7.24: Image analysis of PMCA IHC carried out in sections from rats treated with 150 mg/kg/day of ERKi, 1.4 mg/kg/day of MEKi, 20 mg/kg/day of FGFRi or the respective vehicles.

Group	Study	Time point	N	IHC positivity (%)	P
Vehicle	1	8d	3	0.094 ± 0.037	-
MEKi	1	8d	4	0.724 ± 0.074	**0.034**
FGFRi	1	8d	6	0.335 ± 0.042	**0.020**
Vehicle	2	8d	5	0.924 ± 0.165	-
ERKi	2	3d	4	0.636 ± 0.069	0.327
FGFRi	2	8d	4	1.252 ± 0.181	0.086
Vehicle	3	6h	6	0.331 ± 0.054	-
ERKi	3	6h	6	0.375 ± 0.053	0.749
FGFRi	3	6h	6	0.517 ± 0.064	0.078
Vehicle	4	28d	10	2.331 ± 0.130	-
MEKi	4	28d	8	3.905 ± 0.361	**<0.001**
Vehicle	4	25d	10	0.712 ± 0.090	-
FGFRi	4	25d	10	0.944 ± 0.142	0.174

Table 7.25: Image analysis of Klotho IHC carried out in sections from rats treated with 150 mg/kg/day of ERKi, 1.4 mg/kg/day of MEKi, 20 mg/kg/day of FGFRi or the respective vehicles.

Group	Study	Time point	N	IHC positivity (%)	P
Vehicle	1	8d	3	0.498 ± 0.156	-
MEKi	1	8d	4	0.547 ± 0.097	0.724
FGFRi	1	8d	6	0.710 ± 0.079	0.121
Vehicle	2	8d	6	0.932 ± 0.319	-
ERKi	2	3d	4	0.955 ± 0.645	0.522
FGFRi	2	8d	4	0.957 ± 0.207	0.831
Vehicle	3	6h	6	2.022 ± 1.077	-
ERKi	3	6h	6	0.860 ± 0.294	0.262
FGFRi	3	6h	6	1.634 ± 0.499	0.872
Vehicle	4	28d	9	1.635 ± 0.341	-
MEKi	4	28d	10	2.002 ± 0.466	0.568
Vehicle	4	25d	10	1.497 ± 0.161	-
FGFRi	4	25d	10	1.115 ± 0.137	0.096

Table 7.26: Plasma concentrations of Klotho in animals treated with 1.4 mg/kg/day of MEKi, 20 mg/kg/day FGFRi or vehicle.

Group	Study	Time point	N	Plasma Klotho (ng/mL)	P
Vehicle	1	d8	3	11.17 ± 0.09	-
MEKi	1	d8	6	12.57 ± 0.51	**0.028**
FGFRi	1	d8	5	8.52 ± 0.29	**0.025**

Table 7.27: Image analysis of alkaline phosphatase IHC carried out in sections from rats treated with 150 mg/kg/day of ERKi, 1.4 mg/kg/day of MEKi, 20 mg/kg/day of FGFRi or the respective vehicles.

Group	Study	Time point	N	IHC positivity (%)	P
Vehicle	1	8d	3	0.003 ± 0.001	-
MEKi	1	8d	4	0.007 ± 001	0.077
FGFRi	1	8d	6	0.007 ± 0.002	0.071
Vehicle	2	8d	6	0.252 ± 0.059	-
ERKi	2	3d	4	0.531 ± 0.055	**0.019**
FGFRi	2	8d	4	0.501 ± 0.121	**0.033**
Vehicle	3	6h	6	0.441 ± 0.087	-
ERKi	3	6h	6	0.592 ± 0.168	0.749
FGFRi	3	6h	6	0.497 ± 0.096	0.631

Table 7.28: Image analysis of Pit-1 IHC carried out in sections from rats treated with 150 mg/kg/day of ERKi, 1.4 mg/kg/day of MEKi, 20 mg/kg/day of FGFRi or the respective vehicles.

Group	Study	Time point	N	IHC positivity (%)	P
Vehicle	1	8d	3	0.920 ± 0.334	-
MEKi	1	8d	4	0.704 ± 0.278	0.724
FGFRi	1	8d	6	1.163 ± 0.155	0.439
Vehicle	2	8d	6	1.422 ± 0.122	-
ERKi	2	3d	3	1.186 ± 0.108	0.180
FGFRi	2	8d	4	1.395 ± 0.283	1.000
Vehicle	3	6h	6	1.136 ± 0.128	-
ERKi	3	6h	6	1.014 ± 0.761	0.423
FGFRi	3	6h	6	0.861 ± 0.118	0.150

Table 7.29: Image analysis of osteopontin IHC carried out in sections from rats treated with 150 mg/kg/day of ERKi, 1.4 mg/kg/day of MEKi, 20 mg/kg/day of FGFRi or vehicle.

Group	Study	Time point	N	IHC positivity (%)	P
Vehicle	2	8d	6	0.049 ± 0.011	-
ERKi	2	3d	4	0.064 ± 0.012	0.286
FGFRi	2	8d	4	0.494 ± 0.258	**0.011**
Vehicle	3	6h	6	0.050 ± 0.007	-
ERKi	3	6h	6	0.064 ± 0.013	0.522
FGFRi	3	6h	6	0.056 ± 0.010	0.749

Table 7.30: Plasma concentrations of osteoprotegerin in animals treated with 150 mg/kg/day of ERKi, 20 mg/kg/day FGFRi or the vehicle.

Group	Study	Time point	N	Plasma osteoprotegerin (pg/mL)	P
Vehicle	2	d8	6	360 ± 25	-
ERKi	2	d3	6	570 ± 64	**0.010**
FGFRi	2	d8	6	500 ± 24	**0.004**
Vehicle	3	6h	6	442 ± 63	-
ERKi	3	6h	6	458 ± 56	0.423
FGFRi	3	6h	6	572 ± 132	0.749

Table 7.31: Plasma concentrations of sclerostin in animals treated with 150 mg/kg/day of ERKi, 20 mg/kg/day FGFRi or vehicle.

Group	Study	Time point	N	Plasma sclerostin (pg/mL)	P
Vehicle	2	d8	6	214 ± 10	-
ERKi	2	d3	6	201 ± 15	0.631
FGFRi	2	d8	6	657 ± 81	**0.004**
Vehicle	3	6h	6	279 ± 35	-
ERKi	3	6h	6	252 ± 32	0.522
FGFRi	3	6h	6	250 ± 32	0.631

Table 7.32: Plasma concentrations of DKK1 in animals treated with 150 mg/kg/day of ERKi, 20 mg/kg/day FGFRi or vehicle.

Group	Study	Time point	N	Plasma DKK1 (pg/mL)	P
Vehicle	2	d8	6	881 ± 40	-
ERKi	2	d3	6	1481 ± 162	**0.004**
FGFRi	2	d8	6	1414 ± 111	**0.004**
Vehicle	3	6h	6	1073 ± 110	-
ERKi	3	6h	6	822 ± 107	0.109
FGFRi	3	6h	6	888 ± 165	0.423

Table 7.33: Plasma concentrations of creatinine in animals treated with 150 mg/kg/day of ERKi, 1.4 mg/kg/day of MEKi, 20 mg/kg/day FGFRi or vehicle.

Group	Study	Time point	N	Plasma creatinine (µmol/L)	P
Vehicle	1	d8	3	25.67 ± 1.76	-
MEKi	1	d8	6	30.00 ± 0.86	0.071
FGFRi	1	d8	5	31.60 ± 1.50	0.053
Vehicle	2	d8	6	31.17 ± 1.01	-
ERKi	2	d3	6	60.50 ± 11.50	**0.005**
FGFRi	2	d8	5	38.00 ± 2.21	**0.028**
Vehicle	3	6h	6	3.17 ± 0.95	-
ERKi	3	6h	6	28.83 ± 1.64	0.230
FGFRi	3	6h	6	27.33 ± 0.95	**0.045**
Vehicle	4	d28	10	60.50 ± 1.30	-
MEKi	4	d28	10	61.50 ± 1.15	0.496
Vehicle	4	d25	10	22.30 ± 0.50	-
FGFRi	4	d25	10	28.9 ± 1.05	**0.001**

Table 7.34: ATP contents of rat kidney slices cultured for 1h, 1d, 2d and 3d

Time point	N	nmol ATP / mg wet weight	P
1h	3	50.36 ± 4.23	-
1h (Trit X[1])	3	3.78 ± 1.80	**0.049**
24h	3	32.03 ± 6.94	0.126
48h	3	12.90 ± 5.11	**0.049**
72h	3	0.98 ± 0.80	**0.049**

1 – 1% Triton X

Table 7.35: Image analysis of NaPi-IIa IHC carried out in sections of rat kidney slices incubated for 4h in culture media containing 0 mM or 2 mM of Pi

Group	N	IHC positivity (%)	P
0 mM Pi	4	3.29 ± 0.16	**0.021**
2 mM Pi	4	2.64 ± 0.11	